

Improving the maneuvering performance of diesel hybrid propulsion plants for fast naval combatants

MSc Thesis

SDPO.16.033.m.

Public Version

Improving the maneuvering performance of hybrid diesel propulsion plants for fast naval combatants

By

Jasper Vollbrandt

in partial fulfilment of the requirements for the degree of

Master of Science

in Mechanical Engineering

at the Delft University of Technology,

to be defended publicly on October 27th, 2016

Supervisor TU Delft: LTZ1 (TD) Ir. R.D. Geertsma

Supervisor DMO: LTZ1 (TD) Ir. F.J. Driegen

Ir. E.H. Takken

Thesis committee: Rear-Admiral (ret.) Ir. K. Visser, TU Delft

Dr.ir. H.J. de Koning Gans, TU Delft

LTZ1 (TD) Ir. R.D. Geertsma, TU Delft

LTZ1 (TD) Ir. F.J. Driegen, DMO



Ministerie van Defensie

Preface

After years of arduous work and study, I am taking the final step. This report is the result of my graduation project in mechanical engineering.

The graduation project is part of the MSI – Mechanical Systems and Integration – specialization within Transport Engineering at the Delft University of Technology. This specialization focuses on the characteristics and performance of machinery installations and their integration. A typical MSI-related problem is the design of a ship's propulsion plant.

I worked on my graduation thesis at the Defensie Materieel Organisatie (Defense Material Organization) in the Hague. Part of the Dutch Ministry of Defense, DMO is responsible for the procurement and sale of armed forces material and is involved in planning maintenance and providing logistical services.

The Marine Engineering Bureau, my workplace for the last 9 months, provides advice, regulations and standards for the mechanical and electrical systems onboard vessels belonging to the Royal Netherlands Navy. With specialist knowledge on prime movers, rudder installations, hydraulic and pneumatic systems as well as their control, the Marine Engineering Bureau proved to be the ideal workplace for my research.

Special thanks go to Rinze Geertsma, my supervisor at TU Delft, for many deep discussions and his invaluable feedback on my work.

I would also like to thank Fred Driegen, Kees Posthumus, Isaac Barendregt, Edwin van Dijk, Ab Blokland, Barry Hagenouw, Roel van Zwienen and Nicola Laud for their warm welcome at the Marine Engineering Bureau at the DMO. Thanks, too, to Maarten Cordia for being a helpful roommate. At the DMO, I also want to thank Erik Takken, Jelle Loosman and Joop van Son for contributing to my work, and Ilja Houtman for the opportunity to sail on Zr. Ms. De Ruyter. Furthermore, I would like to thank Peter de Vos at TU Delft for his assistance in finding this interesting subject for my thesis.

Above all, I would like to thank my friends and family - and in particular my parents and my brothers - for their support, guidance and attention, not only in relation to my thesis but also since my first year in Delft.

September 2016,

Jasper Vollbrandt

Abstract

Diesel engines have a bad reputation if considered for propulsion in fast naval combatants. Compared to gas turbines, propulsion systems with diesel engines are regarded to be heavy, prone to thermal overloading and suffer from poor maneuverability. However, diesel engines are efficient and require less expensive maintenance, offering the possibility of significant reduction in operational costs and fuel supply dependency.

This research investigated whether the acceleration performance and the thermal loading can be improved with diesel hybrid propulsion in a CODLAD configuration. The performance and thermal loading was evaluated with dynamic simulation models representing different configurations of propulsion plants for the future M-frigate of the Royal Netherlands Navy.

The study demonstrates that fast naval combatant with diesel hybrid propulsion can accelerate as fast as gas turbine driven vessels. To fulfill the desired NATO standards for acceleration maneuvers an adaptive pitch control strategy in combination with controllable pitch propellers is required. This will enable a fast ramp up of diesel engine speed to provide maximum power without overloading the engine thermally. Furthermore, the electric drives need to assist the diesel engine during the acceleration maneuver for optimum acceleration.

Measurement data is absolutely essential to validate the simulation results and improve the model. Furthermore, an improved turbocharger model can be used to investigate the effect of sequential turbocharging.

Table of Contents

| | |
|--|-----|
| Preface..... | I |
| Abstract..... | III |
| Table of Contents..... | V |
| 1. Introduction..... | 1 |
| 2. Background..... | 4 |
| Replacing the current M-frigate..... | 4 |
| Resistance and Propulsion Power..... | 6 |
| Comparing Diesel Engines and Gas Turbines..... | 8 |
| Propeller Calculations..... | 22 |
| 3. Propulsion Plant Concepts..... | 39 |
| Requirements..... | 39 |
| Determining Concepts..... | 41 |
| Component Selection..... | 46 |
| Matching..... | 53 |
| 4. Propulsion Model..... | 59 |
| Model Description..... | 59 |
| Control Parameters..... | 75 |
| Verification/Validation..... | 77 |
| 5. Simulations..... | 80 |
| 6. Results..... | 84 |
| The problem of thermal overloading..... | 84 |
| Thermal Limits..... | 86 |
| Effects of waves..... | 88 |
| Acceleration maneuvers..... | 92 |
| Angle of Attack CPP vs FPP..... | 126 |
| 7. Conclusions & Recommendations..... | 129 |
| Conclusions..... | 129 |
| Recommendations..... | 131 |
| 8. References..... | 132 |
| 9. Appendix..... | 137 |

1. Introduction

Increasing oil scarcity and increasing awareness of the climate change drive the improvement of fuel economy in the marine industry. Even for military applications improving the fuel economy becomes inevitable. Next to contributing to international climate and energy targets, main reason for military applications is reducing the dependency on fuel supplies. Thus, a good fuel economy is especially important for naval vessels operating in remote areas.

Due to their high efficiency, diesel engines generally are the preferred choice for marine propulsion systems. But these engines are also known for their low power density and poor maneuverability. Therefore, gas turbines remain the favored prime mover in high-performance naval combatants such as destroyers and frigates or patrol vessels intended for high ship speeds.

Many studies on the design of modern and future propulsion concepts show that frigates still rely heavily on the use of gas turbines delivering boost power to achieve high ship speeds. Partridge and Thorp (Partridge & Thorp, 2014) investigated modern frigate design and pointed out the increasing use of one large gas turbine providing boost power either directly or in a hybrid drive configuration. Alexander (Alexander, 2015) studied the benefits of implementing hybrid drive to the gas turbine powered US naval combatants. On the other hand, research by van Es (van Es, 2011) shows that diesel- and diesel-electric-propulsion improves the fuel economy of frigates. His static calculations are suitable to estimate the fuel consumption but unsuitable to predict dynamic performance of different propulsion plants. He concluded limited maneuverability of diesel propulsion based on expert opinion. Thus, the trend of the extensive use of gas turbines for fast naval vessels is supported by the lack of research on improving the maneuverability of diesel engine propulsion.

Research on diesel and diesel electric propulsion could reveal possibilities for the future M-frigate of Royal Netherlands Navy to improve the maneuverability by sustaining the fuel efficiency of the diesel engines. The goal of this research is to gain more insight in the transient performance of diesel propulsion in combination with electric drives for fast naval vessels. Probably, the most important question will be:

Can the maneuvering performance of diesel engines be improved compared to gas turbine driven propulsion plants?

Maneuverability of a ship consist of several elements: acceleration, deceleration and change of heading, but also slow moving in a harbor is part of the ship's maneuverability. Changing heading fast is mainly influenced by the geometry of the hull and rudders and is only partly influenced by the performance of the propulsion plant. Therefore, this aspect of maneuverability will not be covered by this research. The maneuverability is limited to straight line maneuverability, with the focus on acceleration maneuvers which is primarily dependent on the performance of the propulsion plant.

Static calculations that considering the resistance of the vessel, the involved propeller curve and the operating envelope of modern turbocharged diesel engines show diesel engines can propel frigates at high speeds. For example, diesel engine propulsion on the Danish Iver Huitfeldt-class frigate achieves a very good acceleration performance (OMT, 2014). However, evaluating the maneuvering performance of a vessel cannot be quantified with static calculations. Accelerating and decelerating the vessel are a time-dependent process according to Newton's 2nd law of motion, so is accelerating and decelerating shafts and rotating parts within the engine. The available engine power is also a time-dependent process due to the inertia of the turbocharger system. Next to the internal time-dependent processes, also external disturbances like wind and waves are variable in time.

Assessing the performance of every involved component analytically requires solving a system of differential equations with numerous mathematical relations between the components. Obtaining the analytical solution

is hard and only provides solutions for distinct instances of time. On the other hand, modern computers offer sufficient computing power to execute numerical simulations of models that are too complex for solving analytically [e.g. (de Boer & Hardy, 2014); (Geerstma, Negenborn, Visser, & Hopman, 2016); (Grimmelius, Shi, & Stapersma, 2010)]. Therefore, I used a dynamic simulation model to predict the acceleration performance of the dynamic propulsion system with numerical simulation.

Earlier frigates with diesel engines intended for lower ship speeds suffered from overloading of the diesel engines [e.g. (van Spronsen & Tousain, 2001); (Guillemette & Bussieres, 1997)] resulting in increased need for maintenance and a bad reputation of the diesel engine. Preventing overloading for the future M-frigate is of utmost importance. To prevent overloading, limits for the dynamic simulation model have to be introduced.

How can the dynamic overloading limits of the diesel engine be evaluated during the simulation?

Manufacturers of diesel engines determine time dependent load limits for their engines. Furthermore, the diesel engine is also limited by the turbocharger, introducing a charge air dependent load limit. With a dynamic simulation model, these load limits are investigated to introduce limits dependent on predicted engine output data. With limits preventing overloading, the following question arises:

How can high maneuverability be achieved without exceeding the dynamic limitations?

With the limitations in mind, design parameters for the control strategy are developed for high maneuverability while reducing the engine load if possible. These design parameters are tested in the dynamic simulation and evaluated based on the dynamic limitations.

One of the key candidates for the propulsion system is hybrid propulsion with an electric motor for silent speed and low speed loitering. In combination with the diesel engines, the electric drives could provide additional propulsion power, boosting the performance of the propulsion plant.

How can electric drives improve the acceleration performance of diesel engines?

Different propulsion plant layouts are set up in which the size of the electric drives is varied to evaluate the effect on the maneuverability. Next to different propulsion plant layouts also different propulsors are evaluated with dynamic simulations. Controllable pitch propellers offer advantages during maneuvering, in heavy sea and for redundancy reasons [e.g. (Burril, 1949); (Bille, 1970); (Yabuki, Yoshimura, Ishiguro, & Ueno, 2006)]. But with naval requirements, fixed pitch propellers offer advantages as well. FPPs offer a higher efficiency in design conditions, less maintenance and a smaller hub diameter. The smaller hub diameter is in particular important if the propeller is optimized for a cavitation free working point (Witt, Motley, Helfers, & Young, 2012). Currently, fixed pitch propellers are not used in combination with diesel engines on fast naval vessels and research on this configuration is absent. With a dynamic simulation model, it is possible to compare the two propellers in terms of ship speed, maneuverability and the resulting engine load, resulting in the question:

What is the impact of using a FPP?

After evaluating different propulsion concepts, different propulsors and different design parameters for the control strategy, the summarizing question is:

What are the requirements for high maneuverability on diesel engines?

By answering this question, the limitations for propulsion of the future frigate on diesel engines are discussed and the requirements are mentioned. These requirements include requirements on the hardware and on the control strategy.

Setting up simulation models of the propulsion system for dynamic simulation experiments requires a lot of work and a lot of information. Information was gathered in an extensive literature review and a lot of the results are presented in the background section. The background section is introduced with the reasons for replacing the current M-frigate and the roles and requirements of the replacing, future M-frigate. The impact of the Operational Energy Strategy (Dutch: Operationele Energiestrategie (OES)) on the design is addressed, main driver for the required reduction of fuel consumption.

A comparison between the major prime movers for naval vessels, gas turbine and diesel engine, is also made in the background section. For this comparison data on the Luchtverdedigings – en commandofregat (LCF) of the Royal Netherlands Navy is used, in size and weight expected to be comparable to the future M-frigate. The two types of prime mover are compared in power density, performance and operating cost. This section gives reasons why diesel engines are promising in reducing the fuel consumption but also why gas turbines are still extensively used in naval vessels.

Furthermore, the background section covers how the brake power is estimated from a given resistance curve and addresses the influences of off-design conditions on the requested power. To do so this section introduces the necessary equations to predict propeller performance and how the requirements on a naval propeller can be met.

Chapter 3 ‘Propulsion Plant Concepts’ narrows down the requirements for the future M-frigate to requirements that affect the size and layout of the propulsion plant. Possible propulsion plant layouts are discussed and a selection of four different concepts for further investigation is made. Data on the chosen prime movers is presented in this chapter and their parameters for the simulation model introduced.

Chapter 4 ‘Propulsion Model’ explains the propulsion model and introduces the relevant equations needed to predict the performance of the involved components. This chapter also discusses how the simulation model is controlled and which data is required from the user. Chapter 5 covers the simulation experiments. This chapter explains how the simulation experiments are carried out and defines the operational conditions.

The results are presented in chapter 6. The chapter is introduced with a description of the overloading phenomenon and how it can be prevented. The thermal limits to prevent overloading are presented and the method of how they were obtained. Next, the dynamic effect of waves on the propulsion plant is discussed and the consequences for the different concepts are shown. Results of the acceleration maneuvers for the different concepts in trial and design condition are plotted and the performance compared to the reference vessel, the LCF. Also the setpoints for engine speed, propeller pitch and torque of the electric drives are plotted and their effect on the thermal loading of the diesel engines is shown. Further, the performance of the concepts during off-design conditions is evaluated and possibilities discussed to improve the performance. Finally, a method to reduce the angle of attack during acceleration is shown and the results for FPP and CPP are compared against one another.

2. Background

Replacing the current M-frigate

The current class of multipurpose frigates, owned by the Royal Netherlands Navy, were commissioned between 1991 and 1995. After mid-life modernization in 2010 the two remaining ships will be decommissioned in 2023, calling for development of a replacing frigate. In 2011 a design study was started to gather information on the operational needs for the future frigate, leading to the deployment of the operational concept. The operational concept defines the capabilities and requirements on a high level, but act as guidelines for the design of the ship. Since then the conceptual design has made progress and choices on the propulsion plant of the ship were considered. But not only the requirements defined within the operational concept are of large impact on the design of the propulsion plant. The replacement of the frigate is still no official project. All stated requirements and resulting properties and dimensions are given as currently in use for preliminary studies and might change in the final project.

Operationele Energiestrategie

With regard to the increasing awareness of the climate change but also of the depletion of natural resources, especially oil, the European Union agreed on climate and energy targets (European Commission, 2014). These targets include the reduction of greenhouse gas emissions and the increase of renewable energy consumption. The Dutch Ministry of Defense (MoD) contributes to the climate and energy targets by means of the Operational Energy Strategy (Dutch: Operationele Energiestrategie (OES)) (OES, 2015). Next to fulfilling climate targets, reducing the fuel consumption also improves the efficiency of the armed forces. Improving the fuel efficiency increases the operational range of the forces and refueling intervals. Refueling of military equipment in remote operational zones requires vast logistic effort, increasing the cost of delivered fuel significantly and hence reduces the effectiveness of the forces. Within the OES, a 20% reduction in fossil fuel consumption till 2030, compared to 2010, is set as target. For the year 2050, a reduction of 30% is set. These targets hold for the entire armed forces and therefore need to be translated into specific targets valid for the different military branches. For naval combatants an absolute reduction (m^3/year) and a relative reduction ($\text{m}^3/\text{sail day}$) are proposed but not further specified. As the replacing frigate will probably be commissioned as from 2023, the new vessel has to comply with these targets.

The rather superficial targets leave room for discussion on their fulfillment. An absolute reduction can be achieved by deploying less vessels or by reducing the amount of sailing days per year. A relative reduction can be achieved by altering the operational profile and reducing the vessels speed (slow steaming). If the operational conditions remain constant and the reduction has to be achieved per ship, compared to the old M-Frigate, the set targets are not likely to be met. Reason is the increasing ship size of the new frigate, with a displacement ranging between 4500 and 6000 tons, compared to a displacement of 3300 tons of the old frigate. Comparing the new frigate with the current air-defense and command frigates (Dutch: Luchtverdedigings – en commandofregat (LCF)), in size and weight probably comparable, is also not a fair comparison as this frigate has a different operational profile and requirements and might finally deviate in size and weight.

Either way, with the OES the Ministry of Defense will increase the pressure to improve the fuel consumption of the future M-frigate. Relying entirely on diesel engines for propulsion of the future M-frigate, these reductions could potentially be achieved. Another way of reducing the fuel consumption is to reduce the required top speed of the future frigate. Reducing the top speed a bit significantly reduces the required propulsion power as will be shown in the section 'Resistance and Propulsion Power'.

Requirements & the operational profile

With the recent LCF-class specialized in air defense, the future M-frigate likely to focus on counter submarine threats. Anti-Submarine Warfare (ASW) includes the operation of a towed sonar array to detect submerged submarines. A towed sonar array consists of a series of hydrophones mounted to a cable and trailing behind the vessel. In addition to the increased drag force created by the array, towing the sonar array requires specific ship speeds for proper operation, depending on the type of towed array:

- Low Frequency Active Sonar (LFAS): 15 knots
- Towed Array Sonar (TAS): 12 knots

During ASW-operations, the future frigate needs to be as silent as possible. By reducing noise emission to the sea, the vessel reduces the chance of being detected by hostile submarines as well as increasing its own sonar performance by preventing noise polluting the sonar readings. Preventing reciprocating engine noise and low frequent vibrations produced by the diesel engines and noise from the gearbox of reaching the water is nearly impossible as resilient mounting of these components is only partially possible. Therefore, hybrid propulsion is preferred with the option of decoupling the gearbox together with the diesel engines from the propeller shaft. In that case the vessel will be propelled by electric drives directly coupled to the shaft. The electric drives should provide sufficient power to propel the vessel together with a towed sonar array at a speed of 15 knots.

Included in ASW-operations, the frigate also has to be able to perform ‘sprint and drift’ maneuvers while protecting a convoy of other ships. During this maneuver the frigate has to sail with high speed and towed sonar array to the front of the assigned sector and then slowly drift back (based on the type of Sonar: 12 – 15 knots) while listening with the sonar system. The future M-frigate has to be able to reach ship speeds of 28 knots with towed sonar array while performing the ‘sprint and drift’ maneuver.

Next to the operational speed requirements, the vessel has to be able to sail long distances on an economical speed to maximize the range with a limited bunker capacity. This speed is called transit speed. Because transits can take place together with ships from other navies, the transit speed should match transit speeds of other naval vessels. The transit speed is defined to be 18 – 19 knots and the range on transit speed is set to be 5000 nm.

The frigate has to fulfill several additional tasks. These tasks include modern tasks as:

- Maritime Security Operations (MSO), prevention of sea-based illegal activities, such as piracy and human trafficking,
- Maritime Interdiction Operations (MIO), disruption and destruction of supply forces
- Humanitarian operations

For these operations, the frigate is often assigned to a specific sector in the operational area. The vessel will patrol in this sector until further action is necessary. This is called loitering and requires ship speeds between 8 and 12 knots.

Summarized, the following speed ranges are important for the vessel:

- Loitering: 6 – 10 knots
- Sonar Operations: 12 – 15 knots
- Transit: 18 – 20 knots
- Maximum Speed: 28 knots

And the speed profile for the vessel is as follows:

- 0 - <10 knots: 30%
- 10 - <20 knots: 65%
- 20 - 28+ knots: 5%

As the future frigate will be comparable to the LCF in regard to size and speed requirements, the comparison of diesel engines and gas turbines will be based on performance data of the LCF. For the LCF the operational profile is given in the operational concept. (Data from the OC is restricted and left out in the public version).

| | | | | | | | | | | | | | | | |
|-------|------|-----|-----|-----|-----|------|-------|-------|-------|-------|-------|-------|-------|-------|-----|
| Speed | [kn] | 1-3 | 3-5 | 5-7 | 7-9 | 9-11 | 11-13 | 13-15 | 15-17 | 17-19 | 19-21 | 21-23 | 23-25 | 25-27 | >27 |
| Time | [%] | xx | xx | xx | xx | xx | xx | xx | xx | xx | xx | xx | xx | xx | xx |

Table 2.1: Operational profile from operational concept

However, due to increasing maintenance costs of the gas turbines, high speed operations of the vessel are restricted. This results in the following, more realistic operational profile for the LCF, based on measurements of the operating hours on gas turbines and diesel engines:

| | | | | | | | | | | | | | | | | |
|-------|------|------|-----|-----|-----|------|-------|-------|-------|-------|-------|-------|-------|-------|-----|--|
| Speed | [kn] | 1-3 | 3-5 | 5-7 | 7-9 | 9-11 | 11-13 | 13-15 | 15-17 | 17-19 | 19-21 | 21-23 | 23-25 | 25-27 | >27 | |
| Time | [%] | < 17 | | | | | < 76 | | | | | < 8 | | | | |

Table 2.2: Operational profile adjusted to measurements of operating hours

To answer the question why so many frigates are equipped with gas turbines, data on the operational profile alone is not enough, but information on the required propulsion power is needed as well.

Resistance and Propulsion Power

Propulsion power has to be delivered by the propeller to overcome the resistance forces of the hull. For most commercial ships sailing at low speeds, it is acceptable to assume that the resistance forces are proportional to the squared ship speed (Klein Woud & Sapersma, 2002).

$$R = c_1 * v_s^2 \quad (2.1)$$

Where

R = ship resistance in N;

v_s = ship speed in m/s

But for naval vessels sailing on higher speeds, resistance forces are often increasing more rapidly. The rapid increase in resistance is caused by the wave resistance of the vessel. The geometry of the ship hull is responsible for the generation of the wave system of a ship, consisting of divergent and transverse waves. One wave system is generated at the curvature of the bow and one wave system is generated at the stern. The wave length of the generated waves is related to the wave speed, known as the Dispersion Relation:

$$\lambda = \frac{2 * \pi * v_w^2}{g}$$

With λ the wave length in m and v_w the wave propagation speed in m/s. The wave speed is equal to the ship speed as the generated wave system is fixed to the ship.

The speed to length ratio of the ship can be expressed dimensionless in the Froude number F_n :

$$F_n = \frac{v_s}{\sqrt{gL}}$$

At a Froude numbers above 0.4 the wave length exceeds the ship length. In that case the first trough of the bow wave will interfere with the trough of the stern, resulting in an aft trim of the vessel and a distinct transverse wave system causing a steep increase in wave resistance. For the LCF, a ship speed of 29.2 knots results in a Froude number of 0.4. This ship speed is not reached with the LCF, but the effect of constructive interference of bow and stern wave system is already with lower ship speeds noticeable.

Based on resistance data for the LCF, the following relation between ship speed and resistance is more representative. The following resistance curve and deviated power curves of the ship are based on an early concept of the LCF and do not represent the current performance of the vessel.

$$R = c_1 * v_s^3 = xx \frac{kg * s}{m^2} * v_s^3 \quad (2.2)$$

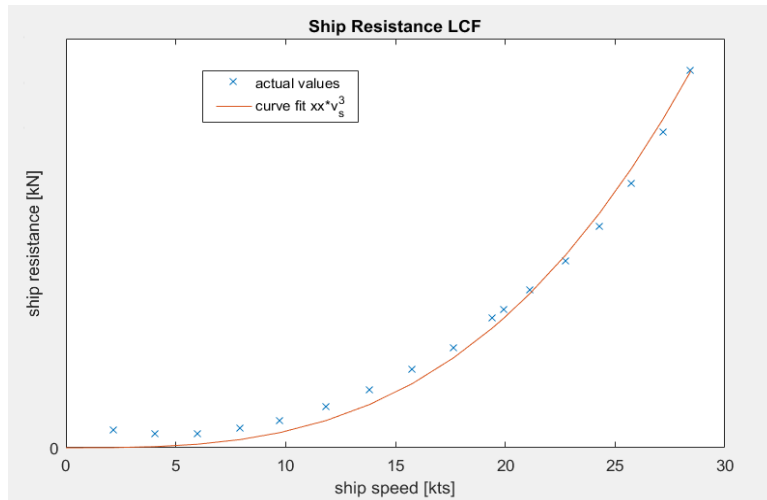


Figure 2.1: LCF Ship Speed vs Resistance

The effective power, required to propel the ship at given ship speed is given by:

$$P_E = R * v_s \quad (2.3)$$

With P_E the effective towing power in W.

But the prime movers of the frigate have to deliver more power to overcome losses in the shafts, transmissions but especially during the conversion of rotational power to thrust force by the propeller. The brake power, requested from the prime movers can then be determined by:

$$P_B = \frac{P_E}{\eta_D * \eta_{TRM}} \quad (2.4)$$

Where

P_B = Brake Power in W

η_D = propulsive efficiency = 0,6 - 0.7 (the exact values are confidential)

η_{TRM} = transmission efficiency = 0,9 – 1.0 (the exact values are confidential)

In reality, the transmission efficiency η_{TRM} and propulsive efficiency η_D are not constant. The propulsive efficiency includes the propeller open water efficiency and strongly depends on pitch, propeller speed and advance speed. Therefore, precise prediction of the propulsive efficiency requires a lot of technical details as well as data on the actual maneuver. However, if a series of steady state conditions is assumed with the propeller at nominal pitch, the propulsive efficiency can be assumed constant in this first comparison.

The transmission efficiency is not only dependent on transferred torque but also on the shaft speed and therefore influenced by the pitch settings of the propeller. Drijver and de Waard [(Drijver, 2013); (de Waard, 2013)] concluded that the efficiency remains fairly constant for a large speed and power range. Efficiency will deviate significantly if the pitch of the propeller is reduced during higher ship speeds in case of bad weather or increased resistance due to fouling or heavy loading. However, these operating conditions will not be included in this first estimation of the propulsion power.



Figure 2.1: LCF Estimated brake power

With the resistance and efficiencies, the brake power for the different speed ranges can be estimated with equations 2.3 and 2.4, resulting in the following table:

| Speed | [kn] | 1-3 | 3-5 | 5-7 | 7-9 | 9-11 | 11-13 | 13-15 | 15-17 | 17-19 | 19-21 | 21-23 | 23-25 | 25-27 | >27 | |
|----------------|------|------|-----|-----|-----|------|-------|-------------|-------|-------|-------|-------|-------|-------|---------|--|
| Time | [%] | < 17 | | | | | < 76 | | | | | < 8 | | | | |
| P _B | [kW] | 53 | 138 | 214 | 369 | 676 | 1229 | 2079 – 3313 | 3313 | 4927 | 7322 | 10205 | 13837 | 18939 | > 26071 | |
| | | – | – | – | – | – | – | – | – | – | – | – | – | – | – | |
| | | 138 | 214 | 369 | 676 | 1229 | 2079 | 4927 | 7322 | 10205 | 13837 | 18939 | 26071 | | | |

Table 2.3: Estimated brake power for operational profile

Whereas transit speed can be reached with slightly less than 10.000 kW of brake power, requested power for higher ship speeds increases steeply. Most frigates, the LCF included, use diesel engines to reach transit speed and add the gas turbines to the propulsion train for higher ship speeds.

Comparing Diesel Engines and Gas Turbines

Power Density

In his study, Frank van Es (van Es, 2011) investigated possible prime movers for a future M-frigate. His findings on the power density for gas turbines and diesel engines will be used in this thesis.

Diesel engines are typically categorized by their speed. Marine engines are divided into three different groups:

- Low speed: engine speeds up to 150 rpm
- Medium speed: 250 – 800 rpm
- High speed: > 1000 rpm

2. Background

Gas Turbines are divided into two groups for this comparison. Smaller gas turbines are usually used in turbo-generators to produce electricity, whereas the larger gas turbines are used as boost turbines to achieve high ship speeds.

The following table lists specific power and weight for the different engines as determined by Frank van Es (van Es, 2011).

| Prime Mover | Power Range | | Specific Volume | | Specific Weight | |
|--------------|-------------|----|-----------------|--------------------|-----------------|--------|
| Low Speed | 4 – 80 | MW | 30 - 35 | m ³ /MW | 20 - 60 | ton/MW |
| Medium Speed | 3 – 24 | MW | 11.4 – 23.1 | m ³ /MW | 6 - 20 | ton/MW |
| High Speed | < 10 | MW | 8.2 – 14.4 | m ³ /MW | 2 - 8 | ton/MW |
| Gas Turbine | 0 - 20 | MW | 6.2 – 3.0 | m ³ /MW | 2.6 – 1.0 | ton/MW |
| Gas Turbine | > 20 | MW | 3.0 – 2.0 | m ³ /MW | 1.0 – 0.6 | ton/MW |

Table 2.4: Power density of different prime movers

This data reveals an interesting trend. With increasing power, specific volume and specific weight tend to increase for the diesel engines. This is the result of the lower engine speed. By reducing the engine speed less energy is lost due to friction and by increasing pressures inside the cylinder the combustion efficiency is also increased. But due to lower piston speeds and increased pressure, forces in all components increase. Therefore, structural requirements increase and as a result engine size and weight increase as well. For gas turbines, the opposite is true. Specific volume and weight tend to decrease with increasing power. This results in a reduced heat loss and improved efficiency.

On frigates space is scarce and additional weight increases the resistance of the ship, implementing high penalties on the maximum speed of the vessel. Hence the prime movers have to be as light and compact as possible. This holds especially for prime movers with high power that are used rarely to achieve high ship speeds. While diesel engines tend to increase in specific weight and volume with increasing power, installing large diesel engines should be avoided, if weight and volume criteria weigh heavily in the design phase. Therefore, gas turbines are often used as they are compact and light and their lower efficiency is accepted as a trade-off. As high ship speeds require a lot of power and therefore a lot of fuel, some efficiency losses of the gas turbines are regained by optimizing the propulsion plant for high speeds (diameter and pitch of the propeller and gearing of the gearbox).

The following example shows dimensions for prime movers delivering sufficient power to propel the LCF to 28 knots. To reach 28 knots, a brake power of about $P_B = 31$ MW has to be delivered [(GE Aviation, 2016); (MTU, 2016); (MAN, 2015)].

| Engine | Amount | Type | Volume | Mass | sfc |
|-----------------|--------|-----------------|---|------------------------------|-----------|
| GE LM2500+ | 1 | Gas Turbine | 59,8 m ³ | 21,9 tons | 226 g/kWh |
| MTU 20V 1163 | 3 | High Speed DE | 89,1 m ³ (3 x 29,7 m ³) | 37,5 tons (3 x 24,5 tons) | 195 g/kWh |
| MAN 14V48/60CR | 2 | Medium Speed DE | 454,2 m ³ (2 x 227,2 m ³) | 426 tons (2 x 213 tons) | 180 g/kWh |
| Wärtsilä X82 L7 | 1 | Low Speed DE | 1013 m ³ | 910 tons | 165 g/kWh |

Table 2.5: Possible prime mover combinations for 28 knots with LCF

Performance

High power density of the gas turbine is not the only reason why many frigates use gas turbines for (a part of) their propulsion. Diesel engines and gas turbines differ also in their drive characteristics. The drive characteristic describes the relation between the engine speed and the maximum deliverable power.

Diesel Engines

The drive characteristics of a naturally aspirating diesel engine can be described as constant torque machine. If the amount of injected fuel is held constant, delivered torque is nearly constant for every engine speed. Delivered power is proportional to engine speed:

$$P_B = M_B * n_e * 2\pi \quad (2.5)$$

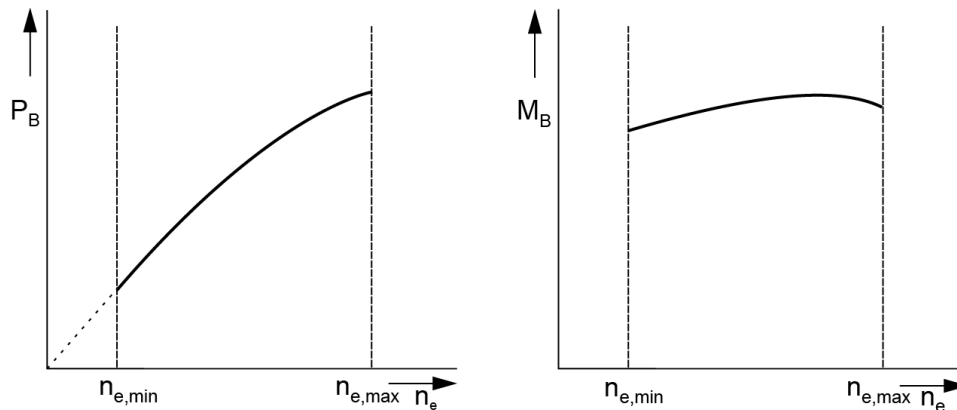


Figure 2.3: Drive Characteristics of a naturally aspirating diesel engine (Klein Woud & Sapersma, 2002)

However, modern marine diesel engines are equipped with forced induction systems. Most common type of forced induction is the one-stage turbocharged system: a turbine, driven by the exhaust gases, drives a compressor, compressing the fresh charge air. By increasing the charge pressure, more air is available during combustion, thus more fuel can be injected and more power can be delivered with constant engine size. In part load conditions, decreasing flow of exhaust gases reduces the work developed by the compressor and as a result charge air pressure drops. To prevent incomplete combustion and thermal overloading, the amount of injected fuel has to be reduced and thus the delivered power reduces. This phenomenon is called the turbocharger limit and results in the engine load limit, see figure 2.4.

Due to the turbocharger limit, the difference between requested power by the propeller and deliverable power of the diesel engine (also called engine margin) can be small. In calm sea states this is favorable as the engine's efficiency is highest if the engine loading is close to the load limit. In heavy sea states the ship resistance increases and the propeller requests more power at the same propeller speed. To prevent the engine from overloading, the engine speed and delivered power have to be reduced and thus the ship speed drops. The same holds if the resistance increased due to towing a sonar array or if the vessels displacement is increased due to heavy loading.

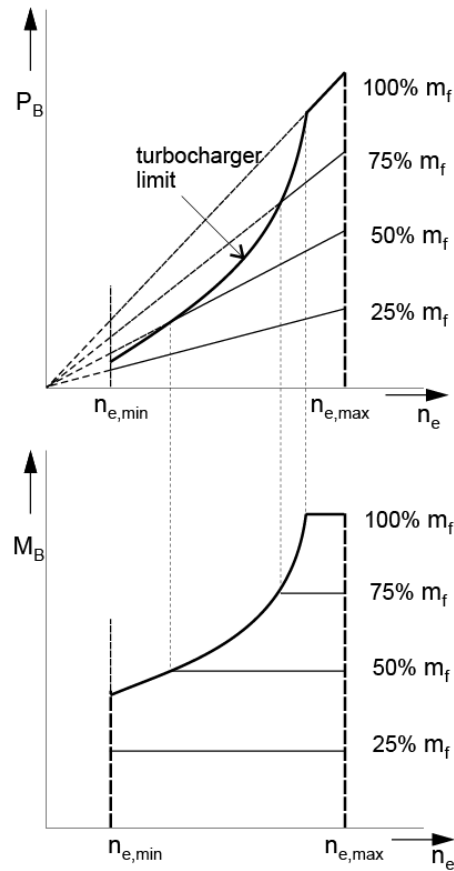


Figure 2.4: Drive characteristics of a one-stage turbocharged engine (Klein Woud & Sapersma, 2002)

An increased engine margin is not only favorable in cases of an increased ship resistance. If the frigate has to accelerate, Newton's 2nd law of motion becomes important for the vessel:

$$m_{ship} * \dot{v}_{ship} = F_{Thrust} - F_{Resistance} \quad (2.6)$$

To achieve high accelerations, more thrust force has to be provided by the propellers than needed to overcome the resistance forces of the hull. To develop more thrust, the propellers request more power from the engine. With the diesel engine loaded close to the load limit the engine is not able to deliver a lot of additional power, resulting in low acceleration values.

For most commercial vessels achieving high accelerations is not important, but for naval vessels it can be crucial to reach their maximum speed as fast as possible. For frigates assigned to ASW, the ability to accelerate fast and change heading abrupt can result in successfully evading incoming torpedoes.

Gas Turbine

Marine gas turbines are often derived from jet engines. On airplanes the jet engines produce thrust for propulsion by accelerating exhaust gases and forcing them through an exhaust nozzle. In marine applications, the exhaust nozzle is removed and a second turbine is added. The accelerated exhaust gas from the original gas turbine (gas generator), drive the second turbine (free power turbine) which is connected to the propeller shaft.

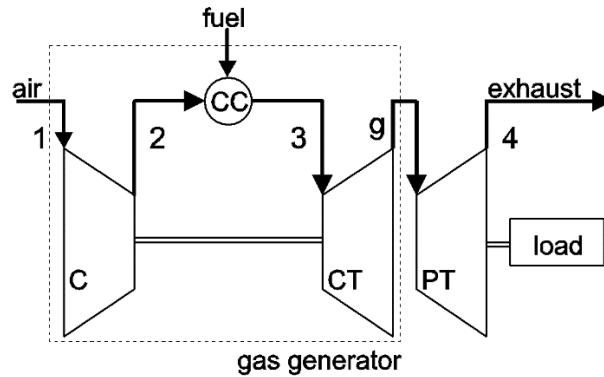


Figure 2.5: Marine gas turbine: Twin-shaft concept (Klein Woud & Sapersma, 2002)

Gas generator and free power turbine are not mechanically connected, but power is transmitted by the hot, accelerated exhaust gases. The gas generator can be operated on maximum power by holding the injected fuel constant while the free power turbine is standing still. Therefore, the gas turbine can be described as a constant power drive. If the gas generator power is held constant, delivered torque of the free power turbine increases with decreasing speed of the turbine.

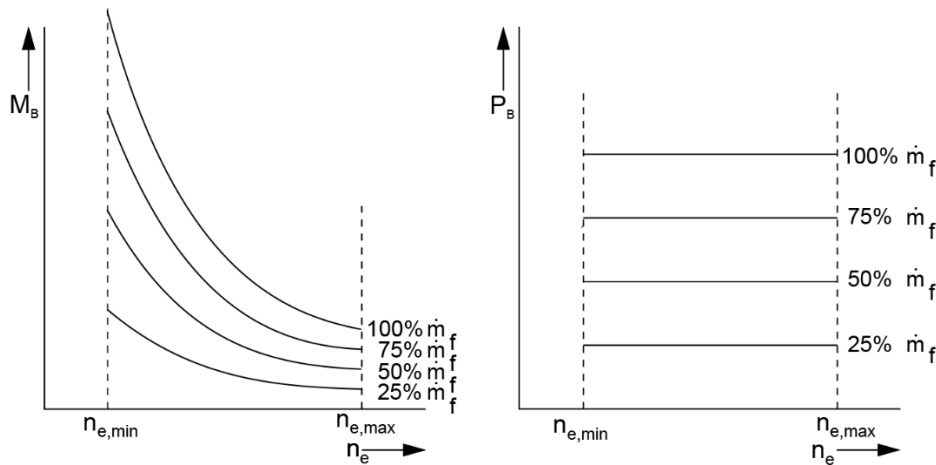


Figure 2.6: Drive characteristics of a gas turbine (Klein Woud & Sapersma, 2002)

In practice, the shaft power generated by the free power turbine decreases with decreasing turbine speed. This is a result from the increasing difference between gas velocity and rotational velocity of the turbine blades and the resulting inflow angles.

When used for ship propulsion, the gas turbine offers plenty additional power. Therefore, the ship speed is unaffected if the ships resistance increases due to heavy sea or other operational conditions. Especially during acceleration of the vessel the difference in additional power compared to the diesel engines has a significant

impact. Figure 2.7 shows the requested power of the propeller for all ship speeds and the engine load limits for the gas turbine and diesel engine of the LCF. From this comparison one would expect a significant difference in acceleration on diesel engines compared to gas turbines.

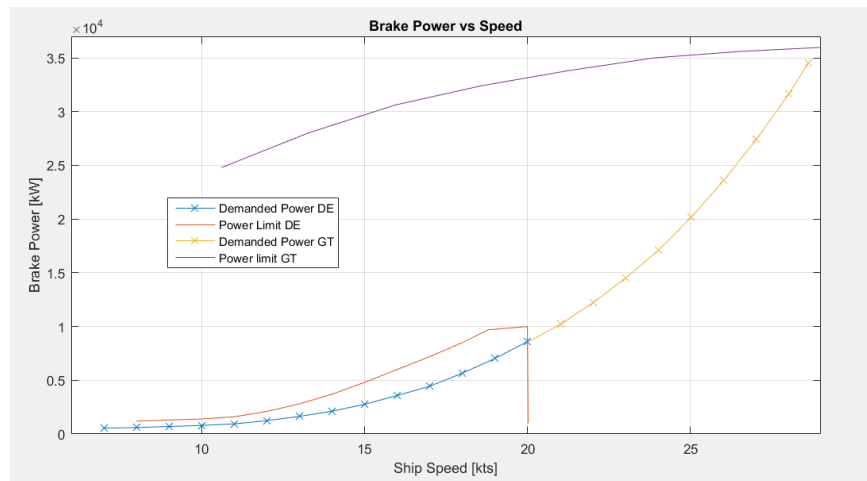


Figure 2.7: Engine Envelop GT & DE LCF

Costs

The costs of the two different prime movers can be split into two different categories:

- Fuel costs
- Repair, maintenance and management costs

Fuel costs are directly related to the requested power of the engine and the operational hours running on the related power level. Repair, maintenance and management costs are partly related to the amount of running hours and respective loading but are also influenced by periodical costs.

Fuel costs

Earlier on, requested power for the different ship speeds was determined and from the operational profile the amount of time spend on the different ship speeds was identified. With data on the efficiency of the two different prime movers the fuel consumption can be determined. The fuel consumption is determined as average consumption per running hour and from the yearly running hours the average fuel consumption per year can be determined.

Diesel Engine

The LCF is equipped with a controllable pitch propeller. Until a ship speed of 10 knots is reached, engine speed is held constant and the speed of the vessel is controlled by the pitch setting of the propeller. With a controllable pitch propeller, the vessel is able to reach very low ship speeds which would not be possible with a fixed pitch propeller due to the engines minimum speed. But due to higher shaft and propeller speeds on low speeds, losses due to friction increase. Values for requested power on low ship speed from table 2.3 are therefore not realistic for the fuel calculations.

To increase the loading of the diesel engines during low ship speeds, the vessel can be propelled by one engine running on one shaft. This propulsion mode produces more underwater noise and accelerating capabilities are worse and therefore won't be used in all cases, but for the further calculations only one engine will be used to reach ship speeds up to 8 knots.

2. Background

Further, for the requested brake power, intermediate values will be used, resulting in the following table for propulsion on diesel engines:

| | | | | | | | | | | | |
|----------------|------|------|------|------|------|------|------|------|------|------|------|
| Speed | [kn] | 2 | 4 | 6 | 8 | 10 | 12 | 14 | 16 | 18 | 20 |
| Time | [%] | < 17 | | | | | < 76 | | | | |
| Engines | [-] | 1 DE | 1 DE | 1 DE | 1 DE | 2 DE |
| P _B | [kW] | 500 | 500 | 500 | 600 | 800 | 1240 | 2120 | 3580 | 5660 | 8600 |

Table 2.6: Operational profile on diesel engines

For the diesel engine of the LCF, the manufacturer provides data on the specific fuel consumption (sfc) of the engine for two different cases: On the generator line and following the propeller law. On the generator line the engine drives a generator and has to run on a constant engine speed to keep the desired frequency of the produced electricity. The propeller law is a special relation between engine speed and requested power, resulting from the resistance forces being proportional to the squared ship speed, eq. (2.1). It can be assumed that shaft speed is proportional to ship speed:

$$n_p = c_3 * v_s \quad (2.7)$$

Combined with eq. (2.1), the following relationship can be derived, known as the propeller law:

$$P_p = \frac{c_2}{c_3 * k_p} * n_p^3 \quad (2.8)$$

The propeller law is not valid for the LCF as the resistance is not proportional with the squared ship speed. However, the requested power does not deviate significantly (figure 2.8) and therefore the specific fuel consumption as stated by the manufacturer can be used. The curve labeled 'LCF' consist of measurement data on the propeller shaft. It includes losses of the gearbox, which are relatively high for low ship speed. This causes a nearly constant brake power for the low ship speeds.

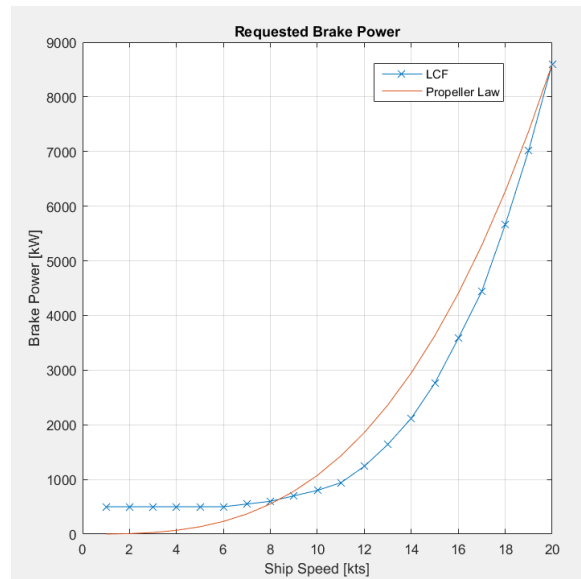


Figure 2.8: Actual Power vs Propeller Law

The manufacturer provides the sfc-values in 4 different load points: 100%, 85%, 75% and 50% of nominal engine power. To estimate the fuel consumption for the whole load-range, a 2nd order polynomial function is fitted through the provided data.

2. Background

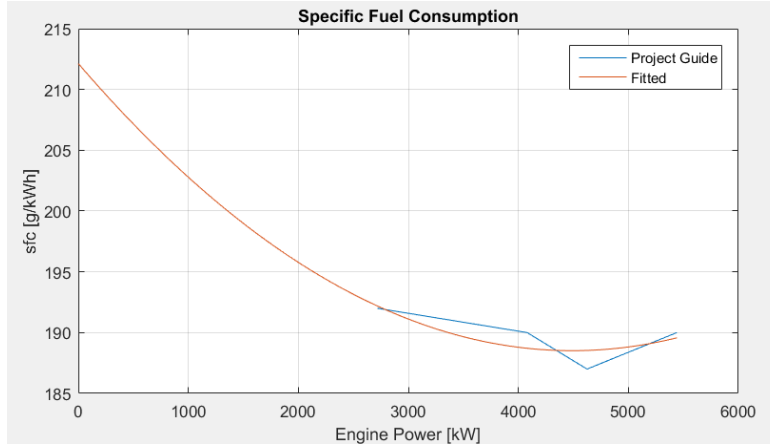


Figure 2.9: Specific Fuel Consumption Wärtsilä 26

With the fitted function of the specific fuel consumption, the sfc-values for the different ship speeds can be calculated as well as the fuel flow per hour:

| Speed | [kn] | 2 | 4 | 6 | 8 | 10 | 12 | 14 | 16 | 18 | 20 | |
|-------------------|---------|-------|-------|-------|-------|-------|-------|-------|-------|--------|--------|--|
| Time | [%] | < 17 | | | | | < 76 | | | | | |
| Engines | [-] | 1 DE | 1 DE | 1 DE | 1 DE | 2 DE | 2 DE | |
| P _B | [kW] | 500 | 500 | 500 | 600 | 800 | 1240 | 2120 | 3580 | 5660 | 8600 | |
| sfc | [g/kWh] | 206,8 | 206,8 | 206,8 | 205,6 | 207,8 | 205,5 | 201,6 | 196,1 | 190,8 | 188,6 | |
| m _{fuel} | [kg/h] | 103,4 | 103,4 | 103,4 | 123,5 | 166,2 | 254,9 | 427,3 | 702 | 1080,2 | 1621,6 | |

Table 2.7: Specific fuel consumption and fuel flow for operational profile on diesel engines

Then the average specific fuel consumption can be calculated by:

$$sfc_{ave} = \frac{\sum(Time * sfc)}{\sum Time} = 197,8 \text{ g/kWh} \quad (2.9)$$

The value for specific fuel consumption can also be expressed as average efficiency:

$$\eta_{ave} = \frac{3600000}{sfc_{ave} * h^L} = 42,62 \% \quad (2.10)$$

For the annual fuel consumption, the annual running hours need to be determined. Data on the running hours until the beginning of 2016 is available for the different vessel. With the time since commissioning the average running hours of the diesel engines is calculated.

The average annual fuel consumption can be calculated by:

$$m_{fuel,ave} = \frac{\sum Time * m_{fuel}}{\sum Time} * 2838,2 \text{ hours/year} = 2055,4 \text{ ton/year} \quad (2.11)$$

2. Background

| | | | | |
|------------------------|---------------|-------------|----------------------------|---|
| Zr Ms Zeven Provinciën | Commissioned: | April 2002 | Active: | 164 months |
| | Starboard: | 16853 hours | Average: 205,9 hours/month | |
| | Port: | 16911 hours | | |
| Zr Ms Tromp | Commissioned: | March 2003 | Active: | 153 months |
| | SB: | 14748 hours | Average: 198,9 hours/month | |
| | PT: | 15680 hours | | |
| Zr Ms De Ruyter | Commissioned: | April 2004 | Active: | 140 months |
| | SB: | 18817 hours | Average: 270,3 hours/month | |
| | PT: | 19022 hours | | |
| Zr Ms Evertsen | Commissioned: | June 2005 | Active: | 126 months |
| | SB: | 17336 hours | Average: 271,1 hours/month | |
| | PT: | 16815 hours | | |
| | | | | Total Average: 236,5 hours/month = 2838,2 hours/year |

Table 2.8: Diesel engine running hours for LCF-class

Gas Turbine

The gas turbines on the LCF are used to cover the speed range from 20 knots to maximum speed (which depends on the sea state and loading condition of the vessel). For high speeds, pitch setting of the controllable pitch propeller is held constant.

For the calculation, the following intermediate values of requested brake power will be used:

| | | | | | | |
|-----------------------|------|-------|-------|-------|-------|-------|
| Speed | [kn] | 22 | 24 | 26 | 28 | max |
| Time | [%] | < 8 | | | | |
| Engines | [-] | 2 GT |
| P _B | [kW] | 10860 | 15340 | 21300 | 28720 | 33600 |
| P _B per GT | [kW] | 5430 | 7670 | 10650 | 14360 | 16800 |

Table 2.9: Operational profile on gas turbines

For the gas turbines, detailed data on the required fuel flow for different speed and power settings of the engine is available. The curve of requested power can be plotted into this fuel map to identify the required fuel flow to the engine.

From the fuel flow the specific fuel consumption can be calculated by:

$$sfc = \dot{m}_{fuel} * \frac{3600}{P_B} \quad (2.12)$$

2. Background

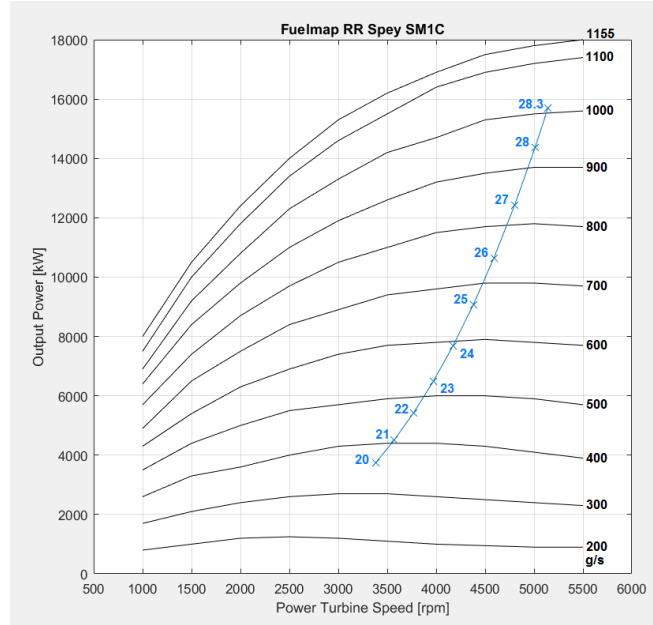


Figure 2.10: Fuel Map RR Spey SM1C

The results for the fuel flow and specific fuel consumption are summarized in the following table:

| Speed | [kn] | 22 | 24 | 26 | 28 | max |
|--------------|---------|-------|-------|-------|-------|-------|
| Time | [%] | < 8 | | | | |
| P_B | [kW] | 10860 | 15340 | 21300 | 28720 | 33600 |
| P_B per GT | [kW] | 5430 | 7670 | 10650 | 14360 | 16800 |
| m_{fuel} | [g/sec] | 470 | 590 | 740 | 935 | 1050 |
| sfc | [g/kWh] | 311,6 | 276,9 | 250,1 | 234,4 | 225 |

Table 2.10: Specific fuel consumption and fuel flow for operational profile on gas turbines

Similar as for the diesel engines, the average specific fuel consumption can be calculated from this data:

$$sfc_{ave} = \frac{\sum Time * sfc}{\sum Time} = 261,36 \text{ g/kWh} \quad (2.13)$$

Which is equivalent to an average engine efficiency of 32,26 %.

To determine the annual fuel consumption, the annual operational hours on gas turbines have to be estimated. For the diesel engines, 2838 operational hours were identified. These hours are equivalent to 91 % of all operational hours. During the remaining 9 % of operational hours, the gas turbines were used. 9 % of all operational hours are equivalent to 315 hours. This is a fairly accurate assumption, by averaging the operational hours reported by Rolls Royce over the last 7 years (see figure 2.13), 300 running hours per year per vessel are recorded.

The average fuel consumption per year follows from:

$$m_{fuel,ave} = \frac{\sum Time * 2 * \dot{m}_{fuel} * 3600}{\sum Time} * 315 \text{ hours/year} = 1436,4 \text{ ton/year} \quad (2.14)$$

Comparing the fuel consumption of the gas turbines and the diesel engines, the gas turbines are responsible for more than 40 % of the total fuel consumption but are used during 9 % of all operational hours. The high fuel consumption of the gas turbines has two reasons:

2. Background

- Requested power from the gas turbines is up to 3 times higher than compared to the diesel engines. Even if the efficiency of the gas turbines were high, to produce a lot of power a lot of fuel is needed.
- The efficiency of the gas turbines is lower. On diesel engines, an average efficiency of 42,6 % is achieved, but the average efficiency of the gas turbines only reaches 32,3 %. Especially during part load the efficiency significantly reduces.

Maximum efficiency on diesel engines, $\eta_{\max} = 44,6 \%$, is reached near nominal power. The efficiency drops about 4 points to 40,6 % at a ship speed of 10 knots.

On gas turbines however, a maximum efficiency of 36,5 % is reached which drops below 25 % with a ship speed of 20 knots, figure 1.12.

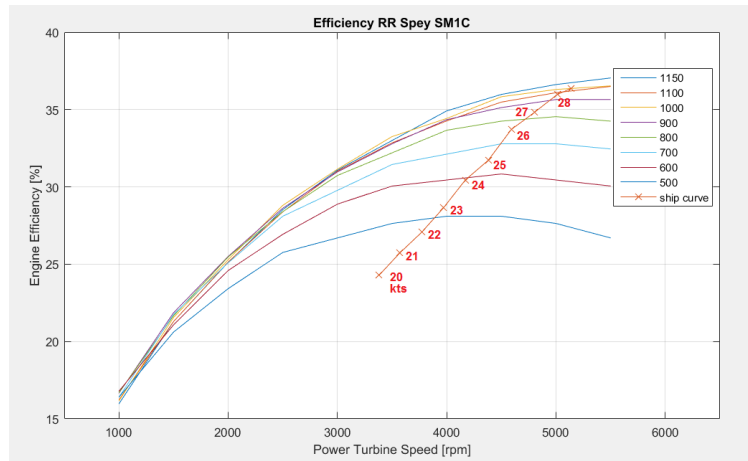


Figure 2.11: Efficiency RR Spey SM1C

Repair, maintenance and management costs

Next to the fuel costs, maintenance and repair on the engines produces additional costs, as well as management of spare parts and replacements.

Diesel engines

Diesel engines need overhaul and repair based on the amount of running hours. The intervals between overhauls and the expected component lifetimes are not fixed, but depend on the operating conditions and loading of the engine. Nevertheless, most engine manufacturers provide overhaul intervals and expected component lifetimes for their engines.

For the diesel engines used on the LCF, the following overhaul intervals are proposed by the manufacturer (Wärtsilä, 2003):

- Small maintenance: 6000-8000 hours
- Large maintenance: 12000-16000 hours
- Turbocharger maintenance: 24000 hours

For the expected component lifetimes, 4 different groups can be identified. Their expected lifetime is proposed by the manufacturer:

- Group 1: 12000 hours
- Group 2: 24000 hours
- Group 3: 36000 hours
- Group 4: 48000 hours

Scheduled maintenance and repairs on the diesel engines on board of the LCF are performed according to the proposed intervals of the manufacturer. Except for small maintenance, all maintenance and repair tasks are performed by DMI (Directie Materiele Instandhouding) in Den Helder. Small maintenance is performed by the crew on board of the vessel.

DMI has also calculated the costs for the scheduled maintenance and repair tasks. The following table shows the costs for the different overhaul and repair intervals as known to DMI.

| Interval | | Costs | |
|----------|-------|-------|---|
| 6.000 | hours | xx | € |
| 12.000 | hours | xx | € |
| 24.000 | hours | xx | € |
| 36.000 | hours | xx | € |
| 48.000 | hours | xx | € |

Table 2.11: DMI maintenance intervals and costs W16V26

Until January 2016, all 4 frigates of the LCF-class underwent the first large maintenance of the diesel engines and the Ruyter already completed the second small maintenance, based on the diesel engine's running hours, table 2.8. Until the end of 2016, all ships are expected to undergo the second small maintenance.

Based on 18.000 running hours, the scheduled maintenance and repair costs per hour are calculated by:

$$\text{Scheduled Maintenance Cost}_{(\text{€}/h)} = \frac{xx \text{ €} + xx \text{ €} + xx \text{ €}}{18.000 \text{ hours}} = 16,5 \text{ €/h} \quad (2.15)$$

In the costs presented by DMI, unscheduled maintenance costs are not included. If the unscheduled maintenance costs are assumed to be 20% of the scheduled maintenance costs, the maintenance costs are:

$$\text{Maintenance Cost}_{(\text{€}/h)} = \text{Scheduled Maintenance Cost}_{(\text{€}/h)} * 1,2 = 19,8 \text{ €/h} \quad (2.16)$$

In his study, Frank van Es (van Es, 2011) determined the following formula for the maintenance costs based on evaluating a large sample group of diesel engines:

$$\text{Maintenance Cost}_{(\text{€}/h)} = (7,70 * P_B^{-0.45}) * P_B = 19,55 \text{ €/h} \quad (2.17)$$

However, Frank van Es used low, medium and high speed engines for his sample group. With decreasing maintenance costs for larger, low speed engines, his formula might be too optimistic to predict the maintenance costs of high speed engines.

In an attempt to give an estimation on the maintenance costs of medium and high speed engines, D. Stapersma (Stapersma, 2001) proposed the following formula:

$$\text{sumc} = 3,65 * \frac{9,5}{c_m} * \frac{\lambda_s}{1.25} * \frac{n}{10} = 5,33 \text{ €/MWh} \quad (2.18)$$

For the diesel engines of the LCF, the following data is given (Wärtsilä, 2015):

- Mean piston speed c_m : 10,67 m/s
- Stroke/Bore ratio λ_s : 1,23
- Nominal Engine Speed n : 16,67 Hz
- Nominal Power P_B : 5,440 MW

$$\text{Maintenance Cost}_{(\text{€}/h)} = \text{sumc} * P_B = 29 \text{ €/h} \quad (2.19)$$

The formula proposed by Stapersma includes costs for unscheduled maintenance, thus the scheduled maintenance costs follow from:

$$\text{Scheduled Maintenance Cost}_{(\text{€}/\text{h})} = \frac{\text{Maintenance Cost}_{(\text{€}/\text{h})}}{1,2} = 24.16 \text{ €}/\text{h} \quad (2.20)$$

With increasing number of running hours, wear within the diesel engine increases and components reach their end of lifetime, thus costs for maintenance increases as can be seen from data provided by DMI. The maintenance costs tend to converge to 24.2 € /h for more than 60000 operational hours. For higher running hours the formula proposed by Stapersma gives a quite accurate estimation on the maintenance costs.

In figure 2.12, the actual costs are obtained by summarizing the costs per interval as specified by DMI and dividing by the amount of running hours.

$$\text{actual costs}_{\text{interval}} = \frac{\sum_0^{\text{interval}} \text{overhaul and repair costs}}{\text{interval}} \quad (2.21)$$

The green line represents a cubic fit function and represents the trend of the overhaul and repair costs.

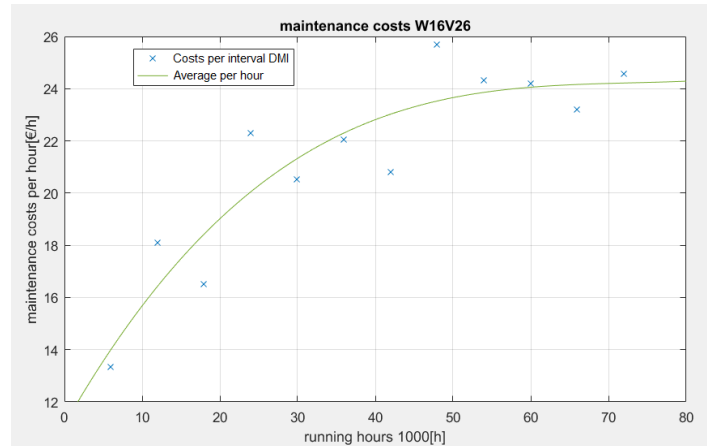


Figure 2.12: Maintenance costs Wärtsilä 16V26

Gas Turbine

In contrast to the diesel engines, the gas turbines are not maintained by the crew of the vessel or DMI, except for small repairs. Large repairs or maintenance on the gas turbines are performed by Rolls Royce. The gas turbines of the LCF are no longer produced and are only used by the Royal Netherlands Navy and the Royal Navy (UK). Because of the small available number of units and therefore scarcity of spare parts, spare parts and replacements are regulated by a memorandum of understanding (MoU) between the United Kingdom and the Netherlands (Bolwell, 2001).

Due to this outsourcing, insight in costs for maintenance, repairs and management is provided as all costs are billed per year by Rolls Royce. The costs are split into repair/overhaul costs for the specific type of gas turbine (RR Spey SM1A or SM1C) and the overall management costs related to the MoU. With the recorded running hours of the gas turbines, the costs per running hour can be specified as well as the average costs per running hour for 2009-2015. At the end of 2015 the cumulative costs per running hour are about 1853 €.

restricted information

Figure 2.13: Maintenance costs RR Spey SM1C

In his study, Frank van Es (van Es, 2011) examined the repair and overhaul costs for the RR Spey SM1A, used in the M-frigate, during a time span of nearly twenty years, from 1991-2010. He concluded costs of 80 € per running hour for repair and overhaul of the RR Spey SM1A. This significant difference is caused by several factors:

- His calculations do not include the (nearly) constant management costs. However, with reduced amount of yearly running hours, management costs per running hour increase (2015: 110 € per running hour)
- Very low repair and overhaul costs in the first 6 years after commissioning of the M-frigate reduce the average costs. After this, maintenance costs increase steeply due to increasing wear and engine failures. For the Spey SM1C, data is available since 2009, 8 years after commissioning of the LCF. Thus, only costs during the phase of increasing wear are considered.
- With the Spey no longer in production and the (originally already small) pool of remaining units decreasing due to engine failures, availability of spare parts and replacements drastically reduces. This drives the costs and is probably the main reason for exploding repair and maintenance costs.

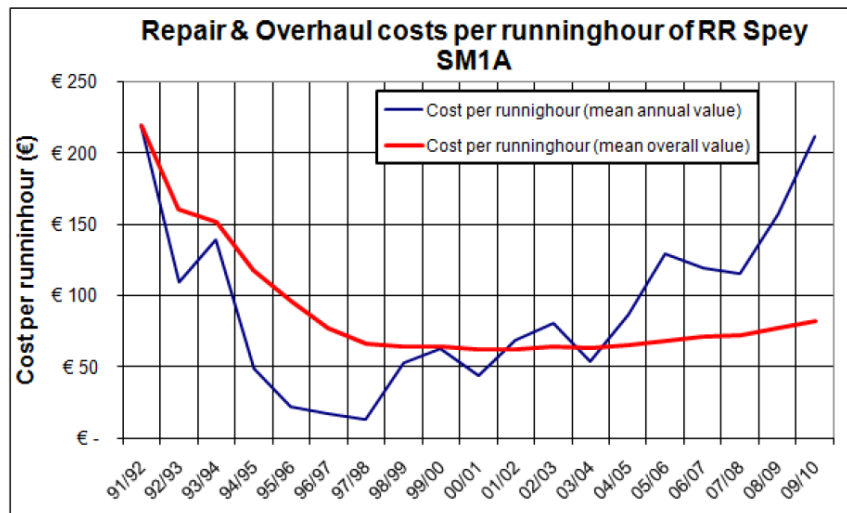


Figure 2.14: Maintenance costs RR Spey SM1A, 1991 - 2010 (van Es, 2011)

Current high repair and maintenance costs are one of the main arguments against the use of gas turbines in the future M-frigate. However, with the RR MT30 discussed as possible boost gas turbine for high ship speeds this could change. Powering the latest frigates and littoral combat ships of the United States Navy as well as the Queen Elizabeth aircraft carriers and possibly future frigates of the Royal Navy, pool size is significantly larger. Especially if the RR Trent 800 aircraft engines are considered as well, sharing 80% of spare parts (Slade, 2015). Repair and overhaul costs for this type of gas turbine should be a lot lower. Quantification of the maintenance costs for late life of these gas turbines is not possible as they were introduced in 2008. However, reliable data could be requested from the US navy as the MT30 is used to power the littoral combat ship since its introduction in 2008 (Nadkarni, 2015).

Propeller Calculations

The propeller of the future M-Frigate has large impact on the performance and capabilities of the vessel. For the frigate two different types of propeller are considered for this study: Fixed Pitch (FPP) and Controllable Pitch Propellers (CPP).

Both types of propeller have their major advantages and severe drawbacks. They will be described shortly in the following paragraph. The cause of the advantages and disadvantages are described in detail during the matching process as well as their impact on the design of the propulsion system and on the performance of the vessel.

FPP vs CPP

Controllable pitch propeller consists of a hub and blades mounted to the hub. Via a hydraulic system the blades can be rotated around their longitudinal axis, thus changing the pitch of the propeller. By changing the pitch of the propeller for a given rotational speed, the load on the engine can be varied. If the ship's resistance decreases due to calm sea, the pitch can be increased to optimize the load on the engine. If the ship's resistance increases due to towing a sonar array or bad weather, the pitch can be decreased to prevent the engines against overloading. By reducing the pitch to almost zero, the vessel is able to achieve very slow ship speeds (which wouldn't be possible otherwise due to required minimal engine speed) and with negative pitch the vessel can also sail backwards without reversing the engine or gearbox.

However, the rotational mechanism increases the hub size, resulting in reduced efficiency of the propeller as well as increased risk of cavitation inception. The hydraulic system also increases complexity of the propulsion system and its space consumption as well as the required maintenance.

Fixed pitch propeller are made from one piece, so the propeller has a fixed pitch setting. As a result, the propeller is cheaper and more robust. The propeller needs nearly no maintenance as it does not contain any moving parts. The one-piece design is favorable for the efficiency of the propeller. As the blades do not have to rotate past each other, blade surface can be increased and thus the blade loading decreased which is favorable for cavitation behavior. However, due to the fixed pitch of the propeller, the engine loading can't be varied for a fixed rotational speed of the engine. If the ship's resistance increases due to heavy weather and the engine is prone to overloading, ship speed needs to be reduced to prevent engine damage.

From ship resistance to required thrust force

The resistance of the hull is determined by its geometry. During the design of the vessel the hull is often modelled by specialized computer software to improve the resistance or other important characteristics (e.g. stability). The software predicts the resistance curve for the vessel, the resistance of the hull on different speeds.

However, in the early phase of the design a detailed model is non-existent. In order to predict the resistance of the vessel, several empirical formulas were developed. The details and the validation of the formulas lie outside the scope of this thesis.

Within DMO the method of Holtrop and Mennen (Holtrop & Mennen, 1982) was slightly altered to fit the results of existing naval vessels of the Royal Netherlands Navy. For the future M-frigate this altered method of Holtrop and Mennen was used to predict the hull resistance for a range of ship speeds and different displacements (Appendix B). With predictions for thrust deduction t and wake factor w , the required thrust force T of the ship and the advance velocity v_a in front of the propeller can be determined:

$$T = \frac{R}{k_p * (1-t)} \quad \text{and} \quad v_a = (1 - w) * v_s \quad (2.22)$$

Considerations for a FPP

The exact geometric layout and the resulting performance characteristics of a naval propeller are classified. However, the performance characteristics of naval propeller optimized for low underwater noise on frigates are comparable to the characteristics of propeller from the Wageningen B-series.

The Wageningen B-Series propellers were a set of 120 model propeller tested at the Netherlands Ship Model Basin (N.S.M.B, now MARIN) in Wageningen in the 60s of the 20th Century. For the screw series the pitch ratio P/D was varied while all other geometric parameters were held constant. Series with different number of blades Z as well as different blade-area ratios A_E/A_0 were tested (Oosterveld & van Oossanen, 1975). With rise of the computer the test results were summarized and generalized by means of multiple regression analysis.

For this thesis the results from Oosterveld and Oossanen (Oosterveld & van Oossanen, 1975) are used. The results are expressed in polynomials in J, P/D, A_E/A_0 and Z for the coefficients K_T and K_Q :

$$K_T, K_Q = \sum C_{s,t,u,v} * (J)^s * (P/D)^t * (A_E/A_0)^u * (Z)^v \quad (2.23)$$

The values for $C_{s,t,u,v}$, s, t, u and v are given in the appendix (appendix A). With the polynomials, open water diagrams for different propellers can be reproduced if the coefficients K_T and K_Q are plotted against the advance ratio J.

The open water diagram for a propeller with Z = 5 and $A_E/A_0 = 0.75$ (simplified called: Wageningen B5-75) is reproduced with the polynomial and given in figure 2.1. Efficiency of the propeller is calculated by:

$$\eta_0 = \frac{1}{2\pi} * \frac{K_T * J}{K_Q} \quad (2.24)$$

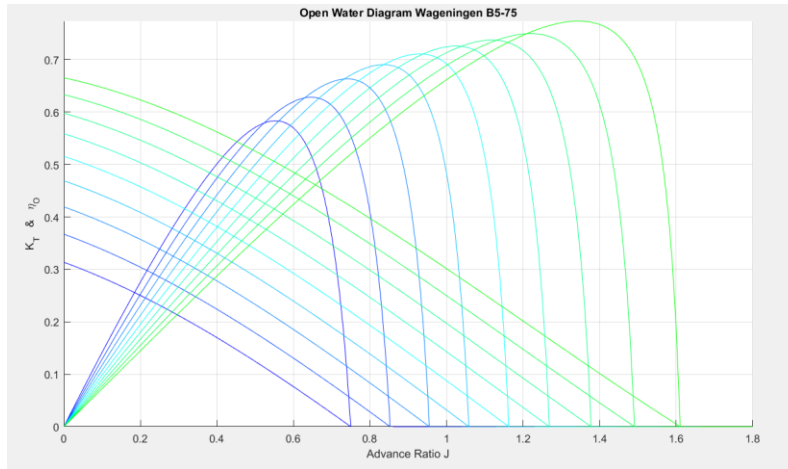


Figure 2.15: Open Water Diagram Wageningen B5-75

The coefficients K_T and K_Q represent the non-dimensional thrust and torque delivered by the propeller:

$$K_T = \frac{T}{\rho * n^2 * D^4} \quad (2.25) \quad \text{and} \quad K_Q = \frac{Q}{\rho * n^2 * D^5} \quad (2.26)$$

And the advance ratio J is given by:

$$J = \frac{v_a}{n_p * D} \quad (2.27)$$

Where:

- T = generated thrust in N
- Q = requested torque in Nm
- n = propeller speed in Hz
- D = propeller diameter in m
- v_a = advance velocity in m/s

For low fuel consumption a propeller with high efficiency is desired. But for different pitch values maximum efficiency will be achieved for different advance ratios. In order to select the most efficient combination of propeller geometry and pitch, the advance ratio for the propeller has to be determined. For the future frigate, a maximum propeller diameter is given. The advance velocity follows from the ship speed for which the highest efficiency is desired. However, the propeller speed remains unknown. Prime movers are limited by a maximum and minimum speed but the gear ratio of the gear box is free to choose, so propeller speed is arbitrary.

By recombining the formulas for non-dimensional thrust and advance ratio, the following relation is found and the propeller speed is eliminated:

$$\frac{K_T}{J^2} = \frac{T}{\rho * v_a^2 * D^2} = c_7 \quad (2.28)$$

By inserting the requested thrust of the ship corresponding to the entered ship speed, the curve for non-dimensional thrust requested by the ship can be set up:

$$K_{T,ship} = c_7 * J^2 \quad (2.29)$$

The curve can be plotted in the open water diagram of the propeller series. Intersections of $K_{T,ship}$ and $K_{T,prop}$ represent working points for which non-dimensional thrust requested by the ship is equal to non-dimensional thrust provided by the propeller. From the intersection the advance ratio can be read and the related propeller speed determined.

The following results were achieved by matching a Wageningen B5-95 propeller with a diameter of 4.8 meter for a ship speed of 18 kn.

| P/D-ratio | J | n _{prop} | η _o |
|-----------|--------|-------------------|----------------|
| [-] | [-] | [rpm] | [%] |
| 0.7 | 0.6484 | 169.6 | 42.44 |
| 0.8 | 0.7324 | 150.1 | 50.66 |
| 0.9 | 0.8131 | 135.2 | 57.41 |
| 1.0 | 0.8910 | 123.4 | 62.74 |
| 1.1 | 0.9666 | 113.8 | 66.69 |
| 1.2 | 1.0402 | 105.7 | 69.43 |
| 1.3 | 1.1124 | 98.9 | 71.15 |
| 1.4 | 1.1836 | 92.9 | 72.22 |
| 1.5 | 1.2544 | 87.7 | 73.12 |

Table 2.12: Wageningen B5-95 comparison of different P/D-ratios

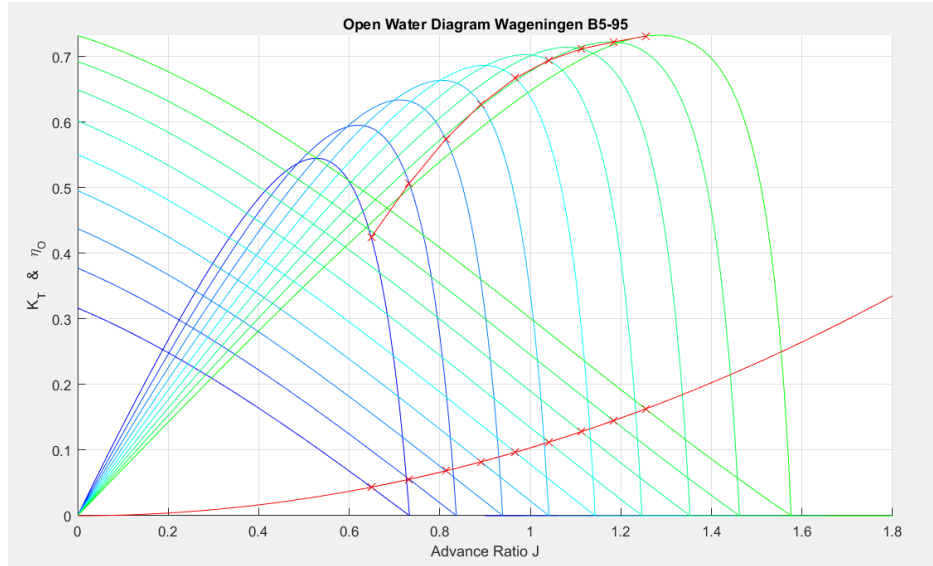


Figure 2.16: Wageningen B5-95 working points

For lightly loaded naval propellers, high efficiency is often achieved by maximizing the pitch ratio.

The future frigate will have to fulfill anti-submarine warfare tasks. During sonar operations as well as in case of a submarine threat, minimizing underwater noise is crucial. For this reason, the propeller will be optimized for cavitation free operation.

Cavitation occurs if the pressure of the water is reduced below the vapor pressure. During cavitation, water changes into its gaseous phase, similar to boiling but without heat addition. Due to the large amount of nuclei in sea water, cavitation nearly immediately starts if the pressure is equal to the vapor pressure. The start of the cavitation process is called cavitation inception. However, not the actual cavitation process causes inconvenience for naval vessels in particular as well as commercial vessels in general, but the reverse process does. If the water vapor hits regions of higher pressure, the gas bubbles become unstable and turn to the liquid phase again. This transition does not occur smoothly but the bubbles implode violently causing noise, vibrations and even damage to the propeller. To prevent cavitation, large pressure dips have to be prevented.

Due to the working principle of a propeller, pressure peaks and dips cannot be prevented. Similar to the wings of an airplane, the airfoil shape of the propeller creates hydrodynamic forces lift and drag. These forces can be rearranged into thrust forces, in shaft direction, and resistance forces, perpendicular to the shaft. For the streamlines around the blade, Bernoulli's principle holds:

$$\frac{1}{2} * \rho * v_0^2 + p_0 = \text{constant} \quad (2.30)$$

Due to the airfoil shape, velocity of the water increases at the back side (or upper side in figure 2.17). According to Bernoulli's principle, pressure decreases at the back side and is therefore called the suction side of the propeller. At the front side, velocity within the stream lines slightly decreases, therefore pressure increases and this side is called pressure side.

2. Background

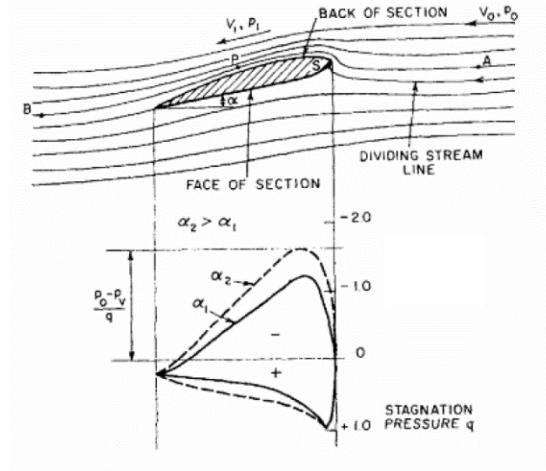


Figure 2.17: Airfoil Pressure Distribution (Lewis E. V., 1988)

If more lift force is created by the same airfoil profile, the thrust force of the propeller increases, but simultaneously the pressure dip at the suction side further decreases until the vapor pressure is reached and cavitation begins. Therefore, propellers with high blade loading (the ratio of generated thrust force to blade area) are prone to cavitation. If the blade area ratio A_E/A_0 is increased while holding the generated thrust constant, the integrated pressure over the suction side will remain constant as well but the pressure dip will improve. However, with increased blade area the friction resistance of the propeller increases and as a result the propeller efficiency decreases slightly. Often this tradeoff is accepted for naval vessels to significantly improve cavitation behavior by decreasing the propeller loading.

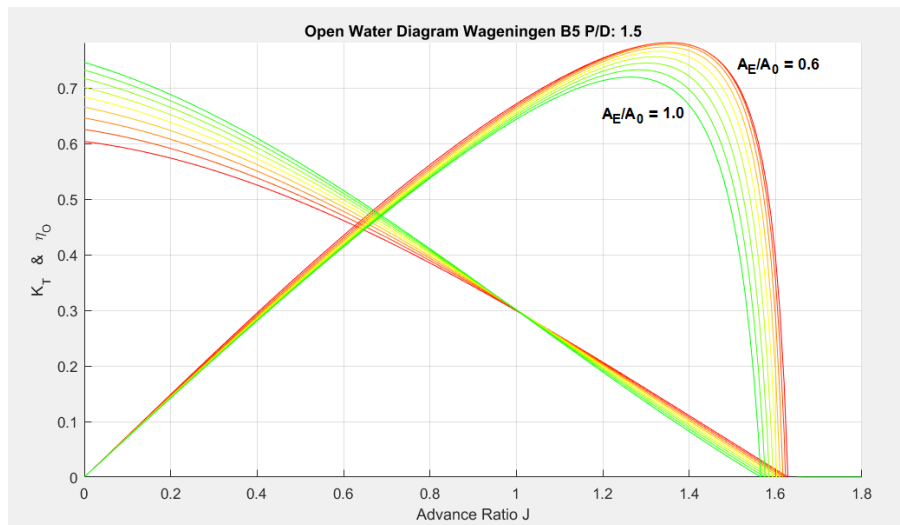


Figure 2.18: Wageningen B-series, A_E/A_0 variation

Next to propeller loading, water velocities over the propeller blade and the angle of attack are also very important for cavitation inception. Cavitation behavior with respect to angle of attack and flow velocities are presented in a diagram called the cavitation bucket, figure 2.19.

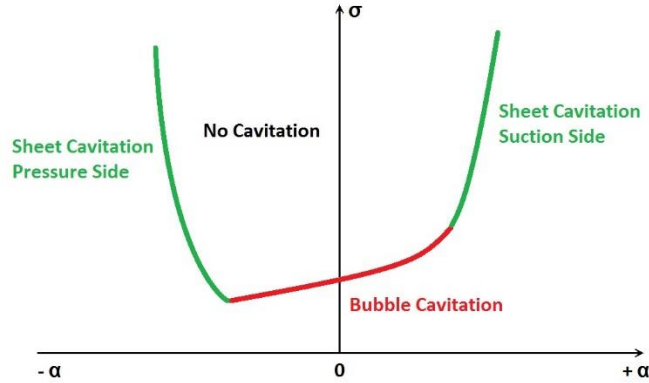


Figure 2.19: Cavitation Bucket

The cavitation number σ can be expressed non-dimensionally, where the water velocities can also be replaced by the rotational velocity of the propeller blades:

$$\sigma = \frac{p_0 - p_v}{\frac{1}{2} * \rho * v^2} = \frac{p_0 - p_v}{\frac{1}{2} * \rho * n_{prop}^2 * D^2} \quad (2.31)$$

If the cavitation number decreases below a certain threshold, i.e. the propeller speed is too high, bubble cavitation occurs. This type of cavitation is typically for high velocities at the midchord regions of the suction side, similar to cavitation due to high blade loading.

The angle of attack is the angle α between the inflowing water and the chordline of the airfoil profile of the propeller. It is defined as the difference between the pitch angle θ of the propeller and the resultant flow angle β of blade speed and advance speed, also called hydrodynamic pitch angle.

$$\alpha = \theta - \beta = \tan^{-1}\left(\frac{P/D}{0.7 * \pi}\right) - \tan^{-1}\left(\frac{v_a}{0.7 * \pi * n_{prop} * D}\right) \quad (2.32)$$

If the angle of attack is increased, velocities at the leading edge of the propeller increase. Due to decreasing pressure, cavitation in form of sheet cavitation can occur. In normal operation sheet cavitation can occur at the suction side if the angle of attack is too high. But if propeller speed is too low or even negative, sheet cavitation can also occur at the pressure side due to a negative angle of attack.

To prevent cavitation as much as possible, the propeller should be chosen in such a way that it falls well within the cavitation bucket. Data on actual cavitation buckets for naval propellers is classified, but rules for proper matching can be identified from the given relations:

- For a high cavitation number, propeller speed should be as low as possible
- For a neutral angle of attack, a high propeller pitch is required. Further, low propeller speeds have also positive influences on the angle of attack, resulting in sufficient margin to suction side cavitation during high ship speeds or acceleration.

Minimizing propeller speed and maximizing the pitch ratio of the propeller also improves the efficiency as stated earlier. For the future M-frigate, research is done on propeller with pitch ratios of 1.7 – 1.8 with blade area ratios of 0.9 -1.0. As optimum propeller speed a range of 130 – 140 rpm is suggested at maximum ship speed of 28 knots.

Unfortunately, the polynomial description of Oosterveld and Oossanen produces reliable results for propellers up to a pitch ratio of 1.6. For further calculations test results of a naval propeller tested by the Maritime Research Institute Netherlands (MARIN) will be used (appendix D). This propeller has a high blade area ratio of 0.92 and a pitch ratio of 1.705 and is optimized for low underwater noise. Therefore, efficiency is slightly reduced as can be seen comparing this propeller to a Wageningen B5-92 with $P/D = 1.6$ (one would expect that higher pitch ratios result in higher efficiencies).

restricted information

Figure 2.20: Wageningen B5-92 vs Navy Design Propeller

Off-design condition FPP

In the previous section the procedure of choosing an optimal propeller was described for a specific ship speed with a specific ship resistance. Due to the operational profile and the resulting different ship speeds and resistances, performance of the propeller in off-design condition is also important. Off-design condition is in case of the frigate somewhat misleading as different ship speeds and resistance requirements are defined well within the operational concept. However, in this chapter the design condition will be defined as matching point of a given prime mover and the propeller.

As stated earlier, with the use of a gearbox between prime mover and propeller, propeller speed in the design condition is arbitrary. However, by determining the gearbox ratio in design condition, the engine speed is prescribed by the propeller speed in all off-design conditions. In most ship designs, the MCR point of the engine is set as design condition. MCR (maximum continuous rating) is defined as the maximum power output that the engine can generate over an extended period of time at maximum engine speed.

Off-Design Speed

In figure 2.21 the design condition is marked by a red 'X'. In the design condition the MTU 8000 delivers 9100 kW at an engine speed of 1150 rpm. The engine is matched to a Wageningen B5-100 propeller with a pitch ratio of 1.5. To calculate the requested propeller torque and propeller speed at a ship speed of 25.6 kn, the working point of the propeller needs to be determined (see previous section). From the working point the advance ratio follows, and from the advance ratio follows propeller speed and requested torque. Requested brake power can be estimated by:

$$P_B = M_{prop} * n_{prop} * 2\pi * \eta_{TRM} \quad (2.33)$$

For a ship speed of 25.6 kn the requested power is equal to the MCR of the MTU diesel engines. The design point is then used to determine the gearbox ratio:

$$i_{GB} = \frac{n_{engine}}{n_{prop}} \quad (2.34)$$

2. Background

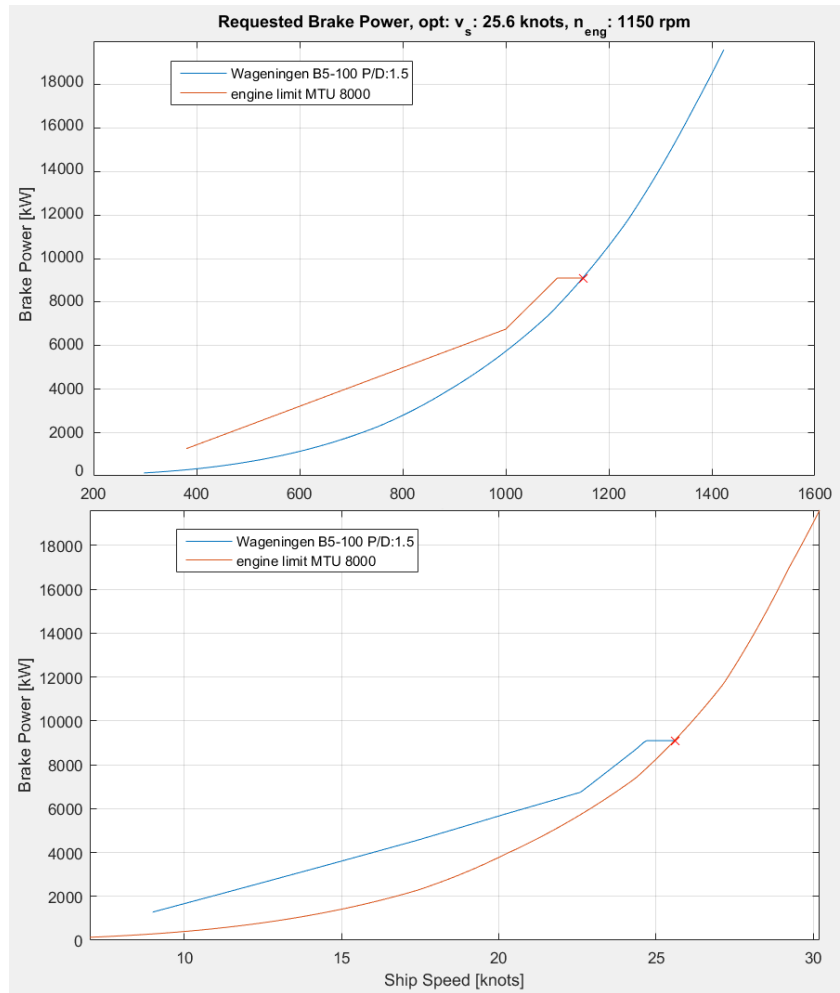


Figure 2.21: Design Point MTU 8000 with Wageningen B5-100

To determine the engine speed and requested power for off-design conditions (in this case for lower ship speeds), the working point of the propeller for every ship speed has to be identified. The working point does change because coefficient c_7 changes for different ship speeds and therefore the curve for non-dimensional thrust requested by the ship.

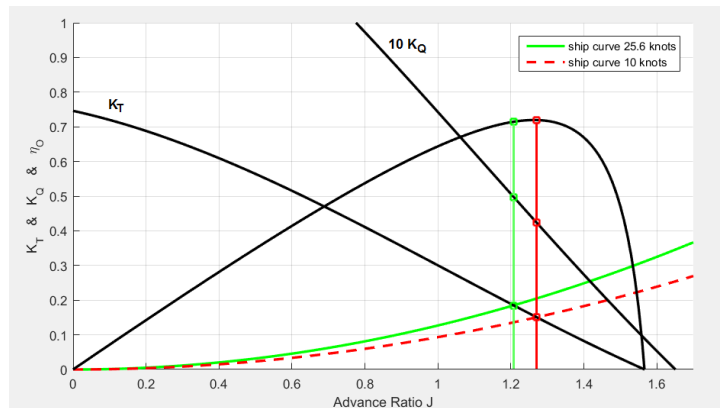


Figure 2.22: Off-Design working point

From the working point, again advance ratio J , propeller speed and requested torque can be determined. With the gearbox ratio fixed from the design point, the engine speed is now defined as well. By automating this procedure with MATLAB, the requested power can easily be determined for each ship speed and the curve of figure 2.7 can be completed. The engine envelope for the MTU 8000 was plotted as well into the figure. This engine can deliver sufficient power in part load conditions to propel the vessel at all ship speed as the power requested by the propeller is lower than the power limit of the engine.

Next to the requested torque and the propeller speed, the open water diagram also produces data on the efficiency of the propeller. The propeller efficiency can be plotted against the ship speeds.

Off-Design Resistance

Similar to the speed in off-design conditions, the working point of the propeller can be calculated if the resistance of the frigate changes. For the off-design calculations, data on the MARIN propeller (appendix D) will be used. The data provided by DMO on the resistance of the future M-Frigate is an estimation of the bare hull resistance. For this data a calm sea, no hull fouling and design displacement is assumed. However, these conditions won't hold for most of the operational time. Higher sea states with waves, increased fouling and heavy loading of the vessel will lead to an increase in resistance. To estimate the increased resistance, the following formula is used, as proposed by Stapersma and Klein Woud (Klein Woud & Sapersma, 2002):

$$SM = y = y_1(\text{fouling}) * y_2(\text{hull form}) * \left(\frac{\Delta}{\Delta_{nom}}\right)^{2/3} * y_3(\text{sea state}) * y_4(\text{water depth}) \quad (2.35)$$

Due to fouling the resistance of the vessel increases. Naval ships can be equipped with fouling release coatings, also known as 'dolphin skin coatings'. If the ships resistance is increased above a certain trigger value, the ship has to sail at speeds exceeding 22 knots for an hour (Brady, 2005). The combination of the special coating and high ship speeds removes the fouling. For frigates the shaft power on a specific speed is measured periodically to determine the increased resistance. Trigger value is an increase in resistance of about 18%. So the average increase due to fouling will be about 9%, $y_1 = 1.09$. According to tests conducted by DMO on fouling release coatings aboard the M-frigate 'Zr. Ms. Van Amstel' new coatings release fouling at significantly lower speeds of 7 – 10 knots. Equipping the future M-frigate with these new fouling release coatings could render obsolete factor y_1 .

In determining the bare hull resistance, a displacement of 5970 tons was used. For a displacement of 6000 tons, coefficient y_2 is set to 1.004.

For the average of the time, sea state 3 of the Douglas Sea Scale (MET Office, 2010) is assumed which is described as slight sea with a significant wave height between 0.5 and 1.25 m. Due to the waves, the resistance of the vessel fluctuates. However, due to the large mass of the vessel the effect of the oscillating resistance is damped. The effect of waves can therefore be represented by an average increase of the resistance. For this sea state the resistance of the vessel is increased about 10%.

So $y_3 = 1.1$.

In shallow water the resistance of the vessel increases as well. For this study, it is assumed that the frigate will sail most of the time in deep water, so $y_4 = 1.0$.

Combining this factors, the service margin (SM) is 1.203, which is a realistic average value for naval vessels. The more realistic resistance of the vessel is then obtained by multiplying the bare hull resistance with the service margin.

Analogous to determining the off-design speed, the working points of the propeller can be determined for every ship speed to achieve requested torque and power, engine speed and the propeller efficiency. The resistance curve with service margin is used as new design condition for the frigate. If the frigate has no fouling (for example after being docked) and is sailing in calm sea, the resistance and thus the loading on the engines is lower. This case is then referred to as light running condition. If the frigate is towing a sonar array, the resistance of the vessel is increased by the drag force of the LFAS (appendix C):

$$R_{tot} = R_{bare\ hull} * SM + R_{LFAS} \quad (2.36)$$

Where the service margin for the design case is equal to $SM = 1$.

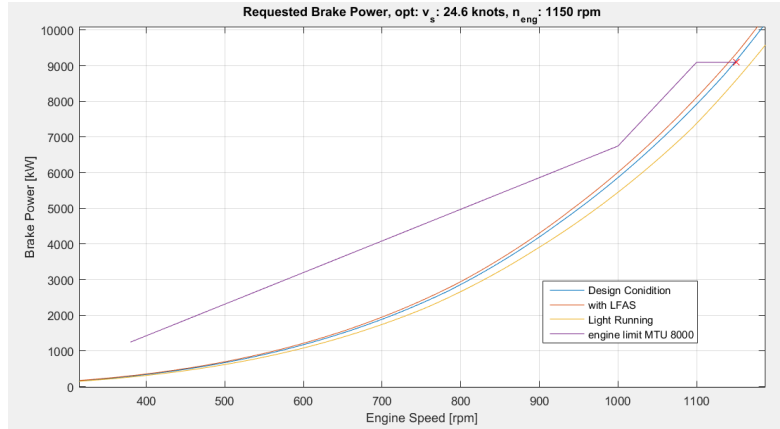


Figure 2.23: Influence of different resistance curves FPP

With the resistance lower than in design condition, the ship will be able to achieve the same ship speeds with less power. But it will not be able to sail faster due to the engines maximum speed. Some manufacturers allow several percent of overspeed for limited amount of time, then the vessel can reach higher speeds in case of light running condition.

If the ship speed resistance however increases, the frigate will probably not reach the design speed. In case of bad weather, increasing wave height increases the resistance of the vessel and thus the propeller curve is shifting upwards. In sea state 8, factor γ_3 increases to 1.76 (was 1.1 in sea state 3, thus the resistance increases by 60%). Requested power increases beyond the engines load limit. Modern engine control prevents overloading of the engines and as a result the ship speed decreases until requested power and delivered power are balanced again (in this case the ship speed reduces to 18.1 kn). But not only increased resistance of the frigate can limit the achievable ship speeds. If a power take-off (PTO) is used to drive an electric generator to supply the vessel with electric power, the engine loading is increased as well and can limit the ship speed (in this case the ship speed reduces to 21.4 kn if the generator requests 1 MW of mechanical power).

2. Background

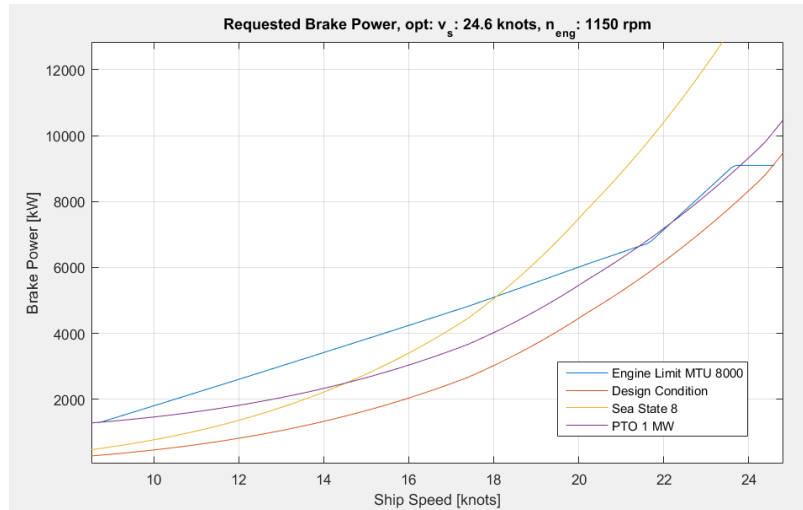


Figure 2.24: Engine overloading

For a fixed pitch propeller, the only way of improving the engine loading in case of bad weather or electric power generation is by anticipating these cases in the design phase. By decreasing the gear ratio, the propeller curves shift downwards but as a consequence, the achievable ship speed in smooth sea decreases because of the engines speed limit. For the example case, the gear ratio is decreased by 0.2% (from 10.44 to 10.42) and maximum power can be delivered in sea state 3 and a PTO requiring 1 MW of mechanical power. In sea state 8 the achievable ship speed increases to 18.5 kn, but the design speed is reduced to 23.8 kn.

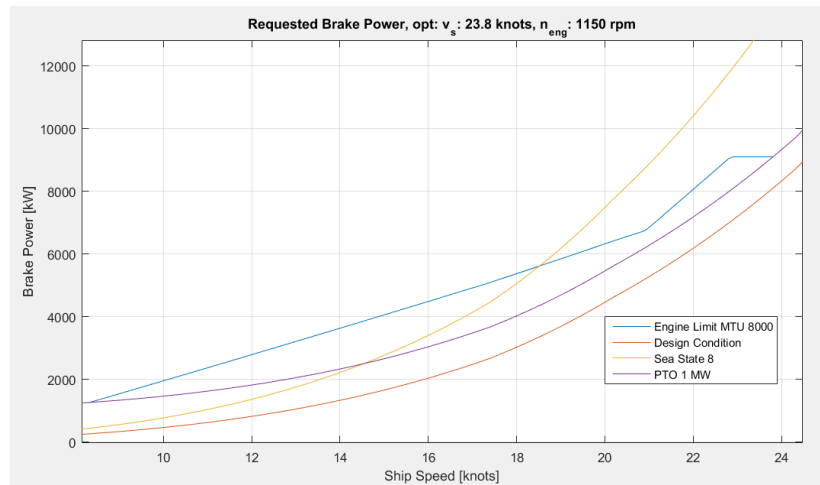


Figure 2.25: Influence of changing the gear ratio

The gear ratio therefore is a very important parameter to adjust in the design of the propulsion plant and has to be selected to fit the specific plant setup and operational requirements. Also the engine load limit of different engines has a large impact on the capabilities in heavy weather and therefore on the selection of a suitable gear ratio. Engines without sequential turbocharging (STC) can produce less power in part load conditions (figure 2.26). As a result, the engines load limit will be reached by lower ship speeds compared to engines with STC. Therefore, engines without STC require lower gear ratios when driving fixed pitch propellers to provide sufficient margin in case of increasing ship resistance.

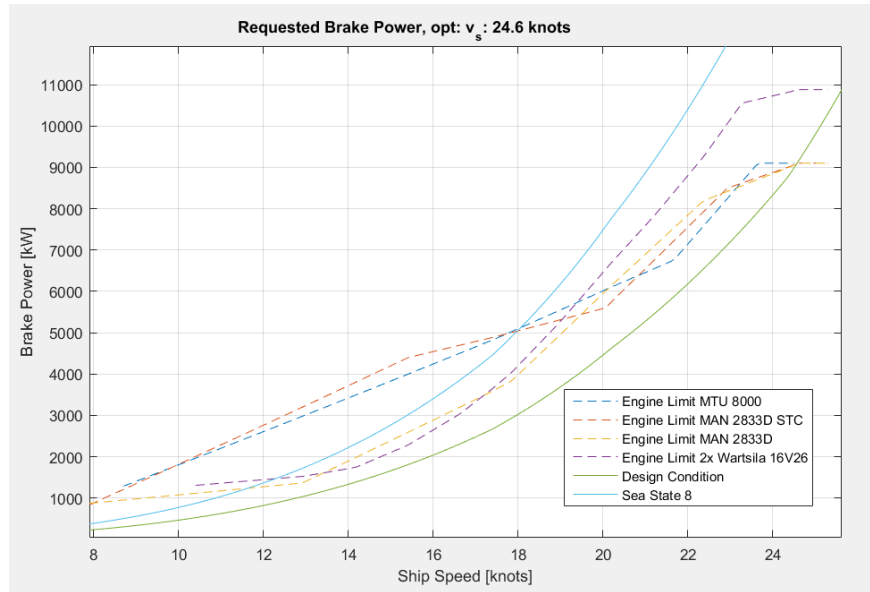


Figure 2.26: Different Engine Envelops

Considerations for a CPP

Important in determining the CPP are efficiency of the propeller and the cavitation behavior. In general, the considerations for a FPP also hold for choosing a CPP.

Similar to a fixed pitch propeller, efficiency is increasing for increasing pitch ratio and decreasing blade area ratio. But due to the larger hub diameter of the CPP, necessary to carry the mechanism for turning the blades, the efficiency is lower than compared to a FPP with comparable geometric ratios. Figure 2.27 shows the efficiency of a Wageningen B5-75 compared to a Wageningen C5-75. The Wageningen C5-75 is a controllable pitch propeller with 5 blades comparable to naval CPPs with respect to cavitation behavior (Dang, van den Boom, & Ligtelijn, 2013). The efficiency of the C-Series propellers is similar to the efficiency of the B-Series propellers with 0.2 lower pitch ratio.

(The original comparison of B5 vs C5 was deleted due to restricted information. The following figure contains the comparison of the Wageningen B4-40 vs C4-40 with similar results)

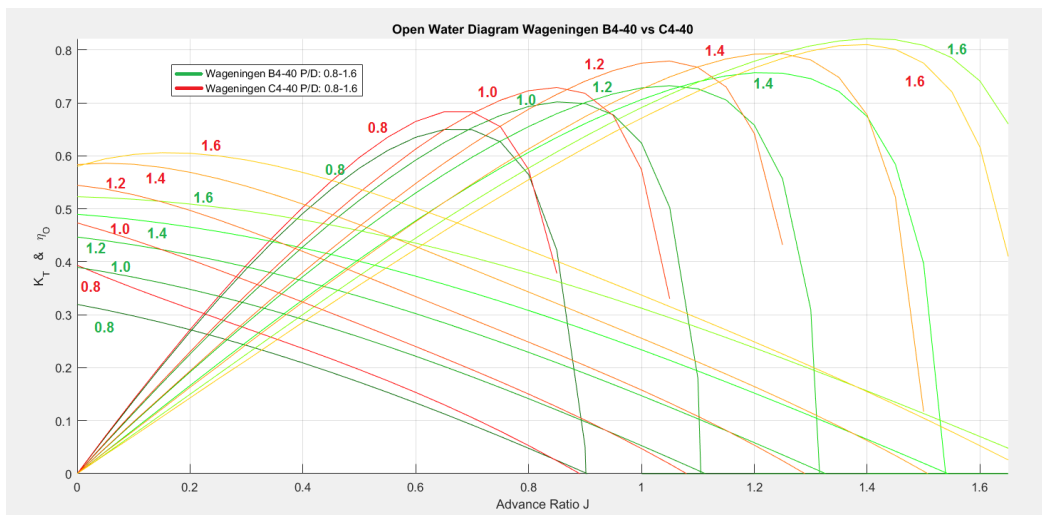


Figure 2.27: Wageningen B4-40 vs C4-40

To improve the cavitation free operation, the blade loading has to be as low as possible. Thus increasing the blade area ratio seems appropriate. However, while changing the pitch of the propeller, the blades need to pass each other. This limits the blade area ratio to 0.75.

With the blade area ratio limited to 0.75 reducing the propeller speed as much as possible is of increased importance for cavitation behavior. With a maximum propeller diameter of 4.8 m for the future m-frigate, the pitch ratio has to be increased if the propeller speed is reduced to deliver constant thrust. Therefore, the pitch of the propeller has to be as large as possible. As beneficial side effect this increases the efficiency of the propeller as well.

Data on systematic propeller tests of CPPs is sparse because extensive testing of these propellers is very expensive due to the different pitch angles and thus expensive. The Wageningen C- and D-Series propellers are the first systematic testing of controllable pitch propellers (Dang, van den Boom, & Ligtelijn, 2013). Tested were 4- and 5- bladed propellers in open and ducted configurations (C- respectively D-Series). From the C-Series propeller design of the 5-bladed propellers aims at application on naval vessels. For this thesis data on the 5-bladed propeller with highest blade area ratio is used. the C5-75 propeller offers a pitch ratio range from -1.4 to + 1.8.

For low propeller speed and high efficiency, the pitch should be kept high if the ship speed is decreasing. If the pitch is held constant, the propeller is equal to a fixed pitch propeller and calculations on the working points of the propeller are similar to the calculations of the previous sections.

With same assumptions and calculations of the previous section on design resistance, light running condition and towing a sonar array, the working point of the propeller at maximum pitch ratio 1.8 for a ship speed of 24.7 kn can be determined. The propeller is again matched with a MTU 8000 diesel engine. With the gear ratio following from the design condition, off-design working points of the propeller can be calculated and the resulting propeller speed related to the engine speed. By comparing the resulting requested power curve (figure 2.27) to results with a fixed pitch propeller (figure 2.23) the propeller performance is nearly identical.

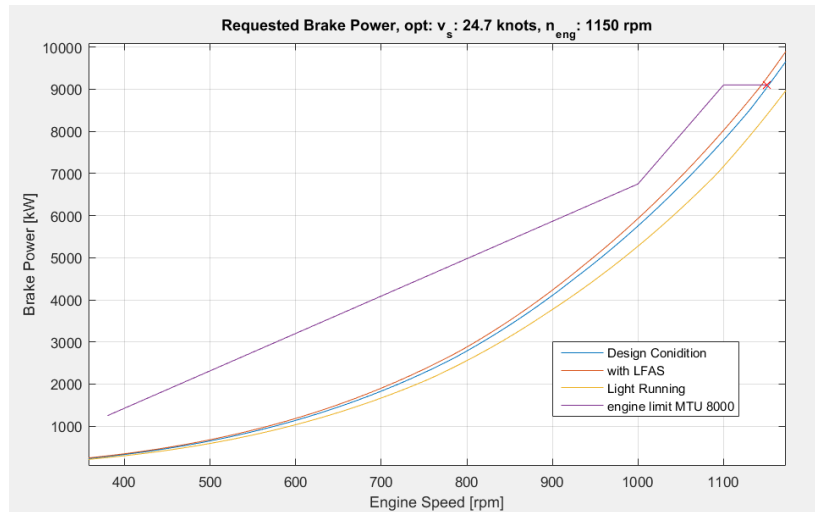


Figure 2.27: Influence of different resistance curves CPP

As a result of the comparable performance the requested power will also for the CPP exceed the engine load limit at heavy sea. But with a controllable pitch propeller, the pitch angle of the blades can be reduced. With lowered pitch the requested power will reduce if the propeller speed is held constant. By decreasing the pitch ratio enough, engine overloading can be prevented while maximizing speed and thus ship speed. If the pitch is reduced too much however, the engine will be limited by its maximum engine speed (see figure 2.28).

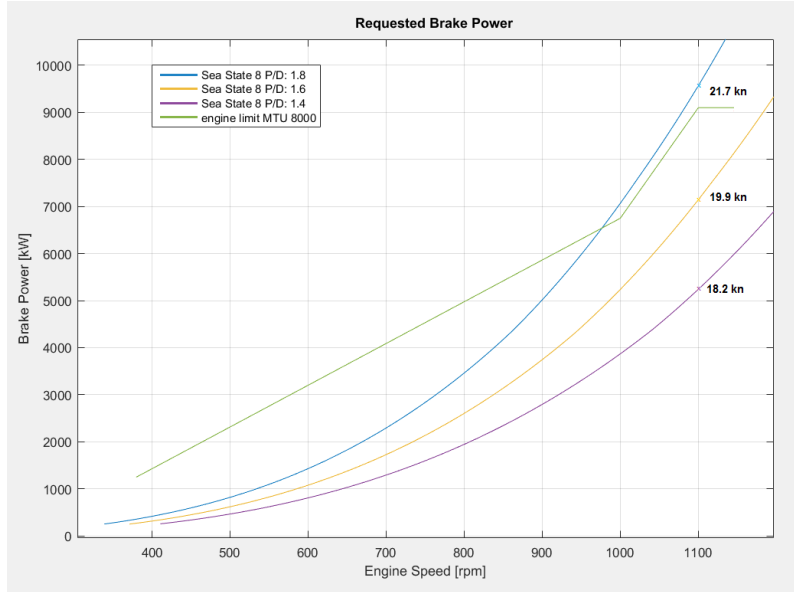


Figure 2.28: Influence of changing propeller pitch

Impact of waves

Next to the average added resistance by heavy sea, expressed as an increase in the service margin, waves also disturb the propeller wake field. Due to these disturbances the advance velocity does not remain constant. By simplifying the irregular wave spectrum to a single wave amplitude and frequency, Geerstma *et al* (Geerstma, Negenborn, Visser, & Hopman, 2016) proposed the following formula for the wake field disturbances in head waves:

$$v_w(t) = \zeta \omega e^{kz} \sin((-kv_{max} - \omega)t) \quad (2.37)$$

Where

ζ = wave amplitude in m

ω = wave frequency in rad/s

k = wave number

z = water depth in m at propeller center

v_{max} = ship speed in m/s

The resulting actual advance velocity can then be obtained by correcting the average advance velocity by the wake field disturbances:

$$v_a(t) = v_{a,ave} + v_w(t) = v_s(1 - w) + v_w(t) \quad (2.38)$$

With $v_{a,ave}$ the average advance velocity, which can be obtained from the ship speed v_s and the wake factor w .

For simplifications we assume a constant engine speed. With a fixed gear ratio and, in case of a CPP, also a fixed pitch setting the propeller speed will remain constant as well. As a result of the oscillating advance speed the advance ratio is also oscillating in phase.

$$J = \frac{v_a}{n_p * D} \quad ref.(2.27)$$

From the relations of the open water diagram, K_T and K_Q will oscillate as well and so will the generated thrust force and requested torque of the propeller. However, with increasing J , K_T and K_Q decrease and vice versa. The resulting thrust force and torque will therefore oscillate in antiphase with the advance velocity.

Figure 2.30 shows the oscillating advance ratio and torque coefficient of two different propellers in waves of sea state 3 and a ship speed of 20 knots. Figure 2.29 shows the steady state working points of the two different propellers in the open water diagram (indicated by an 'X') and the fluctuating working points caused by the oscillating advance velocity (indicated by the solid line).

The two Wageningen C5-75 propellers have different blade diameters (4.8m and 3.35m) and different pitch ratios (1.8 and 1.0). The figures clearly show the antiphase oscillation of K_Q , and the higher absolute values of J and K_Q of the larger propeller. However, due to the larger diameter of propeller 1, the oscillating advance ratio J of this propeller has also a slightly higher amplitude. This will also result in a significantly larger amplitude of the requested torque due to the involvement of D^5 (ref eq. 2.26) and generated thrust due to D^4 (ref eq. 2.25).

(The original figures included restricted data on the Wageningen C5-75 propeller and were deleted. The following figures are based on the Wageningen C4-40 with similar results)

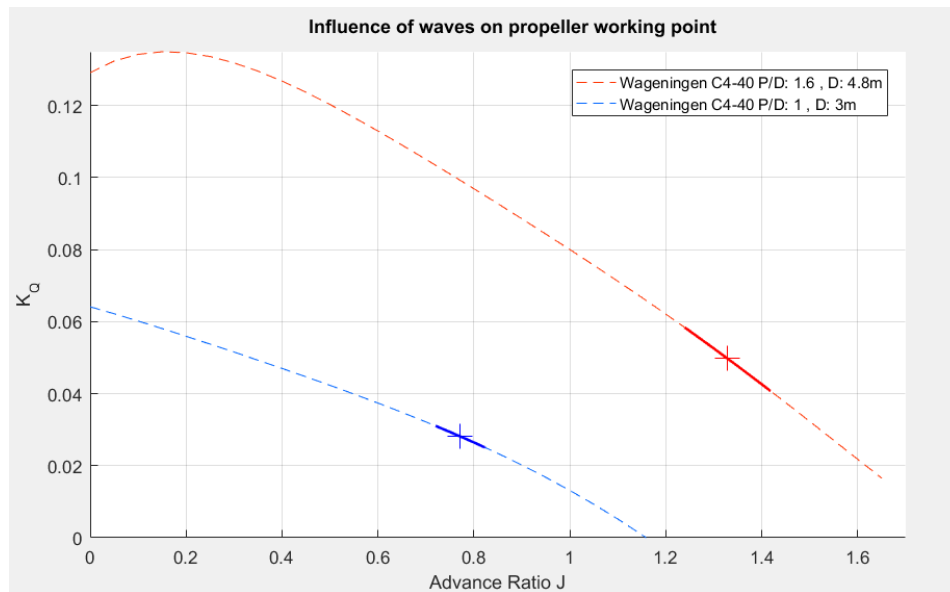


Figure 2.29: Influence of waves on propeller working point in open water diagram

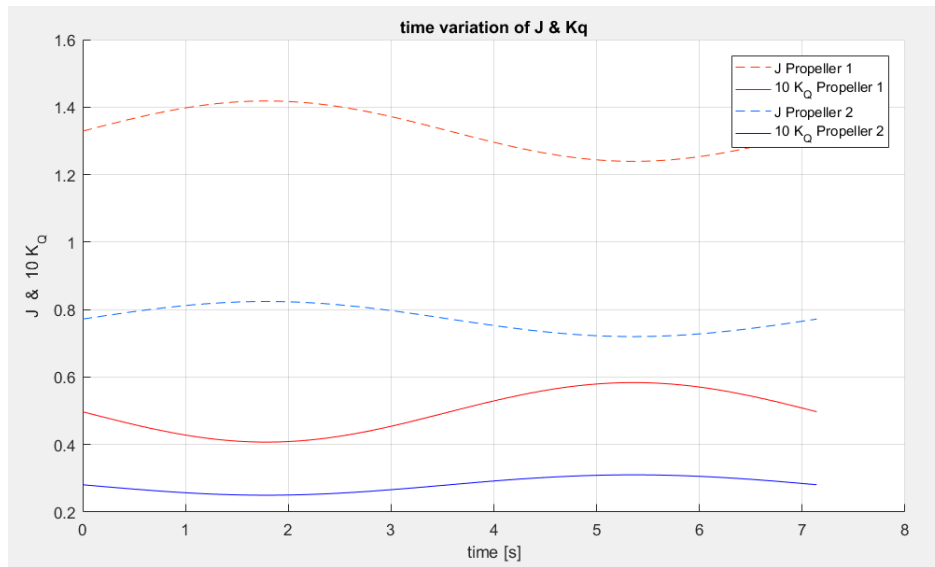


Figure 2.30: Time variation of J and K_Q

Figure 2.31 shows the difference in requested torque by the two propellers. For the smaller propeller the amplitude of the oscillating torque is about 26% of the maximum torque, whereas for the larger propeller the amplitude is about 32%.

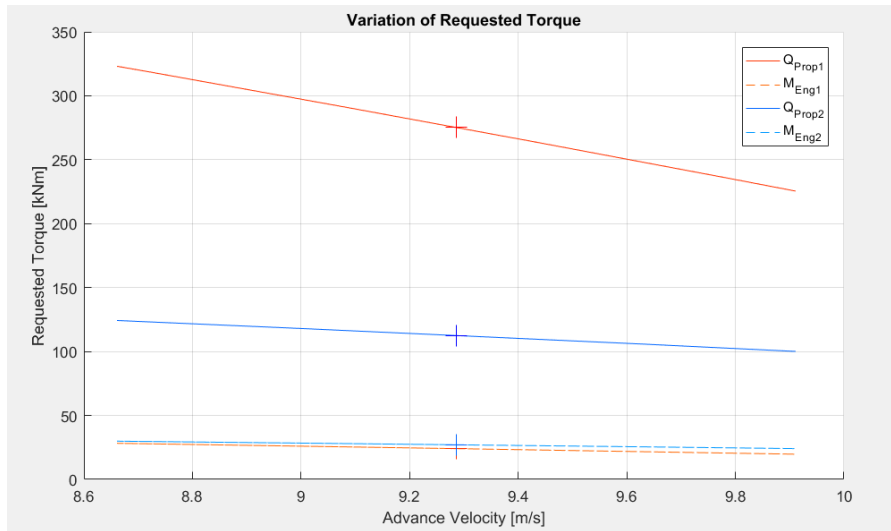


Figure 2.31: Variation of requested torque and advance velocity

One could argue that the difference in amplitude is compensated by the difference in gearbox ratio. In order to develop the same amount of thrust force the smaller propeller has to operate on higher propeller speeds and thus requires a smaller gearbox ratio. The requested brake torque (to be provided by the engines) for the two propellers is also plotted in figure 2.31. The small difference in requested torque is caused by the slightly lower efficiency of the smaller propeller.

However, this conclusion only holds in case of the simplification with constant propeller speed. In an actual propulsion plant the propeller speed will not remain constant. As stated earlier, the requested torque oscillates in antiphase with the advance speed. If v_a decreases, the requested torque increases and, following Newton's 2nd law of motion, the shaft speed will drop:

$$J_{shaft} * \dot{\omega}_{shaft} = M_{eng} - Q_{prop} \quad (2.39)$$

Where:

J_{shaft} = Moment of inertia of the shaft system in kgm²

ω_{shaft} = Rotational speed of the shaft in rad/s

M_{eng} = Provided torque by the engine

Q_{prop} = Requested torque by the propeller

Next to the increasing torque, also the thrust force generated by the propeller is increasing. Therefore, the vessel is accelerated (ref eq. 2.6). The increased ship speed results in a slightly altered propeller working point, requiring even more torque from the engine (see figure 2.22). With speed controlled diesel engines, the governor increases the fuel flow to the engine in order to restore the engine's speed setpoint. The combination of decreasing engine speed and increasing torque can result in an overloading of the engine. Especially if the service margin is chosen too small during the design phase and the diesel engine is already operating close to the maximum engine loading in calm seas. Therefore, the service margin should be sufficient by selecting a higher gearbox ratio. In case of a CPP, this margin can be smaller as the load on the engine can be reduced by reducing the pitch of the propeller.

Determining the exact magnitude of the oscillating torque is very difficult and requires solving the coupled differential equations with the mathematical relations of the involved components and should be analyzed with a dynamic simulation model. However, the fluctuations in engine loading and ship speed will be more severe in case of a large propeller. Installing a large propeller on the future M-frigate could worsen the problem of overloading during increased sea states if the dynamic effects are not fully considered in the design phase.

3. Propulsion Plant Concepts

Requirements

Some requirements of the future frigate were already mentioned earlier in this thesis. More requirements are found on the internet in first publications on possible abilities of the new frigate. And even more requirements were already mentioned by van Es (van Es, 2011), who investigated several possible propulsion plant concepts qualitatively.

However, the replacement of the frigate is still no official project. Once official, large military projects have to pass the four phases of the acquisition process (Defensie Materieel Proces, DMP), (Defensie, 2007):

- A. DMP-A: Defining the need for new military technology
- B. DMP-B: Translating the needs into functional and technical requirements
Evaluation of alternatives
Setting up the budget and timescale
- C. DMP-C: Specification of the requirements
- D. DMP-D: Selection of the product and supplier

At this moment, studies are carried to explore the technical possibilities in order to prepare phase A, DMP-A. As the definitive requirements are defined in phase B, all drafted requirements can change in the (near) future.

The requirements used to set up the propulsion plant concepts in this thesis are based on the requirements currently used for propulsion studies within DMO.

- Maximum speed: 28 knots, with towed sonar in SS3
- Silent speed: 15 knots
- Cruising speed: 18-19 knots
- Displacement: 5000-6000 tons
- Range at cruising speed: 5000 nm
- Auxiliary power: 2000 kW
- Fuel reduction: 20% compared to M-frigate

For this research, two different ship sizes will be considered. Based on the provided resistance curves (see section Background: Propeller Calculations) for displacements of 5200 and 5970 tons, the requested brake power P_B can be calculated. Recombination of equations (2.4), (2.5) and (2.36) gives:

$$P_B = \frac{P_E}{\eta_D * \eta_{TRM}} = \frac{R_{tot} * v_s}{\eta_D * \eta_{TRM}} = \frac{(R * SM + R_{LFAS}) * v_s}{\eta_D * \eta_{TRM}} \quad (3.1)$$

Where

P_E = effective towing power in W

η_D = propulsive efficiency

η_{TRM} = transmission efficiency = 0.96

R = bare hull resistance of the vessel in N

SM = service margin = 1.2

R_{LFAS} = resistance of the towed sonar array if applicable

v_s = ship speed of the vessel in m/s

For the detailed calculations on determining the different efficiencies and the service margin, the reader is referred to the section: Background. The efficiency for the chosen propellers was nearly identical. Therefore, the requested power is equal for propulsion concepts with FPP and CPP. The service margin is based on sea state 3 and some fouling, but the dynamic effect of the waves on the advance velocity is not included. For the two different resistance curves, the following brake powers are determined:

| Ship speed | Requested brake power | |
|------------|-----------------------|---------------------|
| | $\Delta = 5200$ ton | $\Delta = 5970$ ton |
| 28 knots | 29400 kW | 32100 kW |
| 19 knots | 7000 kW | 7800 kW |
| 18 knots | 5900 kW | 6400 kW |
| 15 knots | 3000 kW | 3400 kW |

Table 3.1: Brake power for future M-frigate in design condition (sea state 3, SM = 1.203, with LFAS)

For transit and higher speeds, there are no restrictions in the type of prime movers to use or their amount and configuration, but the silent speed has to be achieved with electric drives. Next to large diesel engines, the gearbox is one of the major producers of underwater noise (Hendriks, 2010). Therefore, the future frigate has to be propelled by electric drives during ASW-operations (Lamerton, Moss, Maltby, & Uhbi, 2008). When the electric drives are used, the gearbox and connected prime movers are decoupled, significantly reducing the underwater noise emission. To decouple the gearbox, the electric drives need to be mounted to the propeller shaft, either directly or by its own reduction gearing.

Next to the quantitative requirements, also some more qualitative requirements are important in setting up the propulsion plants. Although the following requirements are quantifiable, it is difficult to establish limitations.

- Limit maintenance on the prime movers
- Limit complexity of the propulsion plant
- Minimize weight of the propulsion plant
- Minimize volume of the propulsion plant
- Maximize redundancy of the propulsion plant

An indication of the amount of maintenance required for the diesel engines is the amount of cylinders. With increasing amount of cylinders, the engine consists of more maintenance requiring parts like valves and sensors. If possible, few large diesel engines should therefore be chosen above several smaller engines. Another aspect in reducing the maintenance costs lies in avoiding low engine loading for continuous operation. Continuous operation on low engine loading results in increased wear of the engine due to high exhaust temperatures, poor combustion, cold corrosion and fouling of the engine (Wiesmann, 2010). By matching the engine sizes to required propulsion power of frequently occurring ship speeds, low engine loading can be prevented. Thus, considering the operational profile is important.

By limiting the complexity of the propulsion plant, the costs and efforts for operating the propulsion plant is reduced. Although there are a lot of different benefits of reducing the complexity, for this research two aspects are of particular interest: By reducing the amount of different types of prime mover, the required amount of training for the crew in operating the vessel is reduced. Therefore, less and less specialized crew is needed. By reducing the amount of different types per prime mover, the amount of required spare parts is reduced as well as the amount of training for the technical crew in maintaining the systems.

Redundancy for the naval vessels is of critical importance. Being a warship, the future frigate is intended to take part in naval warfare, with the possibility of being damaged. In spite of being damaged, the frigate has to remain operational, although with restrictions (van Es, 2011). In case of damage to the propulsion plant, the vessel still has to be able to reach transit speed. Therefore, at least two propellers, two shafts and two engine rooms are needed. The need for redundancy also has a severe impact in case of a hybrid propulsion plant and if a FPP is used. In case of a hybrid propulsion plant with FPP, the vessel has to reach transit speed on one shaft without overloading the engines. In case the engines are prone to overloading without electric drives, single points of failure for the electric drives have to be removed as well. This will result in a significant increased amount and complexity of electrical equipment aboard.

Determining Concepts

To set up suitable propulsion concepts several requirements narrow down the possible combinations:

- The frigate has to reach a ship speed of 28 knots in sea state 3, with a towed sonar array. To achieve this, a brake power of 29.4 MW or 32.1 MW is required for a vessel of 5200 ton, respectively 5970 ton. Therefore, propulsion diesel engines and electric drives with combined power minimal equal to the requested brake power need to be installed.
- Silent speed during ASW-operations of 15 knots has to be reached on electric drives with towed sonar array in sea state 3. Thus, the electric drives have to deliver 3000 kW, respectively 3400 kW.
- To fulfill redundancy requirements, at least two shaftlines with propellers and two separate engine rooms have to be installed.

Next to these requirements, several assumptions are made. For this thesis, the assumptions are binding. In reality they are not, but deviating from the assumptions is very unlikely:

- No more than two shaftlines are used. The space for fitting propellers limits the propeller diameter to 4.8 m in case two propellers are used. If more propellers (and shafts) were used, the propeller diameter has to be decreased which reduces efficiency. More shaftlines also increase complexity and need for maintenance without any strong advantage.
- During ASW-operations both propellers are used for propulsion as one trailing shaft would increase the flow-induced noise. Therefore, the electric drives on both shafts need to be of equal power, minimal 1500 kW, respectively 1700 kW per drive.
- The power from the electric drives is increased to 2600 kW, including sufficient margin to achieve 15 knots under any circumstance. Silent speed might be possible up to about 18 knots dependent on the operational conditions.
- Due to the strict weight restrictions, only high speed diesel engines are considered.

Analysis of the engine programs of major marine diesel engine manufacturer shows a limited choice of large high speed diesel engines. Considering engines with rated power of minimal 5000 kW, the following diesel engines are left to consider:

| Manufacturer | Type | power per cylinder | Available cylinder configuration | Maximum available power |
|--------------|----------------|--------------------|----------------------------------|-------------------------|
| Wärtsilä | 26 | 340 kW | 6,8,9,12,16 | 5440 kW |
| MAN | V28/33D | 455 | 12,16,20 | 9100 |
| | V28/33D 'Navy' | 500 kW | | 10000 kW |
| MTU | 1163 | 370 kW | 12,16,20 | 7400 kW |
| | 8000 M91 | 455 | 12,16,20 | 9100 |
| | 8000 M91L | 500 kW | | 10000 kW |

Table 3.2: Available high speed diesel engines with rated power of minimal 5000 kW

For high redundancy, the electric drives are optional in assisting the diesel engines but are not required to achieve maximum ship speed. This will result in a COmbined Diesel And Diesel (CODAD) propulsion and the following engine configurations are possible:

- 6 x Wärtsilä 16V26 total: 32.6 MW, 96 cylinders, 227.4 ton
- 4 x MAN 20V38/33D total: 36.4 MW, 80 cylinders, 221 ton
- 4 x MTU 8000 20V total: 36.4 MW, 80 cylinders, 211.6 ton
- 5 x MTU 1163 20V total: 37.0 MW, 100 cylinders, 133 ton

Combinations with smaller diesel engines is possible but this increases complexity of the propulsion plant and the need for maintenance due to the increased amount of cylinders significantly and will not be considered further.

With the installation of electric drives required for silent speed, they offer also the possibility to assist in achieving maximum speed. Therefore, the electric motors need to be operated in the field weakening range as their nominal working point needs to coincide with maximum silent speed. In the field weakening range, the efficiency of induction motors is assumed to be constant (for smaller induction motors this is shown by e.g. (Amrhein, Krein, Chapman, & Fierro, 2007), (Shumei, Chen, & Liwei, 2008)) and thus the mechanical power remains constant as well. For a COmbined Diesel eLEctric And Diesel (CODLAD) propulsion with two 2600 kW electric drives, more combinations are possible:

- E + 5 x Wärtsilä 16V26 total: 32.4 MW, 80 cylinders, 189.5 ton (without Edrives)
- E + 4 x MAN 16V38/33D total: 34.3 MW, 64 cylinders, 183.2 ton (without Edrives)
- E + 3 x MAN 20V38/33D total: 32.5 MW, 60 cylinders, 158.7 ton (without Edrives)
- E + 2 x + MAN 20V38/33D + 2 x 12V38/33D total: 34.3 MW, 64 cylinders, 181.4 ton
- E + 4 x MTU 1163 20V total: 34.8 MW, 80 cylinders, 107 ton (without Edrives)
- Replacing MAN V38/33D with MTU 8000

With the CODLAD propulsion, less diesel engines or smaller diesel engines are needed for the propulsion. Even more possible combinations can be conceived if the size of the electric drives is increased. Some possible combinations are given for an output power of 32.6 MW, but the list of feasible concepts is nearly limitless:

- 2 x Edrive (5.4 MW) + 4 x Wärtsilä 16V26
- 2 x Edrive (4.3 MW) + 3 x MAN 16V38/33D ‘Navy’
- 2 x Edrive (6.3 MW) + 2 x MAN 20V38/33D ‘Navy’
- 2 x Edrive (6.3 MW) + 2 x MAN 12V38/33D + MAN 20V38/33D

Analyzing all proposed concepts requires a lot of work, especially if each concept is evaluated with a fixed pitch and controllable pitch propeller. This work would go beyond the scope of this thesis. Next to the large amount of work, the results of the concepts would probably not vary a lot if two large or four small diesel engines with equal total amount of output power are evaluated. This would decrease the scientific relevance of the large amount of work to evaluate all concepts. Therefore, a few concepts should be chosen with deviating performance.

Comparing the performance of diesel engines and electric drives, major differences can be found in the development of torque across the engine envelope. For turbocharged diesel engines, torque available at minimum engine speed is about 30% – 40% of nominal torque and increasing with increasing engine speed. For induction motors with constant flux control, nominal torque is available from rest up to nominal engine speed and for higher engine speeds the torque is decreasing. Thus, difference in the performance of the propulsion plant can be expected if the size of the electric drives compared to the diesel engines varies. A comparison of CODAD to CODLAD should be included.

Further, the impact on the performance should be investigated in case the electric drives are scaled up. Therefore, a comparison of CODLAD to CODLAD should be included, with differences in size of diesel engines and electric drives.

If Newton’s 2nd law of motion for the accelerating frigate is reconsidered:

$$m_{ship} * \dot{v}_{ship} = F_{Thrust} - F_{Resistance} \quad ref. (2.6)$$

Next to the development of thrust force, depended on time and engine speed, also the mass of the ship and the speed-dependent resistance are important for the acceleration performance of the vessel. Evaluating the performance of a propulsion plant for two different sized vessels could reveal some interesting results.

With regard to the complexity, the weight, size and the need for maintenance of the propulsion plant, concepts with as few engines and cylinders as possible are favored. The following engine combinations were selected for the different concepts:

Concept 1 – CODLAD: 2 x MAN 20V38/33D ‘Navy’ + 2 x Electric Drive (4900 kW), Δ = 5200 ton
 With reduced displacement and lower resistance curve, the vessel might be propelled by two large diesel engines and larger electric drives. The diesel engines make use of the special Navy load profile, allowing for higher engine speed and power output during a limited amount of time. For this concept, the electric drives offer sufficient power to propel the vessel at ship speed of 19-20 knots even with heavier sea and towed array. The diesel engines are used to reach maximum ship speed in combination with the electric drives, or can serve as backup in case the electric propulsion fails. At maximum ship speed, 66% of brake power is delivered by diesel engines and 33% is delivered by the electric drives.

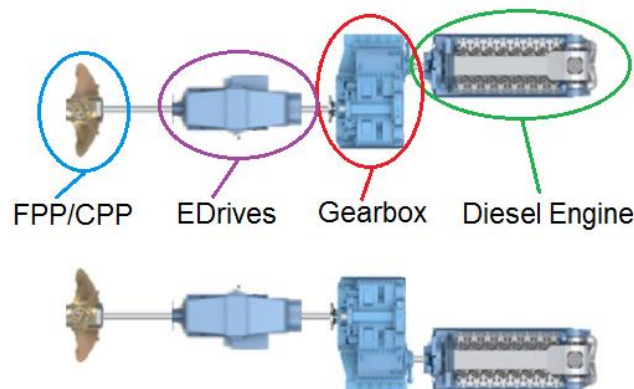


Figure 3.3: Concept 1 – Layout

3. Propulsion Plant Concepts

Concept 2 – CODLAD: 4 x MAN 16V38/33D + 2 x Electric Drive (2600 kW), $\Delta = 5200$ ton

The four diesel engines, two per shaft, deliver 29.1 MW of brake power. Sufficient to propel the frigate in calm sea or without towed array at 28 knots. However, with waves and towed array, the electric drives have to deliver additional power continuously to achieve a ship speed of 28 knots. At maximum ship speed, 85% of brake power is delivered by diesel engines and 15% is delivered by the electric drives.

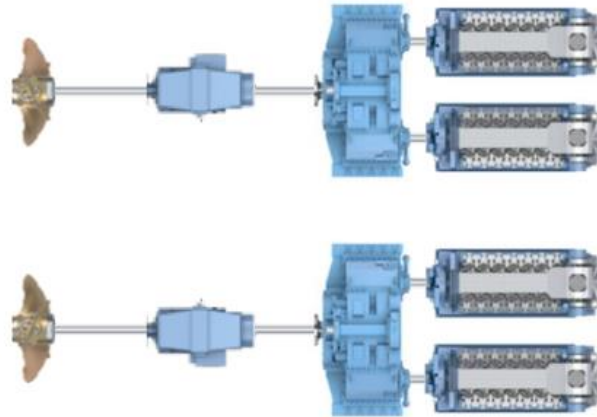


Figure 3.2: Concept 2 & 3 – Layout

Concept 3 – CODLAD: 4 x MAN 16V38/33D + 2 x Electric Drive (2600 kW), $\Delta = 6000$ ton

To investigate the effect of varying ship mass and resistance, the propulsion plant is kept the same. But the displacement of the vessel is increased by 800 tons, also resulting in a higher resistance curve. Due to the higher mass the acceleration will probably be lower and due to the higher resistance curve, a lower maximum ship speed will be achieved. At maximum ship speed, 85% of brake power is delivered by diesel engines and 15% is delivered by the electric drives.

Concept 4 – CODAD: 4 x MAN 20V38/33D, $\Delta = 6000$ ton

Similar to 4 x MTU 8000 20V, but more data is available for the MAN engine. With two engines per shaft driving a CPP, this concept is similar to the propulsion plant of the Danish Iver Huitfeldt-class frigate. With comparable size and maximum ship speed, data on the acceleration of the Iver Huitfeldt-class frigates can be used to develop engine speed and propeller pitch setpoints. In addition, this concept will also be equipped with two 2600 kW electric drives for silent propulsion. The power of the electric drives is not required to achieve maximum ship speed. But during the acceleration maneuver the drives can generate additional torque to assist the diesel engines. At maximum ship speed, 100% of brake power is delivered by diesel engines.

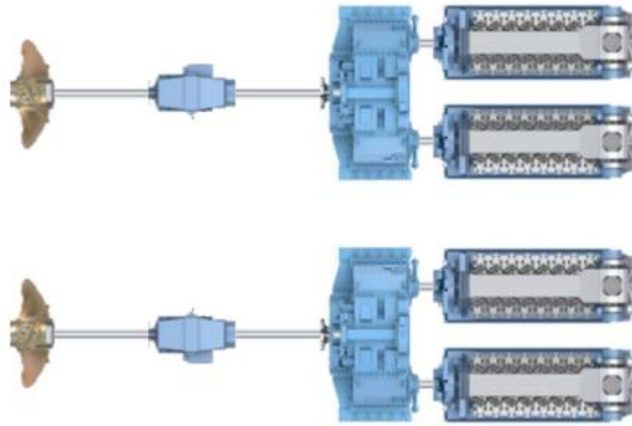


Figure 3.1: Concept 4 - Layout

This four concepts will not represent all possible combinations and configurations possible but provide sufficient variance to show the effect of important variables influencing the acceleration performance of diesel-hybrid propulsion plants.

Component Selection

Electric drives

The hybrid drives discussed in this thesis are a combination of diesel engines and electric motors. With electric motors, often the whole electrical drive is meant. The electric drive consists of the electric motor, a control unit and often a power converter.

In contrast to prime movers where speed control is realized by adjusting the fuel flow to the engine, speed control of electric motors is not that straight forward. Electric motors are not counted as prime movers as they do not use chemical energy to provide mechanical energy, but require electrical energy. Speed control of simple DC motors is achieved by changing the supply voltage, whereas AC motors (Induction and Synchronous) require for voltage- and frequency control of the supplied electrical energy.

For the production of electrical energy an intermediate step is required. Onboard of ships electrical energy is produced by generator sets or turbo generators. In most marine cases, electric motors are connected to the ships power grid and not fed by separated generator sets. Voltage and frequency on the power grid have to be kept constant. Otherwise, the speed uncontrolled electrical consumers (e.g. pumps and motors directly connected) will follow the change of frequency, or suffer from damage in case of voltage peaks. Therefore, power converters are needed to change voltage and, in case of AC motors, the frequency of the electrical energy before supplying the energy to the motors.

The transformation of electric power is not without losses. The power electronics needed to convert frequency and voltage is very efficient but still energy is lost. For the OPV (Oceangoing Patrol Vessel) of the RNLN Ross, Stapersma and Bosklopper determined an efficiency loss of 8% for the electric power transformation of the hybrid drive (Ross, Stapersma, & Bosklopper, 2010). In the future, these losses might be reduced if DC power distributions is introduced in naval vessels [e.g. (Butcher, Maltby, & Parvin, 2009); (Simmonds, 2016)]. With DC power distribution, especially losses in power take offs (PTO) and power take ins (PTI) can be reduced as the amount of power electronics can be reduced and variable speed generators can be used, resulting in better loading of the driving diesel engines.

DC motors offer the lowest underwater noise emission (Butcher, Maltby, & Parvin, 2009), but these motors require brushes to supply the armature windings. Brushes require regular maintenance or the risk of flashovers increase. The use of brushes also limits the current that can be supplied to the armature, limiting the power density of DC motors. Compared to AC motors, DC motors are larger and heavier. Therefore, the application of these motors is limited to submarines where reducing the noise signature is of key importance.

AC synchronous motors offer a high power density, but due to their working principle large synchronous motors are not self-starting. Starting of large synchronous motors can be achieved with use of a smaller induction motor, or by equipping the motor with an induction cage to start up the motor similar to an induction motor. But due to the extra components needed to start the motor, synchronous motors are expensive. However, these type of motor is mainly used as generator in marine applications.

For the electric propulsion of large naval vessels, the induction motor is favored. This type of motor, especially the advanced induction motor (AIM)[(Buckley & Crane, 2007); (Lewis C. , 2002)], offers a good power density and noise signature for a comparably low price.

Induction motors

An electric motor consists of the rotor, located on the shaft and delivering mechanical power, and a stator located in the housing. The stator consists of paired windings, also called poles, creating a rotating magnetic field if connected to an AC supply with frequency f_{set} . The rotational speed of the generated field is also called synchronous speed and can be calculated by:

$$n_s = \frac{2 * f_{set}}{\text{number of poles}} \quad (3.2)$$

The rotor is made up of current-carrying conductors. In case of an induction motor, the current in the conductors of the rotor is generated by magnetic induction due to the relative movement of rotating the magnetic field. Placing a current-carrying conductor in a magnetic field generates Lorentz forces on the conductor, orthogonal to the field and the current in the conductor.

$$F_L = B * I * h \quad (3.3)$$

With magnetic flux density B and length of the conductor h. The conductor, as part of the rotor, rotates with arm $l/2$ and under angle β in the magnetic field (figure 3.4).

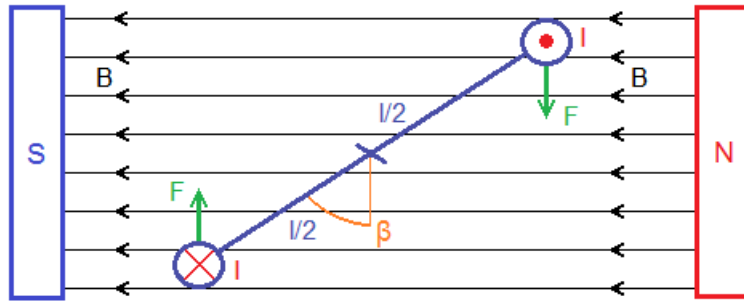


Figure 3.4: Force on conductor in magnetic field

Combined with the opposing conductor, torque is generated on the shaft.

$$M = 2 * F_L * \frac{l}{2} * \sin(\beta) = I * \Phi * \sin(\beta)$$

With magnetic flux Φ :

$$\Phi = B * h * l \quad (3.4)$$

With multiple windings per conductor and several conductors on the rotor, the torque on the shaft is generally given by:

$$M = K_M * I * \Phi \quad (3.5)$$

However, current in the conductors is only induced if the rotor is moving relatively to the magnetic field. Therefore, the current drops to zero if rotor and field are rotating at the same speed. Torque is only generated by the induction motor if the rotor lags to the rotating field. This is expressed in the slip of the engine:

$$s = \frac{n_s - n_{rotor}}{n_s} \quad (3.6)$$

If the slip increases, the resulting torque of the motor increases as well. For large induction motors running on nominal load, the slip is about 0,5 – 1,5%.

Next to the induced current in the conductors of the rotor, due to Faraday's Law also an induced voltage is generated. The faster the conductor is moving through the magnetic field, the higher the induced voltage. For one conductor this can be described as the rate of change of the magnetic flux, equation 3.7.

$$E = -\frac{d\Phi}{dt} \quad (3.7)$$

Similar to the formula for generated torque, for multiple windings and several conductors, the induced voltage can be rewritten as:

$$E = K_E * n * \Phi \quad (3.8)$$

For small slip values, the frequency of the induced voltage is low. In that case, the inductive resistance of the rotor becomes negligible and induced current and voltage are in phase. As the induced voltage is in phase with the magnetic flux, all conductors are contributing in the generation of torque. For low slip therefore, the generated torque is proportional to the slip.

Increasing the slip, the frequency of the induced voltage increases as well. With increasing frequency, the inductive resistance of the rotor becomes increasingly important. Due to the inductive resistance, the induced current increasingly shifts out of phase to the induced voltage. As a result, not all conductors are contributing in generating torque any longer as conductors with different current flow directions are subjected to the same field direction. Thus, with increasing slip the generated torque starts to decrease.

The location of the maximum value is dependent on the resistance of the rotor. If the rotor resistance increases, the maximum torque shifts towards higher slip values and rises less steep, but the drop after maximum torque becomes less as well.

Various standard designs have been developed to drive loads with different characteristics. Figure 3.5 shows the speed-torque-curve for four different classes specified by the National Electrical Manufacturers Association (NEMA). Class B has versatile characteristics with high efficiency and power factor. Other classes can deliver higher starting torque (class C and D) or higher maximum torque (class A) but with a reduced efficiency as trade-off.

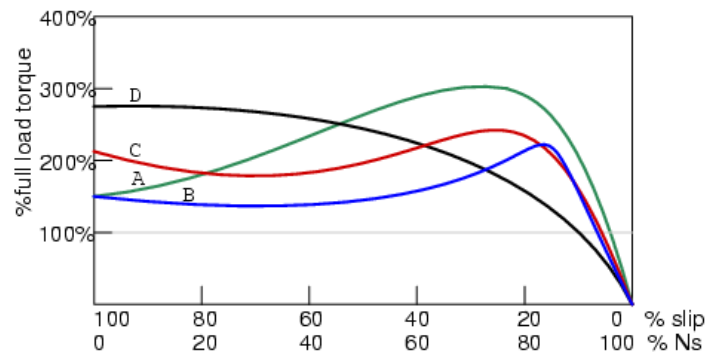


Figure 3.5: NEMA standard design classes A,B,C,D (Kuphaldt, 1999)

Most high voltage induction motors are designed according to NEMA class B, especially induction motors for marine application with emphasis on high efficiency (NEMA, 2009).

If the uncontrolled induction motor is connected to the line, the motor operates with fixed stator voltage and frequency. Therefore, the motor follows the speed-torque curve (figure 3.5) until the delivered torque is equal to the requested torque of the load. With increasing slip, the inductive reactance increases and therefore the power factor drops. As the resistance of the motor remains fairly constant, the absorbed real power of the motor will remain fairly constant as well. Due to the decreasing power factor however, the apparent power S increases, resulting in an increasing current.

$$\text{power factor} = \cos \theta = \frac{P}{S} \quad (3.9)$$

If the motor is started from rest, and thus the slip is maximum and equal to 1, the starting current can be 500 – 600% of the nominal current.

If the uncontrolled induction motor is operated on the power grid, the low power factor and resulting high starting current do not result in an immediate problem as the power company often corrects for decreasing power factors with capacitor banks in their substations. The consumer however will be charged with additional costs for low power factor as the grid infrastructure has to be adapted to support higher currents.

On board of ship, low power factors can cause severe problems. Typical generator sets for marine applications are rated at a power factor of 0,8. The apparent power rating represents the maximum current the generator can deliver whereas the real power rating represents the maximum power the driving engine can deliver. For efficiency-reasons the size of the generator sets is chosen to fit the consumers as the diesel engine driving the generator suffers from fouling and low efficiency in low load conditions. If large uncontrolled induction motors are switched on onboard of the ships, the required current can overload the generator sets. Therefore, advanced control of the induction motor is needed.

Popular control method for induction motors is the control of supply voltage and frequency (variable frequency drives, VFD). During the operation of an induction motor with a VFD, two different speed ranges can be identified. For motor speeds up to nominal speed, the motor is operated with constant flux. For speeds higher than nominal, the motor is operated within the field weakening range.

In the constant flux range, the developed torque is independent of the supplied frequency, thus only depends on the slip of the motor. However, the speed of the motor is still depending on the supplied frequency.

In practice, the stator resistance is so small that the voltage drop across the stator can be neglected, so the induced voltage is nearly equal to the supplied voltage:

$$E \approx U_{set} \quad (3.10)$$

With equations (3.2) and 3.8) the flux can then be expressed by:

$$\Phi = K_f * \frac{U_{set}}{f_{set}} \quad (3.11)$$

For a constant flux, the supplied voltage has to be adjusted proportionally to the supplied frequency. This is possible until the rated frequency is reached. If the frequency and voltage are increased further, the motor would be provided with overvoltage. Therefore, if the supplied frequency is set higher than the rated frequency, the supplied voltage is held constant. Consequently, the flux decreases, eq. 3.11, giving the field weakening range its name. With the developed torque proportional to the flux, the torque is decreasing proportional to the supplied frequency in the field weakening range, resulting in a constant power of the motor.

With proper control, the motor can develop torque as given in figure 3.6, where the red line indicates the trend of the nominal torque.

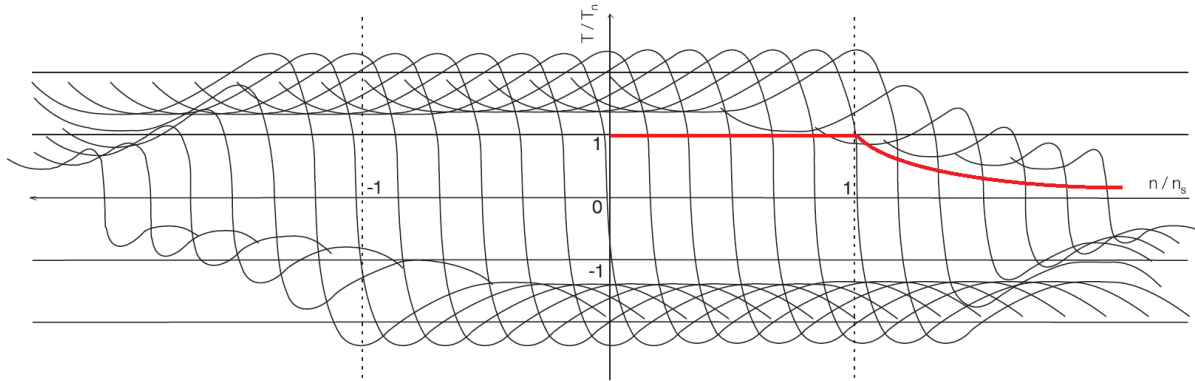


Figure 3.6: Torque of an induction motor controlled by a VFD (ABB, 2011)

Large induction motors are often made according to the customers specification. For induction motors of higher speed (500 – 3000 rpm) manufactures provide standard specifications for a wide range of combinations of speed, voltage and output power (ABB, 2011). For lower speeds, needed to directly couple the electric drive to the propeller shaft, no information is available.

With decreasing engine speed the developed torque has to increase if high output powers are desired. To increase the developed torque, the motor has to be designed to resist higher currents, resulting in increased sizing and weight of all involved components. The power density is thus, similar to diesel engines, decreasing with decreasing speed. Induction motors of high powers on low speed are a niche product, designed and engineered for special applications.

The following table shows the trend for induction motors of 12MW output power (Siemens, 2009).

| Manufacturer | | Converteam | | | Siemens | | |
|--------------|----------------------|------------|------|------|---------------|---------------|---------------|
| Type | | N3HXC | AIM | AIM | 1RP6 712-6 | 1RP6 712-4 | 1RP6 712-2 |
| Speed | [rpm] | 125 | 150 | 200 | 1200 | 1800 | 3600 |
| Mass | [ton] | 122 | 68.5 | 49.2 | 18.9 | 18.6 | 17 |
| Volume | [m ³] | 152.5 | 55.7 | 51.1 | 29.4 | 25 | 23.2 |
| Inertia | [kg*m ²] | 25000 | | | 468 | 300 | 147 |

Table 3.3: Mass and volume for 12 MW induction motors of different speeds

Selecting a motor with higher output speed clearly reduces the weight and space requirements of the propulsion plant on the vessel. However, if an induction motor is selected with higher output speed, reduction gearing is required, with the danger of increasing the underwater noise emission. But recent developments might allow the use of smaller high speed induction motors with special gearing in naval vessels (Hoppe, 2012).

For the implementation of the induction motor within the dynamic simulation model, choosing a low speed motor or medium speed motor does not matter. The output power and torque (in case of an high speed motor after the gearbox) as well as the performance characteristics are identical. Due to the lack of information on low speed induction motors, data on a medium speed induction motor is used for this research.

The following data is used for the induction motor:

| Manufacturer | GE | |
|-------------------|-------------------------|-----------------------|
| Type | MV 560 | MV 710 |
| Power | 2600 kW | 4900 kW |
| Voltage | 6600 V | |
| Frequency | 60 Hz | |
| Poles | 8 | |
| Synchronous Speed | 900 rpm | |
| Inertia | 120.7 kg*m ² | 300 kg*m ² |
| Nominal Torque | 27.57 kNm | 52 kNm |

Table 3.4: Data of induction motors used for the concepts

Diesel Engines

In all concepts, the majority of brake power for propulsion is generated by the large diesel engines. Due to the weight restrictions of the frigate, only high speed diesel engines were considered in determining propulsion plant concepts.

The choice of high-speed diesel engines with sufficient power to propel frigates is limited. While Wärtsilä offers engines of sufficient power to propel the vessel to transit speed, larger engines are not available from this manufacturer. MAN and MTU both offer larger high-speed engines with output power up to 10 MW. The MTU 8000 series is currently used on the Danish Iver Huitfeldt-class frigate and has proved to be capable of accelerating the vessel very fast to maximum speed. Unfortunately, detailed information on the MTU 8000 series is hard to come by. For this thesis the data on the MAN V28/33D engine will be used, in size and output power comparable to the MTU 8000 – series.

The engine is equipped with sequential turbocharging. Up to an engine speed of 700 – 800 rpm only one turbocharger is used to compress the charge air. With higher engine speed, the exhaust mass flow is sufficient to drive the second turbocharger as well. Figure 3.8 shows the engine envelope for the MAN V28/33D STC. With reduced exhaust mass flow at low engine speed, the one small turbocharger can achieve higher charge air pressure than an one-stage turbocharged engine. The engine power is increased at low speed, compared to Figure 2.4 of an one-stage turbocharged engine.

The red area, indicated as Range III, is available for vessels with Navy load profile with limited operating time at full power (> 350 kW/cyl for $<10\%$ operating time). This can be expected for the future M-frigate.

Range II indicates a temporary, increased load limit which can be used during acceleration and maneuvering. Continuous operation within this limit is prohibited to prevent increased wear due to an accumulation of thermal stresses.

3. Propulsion Plant Concepts

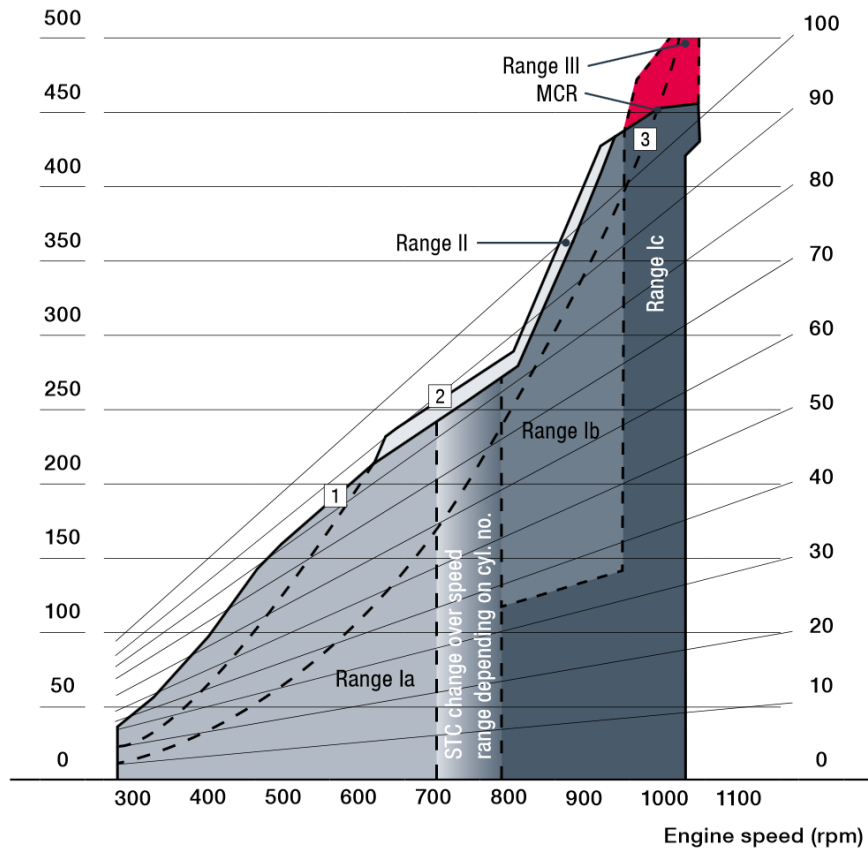


Figure 3.8: Engine Envelope MAN V28/33D STC (MAN, 2012)

For the diesel engines, the following data is used (MAN, 2012):

| | | | |
|--------------------------------|-----------------------|------------------------|------------------------|
| Manufacturer | MAN | | |
| Type | V28/33D STC | | |
| Number of cylinders | 16 | 20 | 20 |
| Power | 7280 kW | 9100 kW | 10000 kW |
| Nominal Speed | 1000 rpm | | 1035 rpm |
| Bore Diameter | 0.28 m | | |
| Stroke Length | 0.33 m | | |
| effective compression ratio | 14.2 | | |
| Nominal charge air pressure | 4.31 bar | | 4.52 bar |
| Nominal charge air temperature | 322 K | | |
| Nominal mechanical efficiency | 0.9 | | |
| Turbocharger delay | 1 s | | |
| Inertia | 830 kg*m ² | 1037 kg*m ² | 1070 kg*m ² |

Table 3.5: Data of diesel engines used for the concepts

Propeller

Many aspects of the propellers (FPP and CPP) were already discussed in the background section. Choice for the propellers is straight forward. For the FPP data on a potential propeller for the future M-frigate was provided by DMO (see Appendix D). For the CPP the choice is limited to the Wageningen C5-75.

For the propellers, the following data is used:

| Type: | FPP | CPP |
|--------------------------|-------------------------|-------------------------|
| Model: | Marin 7496L | Wageningen C5-75 |
| Blades: | 5 | 5 |
| PD-ratio: | 1.705 | Max 1.8 |
| AE/A0: | 0.922 | 0.75 |
| Diameter: | 4.8 m | 4.8 m |
| Inertia Propeller: | 21000 kg*m ² | 23900 kg*m ² |
| Inertia Entrained Water: | 16000 kg*m ² | 16000 kg*m ² |

Table 3.6: Data of propellers used for the concepts

Matching

Next to specifying the size of the components and their performance, important in the process of matching is actual proper matching of propulsion engines with the propulsor.

During the matching process, the operating envelope of the propulsion engine is tuned to the load of the propulsor by fulfilling the following two criteria (Klein Woud & Sapersma, 2005):

- The engine should develop (nearly) full power at the design condition
- The propulsion plant delivers required speed or thrust in all design and off-design conditions without exceeding any limitation

With a fixed pitch propeller or a CPP at maximum pitch, satisfying the second criteria in all conditions with a turbocharged diesel engine is nearly impossible. In trial conditions, the resistance is reduced and the engine cannot deliver maximum power without exceeding the engine speed limit. With heavy sea, the resistance increases and the engine power is limited by the turbocharger limit.

For the MAN V28/33D diesel engine, the manufacturer demands the following matching of engine with propulsor (MAN, 2012), see figure 3.9. In this figure, range 1 indicates the operating range for trial conditions with clean hull and calm sea. For this operating range, an engine speed between 103,5% and 106% is permissible for 1 hour, but for continuous operation the engine speed is limited and full power is not developed. The theoretical propeller curve, indicated by curve 2, represents operation with fouled hull and heavy weather. The exact sea state is not given, but for the theoretical propeller curve the manufacturer demands a service margin of 10% - 15% to the trial conditions. The theoretical propeller curve should run through the maximum continuous rating (MCR) point of the engine.

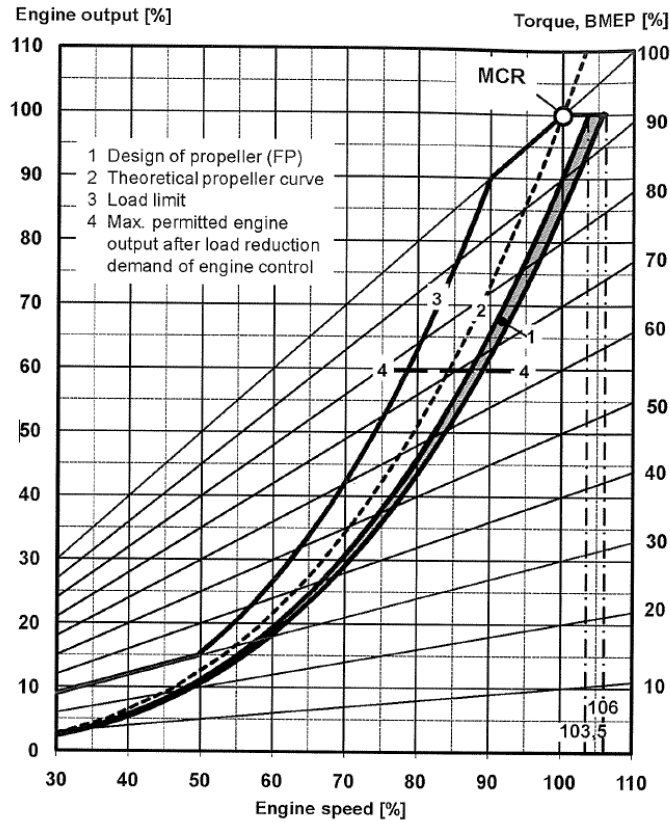


Figure 3.9: Operating range for fixed pitch propeller MAN V28/33D (MAN, 2012)

The propeller curves for the two different propellers were already determined earlier, the reader is referred to the section: Background for the detailed approach of obtaining the propeller curve from the resistance data. For the heavy vessel ($\Delta = 6000$ tons) in design condition (with towed array and a service margin of 20.3% for sea state 3 and some fouling), the FPP curve is given in figure 3.10. With a service margin of 20.3% the margin is chosen to be slightly larger than demanded by the manufacturer.

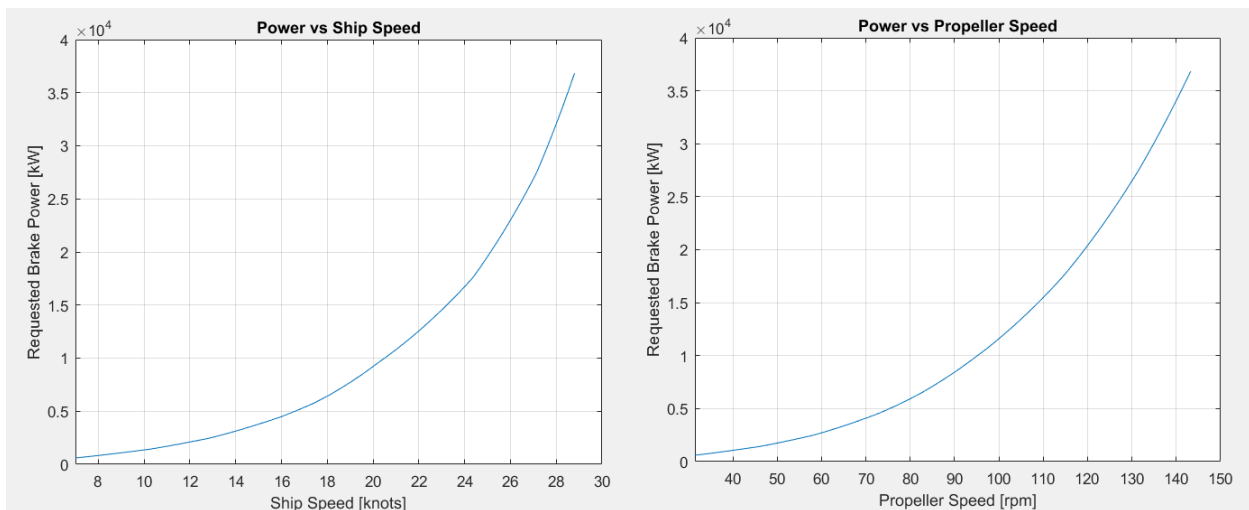


Figure 3.10: Propeller Curve Marin Propeller in design condition

For merchant vessels, the engine is not continuously run in the MCR-point. To increase maintenance intervals and provide a margin in case the vessel is exceptionally heavy loaded, an engine margin (EM) is introduced. This margin lies usually between 10% - 20% and should coincidence with the design speed. In the majority of the operating time, the engines are loaded to but not beyond the engine margin. For a naval vessel, the design speed is only achieved in a fraction of the operational time and the engine margin is not required.

In case the vessel is equipped with a gearbox, the actual process of matching the propeller curve of figure 3.10 to the engine envelope is reduced to determining the gearbox ratio.

$$i_{GB} = \frac{n_{engine}}{n_{prop}} \quad ref. (2.34)$$

Where n_{engine} and n_{prop} are the speed of engine and propeller in case the requested power of the propeller is equal to the MCR of the engine.

For concepts 1 – 3 the electric drives have to provide additional power to achieve maximum ship speed, the power is added to the power envelope of the diesel engines.

Concept 1

The large electric drives of concept 1 allow for a silent speed up to 21 knots. Up to this ship speed, the electric drives operate in the constant torque range. Above 21.1 knots, the electric drives deliver constant power, resulting in a total engine envelope as plotted in figure 3.11. Next to the total engine envelope, also the limits for either the diesel engines or the electric drives is plotted as well. The propeller curve of the FPP in design condition is given as well, full power is delivered at a ship speed of 28 knots. At 28 knots, the propeller rotates at 138 rpm. With a maximum engine speed of 1035 rpm, the gearbox ratio will be 7.4981.

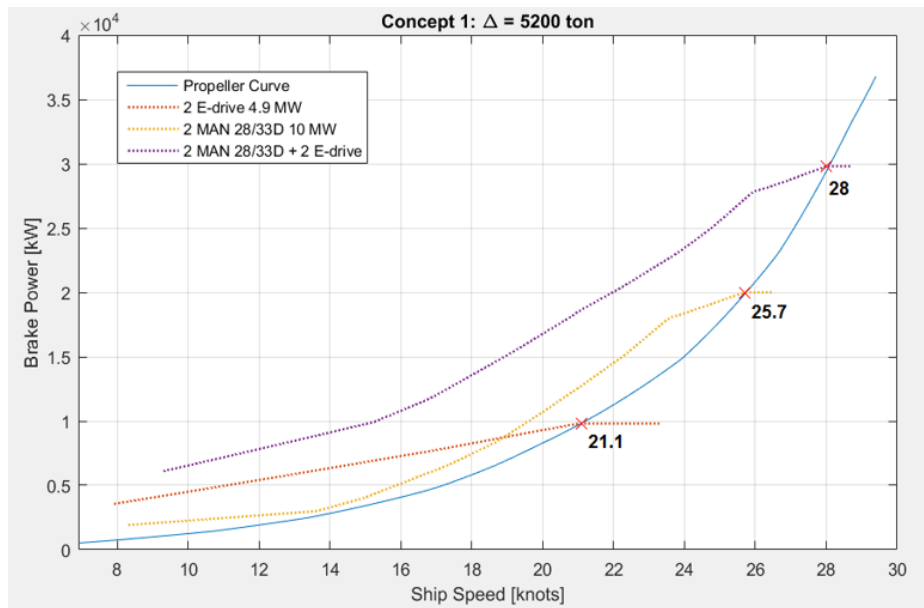


Figure 3.11: Engine envelope Concept 1 – FPP in design condition

At 28 knots, the CPP rotates slightly faster, with 139.2 rpm. Resulting in a gearbox ratio of 7.4378 of Concept 1 equipped with a CPP.

Concept 2

The smaller electric drives of concept 2 limit the silent speed to 18 knots. Therefore, constant torque is only available up to 18 knots. Engine envelopes of propulsion on 2 and 4 diesel engines is plotted as well in figure 3.12. With 4 diesel engines, 28 knots cannot be achieved and the electric drives have to deliver additional power. Nominal engine speed for the diesel engines is 1000 rpm. With FPP, the propeller rotates at 139.5 rpm at maximum ship speed of 28.9 knots, resulting in a gearbox ratio of 7.1677. With CPP, the propeller rotates slightly faster at 140.6 rpm, resulting in a gearbox ratio of 7.1101.

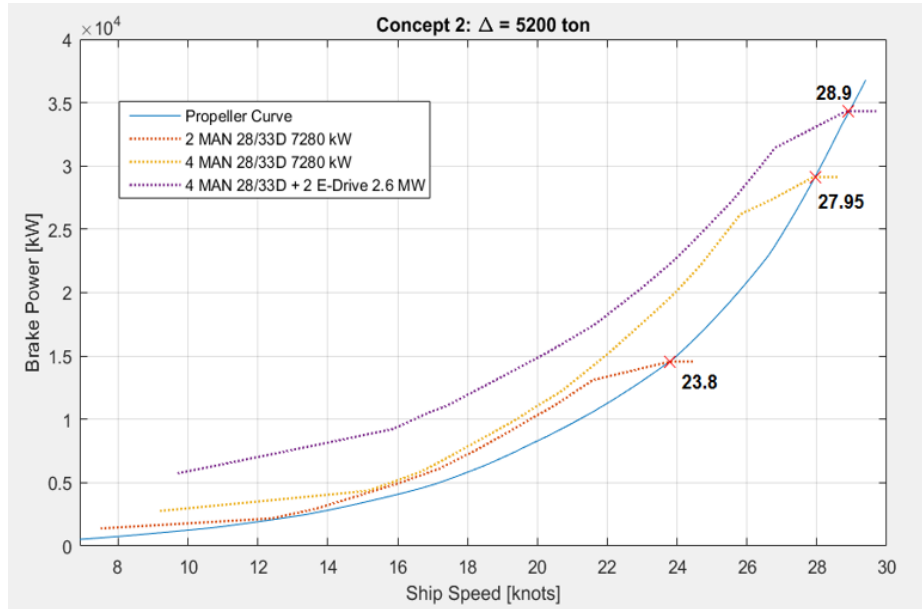


Figure 3.12: Engine envelope Concept 2 – FPP in design condition

Concept 3

Compared to Concept 2, the displacement of the vessel is increased, resulting in an increased resistance. With the power provided by all engines, the maximum achievable ship speed drops to 28.4 knots. Due to the lower ship speed, the propeller rotates with lower speed as well. With FPP, the propeller rotates at 139.2 rpm, resulting in a gearbox ratio of 7.1815. With CPP, the propeller rotates slightly faster at 140.4 rpm, resulting in a gearbox ratio of 7.1237.

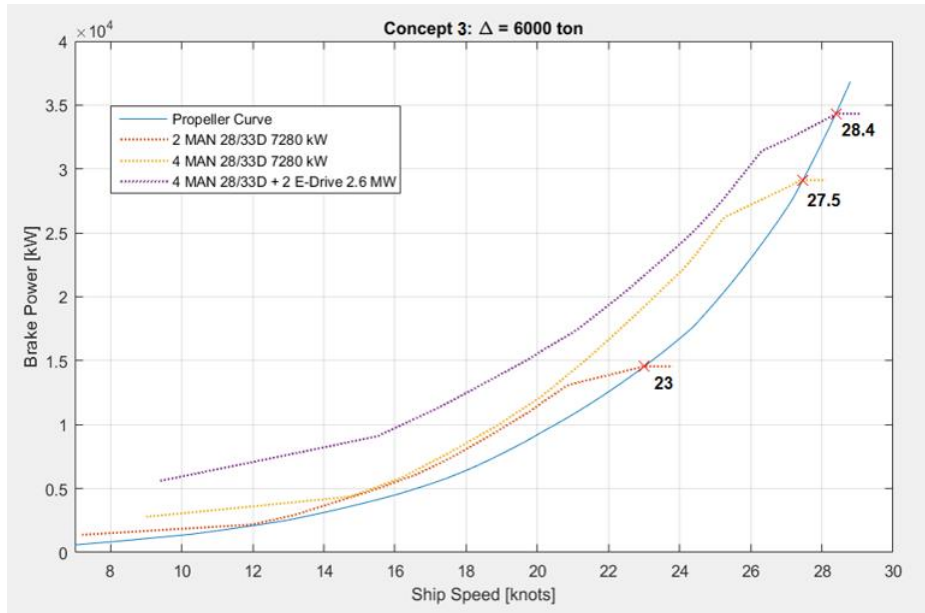


Figure 3.13: Engine envelope Concept 3 – FPP in design condition

Concept 4

The power of the four large diesel engines of concept 4 is sufficient to reach a ship speed of 28.7 knots in design condition. The electric drives are not required and their power is not plotted in the engine envelope, figure 3.14. Equipped with FPP, the propeller rotates at 141.4 rpm a maximum ship speed. This results in a gearbox ratio of 7.0732. With a CPP, the propeller rotates at 142.5 rpm, resulting in a gearbox ratio of 7.0163.

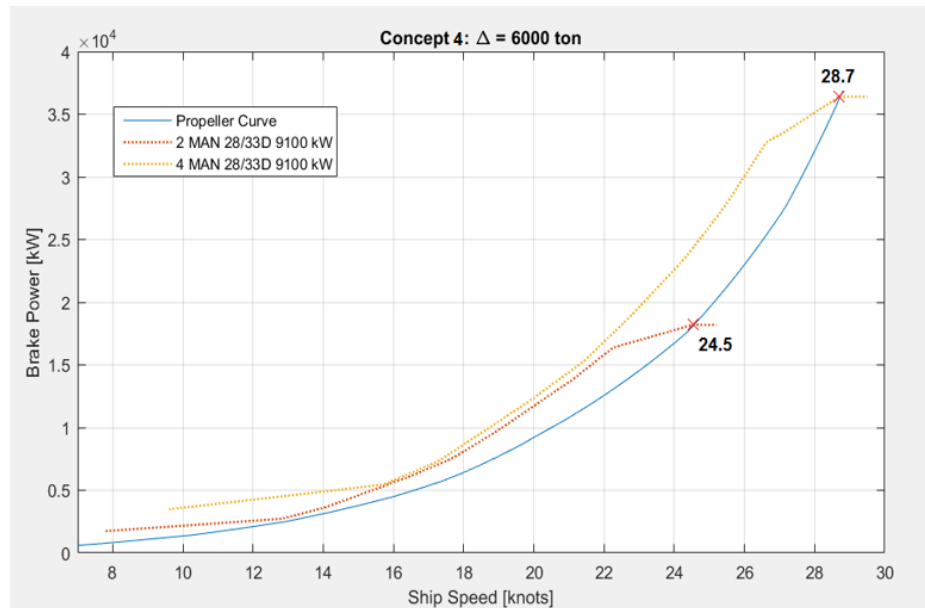


Figure 3.14: Engine envelope Concept 4 – FPP in design condition

Summary

| Concept | Engines per shaft | Propulsion Power | Gearbox ratio | Design Speed | Service Margin |
|----------|-------------------------|------------------------------|---------------|--------------|----------------|
| C1 – FPP | 1 x MV 710 | 29800 kW | 7.4981 | 28 | 0.203 |
| C1 – CPP | 1 x 20V28/33D 'Navy' | | 7.4378 | 28 | 0.203 |
| C2 – FPP | 1 x MV 560 | 34320 kW | 7.1677 | 28.9 | 0.203 |
| C2 – CPP | 2 x 16V28/33D | | 7.1101 | 28.9 | 0.203 |
| C3 – FPP | 1 x MV 560 | 34320 kW | 7.1815 | 28.4 | 0.203 |
| C3 – CPP | 2 x 16V28/33D | | 7.1237 | 28.4 | 0.203 |
| C4 – FPP | 1 x MV 560 | 36400 kW (without edrive) | 7.0732 | 28.7 | 0.203 |
| C4 – CPP | 2 x 20V28/33D | | 7.0163 | 28.7 | 0.203 |

Table 3.7: Summary concepts

4. Propulsion Model

Model Description

The different concepts consist of different components with various size and performance. However, the basic layout of the concepts is identical and a limited amount of types of components can be identified. Every propulsion concept consists of two identical shaftlines, one located on starboard side of the vessel and one on port side. Every shaftline consists of one or more diesel engines, an electric drive, shafts, a gearbox and a propeller, either CPP or FPP. All important model parameters are summarized per concept in Annex F.

Diesel Engine Model

Since their introduction in the beginning of the 20th century, diesel engines achieved broad popularity. Nowadays, these engines are widely used in the transportation sector and electricity generation. Increasing complexity of the engines and their control, drives the need for a better understanding of their working principles and limitations. Studies within the industry and from universities resulted in numerous of modelling approaches with varying complexity. Some approaches aimed at providing insight in the detailed thermodynamical process whereas other approaches offered more insight in the operational limits and application possibilities.

Distinction can be made between empirical and analytical models. Empirical models use polynomial functions or lookup tables to provide solutions to certain input values of a physical process. These models are easy to set up and generate results very fast. However, the table data or coefficients of the polynomial need to be fitted to actual measurement data. If operational conditions deviate from conditions of the actual measurement, results from empirical models may be inaccurate or even incorrect.

Analytical models on the other hand use mathematical equations representing physical characteristics and fundamental laws. With this approach, analytical models can produce results to physical processes with a much wider range of input values. But analytical models of complex processes often include assumptions for simplification or because the fundamental relations are still not fully understood. Therefore, analytical models may produce inaccurate results even if accurate measurement data is available.

The difference between the two approaches can be precisely summarized with a quote of Mike Loonstijn (Loonstijn, 2016):

[P]hysical models are able to predict outcomes based on proven theory, whereas empirical models can replicate outcomes based on experimental data.

Within the approach of analytical diesel engine modelling, many models with varying complexity exist. Based on complexity, Schulten and Stapersma (Schulten & Stapersma, 2003) proposed the following distinction: Mathematical models to solve first order equations of motion and predicting fuel consumption [e.g.

(Grimmelius, Shi, & Stapersma, 2010)]

Mean value models based on first principles and including air and exhaust gas flow dynamics [e.g. (Grimmelius & Stapersma, 2001); (Schulten, 2005)]

Crank angle models describing the heat release per crank angle in the cylinder [e.g. (Koumbarelis & Kyrtatos, 1991); (Stapersma, 2010)]

Phenomenological multizone models describing the phased combustion process based on empirical observations [e.g. (Rajkumar & Sudarshan, 2015)]

CFD diesel engine models [e.g. (Reitz, 1995)]

For this research, the performance of the diesel engine is investigated with a mean value model. To evaluate fuel consumption, dynamic availability of power and the thermal loading of the engine a mean value model is sufficient.

The model used in this thesis is based on research from the Delft University of Technology [(Boetius & Baan, 1998); (Grimmelius, Boetius, & Baan, 1999); (Klein Woud & Sapersma, 2002); (Miedema & Lu, 2002)]

Cylinder process

The core of the diesel engine model is represented by the five point Seiliger cycle (Seiliger, 1922). The Seiliger cycle is an ideal cycle process used to give an approximation for the real thermodynamic process within the combustion engine and therefore also called the cylinder process. The five point Seiliger cycle consists of 5 stages:

- 1-2: Isentropic compression
- 2-3: Isochoric combustion
- 3-4: Isobaric combustion
- 4-5: Isentropic expansion
- 5-1: Isochoric heat rejection

For the model the first 4 stages are of particular interest as they describe the combustion process in the closed cylinder. The last stage, isochoric heat rejection, is not part of the closed cylinder process in a real engine as the exhaust gases are blown out and the cylinder is filled with fresh, relatively cold air. By dividing the complex combustion process of the closed cylinder into the 4 distinct Seiliger stages, thermodynamic state variables (temperature, pressure, volume) and process quantities (work and heat) can be easily calculated by following the first law of thermodynamics for a closed system. The equations for the distinct stages will not be elaborated in this research, the interested reader is referred to scientific literature on thermodynamics [e.g. (Moran & Shapiro, 2006)]. By expressing the state variables as ratios between the different stages, the Seiliger cycle is summarized to a few characteristic parameters, shown in the following table (Klein Woud & Sapersma, 2002):

| Stage | Volume ratio | Pressure ratio | Temperature ratio | Work (per kg trapped air) | Heat (per kg trapped air) |
|-------|-----------------------------------|---|---|--|------------------------------|
| 1-2 | $\frac{V_1}{V_2} = r_c$ | $\frac{p_2}{p_1} = r_c^\kappa$ | $\frac{T_2}{T_1} = r_c^{\kappa-1}$ | $w_{12} = \frac{R(T_2-T_1)}{\kappa-1}$ | – |
| 2-3 | $\frac{V_3}{V_2} = 1$ | $\frac{p_3}{p_2} = a$ | $\frac{T_3}{T_2} = a$ | – | $q_{34} = c_v(T_3 - T_2)$ |
| 3-4 | $\frac{V_4}{V_3} = b$ | $\frac{p_4}{p_3} = 1$ | $\frac{T_4}{T_3} = b$ | $w_{34} = R(T_4 - T_3)$ | $q_{34} = c_p(T_4 - T_3)$ |
| 4-5 | $\frac{V_5}{V_4} = \frac{r_c}{b}$ | $\frac{p_4}{p_5} = \left(\frac{r_c}{b}\right)^\kappa$ | $\frac{T_4}{T_5} = \left(\frac{r_c}{b}\right)^{\kappa-1}$ | $w_{45} = \frac{R(T_5-T_4)}{\kappa-1}$ | – |

Table 4.1: Analytical definition of the Seiliger cycle process

Where:

r_c = effective compression ratio

κ = specific heat ratio of air,

R = gas constant of air in J/kgK

c_v = specific heat at constant volume of air in J/kgK

c_p = specific heat at constant pressure of air in J/kgK

a, b = Seiliger parameters

The effective compression ratio can be estimated within reasonable accuracy based on data of the geometric compression ratio of existing engines. As the compression ratio is adapted from the geometry of the engine, it remains constant across the engine's speed and power envelope. Data on the Seiliger parameters however is not provided by any manufacturer of diesel engines. For the nominal point, these parameters can be estimated with data on the maximum cylinder pressure, p_{max} . In the Seiliger cycle, pressure reaches its maximum in stage 3, after isochoric combustion has taken place, therefore $p_3 = p_{max}$. With pressure in stage 2 determined by the compression ratio, Seiliger parameter can be calculated with equation 4.1.

$$a = \frac{p_{max}}{p_2} \quad (4.1)$$

In case of a turbocharged engine, the inlet pressure of the cylinder is higher than atmospheric. Often the manufacturer gives values of the charge air pressure, corresponding to the pressure of the fresh air after the turbocharger. Due to losses in the inlet duct, this pressure is not exactly equal to the inlet pressure but sufficiently accurate. The inlet pressure corresponds to the pressure in stage 1 of the Seiliger cycle, p_1 .

For Seiliger parameter b , the heat input to the cycle has to be determined, which can be calculated with data on the fuel consumption and the engine's efficiency in the nominal point. Then the parameter b follows from:

$$b = \frac{q_{in} - q_{23}}{c_p * T_3} + 1 \quad (4.2)$$

Where:

q_{in} = total heat input per kg trapped air in kJ/kg

q_{23} = heat input per kg trapped air in kJ/kg during isochoric combustion

Unfortunately, the relation between heat input during isochoric combustion and isobaric combustion does not remain constant if the engine load and speed are reduced. Based on measurements by Schulten (Schulten, 1998), the heat input during isochoric combustion is linearly decreasing with decreasing engine speed.

Work is delivered by the cycle during isobaric expansion and isentropic expansion ($w_{23} + w_{34}$), whereas some of the work is required for the compression (w_{12}). As the Seiliger cycle does not consider mechanical losses, the remaining work delivered is denoted as indicated work W_i (or w_i if the indicated work is expressed per kg trapped air). By comparing the indicated work to the actual delivered power in the nominal point, the losses can be estimated. The losses are assumed to be linearly dependent on the engine speed and therefore represent the findings of the friction model developed by Chen & Flynn (Chen & Flynn, 1965). The mechanical losses are expressed in the mechanical efficiency η_m . The delivered torque of the engine can then be calculated by:

$$M_{eng} = \frac{i * w_i * m_1 * \eta_m}{2\pi * k} \quad (4.3)$$

Where

m_1 = mass of trapped air in the closed cylinder process in kg

i = amount of cylinders

k = number of revolutions per cycle (2 for a four-stroke engine)

Heat release model

The heat release model estimates the heat released during isochoric and isobaric combustion. The total heat input is defined by the amount of injected fuel, m_f , and influenced by heat release efficiency η_{qr} , summarizing the losses to the cooling water and lubrication oil, and the combustion efficiency η_{comb} , being an indicator for the amount of incomplete combustion taking place in the cylinder. In this model the heat release efficiency is assumed constant. The combustion efficiency is of particular interest during incomplete combustion and therefore a function of the air excess ratio λ . The combustion efficiency is modelled according to the combustion model of Betz and Woschni (Betz & Woschni, 1986).

The heat input to the cycle is then split into heat released during isochoric and isobaric combustion according to the following relations:

$$Q_{cv} = Q_{in} * X_a \quad \text{and} \quad Q_{cp} = Q_{in} * (1 - X_a) \quad (4.4)$$

Where Q_{in} denotes total heat input to the cycle, Q_{cv} and Q_{cp} the heat released during isochoric (constant volume: cv) respectively isobaric (constant pressure: cp) combustion. The parameter X_a is calculated by:

$$X_a = 2 * X_{a,nom} - \frac{n}{n_{nom}} * X_{a,nom} \quad (4.5)$$

Where n represents the engine speed (n_{nom} : engine speed in the nominal point) and parameter $X_{a,nom}$ the ratio of heat released during isobaric combustion in the nominal point, determined by Seiliger parameters a and b .

The air excess ratio forms an important parameter in the evaluation of the dynamic performance and the thermal loading of the engine. The air excess ratio describes the amount of actual combustion air in the cylinder to the minimum amount of combustion air needed for complete combustion. If the air excess ratio increases, more air is present in the cylinder at the moment the injected fuel is burned. And therefore the resulting temperature of the gas mixture after combustion is reducing. Thus the maximum cylinder temperature and the air excess ratio are directly related. In practice, the maximum cylinder temperature is impossible to measure, but the air excess ratio can be determined based on the composition of the exhaust gases.

In the model, the air excess ratio is determined by:

$$\lambda = \frac{afr}{\sigma}$$

Where

afr = actual air to fuel ratio

σ = air to fuel ratio for complete combustion (stoichiometric air to fuel ratio) = 14,5 for diesel oil

The actual air to fuel ratio is calculated with:

$$afr = \frac{m_1}{m_f} = \frac{\left(\frac{p_1 * V_1}{R * T_1}\right)}{m_f}$$

Where m_1 denotes the trapped mass of pure air in Seiliger stage 1 and m_f denotes the amount fuel injected per cycle. In practice, the trapped mass of air will also contain remaining exhaust gases of the previous combustion cycle and the trapped mass of pure air will be lower. However, in modern turbocharged 4-stroke engines with Miller timing, scavenging of the cylinder is very good and a scavenge efficiency of 100% can be assumed. In this case the pseudo air excess ratio λ^* , based on trapped air with remaining exhaust gases, is equal to the air excess ratio λ .

Exhaust system model

The exhaust system model represents the turbocharger of the diesel engine. It estimates the inlet pressure p_1 , based on the amount of heat rejected from the cycle Q_{51} . The ideal first-order dynamic model for the turbocharger, consisting of a turbine providing torque, a compressor requiring torque and the shaft dynamics, is simplified to a static system model (Miedema & Lu, 2002).

$$Q_{51} = \frac{m_1 * c_p * T_a}{\eta_{TC}} * \left[\left(\frac{p_1}{p_a} \right)^{\frac{\kappa-1}{\kappa}} - 1 \right] \quad (4.6)$$

Where

T_a = Ambient temperature in °C

p_a = Ambient pressure in Pa

η_{TC} = Efficiency of the turbocharger including losses in the intake and exhaust system

Parameters m_1 and η_{TC} are calculated in the nominal point and held constant for deviating engine speed and load.

To model the turbocharger inertia, a first order transfer function is added:

$$\frac{dp_1}{dt} = \frac{p_{1,est} - p_1}{\tau_{TC}} \quad (4.7)$$

Where $p_{1,est}$ represents the estimated inlet pressure determined with equation 4.6 and τ_{TC} a time delay representing the delayed response of the turbocharger due do its rotary inertia.

Fuel pump model

The fuel pump model relates the amount of fuel injected to the cylinder for each cycle, m_f , to the setpoint of the fuel pump X_{set} . The inertia of the pump is again modelled by a first order transfer function:

$$\frac{dm_f}{dt} = \frac{X_{set} - X_{act}}{\tau_X} * \frac{m_{f,nom}}{X_{nom}} \quad (4.8)$$

With

X_{act} = actual position of the fuel pump

X_{nom} = position of the fuel pump in nominal point

$m_{f,nom}$ = amount of fuel injected in nominal point in g

For a mechanical fuel pump the position of the pump describes the actual displacement of the lever. For an electric fuel pump the position however can be better interpreted as the control voltage.

Governor model

The setpoint of the fuel pump is determined by the governor based on the difference between actual and desired engine speed. In spite of research showing that torque-control of diesel engines in naval applications might be more suitable in preventing thermal overloading (Geerstma, Negenborn, Visser, & Hopman, 2016), the majority of diesel engines uses speed-control strategy.

The governor model consists of a PID-controller as given by the following expression:

$$\frac{X_{set}}{X_{nom}} = K_P \left(\frac{n_{set}}{n_{nom}} - \frac{n_{act}}{n_{nom}} \right) + K_I \int_0^t \left(\frac{n_{set}}{n_{nom}} - \frac{n_{act}}{n_{nom}} \right) dt + K_D \frac{d}{dt} \left(\frac{n_{set}}{n_{nom}} - \frac{n_{act}}{n_{nom}} \right) \quad (4.9)$$

Where:

n_{set} = desired engine speed in Hz

n_{nom} = nominal engine speed in Hz

n_{act} = actual engine speed in Hz

K_P = Proportional gain = 2

K_I = Integral gain = 0.5

In the current version of the model, the derivative term is not used. Therefore the derivative gain, K_D , is set to 0. Further, the governor limits the setpoint of the fuel pump with an upper limit of 105% and a lower limit of 1% of the nominal position.

During part-load operation, the maximum torque is limited due to the turbocharger limit. This results in the well-known engine limit or load limit. The turbocharger limit is dependent on the size of the turbocharger, the efficiency and the resulting charging pressure. If a large turbocharger with high charge pressure is used, the drop in maximum torque in part load is larger than in case of a smaller turbocharger. Because of limited amount of data on the turbocharger on marine diesel engines, the following limit is assumed due to the turbocharger limit:

| Engine speed | Engine Torque |
|---------------------------|------------------------|
| n_{\min} | $\frac{1}{4} T_{\max}$ |
| $n_{\min} < n < n_{\max}$ | Cubic curve |
| $0.9 n_{\max}$ | T_{\max} |
| n_{\max} | T_{\max} |

Table 4.2: Engine torque limit

The resulting limit is shown in the following figure.

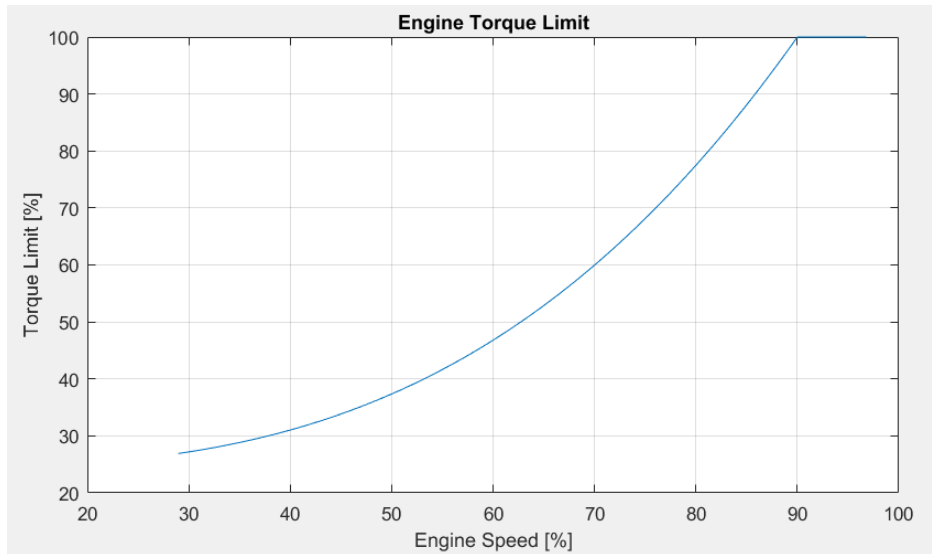


Figure 4.1: Engine Torque Limit

Gas Turbine Model

For gas turbine models the situation is similar to diesel engines. Many different approaches do exist to model the behavior and performance of gas turbines, ranging from simple analytical models based on the Brayton Cycle (Moran & Shapiro, 2006) to very complex CFD-models simulating the combustion process.

For this research the detailed transient performance of the gas turbine is of lesser importance. The gas turbine model is used in the reference model to show the performance of the LCF, meaning a detailed model to improve dynamic performance of the propulsion plant is not necessary.

Further, marine gas turbines can be divided into two components, the gas generator and the free power turbine (see also background section). The two components are mechanically not connected, changes in load of the free power turbine have nearly no effect on the gas generator. Detailed data on the fuel consumption of the gas turbine related to turbine speed and delivered power of the free power turbine is available. With this data a simple empirical model for the free power turbine can be set up.

Free Power Turbine

The free power turbine model determines the delivered power of the turbine based on the free power turbine speed and the fuel flow to the gas generator. Therefore, the data from the fuelmap of the Rolls Royce Spey SM1C gas turbine was fitted to the following function, known as the Mossel model:

$$P^* = 1 - a(1 - n^*) + b(1 - n^*)^2 - c(1 - \dot{m}_f^*) + d(1 - \dot{m}_f^*)^2 + 2e(1 - n^*)(1 - \dot{m}_f^*) \quad (4.10)$$

With:

P^* = non-dimensional power P/P_{nom}

n^* = non-dimensional turbine speed n/n_{nom}

\dot{m}_f^* = non-dimensional fuel flow $\dot{m}_f/\dot{m}_{f,nom}$

The datapoints used to fit the function are given in Appendix E. Fitting resulted in the following values of the fitting parameters a – e:

| a | b | c | d | e |
|---------|---------|--------|---------|--------|
| -0.0470 | -0.8884 | 1.1724 | -0.1904 | 0.4540 |

Table 4.3: Gas turbine fitting parameters

Figure 4.2 shows the data form the fitted function compared to the actual fuelmap. For high fuel flows, the fitted function represents the power of the gas turbine well. With lower fuel flows however, power deviates for low and high turbine speeds. During the simulation, very low fuel flows should be avoided.

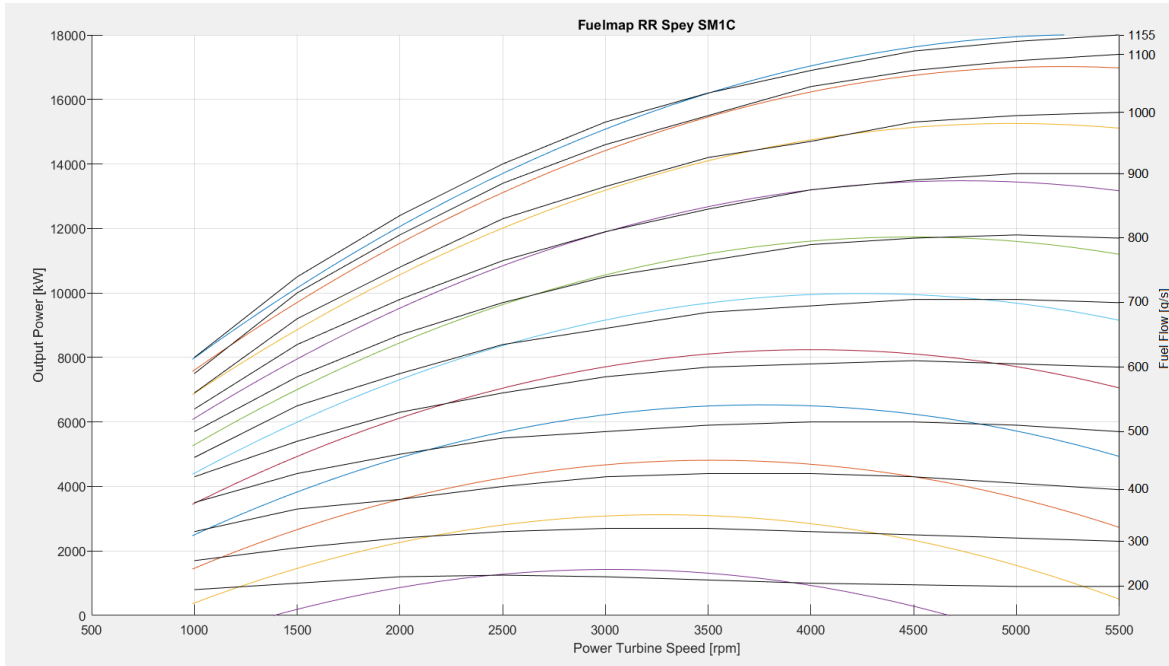


Figure 4.2: Results fitted Mossel model RR Spey SM1C, black lines represent real data

Fuel pump model

The fuel pump model for the gas turbine is adapted from the fuel pump model of the diesel engine. Instead of the fuel pump position X , the opening ratio of the fuel valve θ is used, resulting in:

$$\frac{d\dot{m}_f}{dt} = \frac{\theta_{set} - \theta_{act}}{\tau_\theta} * \frac{\dot{m}_{f,nom}}{\theta_{nom}} \quad (4.11)$$

Governor model

The governor of the gas turbine is also adapted from the diesel engine model. For the gas turbine, the same settings are used compared to the diesel engine. Without the derivative term, the PI-controller is determined by the following expression:

$$\frac{\theta_{set}}{\theta_{nom}} = K_P \left(\frac{n_{set}}{n_{nom}} - \frac{n_{act}}{n_{nom}} \right) + K_I \int_0^t \left(\frac{n_{set}}{n_{nom}} - \frac{n_{act}}{n_{nom}} \right) dt \quad (4.12)$$

With

$K_P =$ Proportional gain = 2

$K_I =$ Integral gain = 0.5

E-Drive Model

Induction motors are known for their reliability and require little to no maintenance. With proper control, induction motors are able to deliver nominal torque for all speeds up to nominal speed. Therefore, the induction motor does not require a strict control system (as e.g. the diesel engine to prevent thermal overloading) and thus a detailed model, based on first principles, is not required for this research. In fact, a detailed model is rather obstructive as these models require specific data of the motor which is hard to come by. An empirical model for the induction motor is sufficient for this research.

In a first attempt to set up an easy model for an induction motor, data on induction motors provided by ABB (ABB, 2011) and the NEMA standards (NEMA, 2009) was used. For induction motors with an output power up to 370 kW, the NEMA standards defines characteristic values on the speed-torque curve for an class B motor. With these values, the torque-speed curve can be fairly easy reproduced, see figure 4.3.

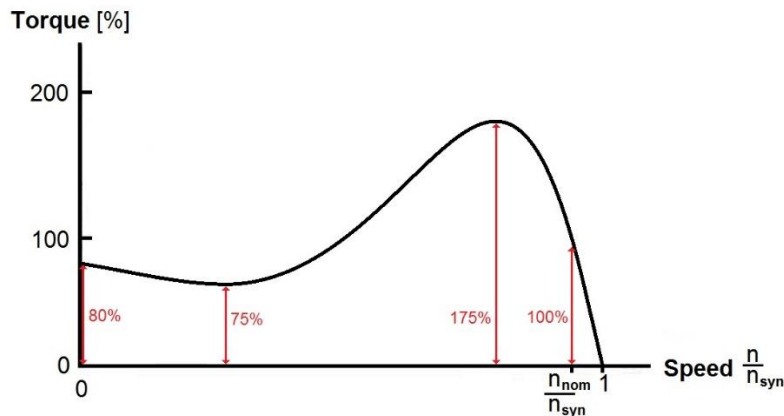


Figure 4.3: Torque-Speed curve NEMA 500 HP Induction Motor

However, the speed-torque curve for larger induction motors deviates from the curve defined in the NEMA standards. The speed torque-curve for large induction motors does not show the typical dip with a minimum torque, the pull-up torque. Due to the small slip values, the break-down torque is reached close to the nominal point, therefore rising sharp till the maximum and afterwards falling slightly less steep, see figure 4.4.

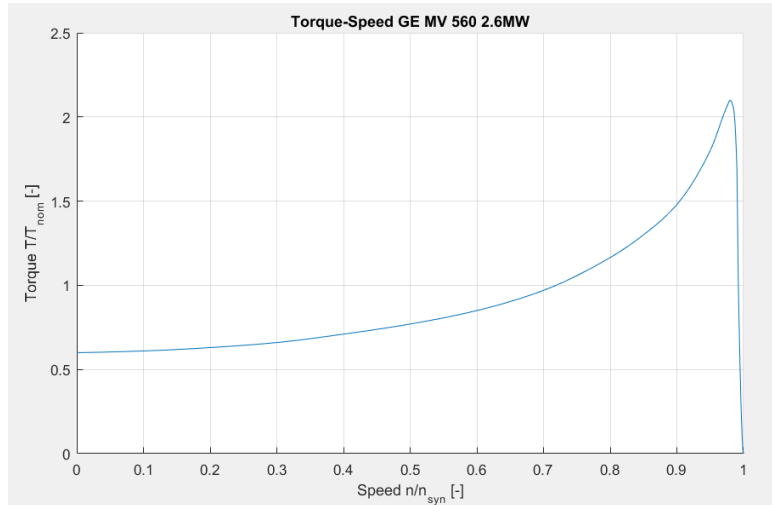


Figure 4.4: Torque-Speed curve large industrial induction motor

This curve is used with a lookup-table in the model to relate the speed of the motor to the maximum generated torque. In the lookup-table, non-dimensional motor speed is set as breakpoints whereas non-dimensional torque is set as table data.

As stated earlier, if the induction motor is controlled by a variable frequency drive, the characteristic speed-torque curve shifts linearly with changing supplied frequency. Up to nominal engine speed, the motor is able to generate the nominal torque with constant slip if the supplied voltage increases linearly with the frequency to keep the motor flux constant. For engine speeds higher than nominal, the delivered mechanical power remains constant, therefore the generated torque decreases. The supplied voltage is held constant at nominal voltage and thus the flux of the motor decreases.

In the model, the speed setpoint is translated into a required supply voltage and frequency, according to the two different speed regimes.

4. Propulsion Model

| | Constant Flux | Field Weakening |
|----------------|---|---------------------------------------|
| | $n_{set} \leq n_{nom}$ | $n_{set} > n_{nom}$ |
| Frequency | $f_{set} = n_{set} * \frac{poles}{2}$ | $f_{set} = n_{set} * \frac{poles}{2}$ |
| Supply Voltage | $U_{set} = f_{set} * \frac{U_{nom}}{f_{nom}}$ | $U_{set} = U_{nom}$ |

Table 4.4: Frequency and supply voltage for two different speed regimes of induction motors

where

- n_{set} = desired speed of the induction motor in Hz
- n_{nom} = nominal speed of the motor in Hz
- f_{set} = frequency provided by the variable frequency drive in Hz
- poles = amount of poles in the motor
- U_{set} = voltage provided by the variable frequency drive in V
- U_{nom} = nominal voltage in V
- f_{nom} = nominal frequency in Hz

The motor speed is normalized by dividing with the set speed. As a result, the speed-torque curve is not shifted linearly to the supplied frequency, but the non-dimensional motor speed is shifted. By doing so, the lookup-table with data on the speed-torque curve is valid for the complete speed range of the motor.

For the constant flux range, the motor produces a constant maximum torque. If the motor is operated in the field weakening range, the maximum torque is reduced so the motor produced constant power. The maximum torque is decreased inversely proportional to the squared motor speed.

$$T_{max} \sim \left(\frac{n_{nom}}{n_{set}} \right)^2 \quad (4.13)$$

The motor current components (active and reactive current) were determined by formulas provided by ABB (ABB, 2011). For the active current I_{sq} below the field weakening point:

$$I_{sq} = I_n * \left(\frac{T_{load}}{T_n} \right) \cos(\varphi_n) \quad (4.14)$$

And for the reactive current I_{sd} below the field weakening point:

$$I_{sd} = I_n * \left(\sin(\varphi_n) + \cos(\varphi_n) \left[\sqrt{\left(\frac{T_{max}}{T_n} \right)^2 - 1} - \sqrt{\left(\frac{T_{max}}{T_n} \right)^2 - \left(\frac{T_{load}}{T_n} \right)^2} \right] \right) \quad (4.15)$$

Denoted with subscripted n for the motor's nominal point: current (I_n), phase angle (φ_n) and torque (T_n). Further requested torque (T_{load}) and maximum motor torque (T_{max}).

Above the field weakening point, the current components also depend on the ratio of current motor speed n to nominal motor speed n_n . For the active current:

$$I_{sq} = I_n * \left(\frac{T_{load}}{T_n} * \frac{n}{n_n} \right) \cos(\varphi_n) \quad (4.16)$$

And for the reactive current:

$$I_{sd} = I_n * \left(\frac{n}{n_n} \left(\sin(\varphi_n) + \cos(\varphi_n) \sqrt{\left(\frac{T_{max}}{T_n} \right)^2 - 1} \right) - \cos(\varphi_n) \sqrt{\left(\frac{T_{max}}{T_n} * \frac{n}{n_n} \right)^2 - \left(\frac{T_{load}}{T_n} * \frac{n}{n_n} \right)^2} \right) \quad (4.17)$$

The total motor current I_m is calculated with:

$$I_m = \sqrt{I_{sd}^2 + I_{sq}^2} \quad (4.18)$$

By determining the power factor, PF, also the electrical power could be calculated:

$$P_{el} = \sqrt{3} * U_{set} * I * PF \quad (4.19)$$

where I is the total motor current.

However, the formulas provided by ABB had a major drawback. Due to their lack of first principles, the formulas were only useful to determine current and power close to the nominal point. In part load conditions or with start-up of the motor, the apparent power deviates from actual values and therefore the resulting power factor is too high.

The following figures (4.4 and 4.6) show the results for direct on line start (the motor is connected directly to the power grid, therefore voltage and frequency are constant) and with control by a variable frequency drive, resulting in a constant slip.

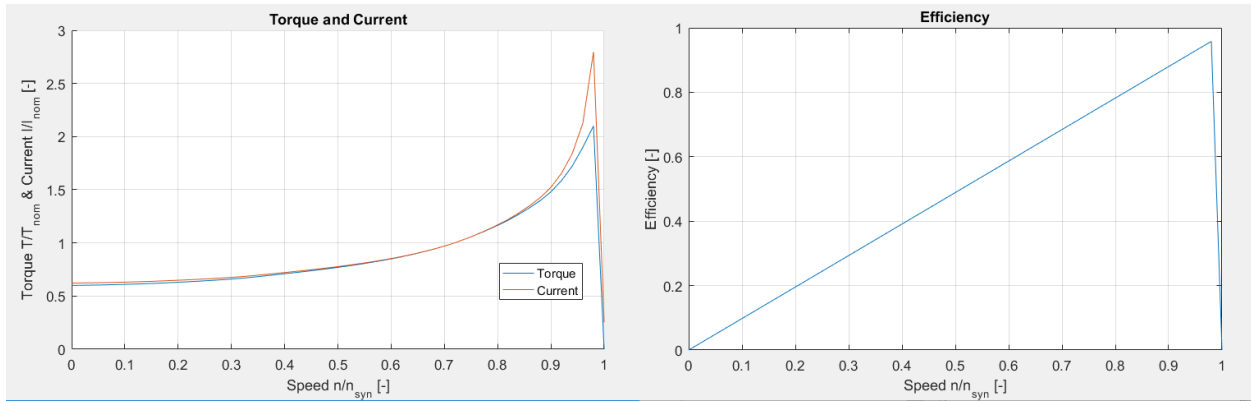


Figure 4.5: Torque, current and efficiency ABB formulas, DOL start

4. Propulsion Model

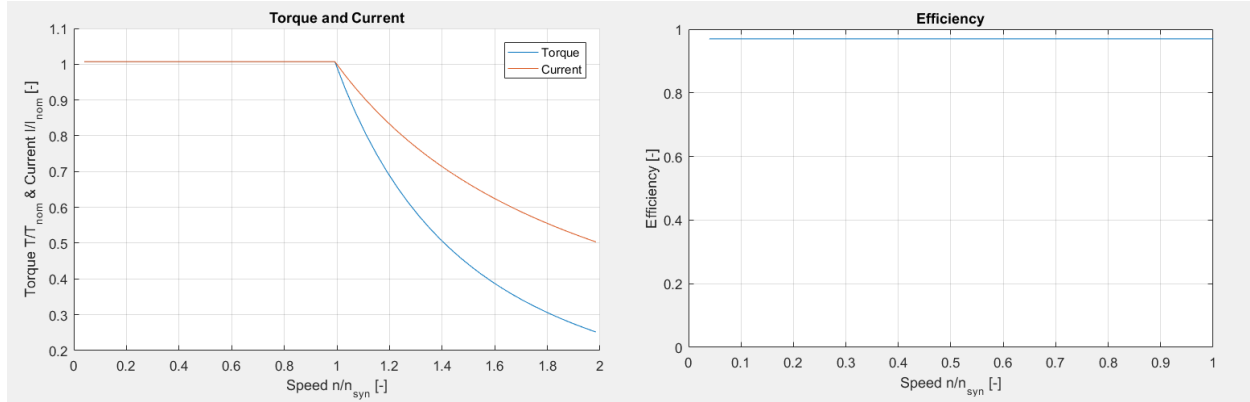


Figure 4.6: Torque, current and efficiency ABB formulas, start-up with VFD

As a result, the model does not generate suitable results for the electric power consumption. But the model does show the possibility of the variable frequency drive. With proper control, the simple motor model can generate constant torque for the constant flux range and constant power for the field weakening range.

But for this research the model can then be simplified even further. A simple look-up table, relating the speed of the motor to the maximum torque is sufficient to represent the characteristics of the induction motor.

Accurate measurements of the efficiency of large induction motors controlled with a variable frequency drive is hard to come by. This also holds for the efficiency of the variable frequency drives suited to control the necessary high powers and currents.

Based on measurements and simulation results of (Shumei, Chen, & Liwei, 2008) and (Heising, Staudt, & Steimel, 2011) for mid-size induction motors and data on the efficiency of VFDs by the U.S. Department of Energy (USDE, 2012), the following two curves for the efficiency of the components was set up. These curves will be used to determine the electric power consumed by the drive based on the delivered mechanical power.

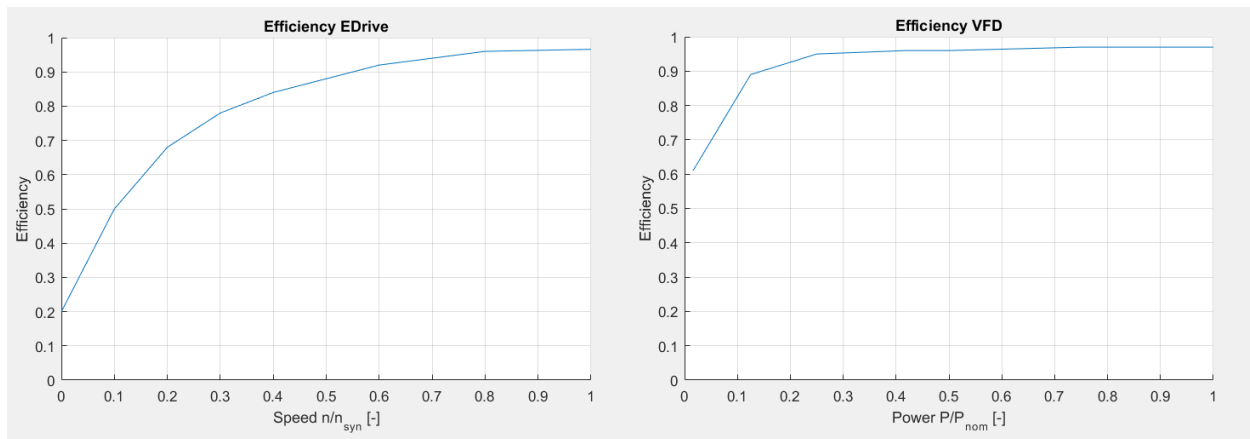


Figure 4.7: Efficiency VFD-controlled induction motor and efficiency of VFD

It should be noted that these curves are not based on measurements/verified models of large induction motors. The efficiency of larger motors increases with size. Therefore, the actual efficiency will probably not deviate much from the presented data. However, for an accurate calculation on the consumed electrical power, more research is needed.

Gearbox Model

Most naval vessels rely on the medium/high speed diesel engines and gas turbines in their propulsion plants. These prime movers run on much higher rotational speed than the propellers of these vessels. Especially considering a frigate designed for ASW-tasks, the propeller speed is desired to be as low as possible. To connect the propellers to the prime movers, a gearbox is therefore essential.

However, as any component in the propulsion plant, the gearbox introduces losses in the transmission of power from the prime mover to the water. Drijver (Drijver, 2013) distinguishes several losses within the gearbox: Losses in bearings and seals, losses due to friction of the mating gear teeth, expulsion (pumping effect of the mating gear teeth), oil churning (drag of the teeth in the oil bath) and aerodynamic friction. These losses are not only dependent on the speed of the gearbox but also dependent on the transmitted power.

Prediction of the individual losses, particularly with limited data on the gearbox, is nearly impossible. In this thesis the losses will be modelled with a simplified linear gearbox loss model proposed by Drijver (Drijver, Godjevac, de Vries, & Stapersma, 2015):

$$M_{loss}^* = a + b * n_{in}^* + c * M_{in}^* \quad (4.20)$$

Where M_{loss}^* is the normalized torque loss, n_{in}^* is the normalized input speed (engine side) and M_{in}^* is the normalized input torque (engine side). Coefficients a, b and c are used to fit the linear model to the a thermal network model, also proposed by Drijver. This linear gearbox model was verified for part-load and heavy loading by a bachelor research project at the Delft University of Technology (de Jong, Rollema, Volger, & Schillings, 2015).

For this research, choices on a specific gearbox are not made. Therefore, the linear gearbox model will be fitted to measurement data on the losses of the gearbox of the LCF, operating in a comparable power and speed range. Fitted to the gearbox losses of the LCF, the coefficients a, b and c are determined:

$$\begin{aligned} a &= 0.6725 \\ b &= 0.1613 \\ c &= 0.1609 \end{aligned}$$

Figure 4.8 shows the results from the linear gearbox model compared to the actual measurements of the LCF.

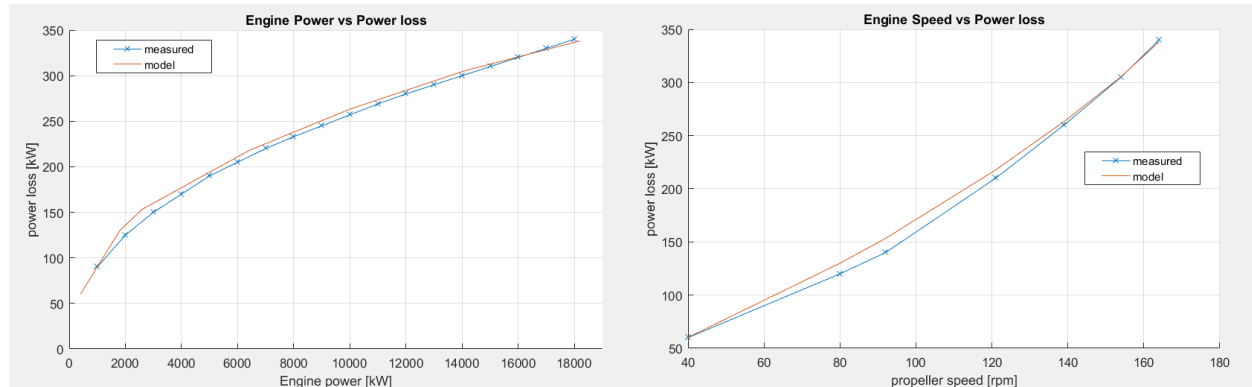


Figure 4.8: Results of fitted gearbox function

The ratio between the input speed, equal to the engine speed n_{eng} , and the speed of the output shaft n_s is introduced as gearbox ratio i_{GB} :

$$i_{GB} = \frac{n_{eng}}{n_s} \quad (4.21)$$

Across the gearbox the law of conservation of energy must hold. Therefore, the ratio of input torque (reduced by the torque loss) to output torque is equal to the inverse of the gearbox ratio.

$$\frac{1}{i_{GB}} = \frac{M_{GB,in} - M_{loss}}{M_{GB,out}} \quad (4.22)$$

Propeller Model

The model will use two different propellers, the fixed pitch MARIN propeller (see appendix D) and the controllable pitch Wageningen C5-75 propeller. As the CPP has to offer the possibility of changing the pitch of the propeller during the simulation, the model of the CPP will have to differ from the model of the FPP.

Another different is caused by the available data of the propellers. For the CPP, data of the four quadrant measurement is available in hydrodynamic pitch angle β versus thrust and torque loading coefficients C_T^* and C_Q^* . This data is of particular interest if stopping and reverse maneuvers are simulated (Klein Woud & Sapersma, 2002). For the FPP, only the open water diagram is available, using other parameters to determine thrust and torque and therefore also requiring a diverging propeller model.

Propeller thrust force and torque are determined with a quasi-static approach of the propeller inflow, based on the data of the four quadrant measurement and open water diagram. With this approach thrust and torque are only dependent on the ship speed (advance speed) and propeller speed. The inertia of the water, resulting in a transient inflow, causes a slight decrease in advance speed just before the propeller. This increases the thrust force of the propeller slightly compared to the static calculations (Amini & Steen, 2012). The effect is very small and is considered negligible as the quasi-static approach is used in several important research publications for marine engineering [e.g. (Vrijdag, 2009); (Geerstma, Negenborn, Visser, & Hopman, 2016)].

CPP

To read out the four quadrant diagram, the model determines the hydrodynamic pitch angle of the working point of the propeller.

$$\beta = \arctan\left(\frac{v_a}{0.7\pi * n_p * D}\right) \quad (4.23)$$

Where

n_p = rotational speed of the propeller in Hz

D = propeller diameter in m

v_a = disturbed advance speed relative to the propeller in m/s

The disturbed advance speed follows from:

$$v_a(t) = v_s(1 - w) + v_w(t) \quad ref. (2.38)$$

A multi-dimensional lookup table is used, linearly interpolating a four quadrant diagram for every pitch setting from the provided data on several specific pitch angles of the propeller. With the hydrodynamic pitch angle, the thrust and torque loading coefficients are read out.

The delivered thrust of the propeller is calculated with:

$$T = C_T^* * \frac{1}{2} \rho * \left(v_a^2 + (0.7\pi * n_p * D)^2 \right) * \frac{\pi}{4} * D^2 \quad (4.24)$$

And the requested torque of the propeller follows from:

$$Q = C_Q^* * \frac{1}{2} \rho * \left(v_a^2 + (0.7\pi * n_p * D)^2 \right) * \frac{\pi}{4} * D^3 \quad (4.25)$$

Due to the interaction of the propeller with the hull, the requested torque of the propeller installed after a ship slightly deviates from the torque in case of an open water propeller. Therefore the relative rotative efficiency η_r is introduced:

$$\eta_r = \frac{Q}{M_p} \quad (4.26)$$

Where M_p is the actual requested torque of the propeller installed after the vessel.

In some literature, the squared hydrodynamic velocity is used in equations 4.24 and 4.25, where the hydrodynamic velocity is given by:

$$v_h = \sqrt{v_a^2 + (0.7\pi * n_p * D)^2}$$

The efficiency of the propeller η_o can also be determined with the data from the four quadrant diagram:

$$\eta_o = 0.35 * \tan \beta * \frac{C_T^*}{C_Q^*} \quad (4.27)$$

FPP

The calculations for obtaining delivered thrust and requested torque of the propeller are similar to the calculations of the CPP. Instead of the hydrodynamic pitch angle, the advance ratio J is used to relate ship speed to propeller speed:

$$J = \frac{v_a}{n_p * D} \quad \text{ref. (2.27)}$$

By using the advance ratio instead of the hydrodynamic pitch angle, it will not be possible to determine thrust and torque if the propeller speed approaches zero as the advance ratio approaches infinity. However, this case will not occur in this model since the minimum propeller speed is limited by the minimum speed of the diesel engine.

With the open water diagram the thrust and torque coefficients K_T and K_Q are obtained. With the coefficients, delivered thrust and requested torque are calculated by:

$$T = K_T * \rho * n_p^2 * D^4 \quad \text{ref. (2.25)}$$

$$Q = K_Q * \rho * n_p^2 * D^5 \quad \text{ref. (2.26)}$$

By using the open water diagram, the efficiency of the propeller follows from:

$$\eta_o = \frac{1}{2\pi} * \frac{K_T * J}{K_Q} \quad \text{ref. (2.24)}$$

Shaft Model

The shaft model consists of the equation of motion of the shaft system:

$$\frac{dn_s}{dt} = \frac{M_{GB,out} - M_p}{I_{tot} * 2\pi} \quad (4.28)$$

Where I_{tot} is the total moment of inertia of the shaft system including all coupled components. This moment of inertia follows from:

$$I_{tot} = I_p + I_{shaft} + I_{GB} + i_{GB}^2(k_{DE} * I_{DE}) + i_{ed}^2(I_{ed}) \quad (4.29)$$

Where:

I_p = inertia of the propeller and entrained water in kgm^2

I_{shaft} = inertia of the shaft

I_{GB} = inertia of the gearbox

k_{DE} = amount of diesel engines per shaft

I_{DE} = inertia of the diesel engine

i_{ed} = gearbox ratio of the e-drive

I_{ed} = inertia of the e-drive

Ship Model

The ship model relates the speed of the ship to the generated thrust of the propellers. The relation between ship speed v_s and thrust is given by:

$$\frac{dv_s}{dt} = \frac{T_{tot} * (1 - t) - R_{tot}}{m} \quad (4.30)$$

Where

T_{tot} = thrust generated by both propellers in kN

t = thrust deduction factor, assumed constant = 0.068

R_{tot} = total resistance of the vessel in kN

m = mass of the vessel in kg

The total resistance of the vessels consists of the hull resistance, R_{hull} , multiplied by the service margin and the resistance of the towed array in case it is towed by the vessel. The service margin, SM, combines additions to the resistance due to fouling, small changes in displacement and the average added resistance due to waves.

For low ship speeds, corresponding with a low Froude-number, the wave resistance of the hull is considered relatively low and thus the following equation holds for the hull resistance:

$$R_{hull} = c_1 * v_s^2 \quad ref. (2.1)$$

Where c_1 is the nominal resistance factor in kg/m .

If the ship speed increases however, the wave resistance plays an increasingly important role. For naval vessels sailing at higher speeds, the resistance curve will be much steeper and the following equation is more accurate:

$$R_{hull} = c_1 * v_s^3 \quad ref. (2.2)$$

For the new vessel, calculations on the hull and its resistance have already been executed by DMO. The resistance curve has been determined (see appendix B) and therefore will be used in the model with a look-up table. The resistance curve of the towed array was also determined by DMO (see appendix C) and the results will also be used with a look-up table, resulting in the following calculation of the total resistance:

$$R_{tot}(v_s) = R_{hull}(v_s) * SM + R_{LFAS}(v_s) \quad ref. (2.36)$$

Control Parameters

The dynamic simulation model is controlled by a set of parameters defined by the user, referred to as control parameters. The simulation model can be executed with different sets of control parameters and their effect on the behavior of the propulsion plant model be studied. Definition of the control parameters is important for evaluating the acceleration performance of the propulsion plant models under different operational conditions. Further a clear definition of the control parameters increases the reproducibility of the simulation experiments.

The control parameters can be divided into three different categories:

- Constants: These parameters are held constant during the entire simulation experiment
- Initial Values: These parameters are starting-point values for the simulation model and may change during the execution of the experiment.
- Time dependent setpoints: These parameters are valid on the related instant of time of the experiment. Defined as breakpoints of a lookup-table, the intermediary values are obtained by linear interpolation.

Constants

The operational conditions are defined as constants. These control parameters are held constant during the entire simulation experiment. Simulation of different operational conditions is only possible by executing the simulation method with an adjusted set of control parameters.

The effect of weather and sea conditions are considered in the simulation experiment by defining the wave frequency in Hz and wave amplitude in m for the effect of the waves on the advance velocity. By setting these two control parameters to zero, calm sea is simulated.

Next to the effect on the advance velocity, the weather and sea conditions also affect the resistance of the vessel. For the hull resistance of the vessel, the resistance curve for trial conditions (no fouling, calm sea, design load and deep water) is used. To consider the average added resistance due to waves and wind, the service margin (SM) is increased. The service margin is a multiplication factor on the hull resistance.

The effects of fouling of the hull, change of displacement due to loading and effects of shallow water are also included in the service margin and need to be defined for the operational conditions.

In case the effect of the towed array is investigated, the resistance of the towed array is added to the hull resistance.

The last constant that needs to be defined for the control parameters is the hotel load in kW. This constant represents the additional electric load on the diesel generators caused by electrical consumers on the vessel.

Initial Values

For the simulation experiments, two initial values are important. The initial engine speed in Hz and the initial ship speed in m/s have to be given by the user. In most cases the initial engine speed will be set to the minimum engine speed to simulate the acceleration from rest or low ship speed. Setting the initial engine speed to a lower value is possible but physically not correct for diesel engines.

While simulating a propulsion plant with CPP, the initial ship speed can be set to zero to simulate an acceleration maneuver from rest. In practice this is possible with a CPP by decreasing the propeller pitch until no thrust is generated. With FPPs, the minimal engine speed also determines the minimal ship speed. An acceleration maneuver from rest is not possible.

Time dependent setpoints

The engine speed, propeller pitch and generated torque of the electric drives are controlled by a series of time dependent setpoints. For every setpoint the corresponding instant of time has to be provided as well. With these setpoints, a lookup table is filled and intermediary values are obtained by linear interpolation.

For the engine speed, the desired engine speed in rpm for an instance in time has to be provided. The governor of the model translates these setpoints, according to the actual engine speed, in a setpoint for the fuel pump.

For the propeller pitch setpoints, the propeller pitch ratio has to be provided. The actual propeller pitch follows the setpoints directly, only limited by the propeller pitch increase/decrease rate.

For the electric drives, the setpoints define the normalized torque (T/T_{nom}) delivered by the drives. Up to nominal engine speed nominal torque is available. For higher engine speeds the generated torque is decreased for constant power output even though the setpoints are set to 1.

Verification/Validation

Unfortunately, verification or validation of the complete propulsion model was not possible. Measurement experiments aboard frigates of the LCF-class of the Royal Netherlands Navy were requested, but until the end of this research project these measurement experiments were not executed.

Requested were measurements of the acceleration of the frigates on diesel engines and, if possible, on gas turbines. The acceleration maneuver contained of the acceleration from rest and the ramping up of the prime mover up until maximum engine speed. During the acceleration maneuver the time-trace of following propulsion plant data had to be recorded:

- Engine speed
- Propeller pitch
- Ship speed
- VRA setpoint
- Engine exhaust temperature
- Charge air pressure

Due to this lack of data, a validation based on real measurements has not been executed and is strongly suggested before further research is carried out with the developed model.

For this research, remaining option is a validation based on the results of the simulation model developed by Imtech. The results from the acceleration maneuver on diesel engines and gas turbines can be found in Appendix G. From these results, the setpoints for diesel engine speed and propeller pitch as used by Imtech can be reproduced. The resulting ship speed is given as well.

For the acceleration maneuver on diesel engines, the following setpoints for diesel engine speed and propeller pitch are used:

| | | | | | | |
|----------|-------|-----|-----|-----|------|------|
| t_set_n | [s] | 0 | 15 | 65 | 140 | 300 |
| n_set | [rpm] | 585 | 750 | 750 | 1000 | 1000 |
| t_set_PD | [s] | 0 | 28 | 65 | 120 | 300 |
| PD_set | [-] | 0 | .7 | .95 | 1 | 1 |

Table 4.5: Engine speed and pitch setpoints for acceleration maneuver LCF on DE

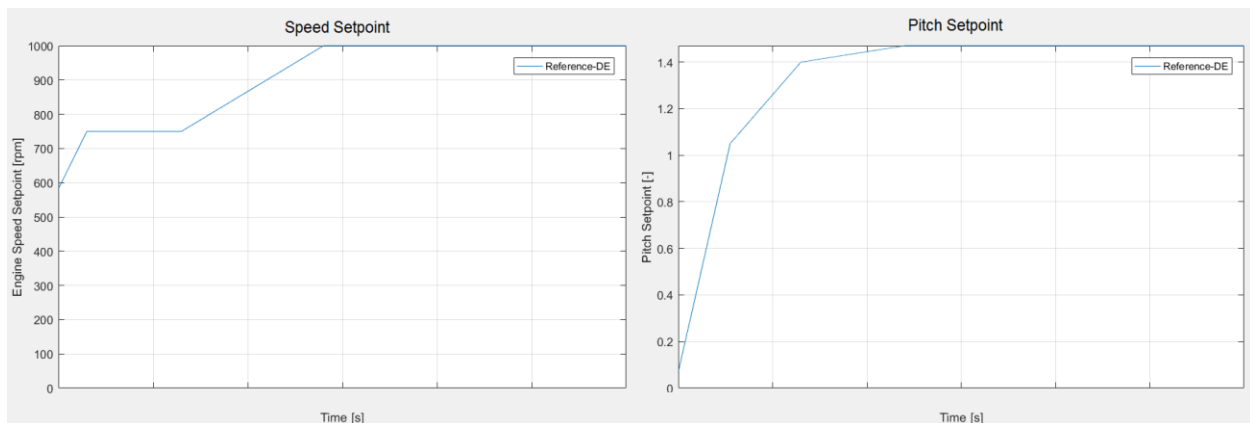


Figure 4.9: Setpoints for Engine Speed and Propeller Pitch of LCF on DE

The resulting ship speed is plotted in figure 4.10. In this figure, the resulting ship speed of the Imtech simulation is plotted as well. For the acceleration maneuver on diesel engines, the developed model is able to reproduce the results closely. However, the setpoints developed by Imtech for their simulation are not implemented in the actual controller of the LCF. The highest ramp rates used by Imtech are:

- Diesel Engine 3.3 rpm/s
- Propeller Pitch: 0.86 °/s

The used propeller pitch rate remains below the actual limit of the LCF with 1 °/s. But the diesel engine ramp up rate for the LCF is limited to 0.5 rpm/s, thus significantly reducing the acceleration of the LCF compared to the simulation model of Imtech.

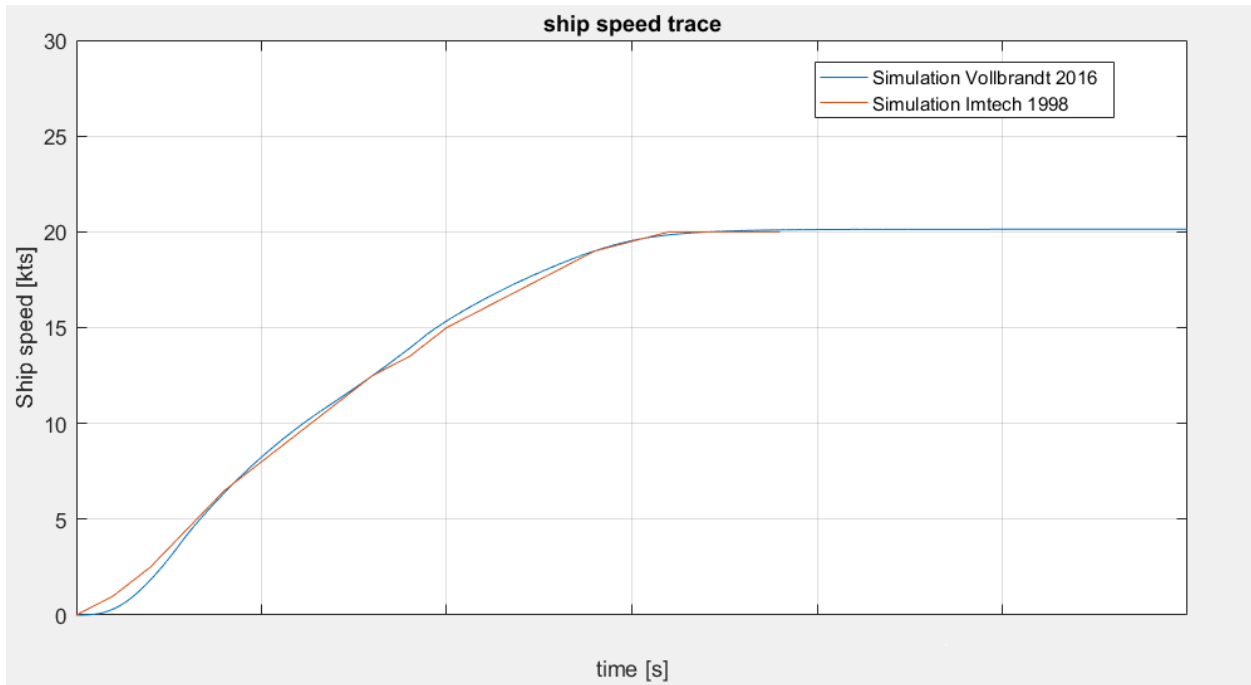


Figure 4.10: Comparison resulting ship speed time trace for acceleration maneuver LCF on DE

Therefore, the model is probably able to estimate the dynamic response of the actual LCF as well, as it is able to reproduce the simulation experiment of Imtech, but the accuracy of other relevant diesel engine data (temperatures, fuel consumption, charge air pressure) remains uncertain.

For the acceleration maneuver on gas turbines, the following setpoints for diesel engine speed and propeller pitch are used:

| | | | | | |
|----------|-------|------|------|------|------|
| t_set_n | [s] | 0 | 50 | 90 | 300 |
| n_set | [rpm] | 2000 | 4300 | 5360 | 5360 |
| t_set_PD | [s] | 0 | 35 | 300 | |
| PD_set | [-] | 0 | 1 | 1 | |

Table 4.6: Engine speed and pitch setpoints for acceleration maneuver LCF on GT

4. Propulsion Model

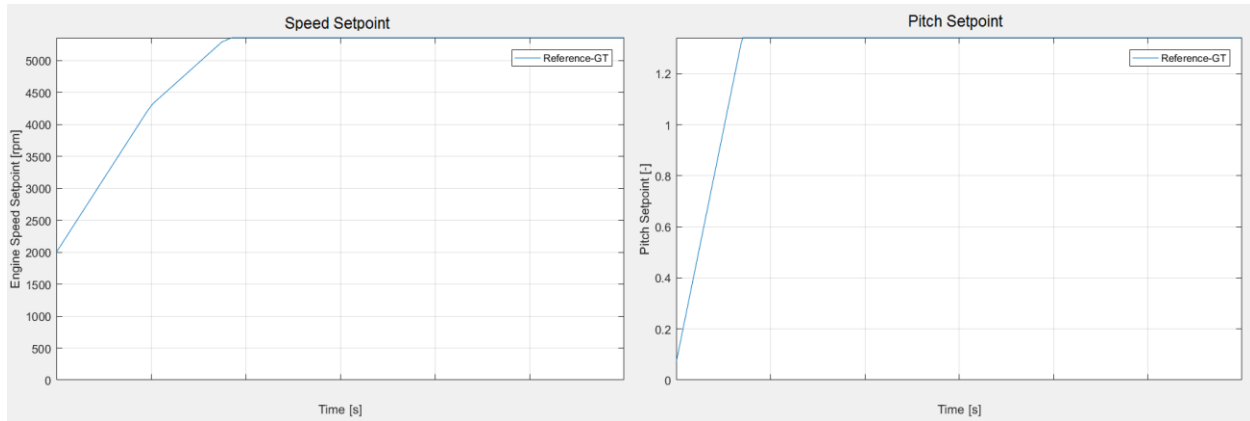


Figure 4.11: Setpoints for Engine Speed and Propeller Pitch of LCF on GT

The ship speed as estimated with both simulation models is plotted in figure 4.12. In contrast to the propulsion model on diesel engines, the propulsion model on gas turbines shows two significant deviations. The ship speed of the developed model is increasing faster than estimated by Imtech. Since the engine speed and propeller pitch setpoints are identical, the gas turbine model developed by the author provides significantly more torque at low engine speeds. Further, the resistance curve for high ship speeds deviates from the resistance curve of Imtech since full power of the gas turbine is not sufficient to propel the vessel to 30 knots. The estimated maximum speed reached is 28.3 knots, which is equal to estimations provided by DMO.

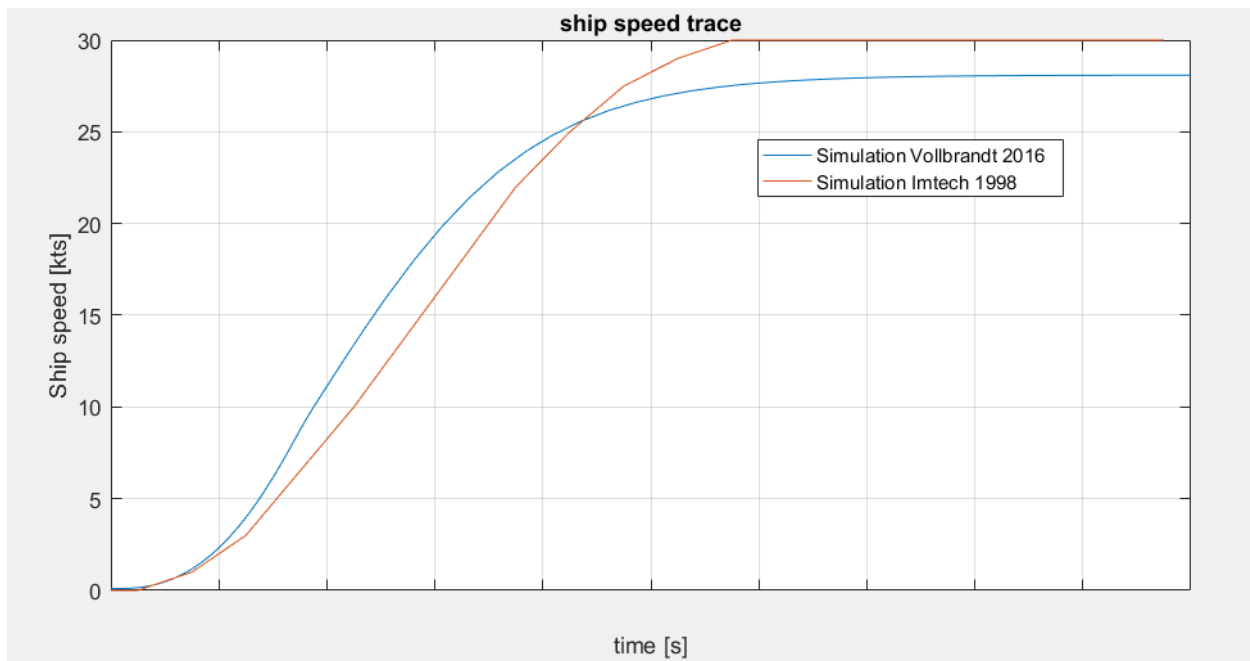


Figure 4.12: Comparison resulting ship speed time trace for acceleration maneuver LCF on GT

Especially for improving the accuracy of estimating the acceleration performance of the vessel on gas turbines, measurement data is required.

5. Simulations

With the developed propulsion models of the different concepts, several different simulations are executed.

Evaluation of thermal limits

With the dynamic simulation models, the performance of the propulsion plant under varying operational conditions can be tested. One very important aspect to evaluate is the load on the diesel engines while performing the simulation experiments. Overloading of the diesel engines should be avoided at any time and the thermal load on the engines should be reduced as much as possible.

However, the load increase rates that manufacturers provide are not very suitable for acceleration simulations with CPP. The load increase rates are time-dependent, whereas the maximum temperature is dependent on the charge air pressure of the turbocharger and thus engine speed-dependent. While the load is proportional to engine speed for a FPP, this does not hold for the CPP due to the variable pitch. New limits are therefore needed to evaluate the different concepts.

With the diesel engine model and included, limited, turbocharger model, some data on the temperatures within the diesel engine can be approximated. To obtain these values, simulation experiments are carried out that match the load increase rate of the manufacturer. Based on these simulations, the maximum values are set as limits for evaluating the concepts.

Maximum ship speed

The experiments for maximum ship speed contain a series of simulations in the static working point of maximum ship speed in design condition, sea state 3. These experiments are used to determine the gearbox ratio and service margin for each concept to achieve the speed close to overloading of the engines at maximum engine speed.

For sea state 3, a wave frequency of 0.14 Hz and a wave amplitude of 0.625 m is set. The service margin is set to 1.203, representing average fouling and average added resistance of sea state 3. During the simulations, the resistance of the towed array is also added.

Acceleration of Reference

This experiments include acceleration simulations of the reference – LCF. For the two propulsion models of the LCF, one with gas turbines and the other with diesel engines, the acceleration of the vessel is investigated.

For the simulations, the engine speed and pitch setpoints are used as determined by the simulation of Imtech, see section ‘Validation/Verification’. During the simulation, the vessel is accelerated from zero ship speed to transit speed on diesel engines and to maximum speed on gas turbines.

Acceleration Maneuvers FPP

This series of experiments investigate the behavior of the 4 concept propulsion plants equipped with fixed pitch propeller. The concepts are accelerated from an initial ship speed of 6 knots to maximum ship speed by increasing the engine speed from 30% to 100%. For concepts 1 – 3, the electric drives assist during the acceleration and after maximum ship speed is achieved. The generated torque is increased from 0% to 100%. For concept 4, the electric drives only assist during the acceleration. The generated torque is increased from 0% to 100% at the beginning of the experiment and after achieving the final ship speed, reduced from 100% to 0%.

For every concept, two simulations are executed: In trial condition and in design condition. During trial condition, calm sea without waves and no fouling is assumed. The service margin is set to 1.0. The towed array is not used. For design condition a wave frequency of 0.14 Hz and a wave amplitude of 0.625 m is set.

The service margin is set to 1.203, representing average fouling and average added resistance of sea state 3. During the simulations, the resistance of the towed array is also added.

| | Trial | Design | Off-Design |
|--------------------------|-----------|---------|------------|
| Service Margin | 1.0 | 1.203 | 1.6 |
| Resistance of LFAS | Not added | Added | Not added |
| Sea state | 0 | 3 | 6 |
| Wave frequency | 0 Hz | 0.14 Hz | 0.1 Hz |
| Wave amplitude | 0 m | 0.625 m | 3 m |
| Wave number | 0 | 0.08 | 0.04 |
| Water depth HL propeller | 4.5 m | 4.5 m | 4.5 m |

Table 5.1: Operational conditions

During the experiments, the following variables are investigated:

- Ship speed
- Ship acceleration
- Maximum cylinder temperature T_4 and air excess ratio λ
- Engine power and speed dependent load limit
- Engine torque

Acceleration Maneuvers CPP

The series of experiments investigating the behavior of the four concept propulsion plants equipped with controllable pitch propeller are similar to the previous experiments regarding FPP. However, next to increasing the engine speed from 30% to 100%, these concepts also offer the possibility to increase the propeller pitch from 0% to 100%.

The performance and thermal load on the diesel engines is highly dependent on the chronological sequence of pitch and engine speed. To determine suitable engine speed ramp-up rates, the engine ramp-up rates of the Danish Iver Huitfeldt-class frigate are used for concept 4 – CPP and the acceleration to maximum ship speed is investigated. For this acceleration maneuver trial conditions are assumed and the electric drives are not used. The pitch rates are fitted to the results of the acceleration times of Iver Huitfeldt-class frigates.

Due to deviating engine specifications of the Iver Huitfeldt-class frigates, the ramp-up rates of the diesel engines need to be slightly modified in terms of minimum and maximum engine speed and the switch-over point between the turbochargers.

With the resulting ramp-up rates the acceleration of the 4 concept propulsion plants equipped with CPP is investigated during trial and design condition. The concepts are accelerated from zero ship speeds to maximum ship speed by increasing the engine speed from 30% to 100% and the propeller pitch from 0% to 100%. For concepts 1 – 3, the electric drives assist during the acceleration and after maximum ship speed is achieved. For concept 4, the electric drives only assist during the acceleration.

During the experiments, the following variables are investigated:

- Ship speed
- Ship acceleration
- Maximum cylinder temperature T_4 and air excess ratio λ
- Engine power and speed dependent load limit
- Engine torque

Acceleration in off-design condition

This series of experiments investigates the behavior of the propulsion concepts while accelerating in off-design conditions. For concepts with FPP, an initial ship velocity of 6 knots is set, for CPP the initial velocity is set to zero. Due to the significantly increased resistance and the dynamic wave load, propeller pitch and engine speed cannot be increased to 100%. The maximum settings will be dependent on the loading of the engine as excess of the load limit should be prevented.

For off-design conditions, sea state 6 is assumed with a wave frequency of 0.1 Hz and a wave amplitude of 2.5 m. The service margin is set to 1.6, representing average fouling and average added resistance of sea state 6. The towed array is not used in this acceleration simulation.

In addition, the behavior of the concepts with FPP is investigated if the load limit is increased to match the engine envelope of a sequentially turbocharged engine. With increased load limit the behavior of the concepts are investigated under design and off-design condition. By changing the load limit, the charge air pressure will not be estimated correctly and results for maximum temperature and air excess ratio will not be representative. Therefore, the following variables are evaluated:

- Ship speed
- Engine power and speed dependent load limit
- Engine torque

Reduction Angle of Attack

Preventing cavitation or reducing the impact of underwater noise emission in case cavitation occurs is mainly influenced by the design and construction of the propeller. During operation of the vessel, the options in preventing cavitation are limited to reducing the ship speed below the cavitation inception speed (CIS). Above the CIS, the water velocity across the propeller blades is too high for cavitation-free operation. The CIS is a well-kept secret as it gives the vessel an edge over possible enemies.

For this research, a cavitation inception speed of 19 knots is assumed, a fair assumption for naval propellers. However, the actual magnitude of the CIS is irrelevant as this research focusses on the dynamic process of acceleration. During the dynamic simulation, the propeller speed is limited due to the cavitation inception speed, shifting the attention to the angle of attack that can be controlled well within a dynamic simulation. Preventing cavitation the angle of attack should be as close to zero as possible.

To minimize the angle of attack, control strategies for CPP and FPP are different. The angle of attack α is determined by:

$$\alpha = \theta - \beta \quad \text{ref. (2.32)}$$

For a FPP the pitch angle θ is fixed. Minimizing the angle of attack is only possible by maximizing the hydrodynamic pitch angle β . The hydrodynamic pitch angle represents the ratio of ship speed to propeller speed:

$$\beta \propto \frac{v_s}{n_p} \quad \text{ref. (2.32)}$$

So β is maximized if the shaft speed remains low compared to the ship speed while accelerating, resulting in a low ramp up of the diesel engines.

For a CPP the pitch angle is increasing while accelerating from zero ship speed. To minimize the angle of attack β has to be minimized as well. To reduce the hydrodynamic pitch angle, the propeller speed has to be increased compared to the ship speed. Therefore, the diesel engine is ramped up to the maximum shaft speed without cavitation as fast as possible while increasing the pitch slowly.

6. Results

The problem of thermal overloading

The current M-frigate (Karel Doorman-class frigate) was the first frigate of the Royal Netherlands Navy with diesel engines for propulsion. With gas turbines delivering power for high ship speeds, the diesel engines were intended for a very fuel-efficient cruising speed. Reducing the propeller pitch was originally intended to achieve ship speeds proportional to shaft speeds lower than the minimum engine speed. Excessive wear of the diesel engines resulted in unexpectedly high maintenance of this vessel. Investigation revealed excessive thermal overloading of the diesel engines in high sea states. As a consequence, the propulsion control system was expanded with a pitch reduction controller, reducing the pitch also in case the engines are close to overloading in high sea states (Vrijdag, 2009). Newer vessels of the RNLN with diesel engine propulsion, such as the LCF and the OPV, make use of low engine speed ramp-up rates and pitch control to sustain large margins to the engine load limit. Since adaption of the propulsion control system of the old M-frigate, thermal overloading of diesel engines on vessels of the RNLN was prevented.

However, the mechanical connection between engine and propeller, as well as the proportional relation between propeller speed and ship speed, couples the ramp-up of the engine speed to the acceleration of the vessel. Preventing overloading by reducing the engine ramp-up rate for all operational conditions cannot permit high maneuverability of the vessel. Therefore, the diesel engine has to be ramped up fast but without overloading the engine thermally.

To prevent thermal overloading of the engine, it is important to understand how and why this phenomenon happens. The term engine load limit was already used in the model description and the background sections. The load limit is a result of forced induction by means of a turbocharger. With decreasing engine speed, the exhaust mass flow through the turbine of the turbocharger reduces and the turbocharger cannot maintain the charge air pressure, see figure 6.1 (Grimmelius & Stapersma, The impact of propulsion plant control on diesel engine thermal loading, 2001). If the fuel rack is held constant, the air excess ratio decreases and as a result, the cylinder temperature increases. Figure 6.1 shows the temperature T_6 , the temperature before the exhaust valve opens.

Excessive temperatures in the cylinder will also result in a large heat transfer to the surrounding engine parts. Parts that are prone to exceeding their allowed temperature limit are: exhaust valve, piston head and cylinder liner. Above this temperature, thermal stresses might be too large, thermal expansion of components too severe or lubrication not guaranteed any longer. But also frequent high temperatures without exceeding the limit can cause harm, results in an accumulation of thermal stresses resulting in thermal fatigue of engine components.

Therefore, the injected amount of fuel is limited in part load conditions. This limit is also plotted in figure 6.1. The fuel limit results in the typical engine envelope with the load limit in part-load operation of the engine.

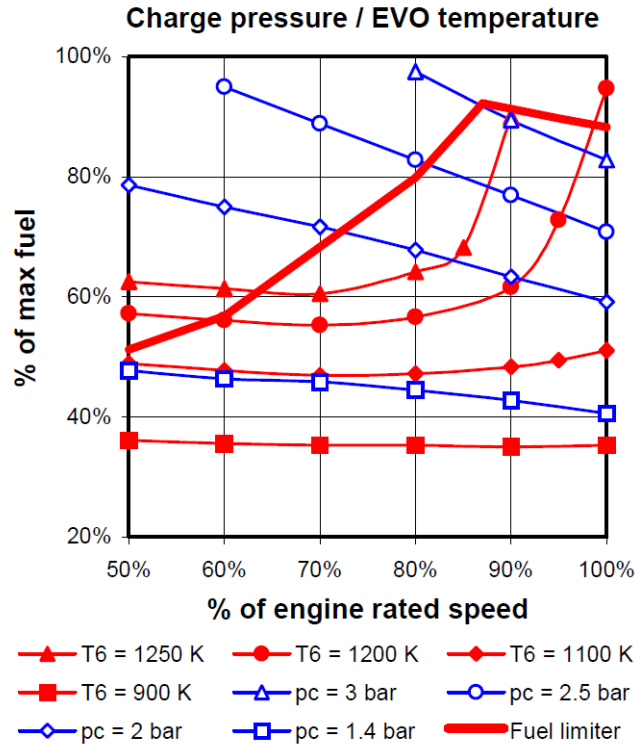


Figure 6.1: Charge air pressure and T_6 (Grimmelius & Stapersma, 2001)

In the design of the propulsion system of the M-frigate, the load limits were well known and the propeller and gearbox ratio were chosen in order to prevent overloading on every ship speed. However, the diesel engines were still overloaded. Measurements on the charge air pressure in a dynamic conditions show a drastically reduced charge air pressure (Grimmelius & Stapersma, The impact of propulsion plant control on diesel engine thermal loading, 2001). Due to the inertia of the turbocharger system, the charge air pressure lags behind in case the engine is accelerated. With a lagging charge air pressure, the air excess ratio is also lower than expected during a static condition. The fuel limit, based on the air excess ratio in static conditions, therefore allows too much fuel to be injected, resulting in excessive engine temperatures. Static calculations are not sufficient to predict and limit the maximum temperatures in the diesel engine.

To prevent clients from the necessity of setting up dynamic simulation models, manufacturers provide load increase rates for their diesel engines. By increasing the load according to the load increase rate, the turbocharger lag is limited and overloading is prevented.

However, the load increase rates are independent of engine speed, whereas the charge air pressure is, on the contrary, very dependent on the engine speed (with the exhaust mass flow). Due to the fixed pitch of a FPP the load increase is a function of the engine speed increase. But with a CPP the load on the engine can be changed without changing the engine speed. In that case a load increase rate might not be suitable to maximize the performance of the engines while preventing overloading. In practice, frigates with CPP and diesel engines also do deviate from the load increase rating to maximize performance, e.g. the Danish Iver Huitfeldt-class frigate.

Thermal Limits

To evaluate the thermal loading during the dynamic simulation, the thermal limits have to be established. Data on the thermal limitations of diesel engines are rare, often even data on the maximum cylinder temperature is not given and detailed data on the temperature increase in part load does not exist. However, manufacturers provide time-dependent limits of the engine loading, referred to as load increase rates.

Figure 6.2 shows the allowable load increase rate of two high-speed diesel engines. Per manufacturer two lines are given, the dotted line represents the allowable load increase rate in case of emergencies, the solid line represents the allowable load increase in case of normal operational conditions. The reason for the large deviation between the two manufacturers remains unclear. For a conservative approach, the engine rating of MAN will be considered for an engine operation under normal conditions. For this load increase rate, the load on the engine is limited to 60% after 30 seconds and full power is allowed after 180 seconds.

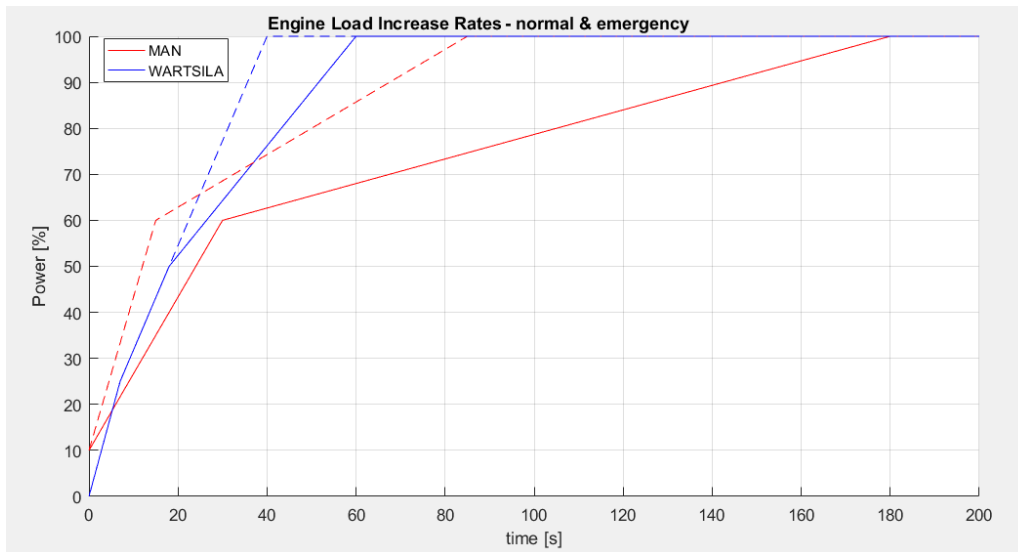


Figure 6.2: Engine load increase rates: MAN 28/33 STC & Wärtsilä 26

Another limit of the diesel engine is formed by the turbocharger and discussed earlier as the engine limit or load limit. The load limit is not time dependent but speed dependent. The ratio between the two limits is shown in figure 6.3. In case of a FPP, the cubed engine speed is increasing proportionally with the engine loading. As a result, the margin between delivered power and the engine margin is small. In this case the engine will be limited rather by the turbocharger than by thermal load limit. In case of a CPP, while ramping up the engine to maximum speed before slowly increasing the propeller pitch, the load limit becomes irrelevant as the turbocharger is operating at full speed. In this case the engine will rather be limited by thermal load limit.

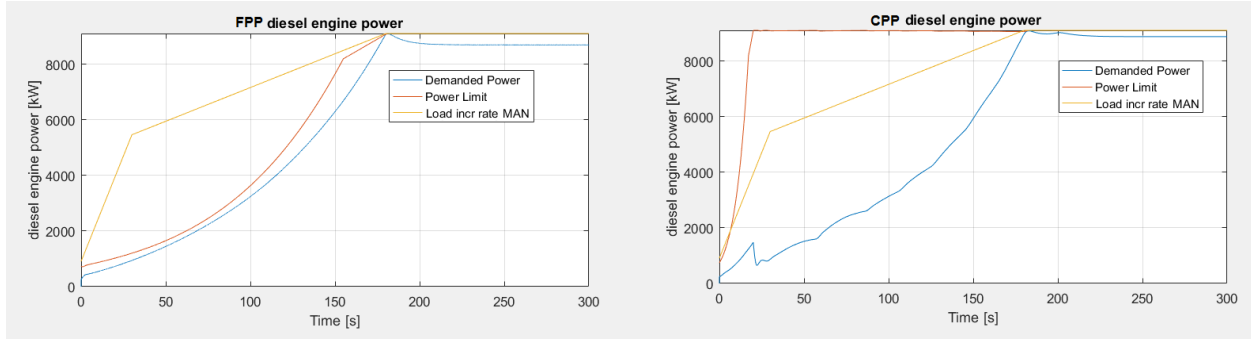


Figure 6.3: Acceleration maneuver Concept 4 – FPP vs CPP, nominal load after 180 s
 FPP: DE-ramp up 3.9 rpm/s; CPP: fast ramp up DE, pitch 0.2 °/s

However, in case of a slow acceleration maneuver, both limits will not be exceeded. To evaluate the thermal limits, the vessel has to accelerate faster. If the engine load matches the engine load increase rate, the effect on maximum cylinder temperature, air excess ratio and the temperature increase rate can be investigated. Evaluation is only possible with CPP, because more aggressive increasing of the pitch results in a higher engine loading without exceeding the engines load limit.

For the evaluation, the propulsion plant of concept 4 is used. With this concept, the vessel can be accelerated to maximum ship speed without the assistance of the electric drives, making it easier to precisely control the load by adjusting the pitch setpoints of the propeller.

The following engine speed and pitch setpoints were used:

| | | | | | | | |
|----------|-------|-----|------|------|------|------|-----|
| t_set_n | [s] | 0 | 30 | 80 | 110 | 300 | |
| n_set | [rpm] | 300 | 800 | 910 | 1000 | 1000 | |
| t_set_PD | [s] | 0 | 30 | 60 | 150 | 180 | 300 |
| PD_set | [-] | 0 | 0.68 | 0.86 | 0.97 | 1 | 1 |

Table 6.1: Engine speed and pitch setpoints for engine loading equal to increase rates of manufacturer

The resulting engine loading matched the engine load increase rate acceptable close, see figure 6.4

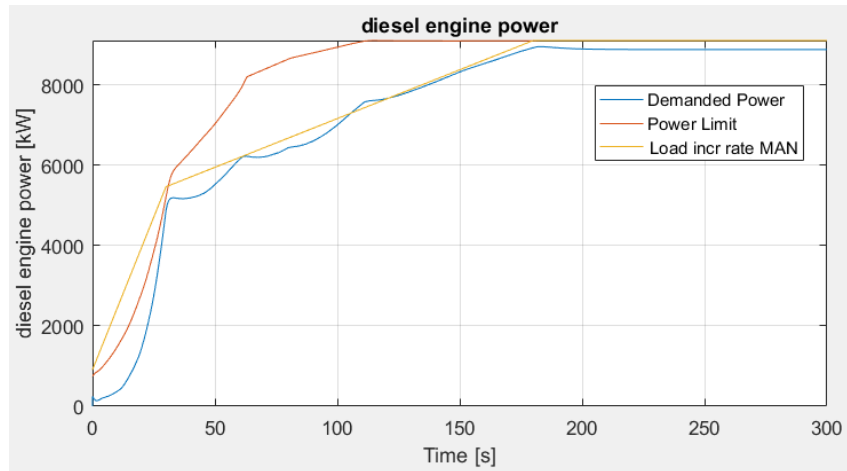


Figure 6.4: Engine loading equal to engine load increase rate for Concept 4 - CPP

6. Results

The resulting engine data from the simulation model is used to generate the thermal load limits. The position of the maximum cylinder temperature corresponds with the position of the minimum air excess ratio, see figure 6.5. As expected, the highest value for the maximum cylinder temperature occurs after a phase of steep load increase, after 30 seconds. By differentiating the results for the maximum cylinder temperature with respect to time, the temperature increase rate is obtained. The maximum temperature increase occurs before the maximum temperature. The data is shown in figure 6.6.

From the data, the following thermal limits were obtained:

- $\Lambda_{\min} = 1.7$
- $T_{\max} = 2070^{\circ}\text{C}$
- $(dT/dt)_{\max} = 102^{\circ}\text{C/s}$

The limit of the maximum cylinder temperature is considered to be very strict. The limiting temperature increase rate can assumed to be less strict, but frequent exceeding of the limit results in an accumulation of thermal stresses resulting in thermal fatigue of engine components.

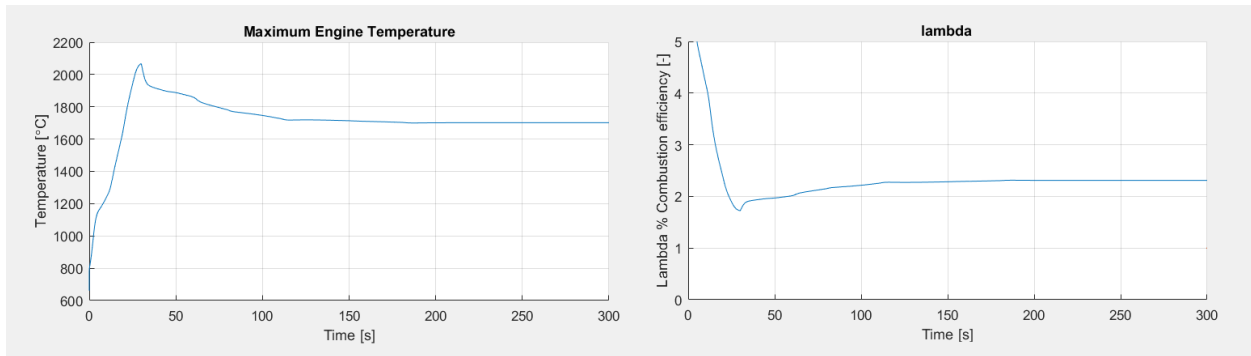


Figure 6.5: Maximum Engine Temperature & Air Excess Ratio for acceleration maneuver
Engine loading equal to engine load increase rate for Concept 4 - CPP

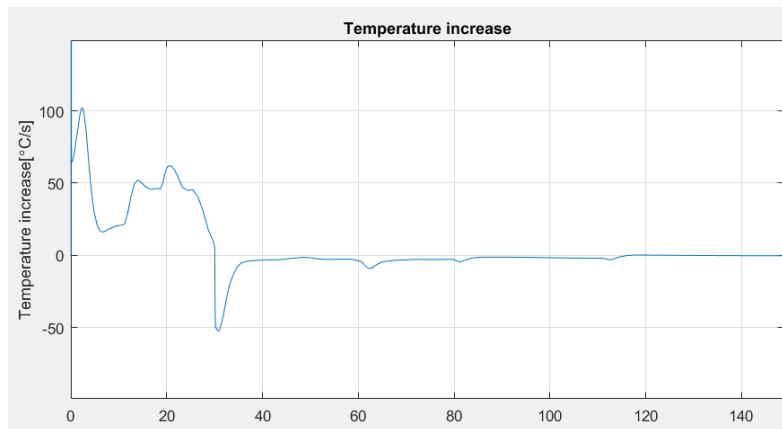


Figure 6.6: Temperature Increase Rate

It should be noted that these limits are only valid for this research to evaluate the different concepts and control schedules. The maximum cylinder temperature and air excess ratio in an actual engine are also highly influenced by the scavenging process, the process of forcing the exhaust gases out of the cylinder and filling the cylinder with fresh air. This process is not modelled with the current diesel engine model. Further, the resulting cylinder temperature is based on several assumptions for and within the Seiliger cycle process.

Effects of waves

In design and off-design conditions, the oscillating advance velocity causes the generated thrust force and required torque of the propeller to oscillate as well. With dynamic simulations it is possible to analyze the effect of oscillations in torque on the rotational speed of shafts and engines.

An increase in requested torque results in a decrease of shaft speed, according to Newton's 2nd law of motion (ref. eq. 2.39). With decreasing shaft speed and engine speed, the engine limit is decreasing, resulting in an oscillating engine limit. For concept 1 – CPP on maximum speed, the requested brake power exceeded the load limit by 450 kW, or 5%, figure 6.7. Due to the fluctuations of requested torque, the maximum engine speed was exceeded by 20rpm, or 2%.

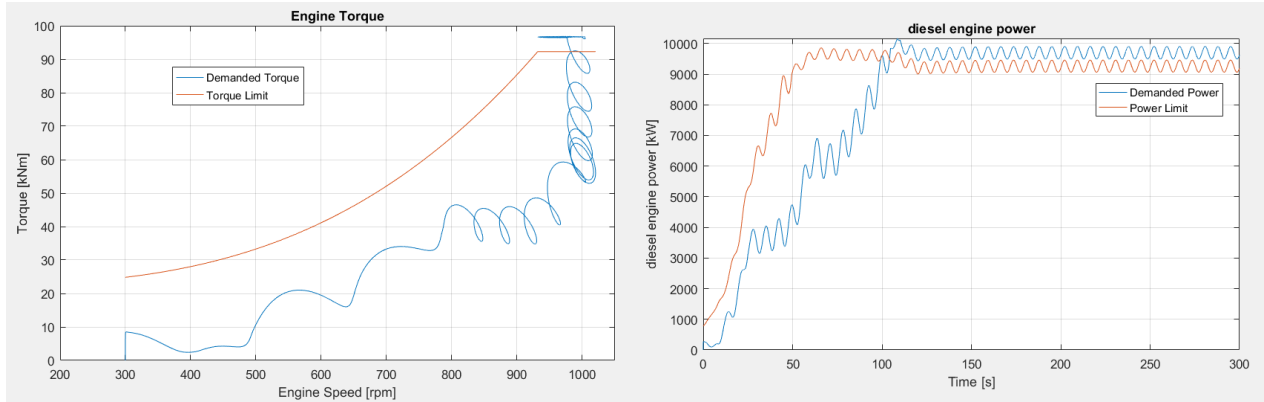


Figure 6.7: Acceleration maneuver in design condition concept 1 – CPP with SM = 0.203

To reduce the engine loading at maximum speed, the service margin was increased by increasing the gearbox ratio by 9% for concept 1 – CPP. As a result, the overloading of the engine was prevented, but due to a lower propeller speed the ship's maximum speed was reduced as well. The increased service margin resulted in a drop of 0.5 knots (or 2%) of maximum speed in design condition. For the trial conditions, the achievable maximum speed dropped as well due to the maximum engine speed. The results are shown in figure 6.8.

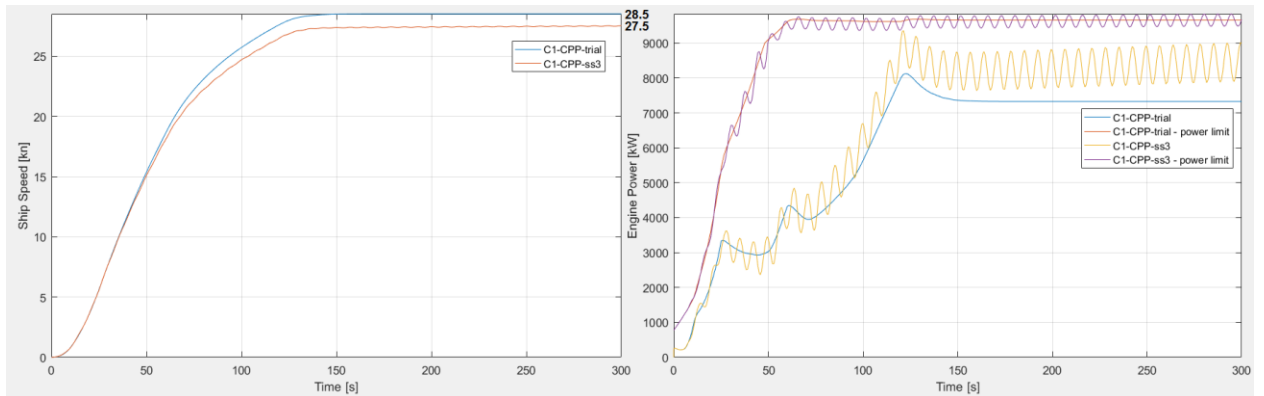


Figure 6.8: Acceleration maneuver in design condition concept 1 – CPP with SM = 0.2745

The service margin had to be adjusted for every concept. However, based on the layout of the propulsion plant and the type of propulsor, the increase in service margin differed.

For this research, a torque control strategy is used for the electric drives, resulting in constant torque output. Thus, the fluctuations in torque caused by the waves have to be compensated by the diesel engines. Due to equal operational conditions and equal sizing of the propeller, the oscillation of the requested torque by the

propeller will have nearly the same amplitude for all concepts. However, with decreasing size of the diesel engines, relative fluctuations of the engine's torque compared to nominal torque will be larger. The larger oscillations will require larger service margins. This is the case for concept 1, by relying on large electric drives providing constant torque the smaller diesel engines have to compensate for the wave load with large variations in torque and engine speed. With increasing size of the diesel engines compared to the electric drives, the oscillation in torque and speed of the diesel engines decreases. In figure 6.9, the engine speed and torque is plotted for concepts 1, 2 and 4 in design condition on maximum ship speed. The large variations for concept 1 are plotted in dark blue (CPP) and red (FPP). In comparison the variations of concept 4 are significantly smaller, plotted on top in green (CPP) and bright blue (FPP). Results for concept 2 are plotted in purple (CPP) and yellow (FPP).

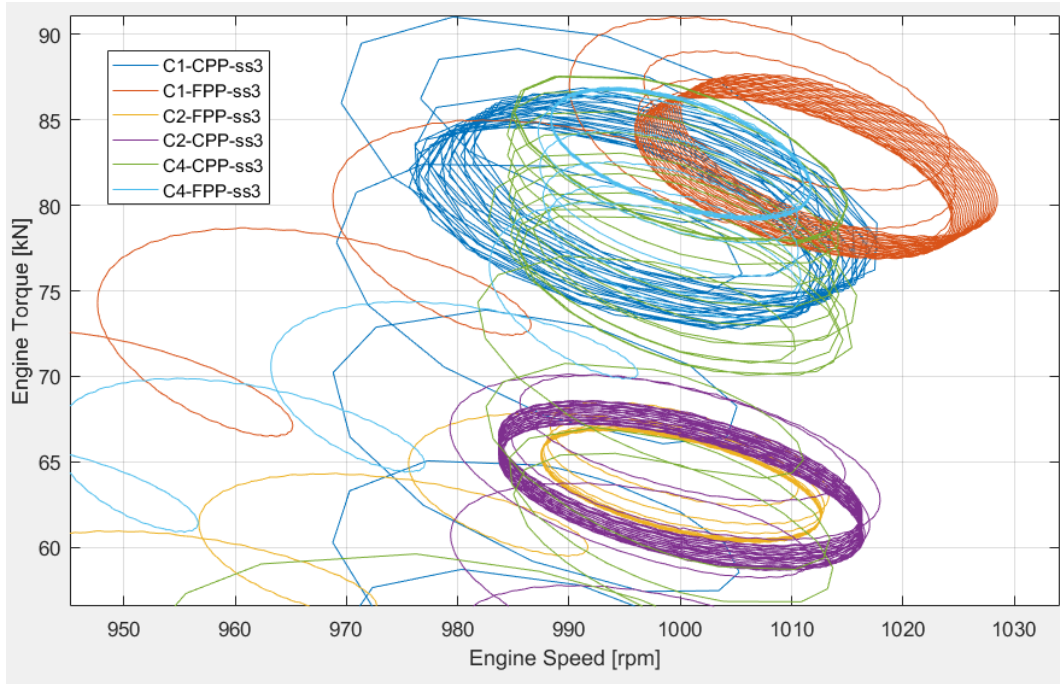


Figure 6.9: Effect of waves in phase plane for Concepts 1, 2 & 4 in design condition

Comparing the increase in gearbox ratio and the resulting service margin for concepts with CPP to concepts with FPP, two important aspects can be noticed. See figure 6.10 for a comparison between CPP and FPP for concept 3. In both cases the propeller rotates with an average of 137.5 rpm at maximum ship speed of 28 knots with FPP, respectively 28.1 knots with CPP. However, the amplitude of the oscillating propeller torque for the CPP is higher, resulting in an higher amplitude of the oscillating requested brake power. For the CPP, the amplitude of the oscillating power is 790 kW, whereas the amplitude for the FPP is 600 kW, reduced by 24%. Therefore one could argue that the service margin for the CPP should be larger.

Though this can be put in perspective by considering the second aspect. By ramping up the diesel engine before increasing the propeller pitch to maximum, the load margin to the engine limit is larger for the CPP, see figure 6.11 for the engine torque. If the last part of the acceleration in waves is considered, the FPP shows a peak in engine power just before the maximum ship speed is reached. This peak is caused by additional power required for acceleration of the ship and the shaft system including the engine. For the CPP however, the shaft system and engine already run maximum speed towards the end of the acceleration maneuver. By increasing the pitch of the propeller slowly towards the end, the peak in engine power of the FPP can be prevented. Therefore, not only the dynamic effects of the waves but also of the acceleration maneuver need

to be considered in determining the service margin if a FPP is used. For the CPP it is sufficient to consider the dynamic effects of the waves to determine the service margin.

With a CPP it is possible to design the propulsion system even without service margin. But then the pitch of the propeller needs to be reduced if the vessel operates in waves with an adaptive pitch control, resulting in roughly the same drop in speed compared to increasing the service margin in the design process.

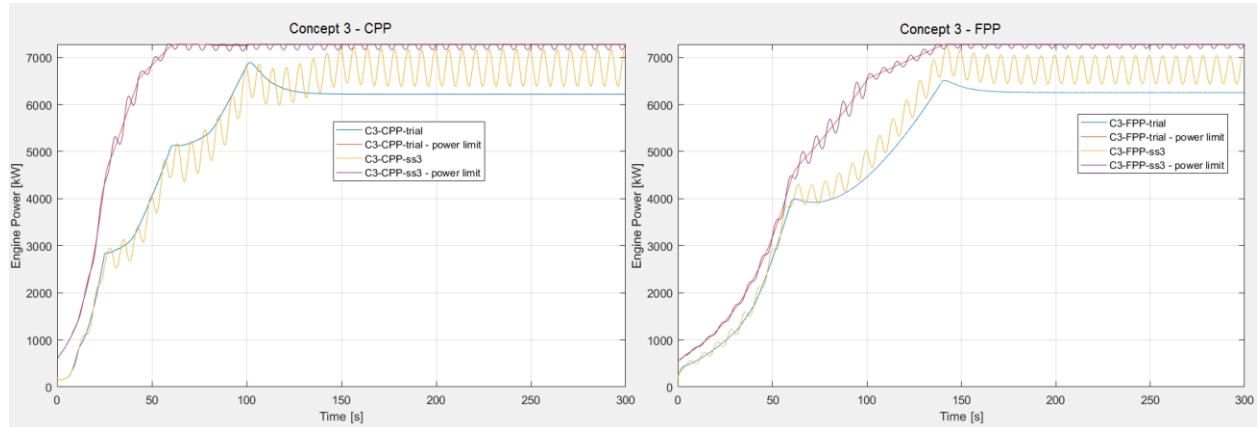


Figure 6.10: Engine Power during acceleration for concept 3, CPP vs FPP, SM = 0.22 & 0.215

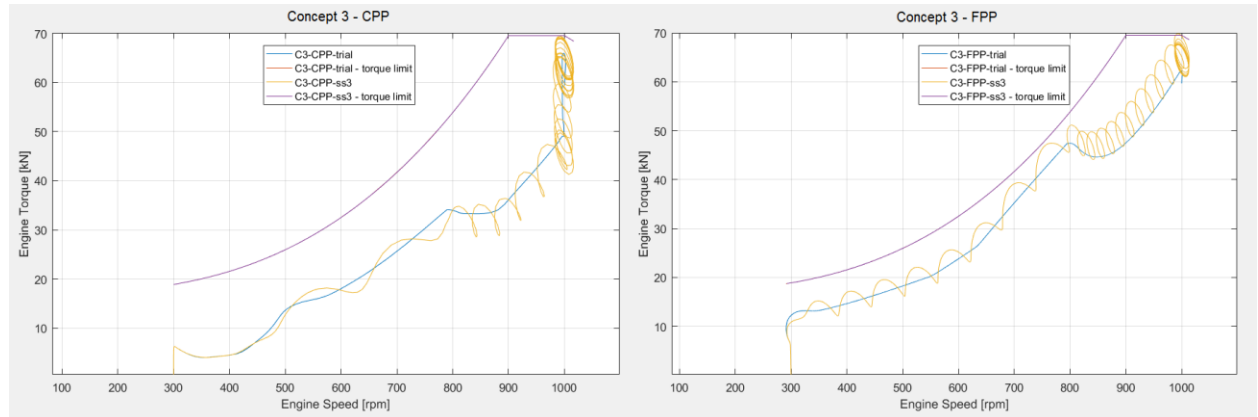


Figure 6.11: Engine Torque during acceleration for concept 3, CPP vs FPP, SM = 0.22 & 0.215

For the concepts, the gearbox ratios and the resulting design speeds are given in the following table. Due to the slightly lower efficiency of the FPP, the concepts with FPP achieve a lower design speed than concepts with CPP. Next to the lower efficiency, also the increased service margin for the FPP causes deviation in design speed.

The service margin was determined by calculating the trial brake power belonging to the design speed and compared to the maximum available power. Initially, a service margin of 20.3% was assumed, representing average fouling and average added resistance of sea state 3. Due to the dynamic effect of the waves, the service margin had to be increased for all concepts.

| Concept | Gearbox ratio | Design Speed | P _B Trial | P _B Max | Service Margin | Increase SM |
|----------|---------------|--------------|----------------------|--------------------|----------------|-------------|
| C1 – FPP | 7.65 | 27.3 | 21.53 MW | 29.8 MW | 27.75 | 7.45 |
| C1 – CPP | 7.65 | 27.5 | 21.62 MW | 29.8 MW | 27.45 | 7.15 |
| C2 – FPP | 7.25 | 28.4 | 26.26 MW | 34.32 MW | 23.48 | 3.28 |
| C2 – CPP | 7.25 | 28.6 | 26.36 MW | 34.32 MW | 23.19 | 2.89 |
| C3 – FPP | 7.275 | 28.0 | 26.77 MW | 34.32 MW | 22.2 | 1.9 |
| C3 – CPP | 7.275 | 28.2 | 26.93 MW | 34.32 MW | 21.53 | 1.23 |
| C4 – FPP | 7.1 | 28.5 | 29.27 MW | 36.8 MW | 20.46 | 0.16 |
| C4 – CPP | 7.1 | 28.6 | 28.93 MW | 36.8 MW | 21.39 | 1.09 |

Table 6.2: Gearbox ratios and service margins (total and due to dynamic effects of waves)

The results show that the required service margin depends on the type of propulsor and the layout of the propulsion plant. In case of large diesel engines and additional electric drives only assisting in the acceleration maneuver, the increase in required service is small. For hybrid propulsion plants relying heavily on the additional power of electric drives, the dynamic effects of waves are of larger impact and require large margins. In that case the service margins proposed by the manufactures might not be sufficient.

Acceleration maneuvers

With the dynamic thermal load limits established and the maximum ship speed of the concepts fixed, the different acceleration maneuvers could be simulated, evaluated and adjusted where needed. The parameters used for the different propulsion concepts and the operational conditions can be found throughout the previous chapters, but are also summarized in tables of Annex F. In short, the following concepts are tested with FPP and CPP:

- Reference: $\Delta = 6050$ ton; per shaft: 1 DE 5440 kW, 1 GT 18000 kW
- Concept 1: $\Delta = 5200$ ton; per shaft: 1 DE 10000 kW, Edrive 4900 kW
- Concept 2: $\Delta = 5200$ ton; per shaft: 2 DE 7280 kW, Edrive 2600 kW
- Concept 3: $\Delta = 6000$ ton; per shaft: 2 DE 7280 kW, Edrive 2600 kW
- Concept 4: $\Delta = 6000$ ton; per shaft: 2 DE 9100 kW, Edrive 2600 kW

Reference – LCF

For the reference vessel, the setpoints for the diesel engine speed and the pitch of the propeller are based on an earlier simulation model developed by Imtech. For the acceleration maneuvers of the reference trial condition is assumed. During the acceleration maneuver on diesel engines, the pitch is increased first, while the engine speed is just slightly increased to 750 rpm.

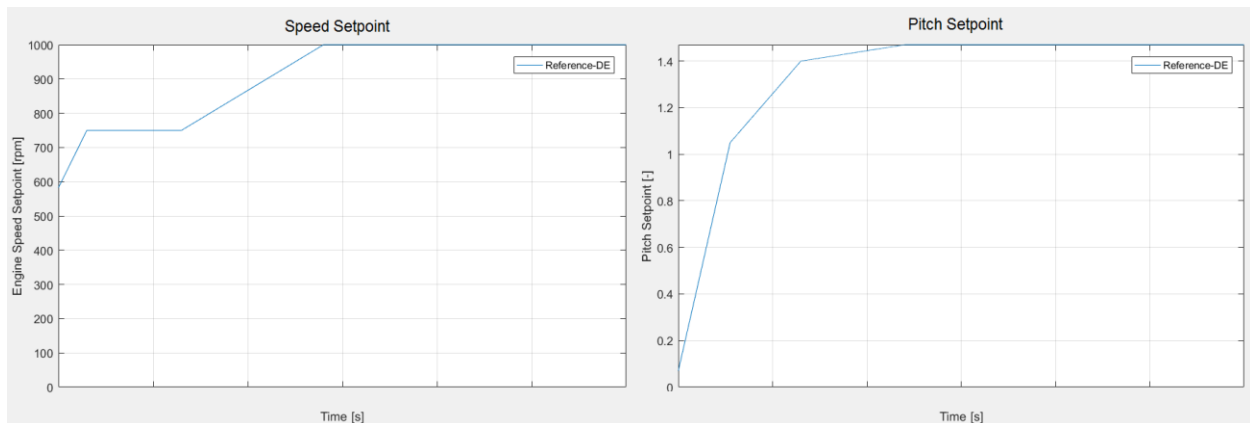


Figure 6.12: Setpoints for engine speed and propeller pitch of reference vessel on diesel engines during acceleration

For the acceleration maneuver, the following setpoints are used:

| | | | | | | |
|----------|-------|-----|-----|-----|------|------|
| t_set_n | [s] | 0 | 15 | 65 | 140 | 300 |
| n_set | [rpm] | 585 | 750 | 750 | 1000 | 1000 |
| t_set_PD | [s] | 0 | 28 | 65 | 120 | 300 |
| PD_set | [-] | 0 | .7 | .95 | 1 | 1 |

Table 6.3: Engine speed and pitch setpoints for acceleration maneuver reference on DE

The setpoints result in a ramp up rate of the diesel engine of 3.3 rpm/s for 750 – 1000 rpm.

On diesel engines, the reference vessel achieves a maximum acceleration of 0.134 m/s². The maximum speed of 19.4 knots is reached after 175 seconds, resulting in an average acceleration of 0.057 m/s².

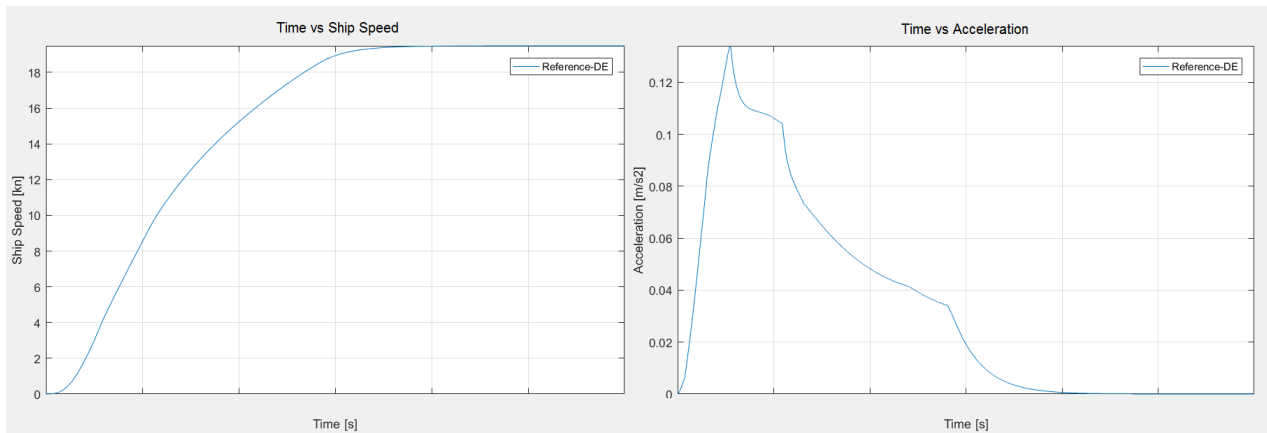


Figure 6.13: Speed and acceleration of LCF on DE during acceleration

The load limit used for the diesel engines in this simulations is not representative as the LCF uses diesel engines equipped with sequential turbocharging (STC). With STC, maximum charge air pressure on one turbocharger is reached at 570 rpm, increasing the amount of air in the cylinder and thus the load limit in part load. The limit will not be exceeded during the acceleration maneuver of the actual vessel. The same holds for the results of maximum cylinder temperature and air excess ratio. With STC, more air is available at lower rpm due to the higher charge air pressure, increasing the air excess ratio and thus decreasing the cylinder temperature. But the results show the current trend of the engine loading very well. While the engine speed remains low, the rapid increase in pitch causes a steep increase in engine torque, figure 6.14. Also with the STC engines, the remaining margin to the load limit will probably be small. The results for the maximum temperature and the air excess ratio, figure 6.15, can be used to compare the load increase of the reference to the different concepts.

6. Results

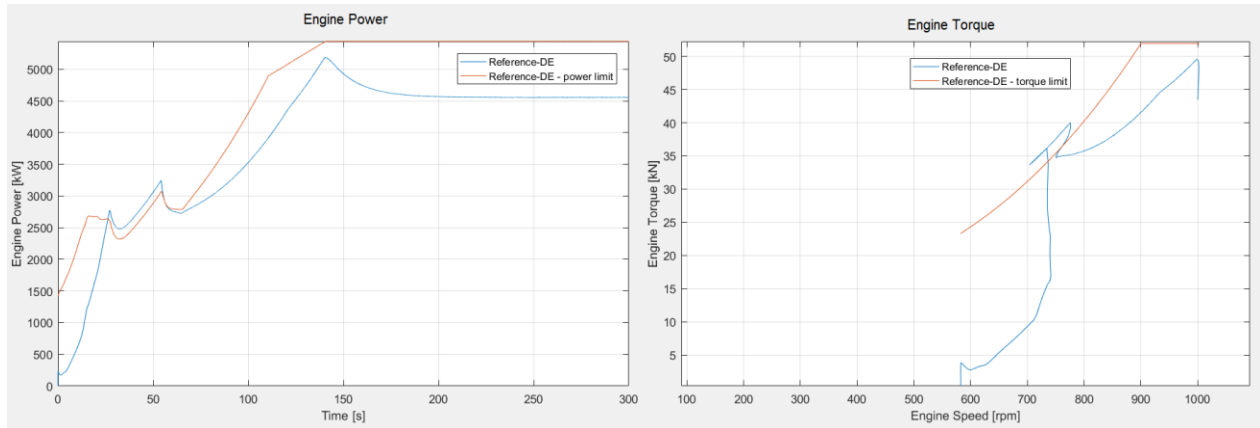


Figure 6.14: Engine power and torque of LCF on DE during acceleration engines are overloaded as the model does not support STC

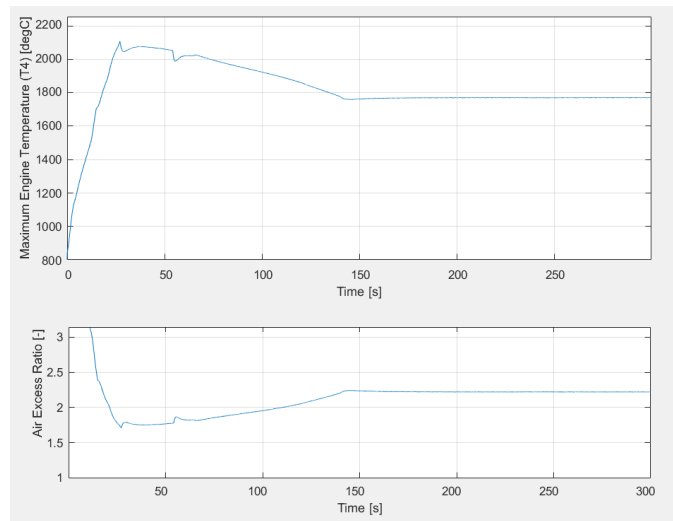


Figure 6.15: Maximum cylinder temperature and air excess ratio of LCF

The gas turbines of the vessel provide sufficient torque to drive the propeller with maximum pitch. However, due to the minimum engine speed, the pitch also has to be reduced if the ship speed is reduced to zero. During the acceleration maneuver, the pitch is therefore increased to maximum with the maximum pitch increase rate of $1^\circ/\text{s}$. Simultaneously the gas turbine speed is ramped up, figure 6.16.

6. Results

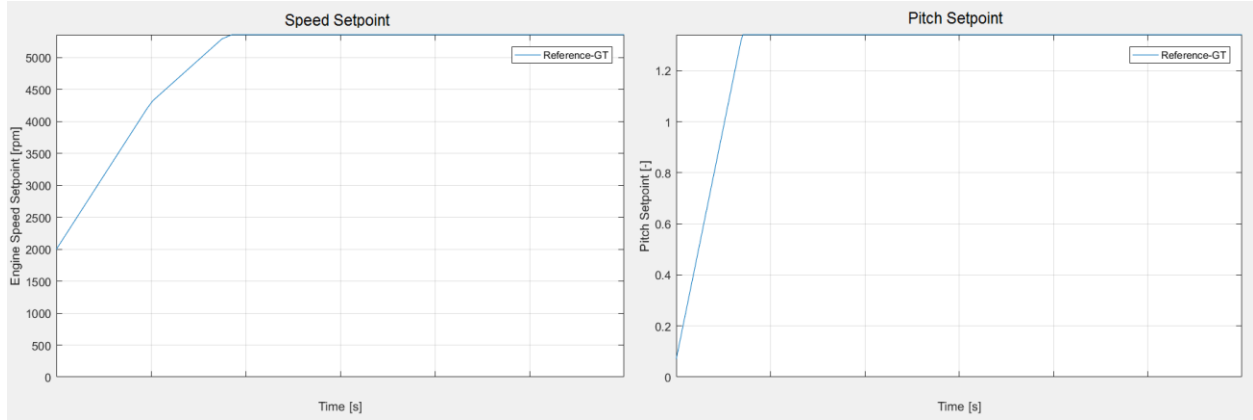


Figure 6.16: Setpoints for engine speed and propeller pitch of reference vessel on gas turbines during acceleration

| | | | | | |
|----------|-------|------|------|------|------|
| t_set_n | [s] | 0 | 50 | 90 | 300 |
| n_set | [rpm] | 2000 | 4300 | 5360 | 5360 |
| t_set_PD | [s] | 0 | 35 | 300 | |
| PD_set | [-] | 0 | 1 | 1 | |

Table 6.4: Engine speed and pitch setpoints for acceleration maneuver reference on GT

The results for the reference vessel propelled by the gas turbines is plotted in figure 6.17. The vessel achieves a peak acceleration of 0.278 m/s^2 . In contrast to propulsion with diesel engines and CPP, the maximum acceleration is reached with maximum pitch due to the high generated torque of the gas turbines. The maximum speed of 29 knots is reached after 150 seconds, resulting in an average acceleration of 0.097 m/s^2 . On gas turbines, the vessel could perform much better with higher pitch increase rate. The maximum allowable pitch increase rate for the LCF is $2.4 \text{ }^\circ/\text{s}$. However, during normal operation the pitch increase rate is limited to $1 \text{ }^\circ/\text{s}$.

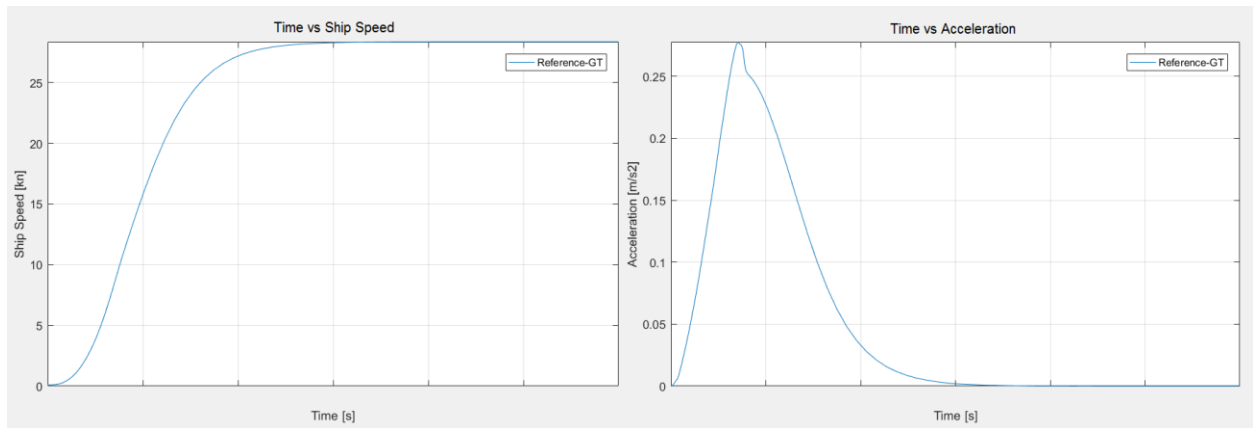


Figure 6.17: Speed and acceleration of LCF on GT during acceleration maneuver

FPP – Trial Conditions and Design Condition

With a fixed pitch propeller, setpoints for the engine speed and the torque of the electric drive have to be defined. As the not all generators required to provide for the electric drives are assumed to be on the line at the start of the acceleration maneuver, the drives cannot provide instant maximum torque. Therefore maximum torque from the electric drives is available after a short delay. However, instant switching on and off should be prevented as this causes load steps on the diesel engines. In figure 6.18 the engine loading is plotted in case the electric drives are instantly switched on after 10 seconds and switched off after 130 seconds.

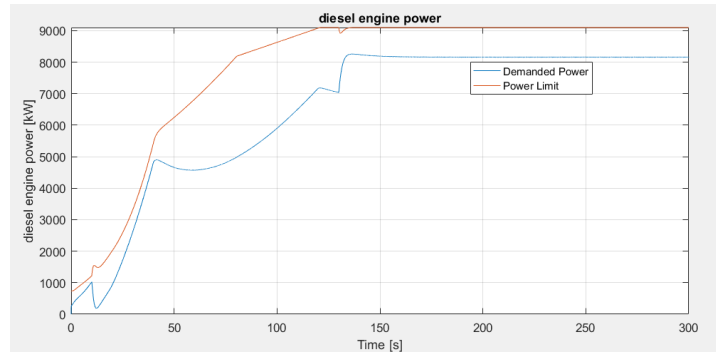


Figure 6.18: Load steps due to instant switching electric drive

The resulting response on the engine speed and the cylinder temperature is plotted in figure 6.19. The effect on the engine speed is not severe due to the large inertia of the shafting systems. But the step response of the cylinder temperature causes unacceptable high temperature increase/decrease rates in the cylinder. By ramping up and down the generated torque of the electric drives, load steps on the diesel engines are prevented.

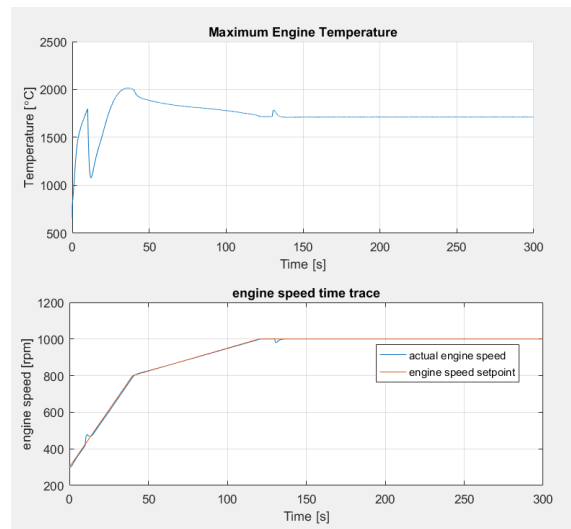


Figure 6.19: Response on cylinder temperature and engine speed due to instant switching electric drive

The setpoints for the diesel engine speed were divided into two ramp up rates. By changing the ramp up rates and adjusting the switch over point (the engine speed where transition between the two ramp up rates occur), the engine loading during the dynamic simulation can be adjusted to fit the engine load limit. Especially the rate of the first ramp up determines the temperature increase rate in the engine. Whereas the switch over point determines the margin to overloading and therefore also the maximum temperature in the cylinder. The

first ramp up rate can be significantly larger because the electric drives provide a lot of additional torque. The second ramp up rate has to be smaller as the torque developed by the electric drives decreases in absolute number as well as compared to the torque of the diesel engines. In addition the requested brake power increases proportionally with the cubed engine speed.

By defining more switch over points and thus more ramp up rates, the load on the engines could be matched closer to the load limits, however significantly increasing the effort to tune the rates to the different operational conditions.

Concept 1 – FPP

The setpoints for diesel engine speed and torque of the electric drives are given in figure 6.20. The ramp up of the generators is simulated as a gradual increase in the torque setpoint of the electric drives. In spite of the torque set to nominal torque, the generated torque is reduced once the electric drives operate in field weakening range.

For design condition the second ramp up rate of the diesel engines is slightly reduced and the maximum engine speed limited to 1014 rpm to prevent overloading of the engines. The change between the two ramp up rates after 60 seconds can also found back in the engine load as a peak, figure 6.22. After reduction of the ramp up rate, also the required load increase rate reduces.

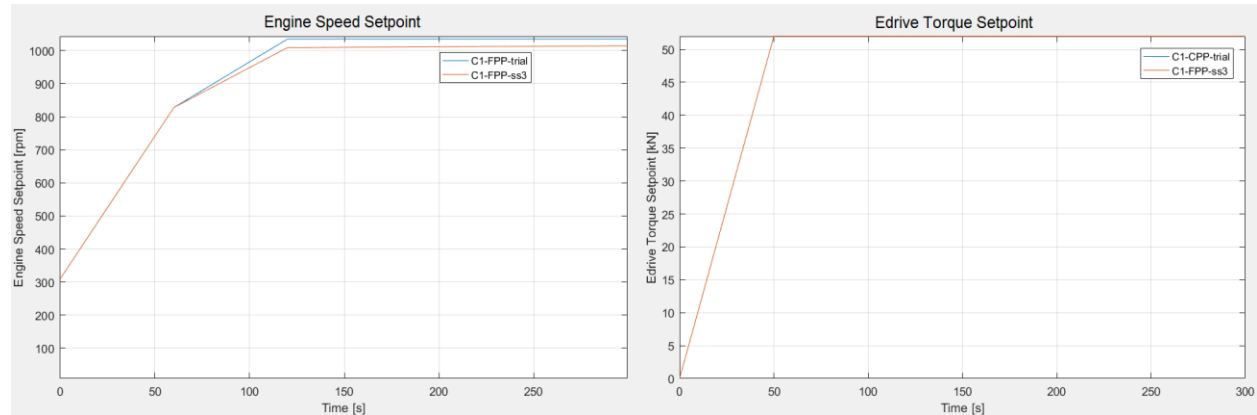


Figure 6.20: Setpoints for engine speed and edrive torque of Concept 1 – FPP

| | | | | | |
|----------|-------|-----|-----|------|------|
| t_set_n | [s] | 0 | 60 | 120 | 300 |
| n_set | [rpm] | 310 | 830 | 1035 | 1035 |
| t_set_ed | [s] | 0 | 50 | 300 | |
| T_set | [kNm] | 0 | 52 | 52 | |

Table 6.5: Engine speed and edrive setpoints for acceleration maneuver Concept 1 – FPP in trial conditions

The setpoints result in the following ramp up rates:

- 310 – 830 rpm: 8.7 rpm/s
- 830 – 1035 rpm: 3.4 rpm/s

For sea state 3, the engine speed setpoint is slightly reduced to:

| | | | | | |
|----------|-------|-----|-----|------|------|
| t_set_n | [s] | 0 | 60 | 120 | 300 |
| n_set | [rpm] | 310 | 830 | 1014 | 1014 |
| t_set_ed | [s] | 0 | 50 | 300 | |
| T_set | [kNm] | 0 | 52 | 52 | |

6. Results

Table 6.6: Engine speed and edrive setpoints for acceleration maneuver Concept 1 – FPP in design conditions

Resulting in the following ramp up rates for sea state 3:

- 310 – 830 rpm: 8.7 rpm/s
- 830 – 1035 rpm: 3.1 rpm/s

Figures 6.21, 6.22 and 6.23 show the result of the acceleration simulation for trial conditions and design condition. During large part of the acceleration maneuver, the margin between engine load and load limit is large. However, due to the lagging of the electric drives, the diesel engine is heavily loaded in the first few seconds. As a result the maximum cylinder temperature increases rapidly and peaks just above the allowable limit, $T_{\max} = 2086^{\circ}\text{C}$. More severe however is the temperature increase rate during the first few seconds. With 156°C/s the allowable rate is exceeded by 53%.

This is particular problem of the large electric drives as they need all generator sets being on the line to develop full power. Especially with these large electric drives, electric energy storage favorable to avoid lagging of the electric drives.

The NATO standards for acceleration is based on the trial conditions. Maximum acceleration is reached after 50 seconds and peaks with 0.153 m/s^2 . The maximum ship speed of 29.1 knots is reached after 148 seconds, which results in an average acceleration of 0.08 m/s^2 .

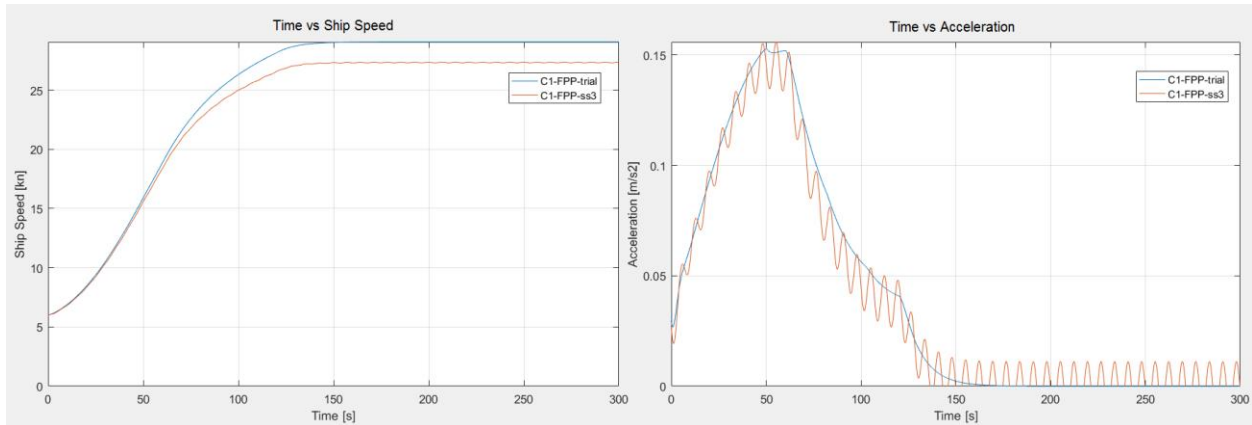


Figure 6.21: Speed and acceleration of Concept 1 – FPP during acceleration in trial and design condition

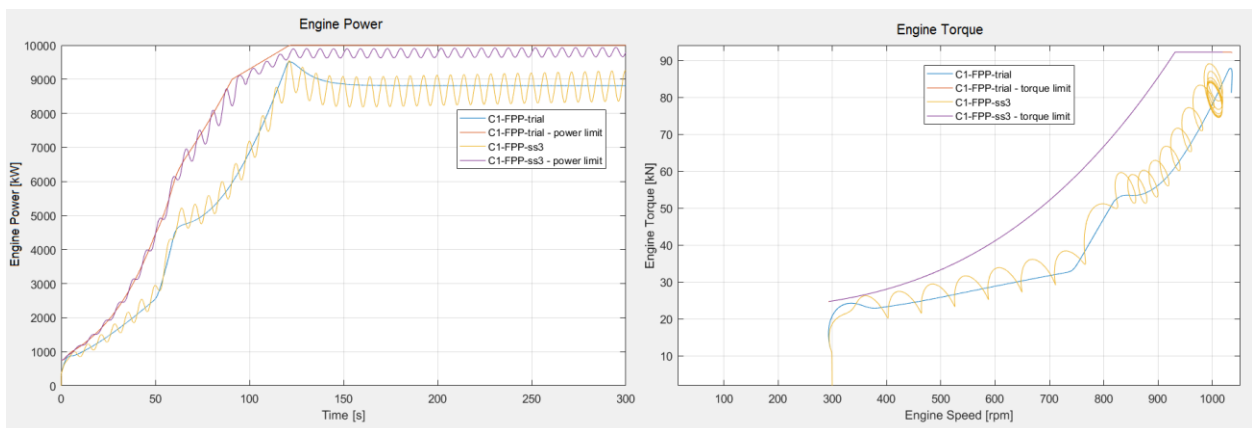


Figure 6.22: Engine power and torque of Concept 1 – FPP during acceleration in trial and design condition

6. Results

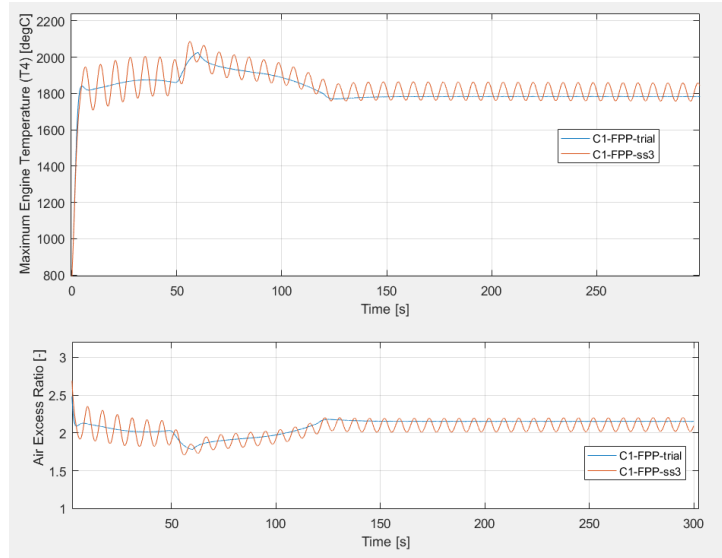


Figure 6.23: Maximum cylinder temperature and air excess ratio of Concept 1 – FPP during acceleration in trial and design condition

| | |
|------------------|------------------------|
| a_{\max} | 0.153 m/s^2 |
| a_{ave} | 0.08 m/s^2 |
| T_{\max} | 2086°C |
| λ_{\min} | 1.71 |
| $(dT/dt)_{\max}$ | 156°C/s |

Table 6.7: Results of acceleration maneuver Concept 1 - FPP

Concept 2 – FPP

The electric drives of this concept are smaller, less generators need to be brought on the line to supply electric power. Therefore the electric drives can generate the maximum torque earlier. Next to the faster ramp up of the electric drives also the diesel engines can be ramped up faster, because the increased amount of diesel engines can produce more torque in the beginning of the acceleration maneuver. This results also in an increased available engine margin and thus a lower temperature increase rate in the cylinder.

The ramp up rates for trial conditions and design condition can be kept the same, defined by the following setpoints:

| | | | | | |
|-----------------------|-------|-----|------|------|------|
| t_{set_n} | [s] | 0 | 55 | 130 | 300 |
| n_{set} | [rpm] | 300 | 800 | 1000 | 1000 |
| $t_{\text{set}_{ed}}$ | [s] | 0 | 40 | 300 | |
| T_{set} | [kNm] | 0 | 27.6 | 27.6 | |

Table 6.8: Engine speed and edrive setpoints for acceleration maneuver Concept 2 – FPP in trial and design conditions

The setpoints result in the following ramp up rates:

- 300 – 800 rpm: 9.1 rpm/s
- 800 – 1000 rpm: 2.7 rpm/s

6. Results

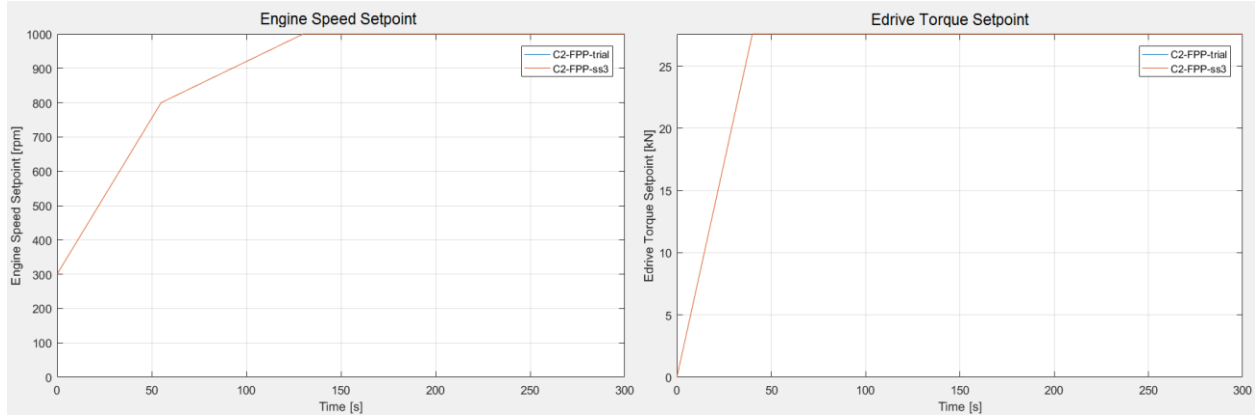


Figure 6.24: Setpoints for engine speed and edrive torque of Concept 2 – FPP

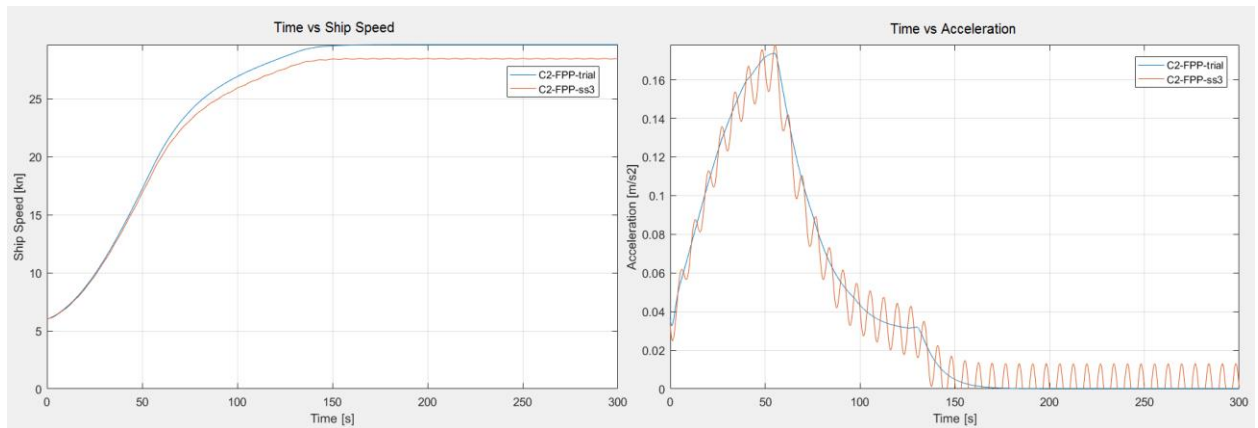


Figure 6.25: Speed and acceleration of Concept 2 – FPP during acceleration in trial and design condition

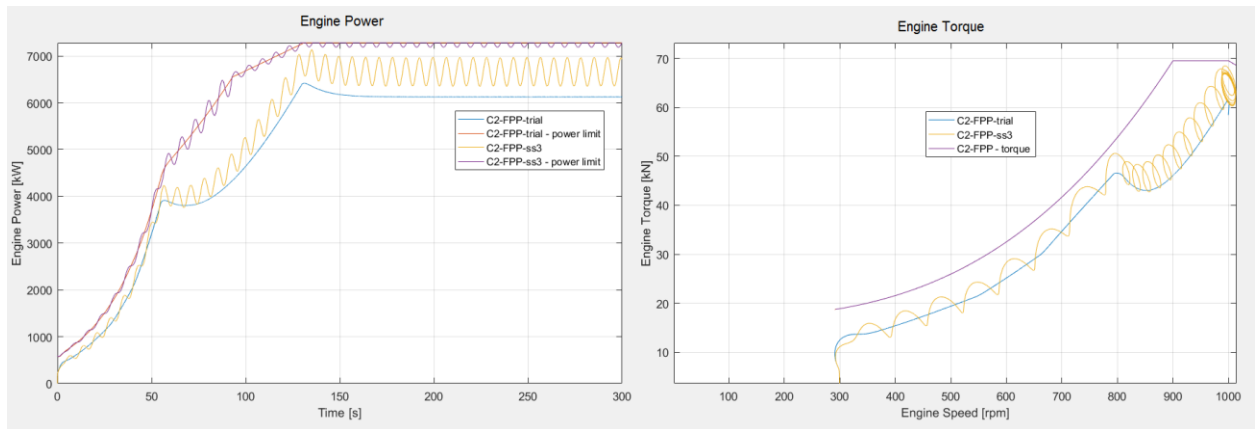


Figure 6.26: Engine power and torque of Concept 2 – FPP during acceleration in trial and design condition

6. Results

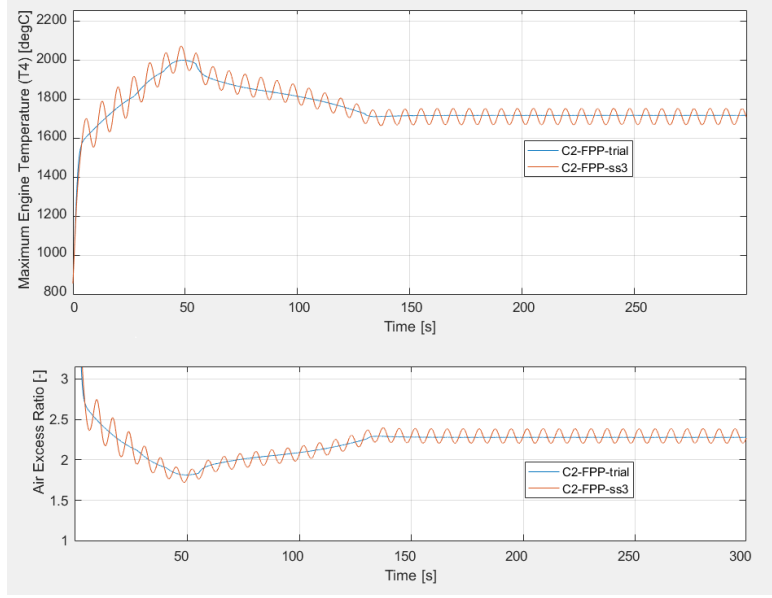


Figure 6.27: Maximum cylinder temperature and air excess ratio of Concept 2 – FPP during acceleration in trial and design condition

The acceleration peaks with 0.173 m/s^2 after 55 seconds. The maximum ship speed of 29.6 knots is reached after 155 seconds, resulting in an average acceleration of 0.084 m/s^2 .

| | |
|------------------|-----------------------|
| a_{\max} | 0.173 m/s^2 |
| a_{ave} | 0.084 m/s^2 |
| T_{\max} | 2070°C |
| λ_{\min} | 1.72 |
| $(dT/dt)_{\max}$ | 102°C/s |

Table 6.9: Results of acceleration maneuver Concept 2 – FPP

Concept 3 – FPP

Compared to concept 2 – FPP, the propulsion plant is kept the same. But the displacement of the vessel is increased and thus also the bare hull resistance. The maximum engine power remains the same as in concept 2, the increased hull resistance therefore causes a reduction in achievable maximum ship speed. For the acceleration maneuver, the increased displacement means an increased inertia and the achievable acceleration will be lower. To prevent overloading of the engines, the ramp up rates also reduced.

The ramp up rates for trial conditions and design condition are defined by the following setpoints:

| | | | | | |
|-----------------------|-------|-----|------|------|------|
| t_{set_n} | [s] | 0 | 60 | 140 | 300 |
| n_{set} | [rpm] | 300 | 800 | 1000 | 1000 |
| $t_{\text{set}_{ed}}$ | [s] | 0 | 40 | 300 | |
| T_{set} | [kNm] | 0 | 27.6 | 27.6 | |

Table 6.10: Engine speed and edrive setpoints for acceleration maneuver Concept 3 – FPP in trial and design conditions

The setpoints result in the following ramp up rates:

- 300 – 800 rpm: 8.3 rpm/s
- 800 – 1000 rpm: 2.5 rpm/s

6. Results

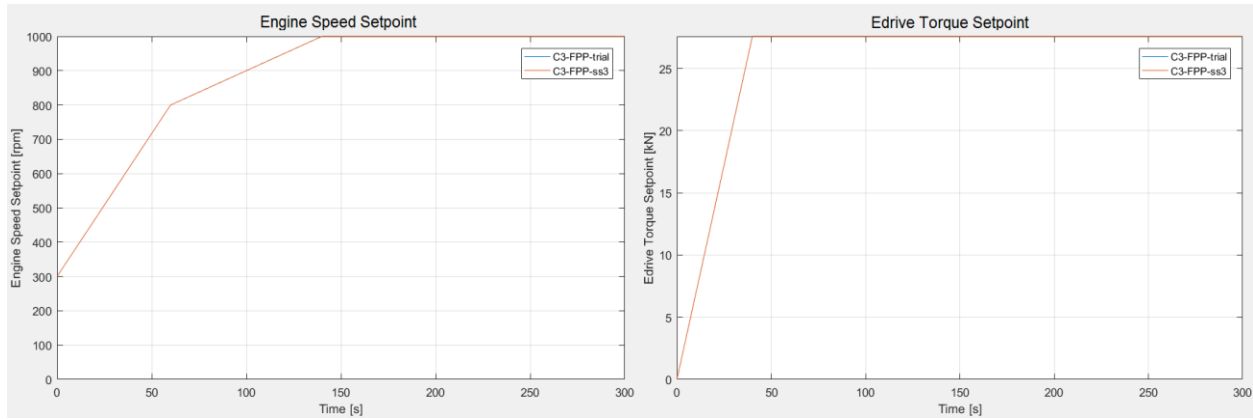


Figure 6.28: Setpoints for engine speed and edrive torque of Concept 3 – FPP

Compared to concept 2, the maximum acceleration drops to 0.155 m/s^2 . With the maximum ship speed of 29.1 knots reached after 159 seconds, the average acceleration reached 0.075 m/s^2 , a reduction of 11% compared to concept 2.

6. Results

During the acceleration maneuver, the margin to the load limit of the diesel engine is comparable, resulting in a nearly equivalent maximum engine temperature of 2065 °C, see figure 6.31. However, due to the reduced ramp up rates of the diesel engines in this heavier vessel, the temperature increase rate reduced as well. The temperature increase rate of concept 2 is equal to the allowable limit, whereas the temperature increase rate for concept 3 reduces to 92 °C/s, a reduction of 10%. Ultimately, the accumulated thermal stresses for this concept will be lower.

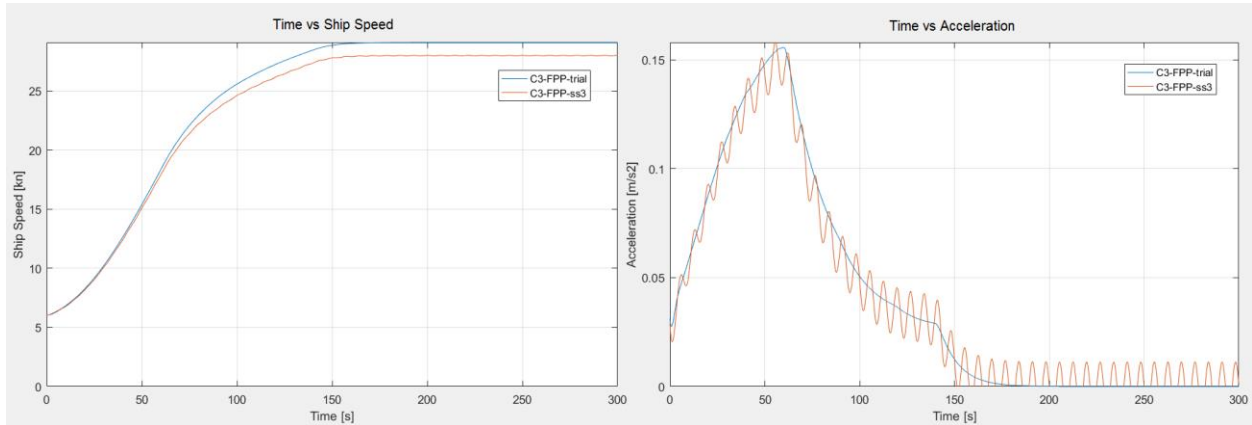


Figure 6.29: Speed and acceleration of Concept 3 – FPP during acceleration in trial and design condition

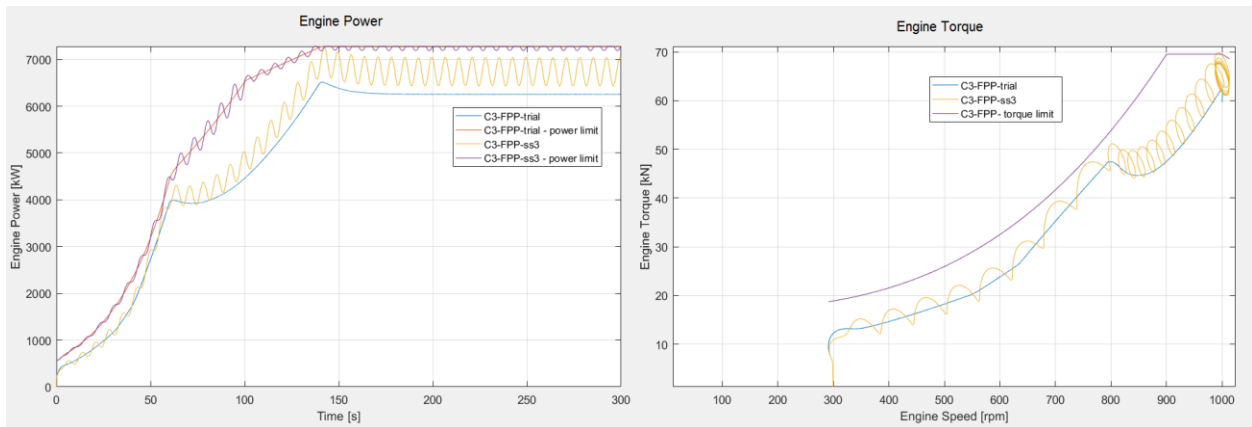


Figure 6.30: Engine power and torque of Concept 3 – FPP during acceleration in trial and design condition

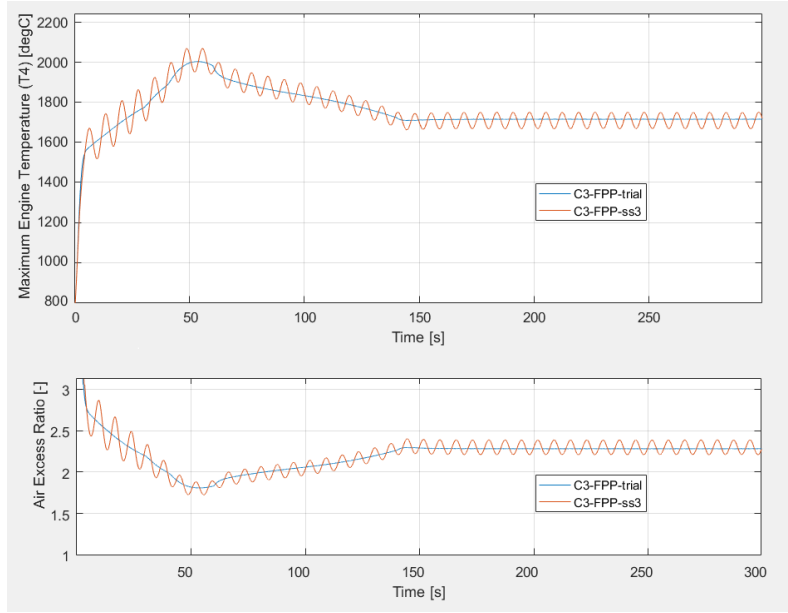


Figure 6.31: Maximum cylinder temperature and air excess ratio of Concept 3 – FPP during acceleration in trial and design condition

| | |
|------------------|------------------------|
| a_{\max} | 0.155 m/s ² |
| a_{ave} | 0.075 m/s ² |
| T_{\max} | 2065 °C |
| λ_{\min} | 1.73 |
| $(dT/dt)_{\max}$ | 92 °C/s |

Table 6.11: Results of acceleration maneuver Concept 3 - FPP

Concept 4 – FPP

The diesel engines of concept 4 are sufficiently large dimensioned to propel the frigate at design speed. Therefore the electric drives do not have to assist if the acceleration maneuver is completed and the torque setpoint is reduced gradually, see figure 6.32. By reducing the generated torque of the drives gradually, the load is transferred to the diesel engines gradually, preventing a load peak on the diesel engine. The gradual load increase of the diesel engines is visible in figure 6.34, from 120 – 150 seconds.

The ramp up rates for trial condition and design condition are defined by the following setpoints:

| | | | | | | |
|----------|-------|-----|------|------|------|-----|
| t_set_n | [s] | 0 | 50 | 120 | 300 | |
| n_set | [rpm] | 300 | 800 | 1000 | 1000 | |
| t_set_ed | [s] | 0 | 40 | 110 | 150 | 300 |
| T_set | [kNm] | 0 | 27.6 | 27.6 | 0 | 0 |

Table 6.12: Engine speed and edrive setpoints for acceleration maneuver Concept 4 – FPP in trial and design conditions

The setpoints result in the following ramp up rates:

- 300 – 800 rpm: 10 rpm/s
- 800 – 1000 rpm: 2.86 rpm/s

6. Results

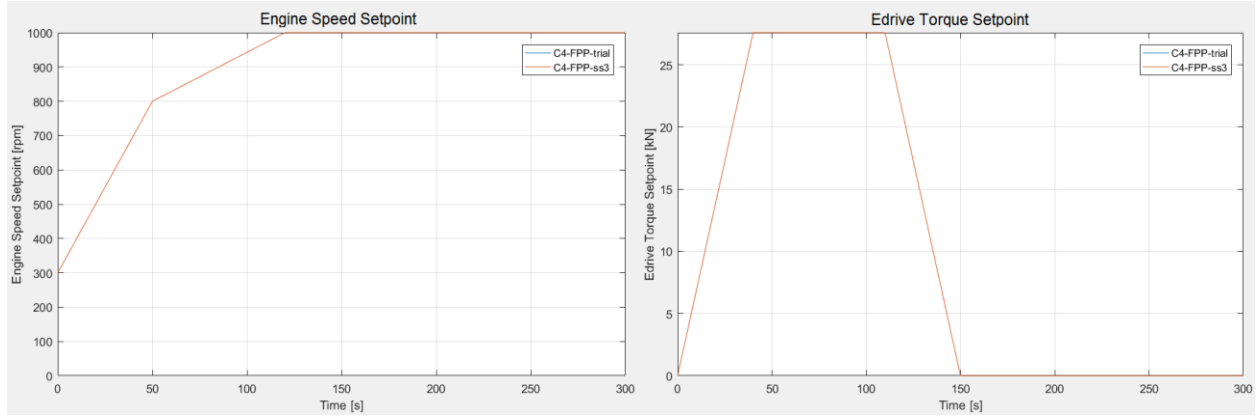


Figure 6.32: Setpoints for engine speed and edrive torque of Concept 4 – FPP

Due to the large diesel engines, providing a lot of torque towards the end of the acceleration maneuver, concept 4 can accelerate the fastest. The required NATO standard is nearly met for the maximum speed. The maximum speed is reached in 140 seconds, resulting in an average acceleration of 0.087 m/s^2 , peaking after 50 seconds with 0.187 m/s^2 . 28 knots are reached after 108 seconds, which results in an average acceleration of 0.105 m/s^2 .

Designed for both combinations, CODLAD and CODLOD, this concept offers also sufficient margin to the load limit of the diesel engines while accelerating from low ship speeds. This results in the lowest maximum cylinder temperature of all FPP concepts, and especially in the lowest temperature increase rate.

In combination with an electric energy storage, the electric drives could provide instant power at the beginning of the acceleration maneuver. This would probably result in this concept fulfilling the NATO requirements for the average acceleration.

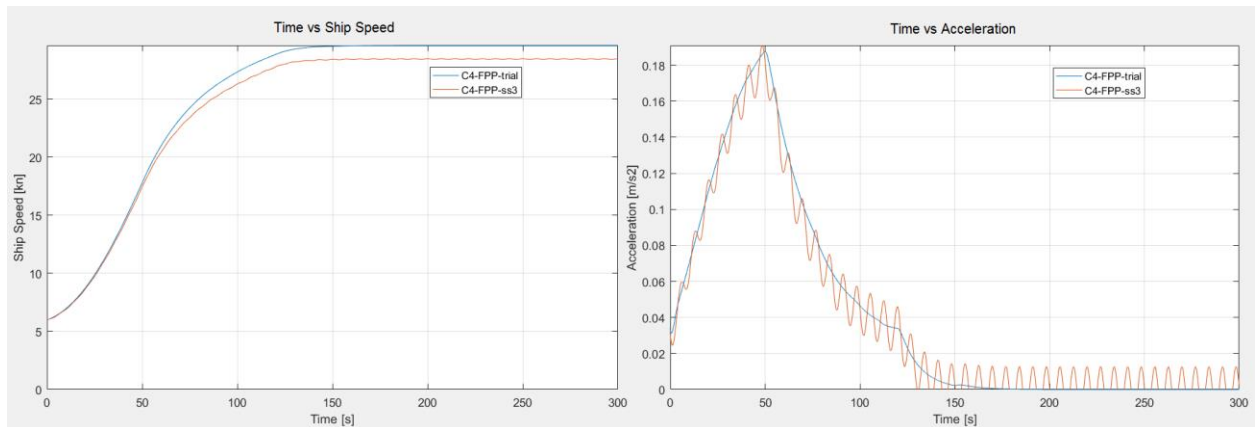


Figure 6.33: Speed and acceleration of Concept 4 – FPP during acceleration in trial and design condition

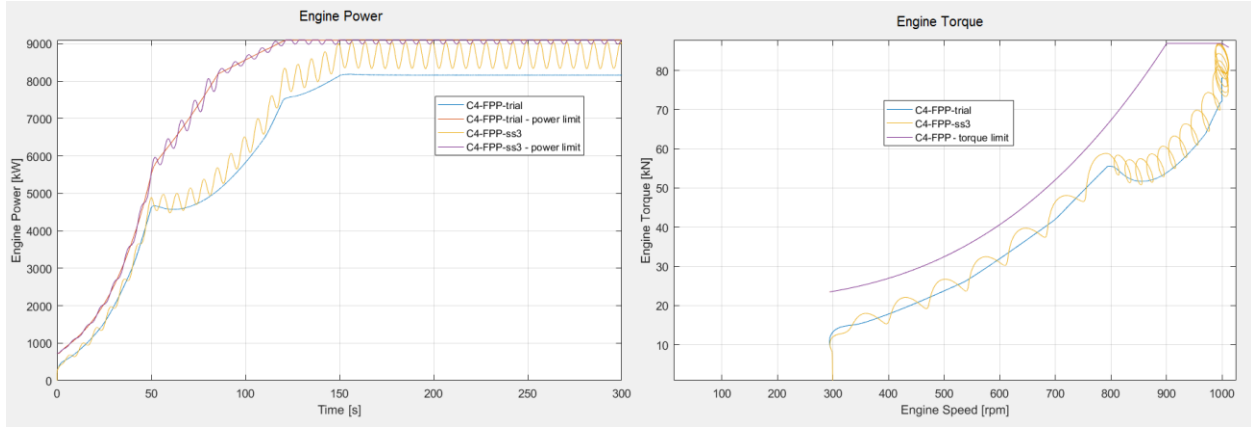


Figure 6.34: Engine power and torque of Concept 4 – FPP during acceleration in trial and design condition

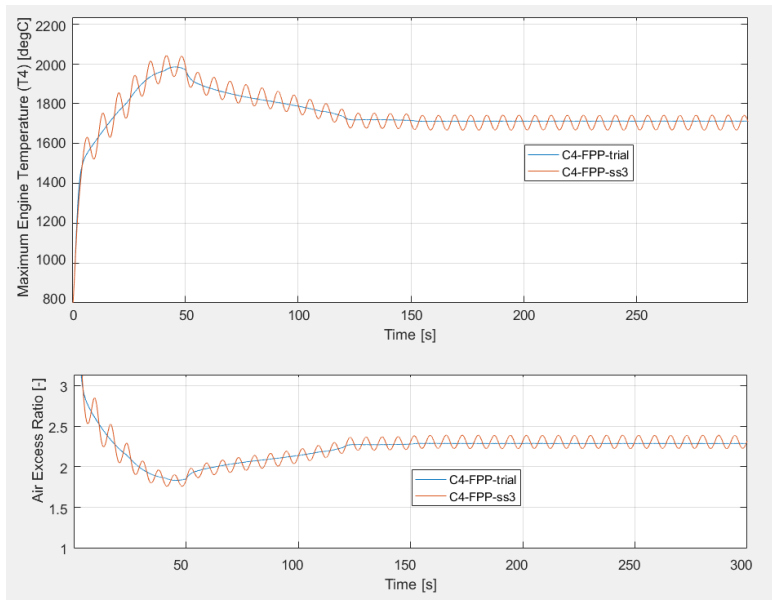


Figure 6.35: Maximum cylinder temperature and air excess ratio of Concept 4 – FPP during acceleration in trial and design condition

| | |
|------------------|------------------------|
| a_{\max} | 0.187 m/s ² |
| a_{ave} | 0.087 m/s ² |
| T_{\max} | 2040 °C |
| λ_{\min} | 1.76 |
| $(dT/dt)_{\max}$ | 58 °C/s |

Table 6.13: Results of acceleration maneuver Concept 4 - FPP

CPP – Trial Conditions and Design Condition

For high performance and low thermal loading on the engines, the right combination of pitch and engine speed ramp up is crucial. The amount of combinations is endless and as is the amount of combinations that result in poor performance, overloading or both. Picking a reference is not easy as the amount of fast naval vessels on diesel engines is limited and detailed data on the control of their propulsion plant even more scarce. Due to their poor performance and problems with overloaded diesel engines, the old M-frigate and the LCF are not the best starting point to develop setpoints for high performance.

However, some data on the Danish Iver Huitfeldt-class frigate is available. This vessel with $\Delta = 6600$ tons is slightly larger than concept 4 – CPP. It is propelled up to 29.3 knots by four diesel engines of comparable size, driving two shafts with CPPs. For the acceleration maneuver, the following diesel engine ramp up rates were provided:

- 400 – 700 rpm: 19 rpm/s
- 700– 1000 rpm: 7 rpm/s

During the acceleration maneuver in calm sea, the vessel achieves the following performance:
(The data of the following table was altered due to restricted information)

| | | | | | |
|------------|------|----|----|-----|------|
| Time [s] | 35 | 60 | 80 | 110 | 120 |
| Speed [kn] | 10.0 | 22 | 27 | 29 | 29.3 |

Table 6.14: Acceleration Danish Iver Huitfeldt-class frigate

The pitch setpoints are not known, but with the provided acceleration times, pitch setpoints could be developed experimentally with the propulsion model of concept 4 – CPP:

| | | | | | |
|----------|-------|-----|-----|------|------|
| t_set_n | [s] | 0 | 16 | 59 | 300 |
| n_set | [rpm] | 400 | 700 | 1000 | 1000 |
| t_set_PD | [s] | 0 | 10 | 90 | 300 |
| PD_set | [-] | 0 | 0.5 | 1 | 1 |

Table 6.15: Engine speed and pitch setpoints concept 4 – CPP for acceleration maneuver similar to Iver Huitfeldt

With this settings, concept 4 – CPP achieves the comparable performance:

| | | | | | |
|------------|------|------|------|------|------|
| Time [s] | 32.5 | 60 | 75.5 | 87 | 118 |
| Speed [kn] | 10.0 | 20.8 | 25.4 | 27.6 | 29.6 |

Table 6.16: Results concept 4 – CPP for acceleration maneuver similar to Iver Huitfeldt

The electric drives were not used for this simulation. The resulting engine loading and the ship speed are plotted in figure 6.36. Even though the engines of the Iver Huitfeldt (MTU 20V 8000) are equipped with sequential turbocharging, the engine load remains below the load limit of the one-stage turbocharged engines of the simulation model. This is a result of the fast ramp up of the diesel engines.

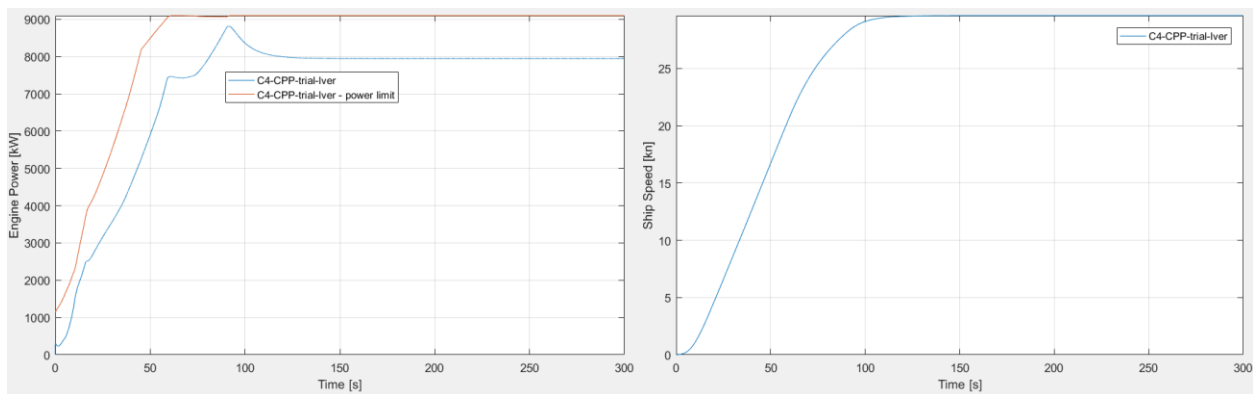


Figure 6.36: Power and ship speed for concept 4 – CPP, settings close to propulsion Iver Huitfeldt class frigates

The engine ramp up for the concepts with CPP is lightly altered compared to the ramp up rates of the Iver Huitfeldt:

- Minimum engine speed of the engines used in the concept is 300 rpm
- The switch over speed of the turbochargers differ as well. The MTU engine creates maximum charge air pressure with 2 of 4 turbochargers at 700 rpm, whereas the MAN reaches maximum pressure with 1 of 2 TC at 800 rpm. Therefore, the MAN engines are ramped up fast to 800 rpm.

With this slight changes, the following engine speed setpoints are set up:

| | | | | | |
|---------|-------|-----|-----|------|------|
| t_set_n | [s] | 0 | 25 | 60 | 300 |
| n_set | [rpm] | 300 | 800 | 1000 | 1000 |

Table 6.17: Engine speed setpoints for all concepts with CPP

The setpoints result in the following ramp up rates:

- 300 – 800 rpm: 20 rpm/s
- 800 – 1000 rpm: 5.7 rpm/s

To increase the comparability of the different concepts, the engine ramp up rates are held constant for all concepts with CPP.

Concept 1 – CPP

With the engine speed setpoints fixed, the pitch setpoints are adjusted to prevent overloading of the diesel engines. For trial condition and design condition the following setpoints are defined:

| | | | | | |
|----------|-------|---|-----|-----|-----|
| t_set_PD | [s] | 0 | 10 | 120 | 300 |
| PD_set | [-] | 0 | 0.5 | 1 | 1 |
| t_set_ed | [s] | 0 | 50 | 300 | |
| T_set | [kNm] | 0 | 52 | 52 | |

Table 6.18: Pitch and edrive setpoints for acceleration maneuver Concept 1 – CPP in trial and design conditions

The setpoints result in the following pitch rates:

- Rate 1: 2 °/s
- Rate 2: 0.18 °/s

Due to the slightly higher efficiency of the CPP, the engine speed does not have to be reduced if the sea state is increased to sea state 3, as needed with a FPP.

6. Results

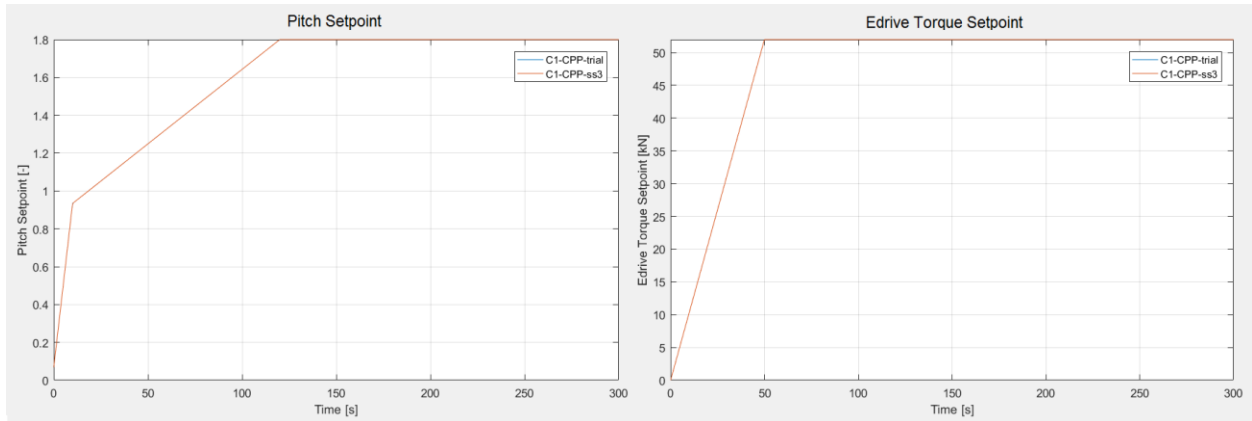


Figure 6.37: Setpoints for propeller pitch and edrive torque of Concept 1 – CPP

Due to the fast ramping up of the diesel engine, the engine can provide more torque during the acceleration maneuver. This results in a much higher acceleration, peaking at 0.227 m/s^2 after just 26 seconds. The maximum ship speed of 28.5 knots is reached in 148 seconds. This is comparable to the concept with FPP, but due to the minimum engine speed the initial velocity of the concept with FPP was 6 knots. The average acceleration from stand still with CPP therefore is 0.1 m/s^2 , an increase of 25%. The acceleration of concept 1 with CPP fulfills the required NATO standards.

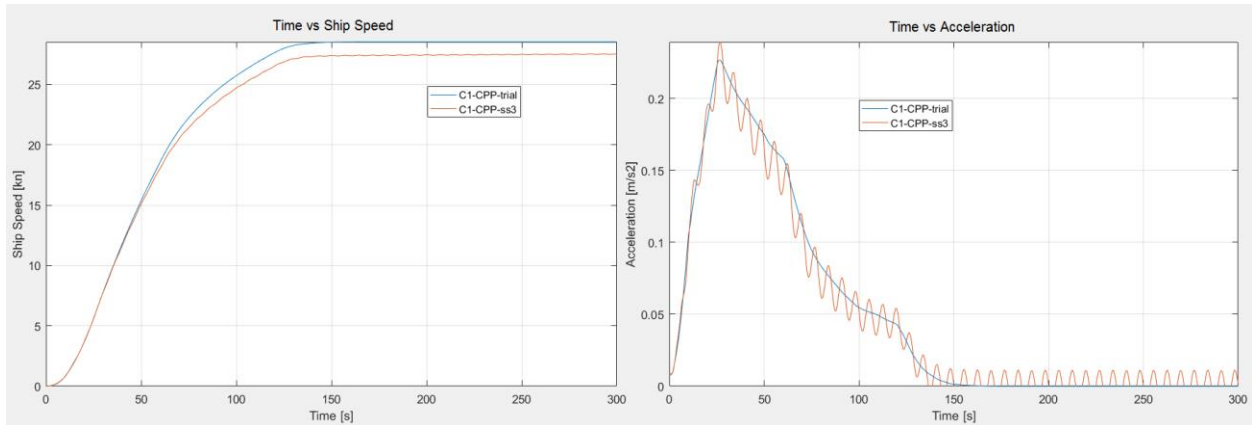


Figure 6.38: Speed and acceleration of Concept 1 – CPP during acceleration in trial and design condition

Next to the increased acceleration, the fast ramp up of the diesel engine has another advantage. Due to the higher engine speed, the charge pressure increases and more air is available in the cylinder. This increases the load limit, see figure 6.39, and decreases the maximum cylinder temperature.

The maximum cylinder temperature stays well below the temperature limit. Unfortunately, the temperature increase rate is improved as well but remains close to the allowable increase limit.

6. Results

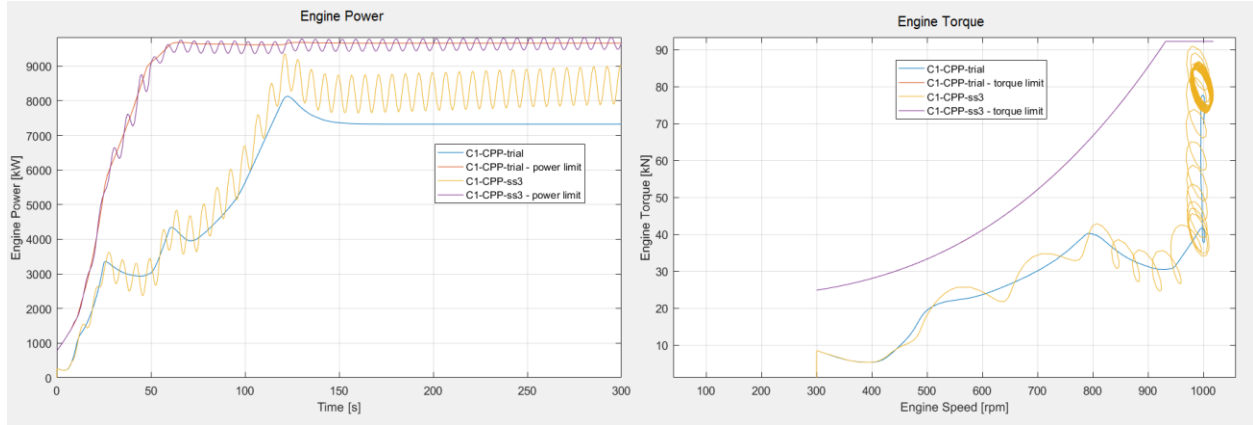


Figure 6.39: Engine power and torque of Concept 1 – CPP during acceleration in trial and design condition

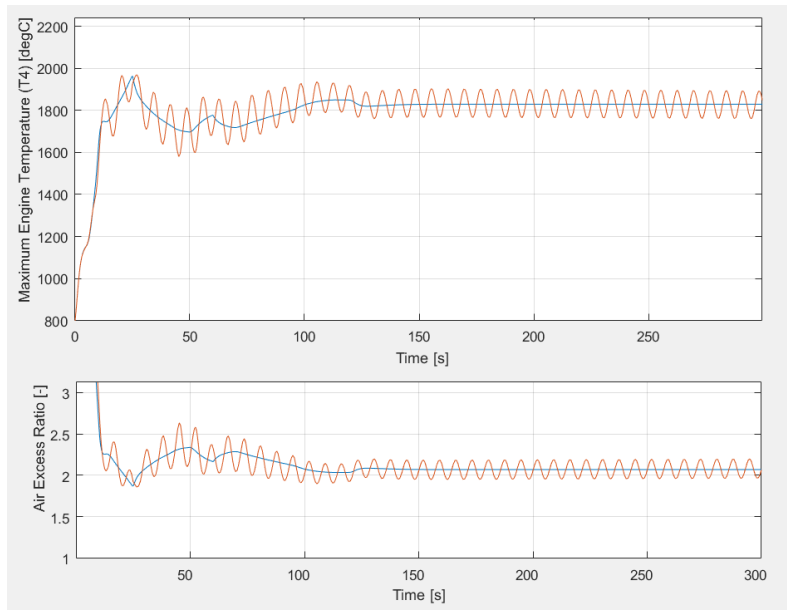


Figure 6.40: Maximum cylinder temperature and air excess ratio of Concept 1 – CPP during acceleration in trial and design condition

| | |
|------------------|------------------------|
| a_{\max} | 0.227 m/s ² |
| a_{ave} | 0.1 m/s ² |
| T_{\max} | 1963 °C |
| λ_{\min} | 1.86 |
| $(dT/dt)_{\max}$ | 100 °C/s |

Table 6.19: Results of acceleration maneuver Concept 1 – CPP

Concept 2 – CPP

Compared to concept 1 – CPP, the four diesel engines of concept 2- CPP deliver more torque after ramped up to maximum engine speed. With more torque available towards the end of the acceleration maneuver, the pitch rate can be increased without overloading the engine. The setpoints for propeller pitch and torque of the electric drives are:

6. Results

| | | | | | |
|----------|-------|---|------|------|-----|
| t_set_PD | [s] | 0 | 10 | 100 | 300 |
| PD_set | [-] | 0 | 0.5 | 1 | 1 |
| t_set_ed | [s] | 0 | 40 | 300 | |
| T_set | [kNm] | 0 | 27.6 | 27.6 | |

Table 6.20: Pitch and edrive setpoints for acceleration maneuver Concept 2 – CPP in trial and design conditions

The setpoints result in the following pitch rates:

- Rate 1: $2^\circ/\text{s}$
- Rate 2: $0.22^\circ/\text{s}$

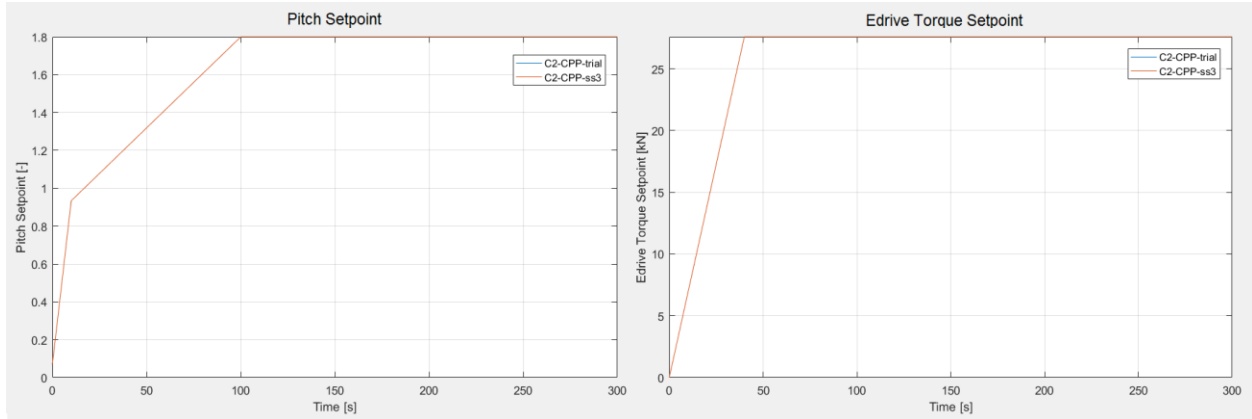


Figure 6.41: Setpoints for propeller pitch and edrive torque of Concept 2 – CPP

With the increased pitch rates, the maximum acceleration is also increased to 0.256 m/s^2 . The maximum ship speed of 29.75 knots is reached in 140 seconds, resulting in an average acceleration of 0.109 m/s^2 . Compared to concept 2, with FPP the acceleration is increased by 30% while the margin to the load limit is increased.

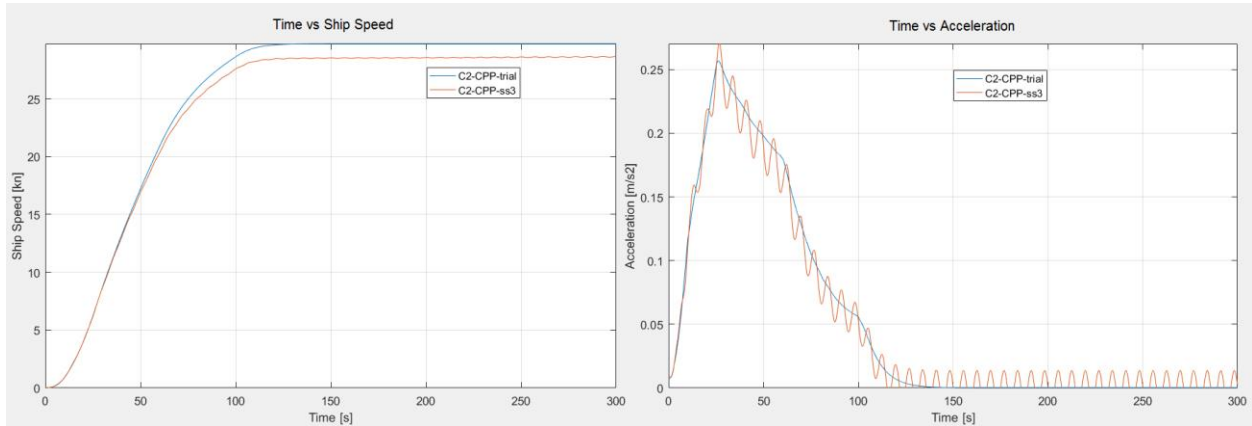


Figure 6.42: Speed and acceleration of Concept 2 – CPP during acceleration in trial and design condition

6. Results

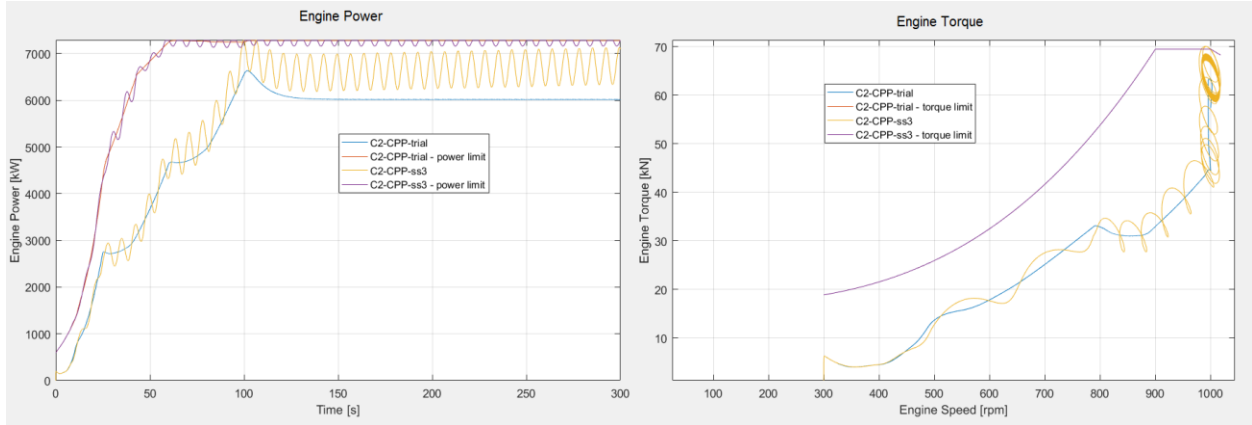


Figure 6.43: Engine power and torque of Concept 2 – CPP during acceleration in trial and design condition

The margin to the load limit is significantly improved, resulting in decreased values for maximum engine temperature and the air excess ratio. The maximum cylinder temperature peaks at 1895 °C, increasing the minimum air excess ratio to 1.97.

Before the electric drives provide maximum torque, the four diesel engines can provide more torque than the two diesel engines of concept 1. With equal ramp up rates for diesel engine speed and propeller pitch the load on the four diesel engines increases slower, resulting in lower temperature increase rates. The maximum temperature increase rate is 90 °C/s.

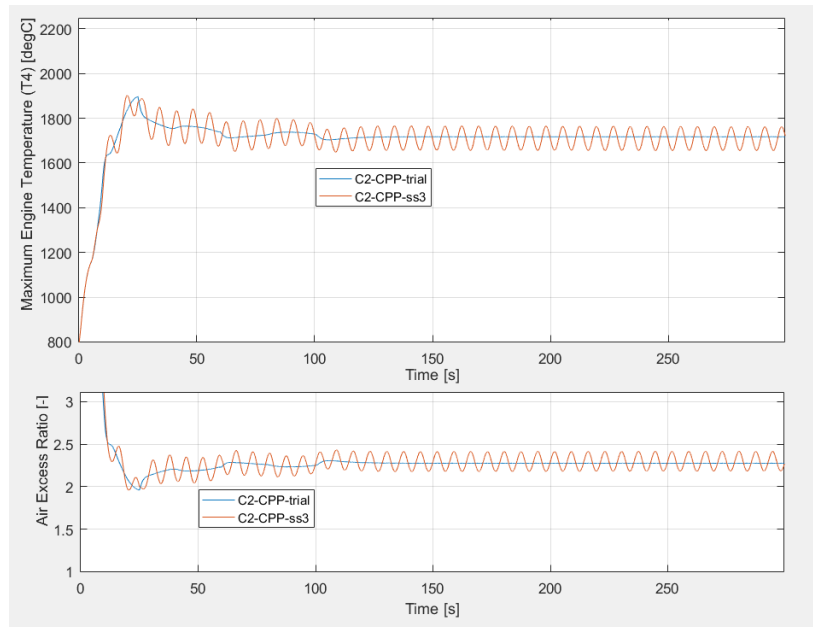


Figure 6.44: Maximum cylinder temperature and air excess ratio of Concept 2 – CPP during acceleration in trial and design condition

| | |
|------------------|------------------------|
| a_{\max} | 0.256 m/s ² |
| a_{ave} | 0.109 m/s ² |
| T_{\max} | 1895 °C |
| λ_{\min} | 1.97 |
| $(dT/dt)_{\max}$ | 90 °C/s |

Table 6.21: Results of acceleration maneuver Concept 2 – CPP

Concept 3 – CPP

Comparing concept 3 and 2 with the CPP, the same considerations hold as for these two concepts equipped with a FPP. The propulsion plant is kept the same, but due to the increased displacement hull resistance and inertia of the vessel increases. Resulting in a higher load on the diesel engines. For the trial conditions, the setpoints can be kept the same without overloading the engine. But for design condition, the propeller pitch setpoints are adjusted to reduce the dynamic load of the acceleration maneuver.

A slight reduction of the second pitch rate was not sufficient to reduce the dynamic loading on the engines and prevent overloading. To further reduce the dynamic load caused by the acceleration, a third pitch rate was introduced.

For the trial condition, the setpoints are equal the concept 2 – CPP:

| | | | | | |
|----------|-------|---|------|------|-----|
| t_set_PD | [s] | 0 | 10 | 100 | 300 |
| PD_set | [-] | 0 | 0.5 | 1 | 1 |
| t_set_ed | [s] | 0 | 40 | 300 | |
| T_set | [kNm] | 0 | 27.6 | 27.6 | |

Table 6.22: Pitch and edrive setpoints for acceleration maneuver Concept 3 – CPP in trial conditions

Resulting in the following pitch rates:

- Rate 1: $2^\circ/\text{s}$
- Rate 2: $0.22^\circ/\text{s}$

For sea state 3, the setpoints for the propeller pitch are adjusted to:

| | | | | | | |
|----------|-----|---|-----|------|-----|-----|
| t_set_PD | [s] | 0 | 10 | 100 | 150 | 300 |
| PD_set | [-] | 0 | 0.5 | 0.95 | 1 | 1 |

Table 6.23: Adjusted pitch setpoints for acceleration maneuver Concept 3 – CPP in design conditions

Resulting in the following pitch rates:

- Rate 1: $2^\circ/\text{s}$
- Rate 2: $0.21^\circ/\text{s}$
- Rate 3: $0.02^\circ/\text{s}$

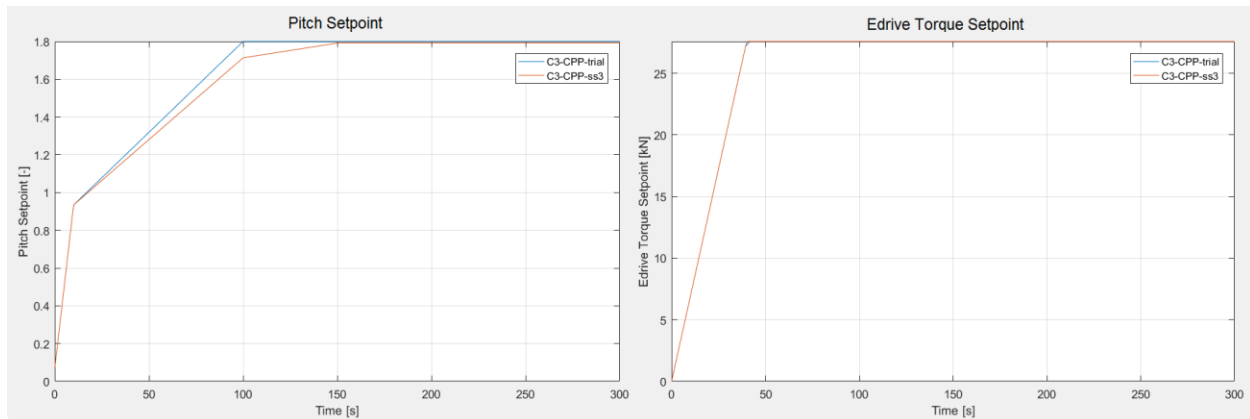


Figure 6.45: Setpoints for propeller pitch and edrive torque of Concept 3 – CPP

As a result of the decreasing pitch rates and the increased inertia of the vessel, the maximum acceleration decreases compared to concept 2 – CPP. The acceleration peaks with 0.235 m/s^2 . The maximum ship speed of 29.2 knots is reached in 132 seconds, resulting in an average acceleration of 0.114 m/s^2 . This value is higher than the average acceleration of the lighter vessel of concept 2. However, the average acceleration is only higher for the trial condition and the lower final ship speed of concept 3, resulting in a larger engine margin. For design condition, concept 2 reaches final ship speed after 128 seconds whereas concept 3 requires 163 seconds due to the decreased pitch rate.

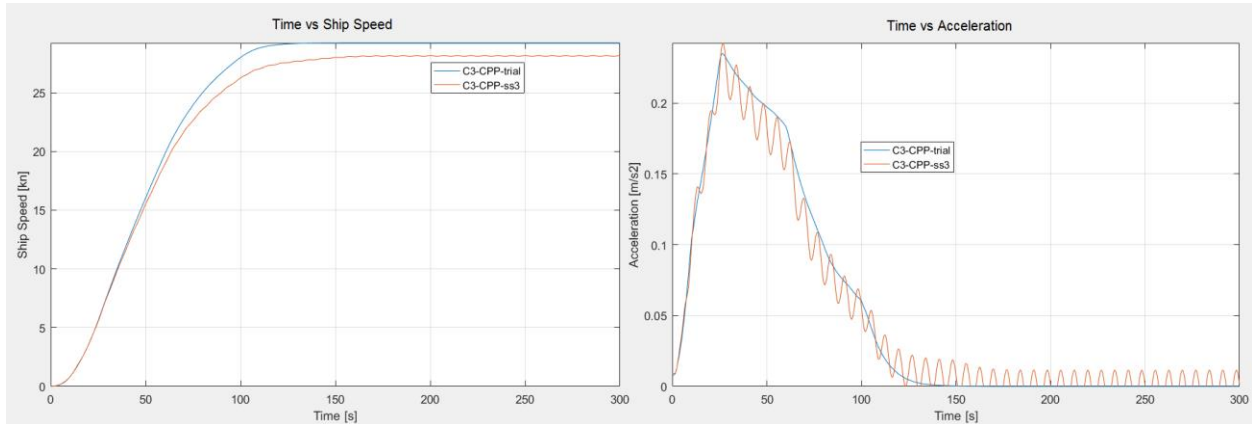


Figure 6.46: Speed and acceleration of Concept 3 – CPP during acceleration in trial and design condition

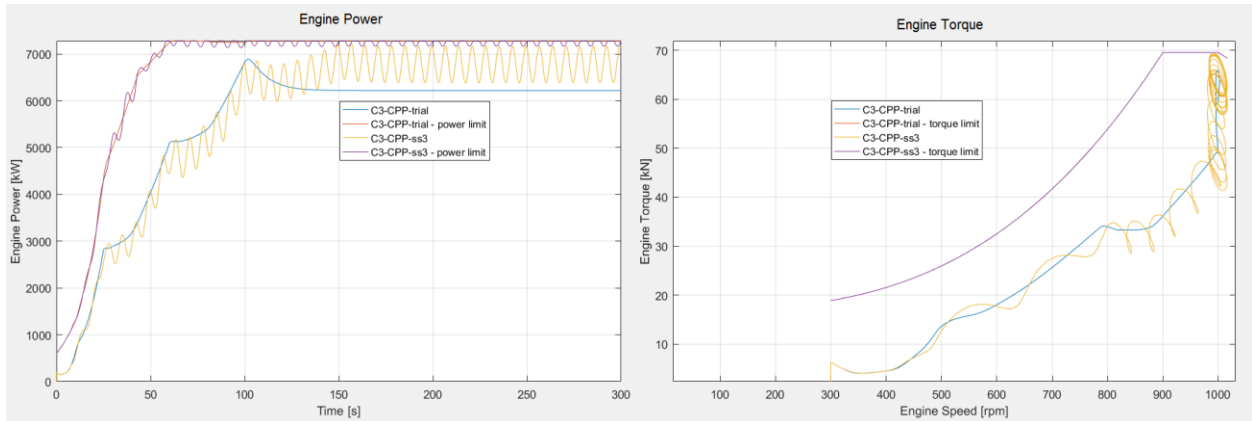


Figure 6.47: Engine power and torque of Concept 3 – CPP during acceleration in trial and design condition

The diesel engines are slightly heavier loaded, the maximum cylinder temperature increases slightly but stays well below the temperature limit. Due to the increased inertia but equal setpoints, the load increases faster resulting in an increased temperature increase rate. With the temperature increase equal to the limit, the concept stays within the thermal limits.

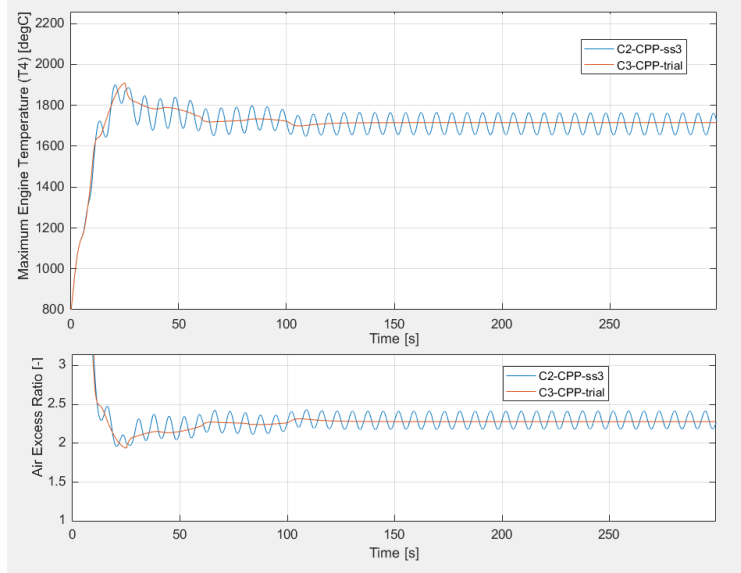


Figure 6.48: Maximum cylinder temperature and air excess ratio of Concept 3 – CPP during acceleration in trial and design condition

| | |
|-----------------|------------------------|
| a_{max} | 0.235 m/s ² |
| a_{ave} | 0.114 m/s ² |
| T_{max} | 1911 °C |
| λ_{min} | 1.94 |
| $(dT/dt)_{max}$ | 102 °C/s |

Table 6.24: Results of acceleration maneuver Concept 3 – CPP

Concept 4 – CPP

Due to the large diesel engines, concept 4 offers also with a CPP the highest acceleration combined with the lowest thermal load of the engines. With the diesel engines providing sufficient power to propel the vessel at design speed, the electric drives can be switched off after the acceleration maneuver. By gradually decreasing the generated torque after the frigate is accelerated to maximum speed, the diesel engines can be loaded close to the load limit without overloading.

The ramp up rates for trial condition and sea state 3 can be kept the same, defined by the following setpoints:

| | | | | | | |
|----------|-------|---|------|------|-----|-----|
| t_set_PD | [s] | 0 | 10 | 80 | 300 | |
| PD_set | [-] | 0 | 0.5 | 1 | 1 | |
| t_set_ed | [s] | 0 | 30 | 90 | 160 | 300 |
| T_set | [kNm] | 0 | 27.6 | 27.6 | 0 | 0 |

Table 6.25: Pitch and edrive setpoints for acceleration maneuver Concept 4 – CPP in trial and design conditions

Resulting in the following pitch rates:

- Rate 1: 2 °/s
- Rate 2: 0.25 °/s

6. Results

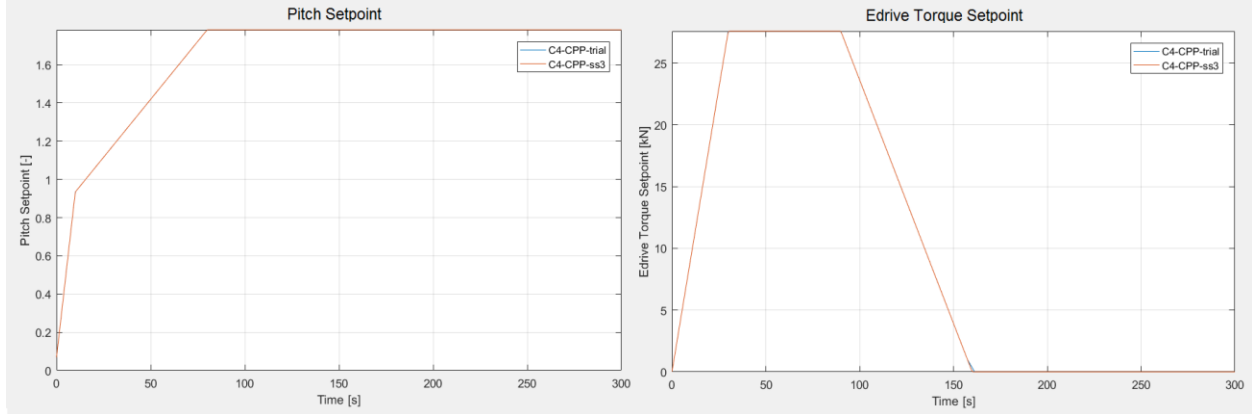


Figure 6.49: Setpoints for propeller pitch and edrive torque of Concept 4 – CPP

The combination of large diesel engines and electric drives provide sufficient power to accelerate the vessel to the maximum ship speed of 29.6 knots in 119 seconds. This results in an average acceleration of 0.128 m/s^2 , fulfilling the NATO desired requirements for acceleration. The acceleration peaks with 0.256 m/s^2 .

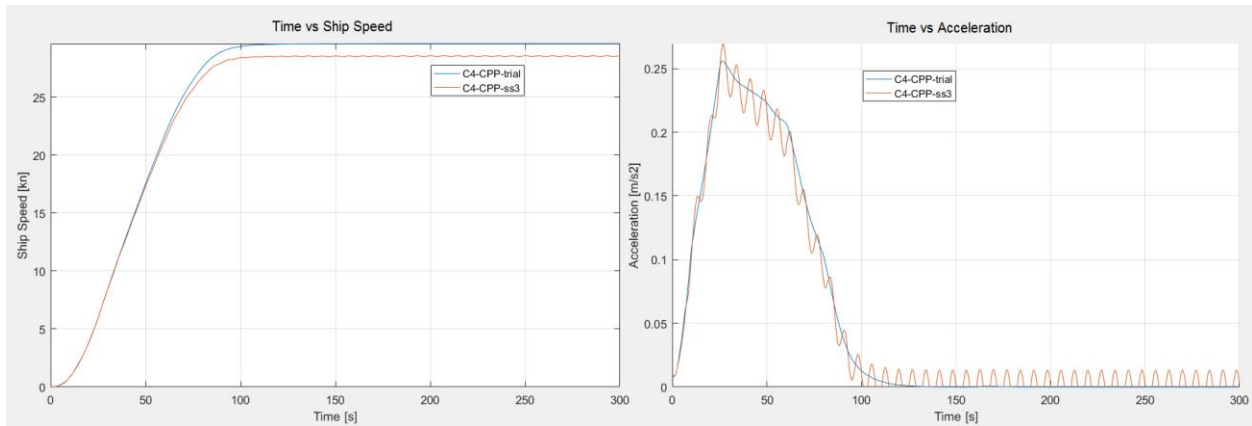


Figure 6.50: Speed and acceleration of Concept 4 – CPP during acceleration in trial and design condition

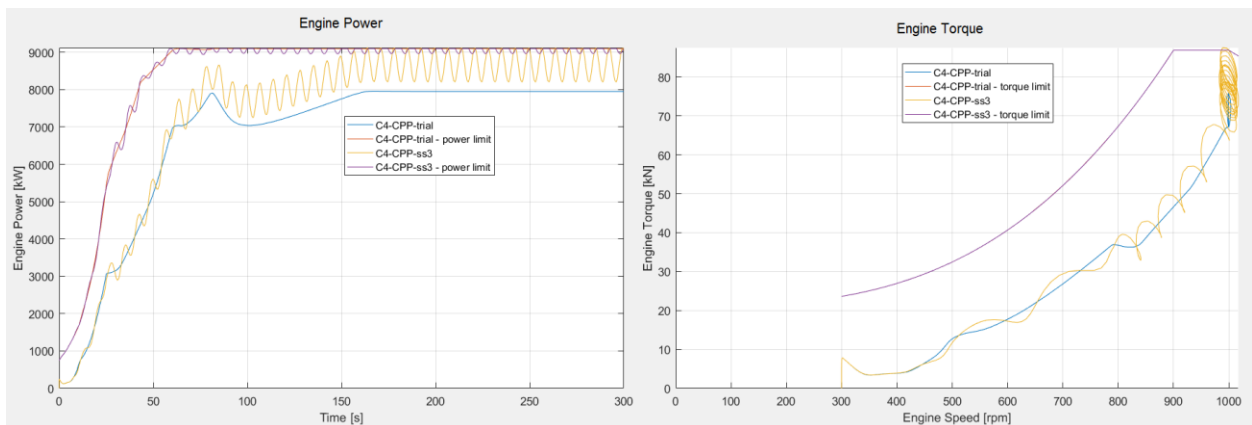


Figure 6.51: Engine power and torque of Concept 4 – CPP during acceleration in trial and design condition

6. Results

The setpoints for this concept are rather conservative, resulting in a large margin to the load limit of the engines. Maximum cylinder temperature is 1850 °C and the minimum air excess ratio is 2.04. Due to the low engine load during the first seconds of the acceleration maneuver, the cylinder temperature increase rate is very low and has a small peak of 59 °C/s.

| | |
|------------------|------------------------|
| a_{\max} | 0.256 m/s ² |
| a_{ave} | 0.128 m/s ² |
| T_{\max} | 1850 °C |
| λ_{\min} | 2.04 |
| $(dT/dt)_{\max}$ | 59 °C/s |

Table 6.26: Results of acceleration maneuver Concept 4 – CPP

The effect of the acceleration maneuver assisted by the electric drives is studied also with concept 4 – CPP. To maintain the same maximum cylinder temperature and temperature increase rates, the setpoints for propeller pitch and engine speed are reduced. Especially the engine ramp up and pitch increase during the beginning of the acceleration maneuver have to be decreased. Figure 6.52 shows results of the acceleration maneuver with and without the assistance of the electric drives. The more conservative settings in the beginning of the acceleration maneuver are reflected with a lagging ship speed. The maximum ship speed of 29.6 knots is achieved in 141 seconds. This results in an average acceleration of 0.108 m/s². With these settings the desired NATO standards are not achieved, but the current low loading on the engines allow for more aggressive increase rates.

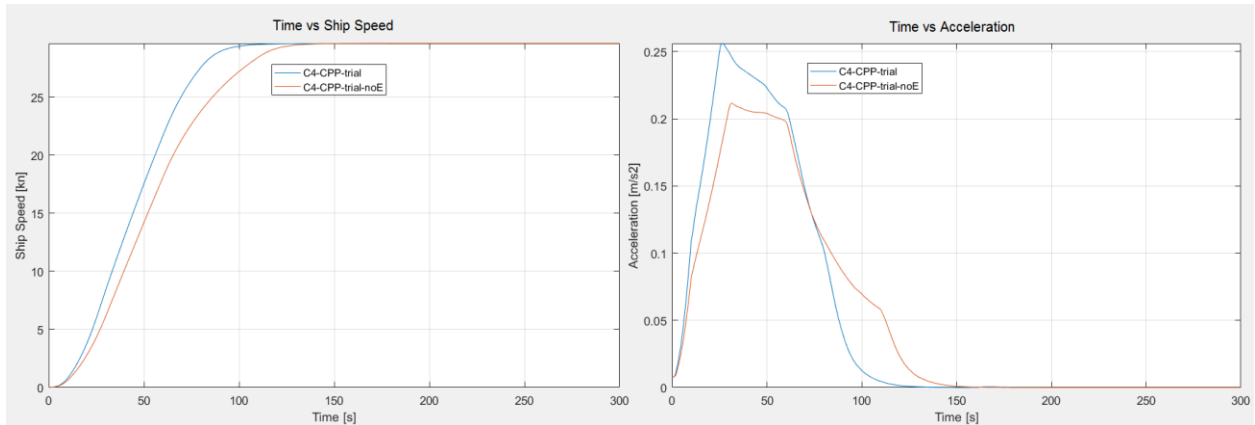


Figure 6.52: Speed and acceleration Concept 4 – CPP, edrive vs no edrive

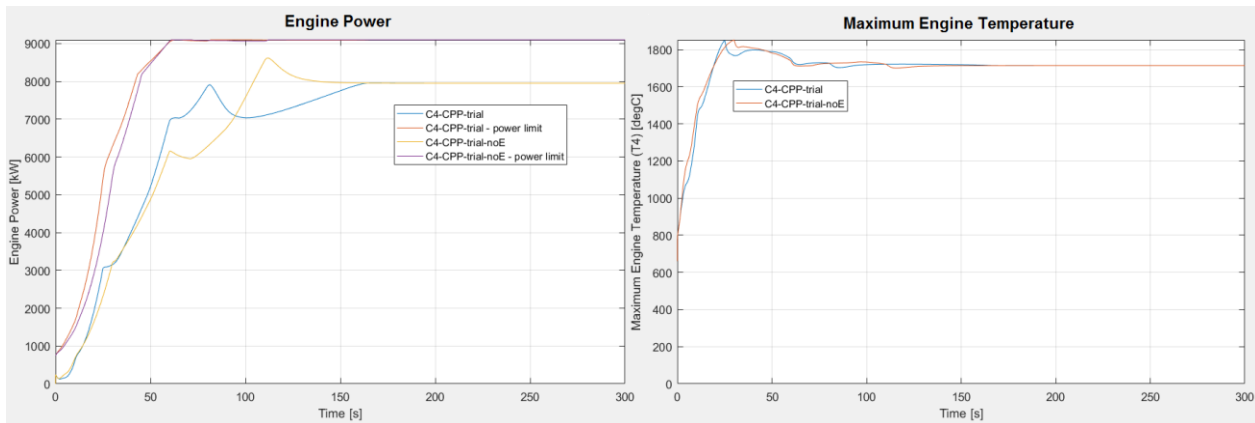


Figure 6.53: Engine power and maximum temperature Concept 4 – CPP, edrive vs no edrive

Overview

The results from the different concepts can be summarized in a table:

| Concept | Ship speed SS3 | Average Acceleration | Thermal Limits | | Angle of Attack |
|-----------|----------------|------------------------|----------------|------------------|-----------------|
| | | | T_{\max} | $(dT/dt)_{\max}$ | α_{\max} |
| LCF - GT | 29 kn | 0.097 m/s ² | | | |
| LCF - DE | 19.4 kn | 0.057 m/s ² | | | |
| C1 – FPP | 27.3 kn | 0.08 m/s ² | 2086 °C | 156 °C/s | 17.5 ° |
| C1 – CPP | 27.5 kn | 0.1 m/s ² | 1963 °C | 100 °C/s | 20.9 ° |
| C2 – FPP | 28.4 kn | 0.084 m/s ² | 2070 °C | 102 °C/s | 18 ° |
| C2 – CPP | 28.6 kn | 0.109 m/s ² | 1895 °C | 90 °C/s | 20.8 ° |
| C3 – FPP | 28.0 kn | 0.075 m/s ² | 2065 °C | 92 °C/s | 18.1 ° |
| C3 – CPP | 28.2 kn | 0.114 m/s ² | 1911 °C | 102 °C/s | 21 ° |
| C4 – FPP | 28.5 kn | 0.087 m/s ² | 2040 °C | 58 °C/s | 18.9 ° |
| C4 – CPP | 28.6 kn | 0.128 m/s ² | 1850 °C | 69 °C/s | 21 ° |
| C4 – CPP* | 28.6 kn | 0.108 m/s ² | 1853 °C | 74 °C/s | 21 ° |

Table 6.27: Summarized results of acceleration maneuvers for all concepts in design conditions.

* without electric drives.

Only concept 4 with CPP fulfills the requirements and stays within the thermal limits. Concept 2 and concept 3, with CPP, fulfill the required NATO standards for acceleration, but not the desired standards.

Comparing the acceleration for the different concepts, figure 6.54, the difference between concepts with CPP and FPP is clear. The performance of the concepts with CPP, especially concept 4, is close to the performance of the reference frigate on gas turbines. The acceleration performance of the concepts with FPP is significantly lower and the maximum acceleration is reached a lot later.

Neither the gas turbine nor concept 4 – CPP is designed to the limit. The reference vessel on gas turbines could perform better if the pitch rate is increased. Concept 4 – CPP could also perform better (read: achieve higher accelerations) with increased pitch rates as the loading on the engine is still relatively low.

All concepts with CPP require higher pitch increase rates than currently handled on the LCF. However, the increased pitch rates of 2 °/s are feasible, even with the propulsion system currently used on the LCF which allows for pitch increase rates of 2.4 °/s.

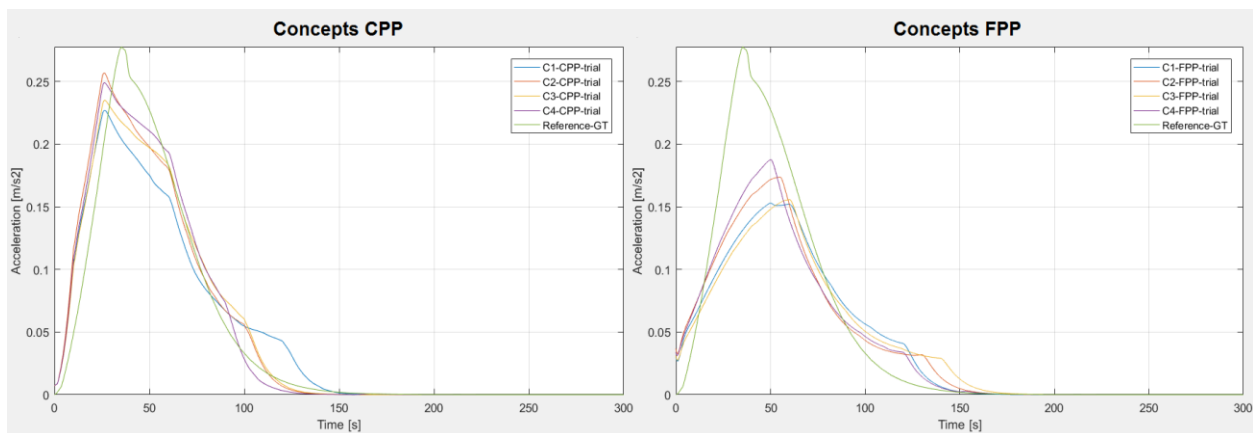


Figure 6.54: Comparison acceleration CPP and FPP during acceleration in trial condition

Figure 6.55 shows the comparison for the maximum cylinder temperature. Concepts with CPP show a clear peak in the maximum cylinder temperature, coinciding with the maximum acceleration (after 25 seconds). The peak also coincides with the diesel engines ramped up to 800 rpm. The high ramp up rate also causes the high load increase on the engine as the engine with its own inertia needs to be accelerated as well. It is followed by the drop in engine ramp up rate, causing the load increase rate on the engine to decrease and so does the maximum engine temperature.

For the FPP the peak is not that distinctive, but coincidences as well with the change in engine ramp up rates. Due to the much lower ramp up rates of the diesel engines for FPP, the effect of the inertia of the engine is of lesser impact. As a result reducing the ramp up rate of the engine has a lower impact on reducing the maximum cylinder temperature.

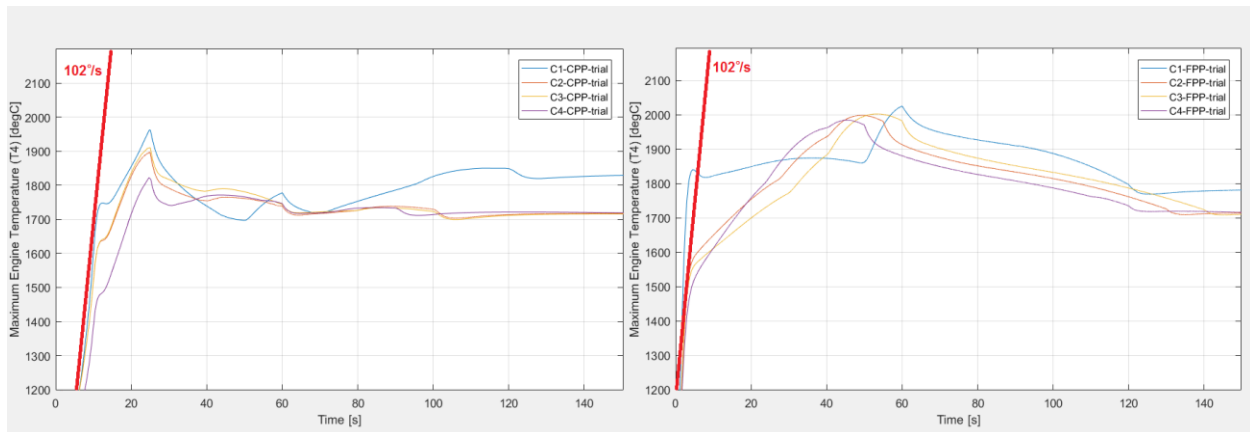


Figure 6.55: Comparison maximum cylinder temperature CPP and FPP during acceleration in trial condition

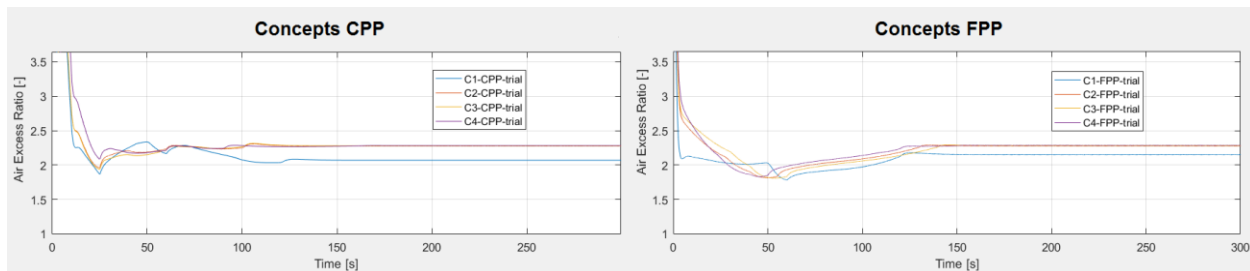


Figure 6.56: Comparison minimum air excess Ratio CPP and FPP during acceleration in trial condition

Concepts in off-design condition

In off-design condition (sea state 6) the effect of waves on the propulsion plant and the performance of the frigate significantly increases. The increased average added resistance increases the load on the engines and the oscillating advance velocity reduces the engines load limit. As a result, the maximum ship speed cannot be achieved any longer. To handle the increased resistance, control strategies for FPP and CPP are different.

CPP in off-design condition

By reducing the pitch of the propeller for a CPP, a high engine speed can be remained and maximum engine power is available. Accelerating in off-design condition, the engine ramp up rates are held constant, as determined for trial conditions. To prevent overloading, pitch rates are reduced slightly but the largest effect has the reduction of maximum propeller pitch to 37°.

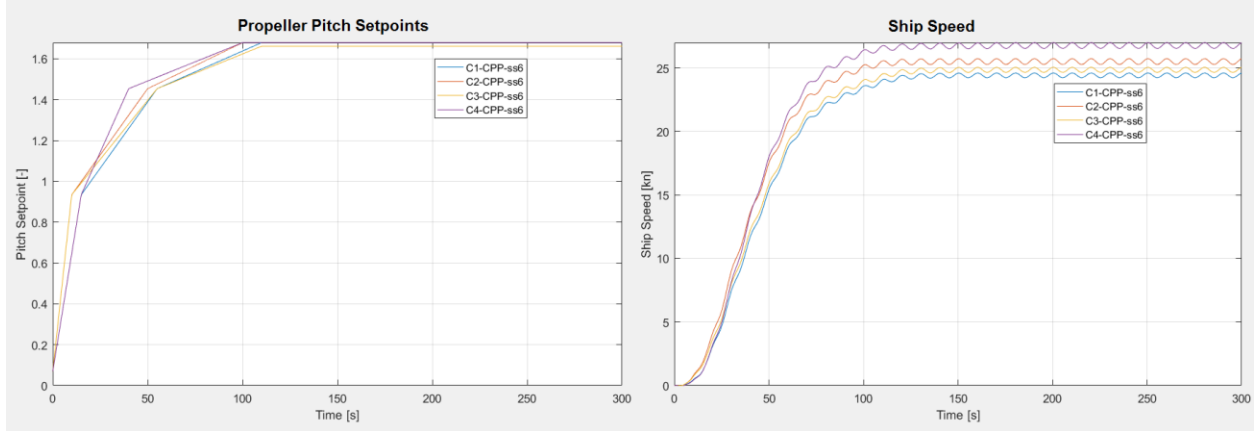


Figure 6.57: Propeller pitch setpoints and ship speed CPP in off-design condition

The achievable ship speed remains high, compared to design condition, the speed is reduced by 8 – 11%.

However, the load on the engines oscillates as well. For concept 1, relying on large electric drives, the load oscillates with smaller amplitude. For concept 4, after switching off the electric drives after the acceleration maneuver, the amplitude of the oscillation is the largest, see figure 6.58.

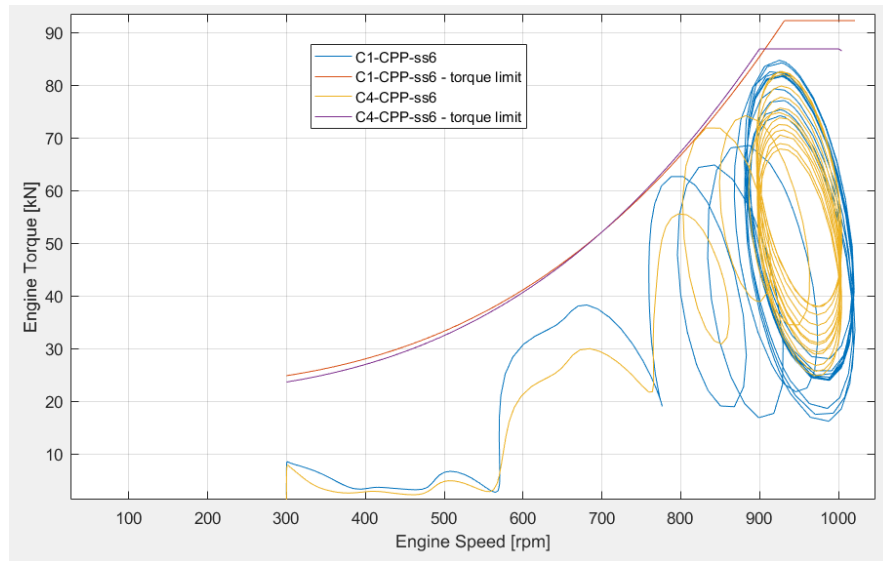


Figure 6.58: Oscillating torque and engine speed in off-design condition

For concept 1, the amplitude has a magnitude of 57.2 Nm, or about 60% of the total available torque. The amplitude for concept 4 increases to 68.5 Nm, or about 79% of the total available torque. These load changes introduce large disturbances on the engine speed, oscillating with an amplitude of up to 135 rpm, resulting in discomfort on the vessel itself and thermal stresses in the engine.

The oscillations on the load of the engine seemed very high. Therefore the results were compared to measurements on the old M-frigate showing the oscillating fuel rack position due to the countermeasures of the governor in sea state 6, figure 6.59 (van Spronsen & Tousain, 2001). In an attempt to counter steer the oscillating engine speed/shaft speed, the fuel rack setpoints, determined by the governor, oscillate as well. This figure also shows the clear overloading of the diesel engine as the governor was mechanically not limited

to keep the fuel rack position within the overloading criterion. The maximum amplitude of oscillation of the fuel rack is about 12 mm for a ship speed of 16 knots.

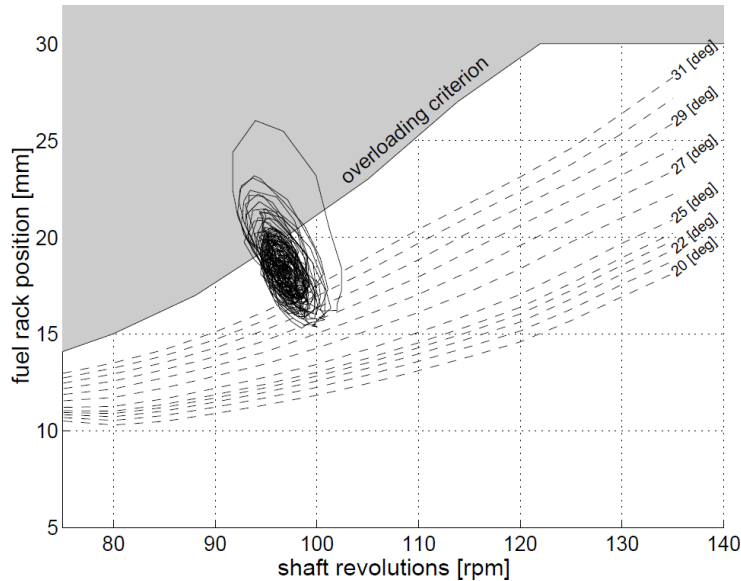


Figure 6.59: Fuel rack position in sea state 6 from M-frigate (van Spronsen & Tousain, 2001)

Figure 6.60 show simulation results for the fuel rack position of concept 4 – CPP in off-design condition (sea state 6). The engine speed was set to 700 rpm and the propeller pitch to 31°, resulting in a ship speed of 16.7 knots.

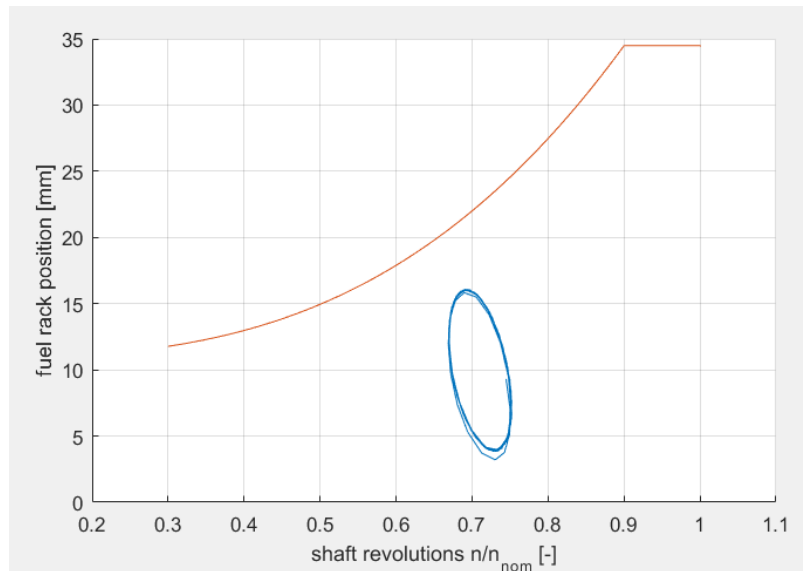


Figure 6.60: Fuel rack position in sea state 6 for Concept 4 – CPP

Due to the much larger engines, the overloading criterion is not violated in this condition. But the oscillating wave load has the same effect on the fuel rack position. The resulting amplitude of the fuel rack oscillation is 11.7 mm, only slightly reduced compared to the real measurements of the M-frigate. Another effect of the larger engines, providing more torque, is visible in the results. The ovals described by oscillating fuel rack position are less tilted for the simulation, corresponding with less fluctuations in the engine speed.

With proper control of the electric drive, the load oscillation on the engine could be reduced. If the electric drives generate torque in antiphase with the advance speed, thus in phase with the oscillating engine torque, part of the fluctuations is taken over by the electric drives. The reduction of load peaks on the diesel engine is also called peak shaving.

Figure 6.61 shows the setpoint for the electric drives in antiphase with the advance speed for concept 4 – CPP. The load oscillation on the diesel engine significantly reduces. The amplitude of the oscillating engine torque reduces to 35 Nm and as a result the amplitude of the oscillating engine speed reduces to 73 rpm.

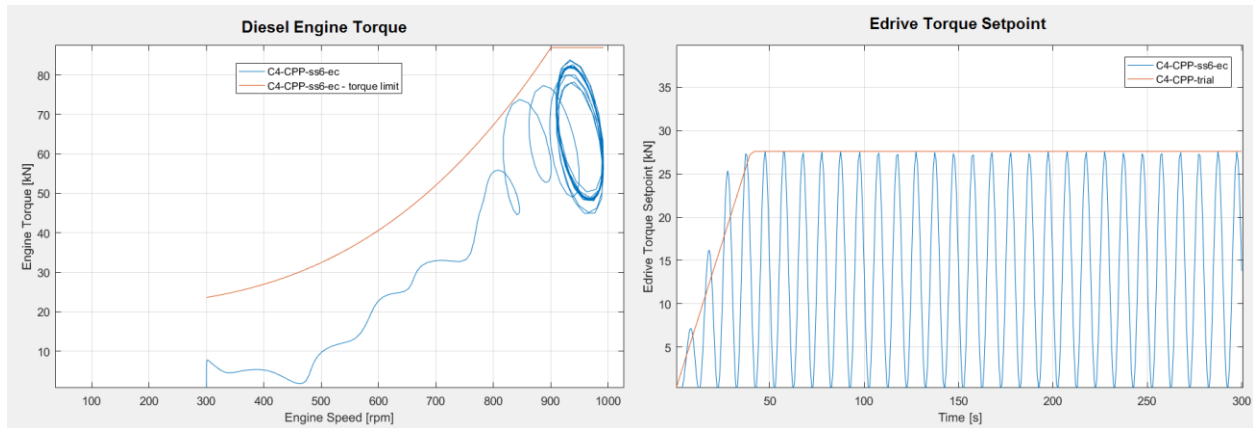


Figure 6.61: Diesel engine torque with controlled edrive in off-design condition

Figure 6.62 shows the effect on lambda compared to constant torque generation of the electric drives. The amplitude of oscillating air excess ratio reduces and thus also the fluctuations in engine temperature will reduce.

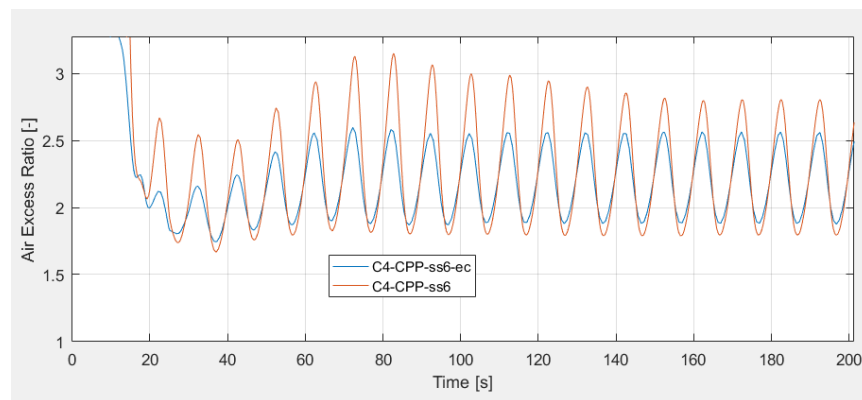


Figure 6.62: Effect of controlled edrive on air excess ratio in off-design condition

For an actual controller the shaft speed or engine speed could be used as process variable as the engine speed oscillates in phase with the advance speed. Next to the advanced controller also a fast responding electric energy storage is needed, otherwise the load oscillations would just be passed onto the generator sets.

FPP in off-design condition

With an FPP the options in off-design condition are limited to reducing the engine speed and thus the propeller speed. However, with reduction of engine speed, the load limit of the diesel engines reduces as well. This can result in a still overloaded engine if the margins between propeller curve and load limit for the design case already were small. In that case the ship can lose its propulsion and should be prevented in any circumstance.

For concept 4 – FPP the electric drives are switched off after the acceleration maneuver, showing the severe reduction in engine performance, figure 6.63. The engine speed is limited to 500 rpm to prevent overloading of the diesel engines, reducing the ship speed to 14.8 knots. The effect of switching off the electric drives is clearly visible in the speed – torque curve of figure 6.63. During the acceleration maneuver the electric drives are providing additional torque and the margin between delivered torque and the torque limit is sufficient (300 – 500 rpm). With gradually decreasing the generated torque of the electric drives the torque of the diesel engine increases to the limit. This situation is very unfavorable for the diesel engine:

- the engine is operating in low speed and low absolute load (compared to the nominal power), resulting in increased wear of the engine.
- The relative load (compared to the speed dependent load limit) is oscillating between maximum and close to zero, resulting in high fluctuations of the cylinder temperature and thus increases the thermodynamic stresses.
- With the load limit reached the engine cannot provide any additional power for acceleration or if the resistance increases further due to an increasing sea state.

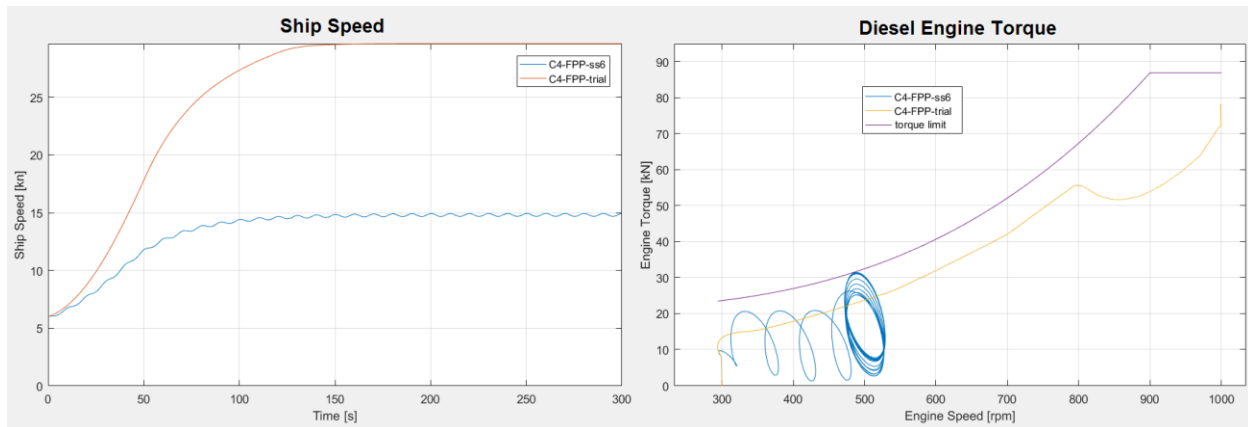


Figure 6.63: Ship speed and diesel engine torque for Concept 4 – FPP in off-design condition

For concepts 1 – 3 with FPP the situation is slightly better. Due to the continuous assistance of the electric drives, higher engine speeds are achieved and thus higher ship speeds. Figure 6.64 shows the results for ship speed and engine setpoints for the four concepts equipped with FPP. The engine ramp up rates are reduced to prevent overloading of the diesel engines during the acceleration.

Figure 6.65 shows the diesel engine torque for concepts 1 – 3 with FPP. The engines are close to overloading, the ramp up rates could be further reduced to reduce the load while accelerating. During the acceleration maneuver, the oscillating torque on the diesel engines is severe. For the final ship speed however, the torque oscillates less severe than for the concepts equipped with CPP.

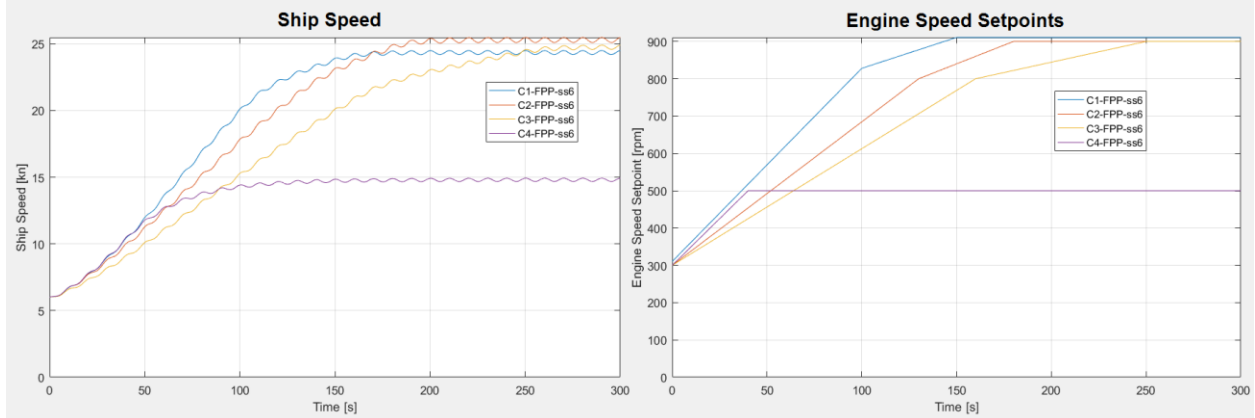


Figure 6.64: Ship speed and engine setpoints for concepts with FPP in off-design condition

This results show clearly that sea state 6 is the limiting sea condition for all concepts with FPP. A further increased sea state will result in a loss of propulsion. Even more important is the assistance of diesel engines by the electric drives. Without the additional power of the electric drives concepts 1 – 3 will lose propulsion completely and concept 4, due to the increased margin in design condition, will be limited to 14.8 knots.

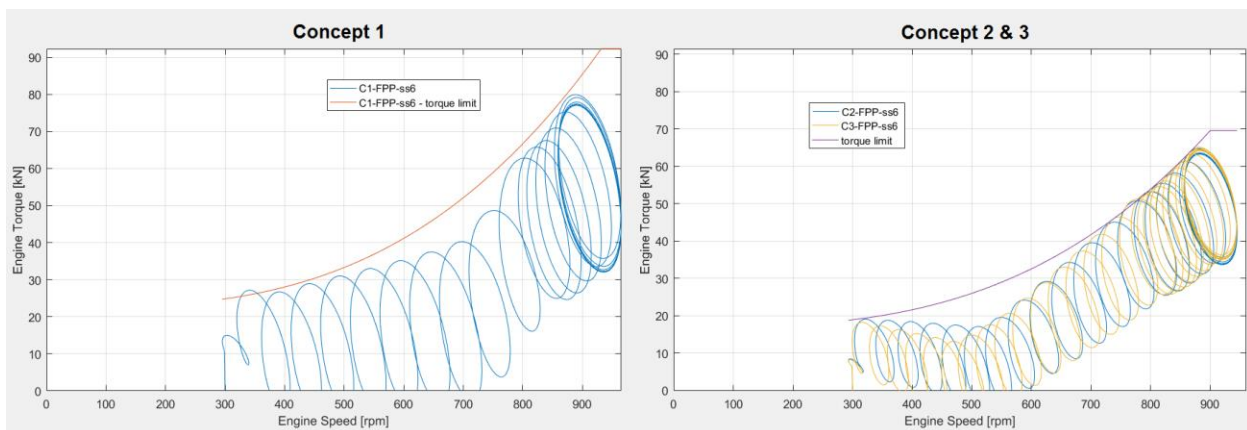


Figure 6.65: Engine torque for concepts 1 – 3 with FPP in off-design condition

Improving performance with STC

Limiting to the performance of the propulsion concepts with FPP in off-design condition is the decreasing load limit with decreasing engine speed. The load limit used in the simulations is a decent assumption for a one-stage turbocharged system. Actual load limits for these engines might change slightly, improving or worsen the actual performance slightly but not considerable.

Extending the load limit can be achieved by equipping the diesel engines with sequential turbocharging. The load limits for an engine equipped with STC are easy to add to the model. However, results for the engine temperature are not representative. On low rpm, an engine equipped with STC decreases the amount of turbochargers in use, therefore increasing the mass of air through each turbocharger and increasing the charge air pressure. With higher charge air pressure the maximum cylinder temperature decreases. As a result, the predicted cylinder temperature on low engine speed will be higher than temperatures of an actual engine equipped with STC.

Figure 6.66 shows the resulting ship speed and engine load for the diesel engines of concept 4 – FPP equipped with STC. The increased load limit represents the actual load limit of the MAN 28/33 with STC. Due to the increased load limit a higher engine speed can be achieved, resulting in a ship speed of 22.5 knots. More important however is the reduced relative engine load (compared to the speed dependent load limit).

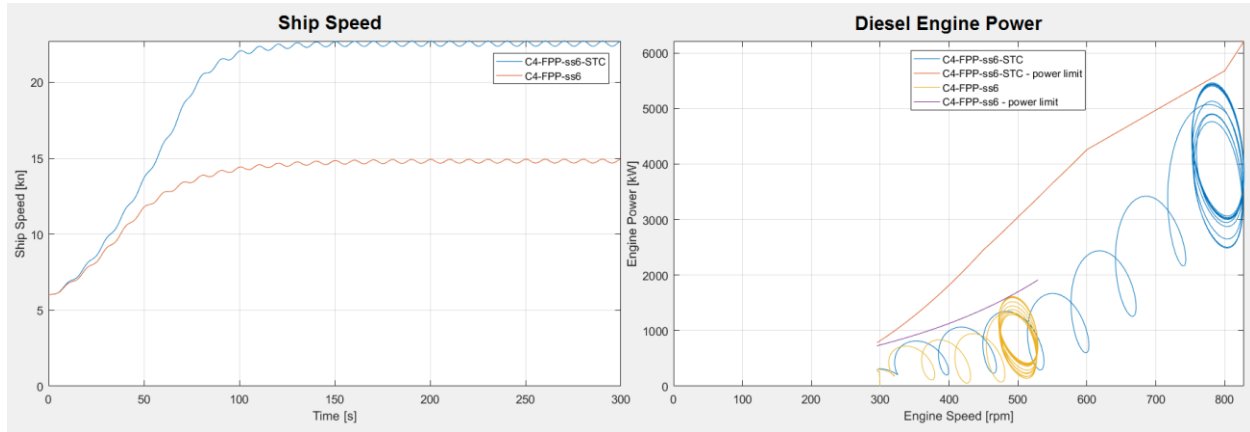


Figure 6.66: Concept 4 – FPP comparison performance non-STC with STC in off-design condition

Improving redundancy with STC

Equipping the vessel with sequentially turbocharged diesel engines could also improve the redundancy of concepts 2 and 3 with FPP. Simulating the acceleration maneuver without electric drives, the vessel can be accelerated without overloading the engine, see figure 6.67. By accelerating the vessel very slow, the load limit is not exceeded, but the margin reduces to zero. This situation will certainly not be accepted for the actual vessel as a slight increase in resistance or sea state will result in a loss of propulsion.

Engines with STC however provide sufficient additional power to improve the acceleration increase the margin to overloading. In this case the acceleration is possible without the additional power of the electric drives.

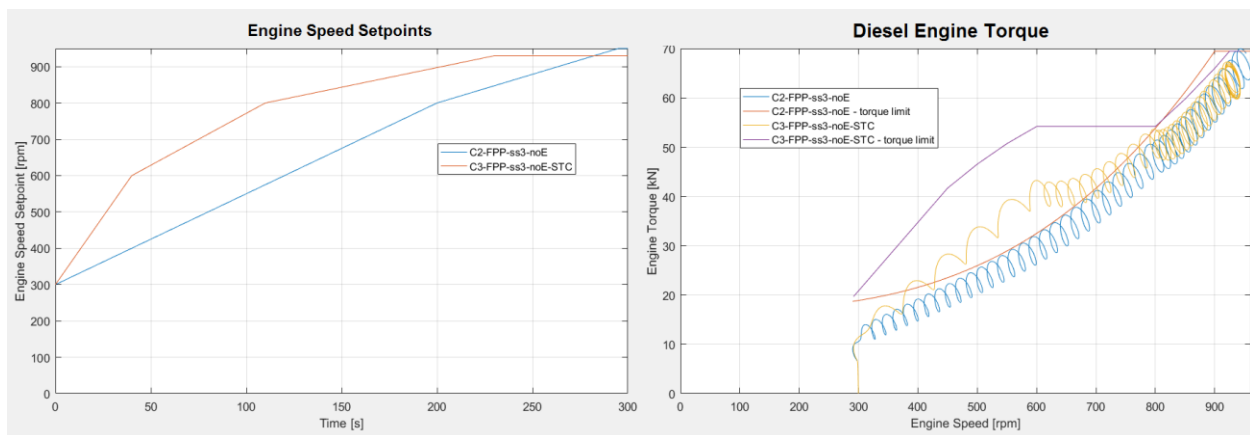


Figure 6.67: Concept 3 – FPP comparison performance non-STC with STC without edrives in design condition

CPP and STC

Concepts with FPP benefit from diesel engines with STC. Improvements in the redundancy and off-design performance was shown with two examples. The acceleration in trial condition and design condition could probably be improved as well by simultaneously reducing the thermal load on the engines. Simulations to show these effects were not possible due to the lack of data on the charge air pressure of STC engines.

Concepts with CPP on the other hand will not or just slightly benefit from diesel engines with STC. Key to achieve good performance and low thermal loading of concepts with CPP was ramping up the diesel engines to maximum speed. STC engines use a reduced amount of turbocharger until the STC change over speed, usually between 70 – 80% of nominal engine speed. After the STC change over speed the exhaust mass flow has increased sufficiently to drive all turbochargers and the engine offers the same performance as a one-stage turbocharged engine, see the load limits in figures 6.66 and 6.67.

Angle of Attack CPP vs FPP

The results are generated with concept 4 in trial condition. With given gearbox ratio, the cavitation inception speed of 19 knots corresponds with a propeller speed of 84.5 rpm and an engine speed of 600 rpm. The electric drive is not used in this simulation. However, for silent ASW-operations, the electric drives might be used instead of the diesel engines. In that case the ramp up rates for the diesel engine speed can be simply translated to the ramp up rates for the electric drives.

The initial ship velocity for the FPP is 8 knots, roughly corresponding with an engine speed of 250 rpm. Before acceleration with the FPP, 15 seconds on 250 rpm are simulated to stabilize the ship speed, otherwise peaks in the angle of attack occur due to short, high accelerations.

For the acceleration maneuvers, the following setpoints were used for FPP:

| | | | | | |
|---------|-------|-----|-----|-----|-----|
| t_set_n | [s] | 0 | 15 | 180 | 300 |
| n_set | [rpm] | 250 | 250 | 600 | 600 |

Table 6.28: Engine speed setpoints concept 4 – FPP acceleration maneuver with low angle of attack

And CPP:

| | | | | | |
|----------|-------|-----|-----|-----|--|
| t_set_n | [s] | 0 | 10 | 300 | |
| n_set | [rpm] | 300 | 600 | 600 | |
| t_set_PD | [s] | 0 | 180 | 300 | |
| PD_set | [-] | 0 | 1 | 1 | |

Table 6.29: Engine speed and pitch setpoints concept 4 – CPP acceleration maneuver with low angle of attack

Resulting in the following ramp-up rates:

- FPP: engine: 2.1 rpm/s
- CPP: engine: 30 rpm/s
pitch: 0.22 °/s

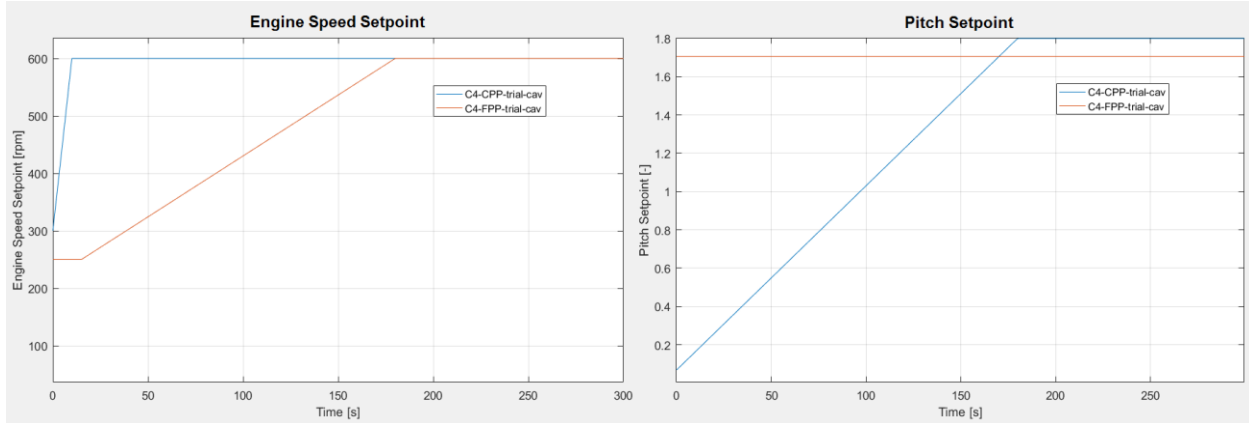


Figure 6.68: Setpoints for low angle of attack concept 4, FPP vs CPP

Figure 6.69 shows the resulting angle of attack for FPP and CPP in the left plot. The right plot shows the angle of attack for the fast acceleration maneuver with the earlier determined setpoints for concept 4.

For the FPP the angle of attack shows the same characteristic development for both simulations with a maximum angle of attack close to the start of the acceleration. The reduced magnitude was expected due to the slower ramp-up rate of the engine.

Simulation of the CPP shows some interesting results. For the fast acceleration the angle of attack reveals a sharp peak due to the fast ramping up of engine speed and propeller pitch within the first 10 seconds of the simulation. By reducing the pitch rate, the sharp peak in the angle of attack can be eliminated completely, resulting in a smooth development of the angle of attack for the start of the acceleration maneuver.

The FPP might achieve better cavitation performance in static conditions due to its design, but once equipped to the vessel very low acceleration is the only option to prevent cavitation in dynamic conditions. With CPP, on the contrary, the cavitation inception can be influenced by propeller speed and pitch. This results in a lower angle of attack of the CPP and probably also less underwater noise.

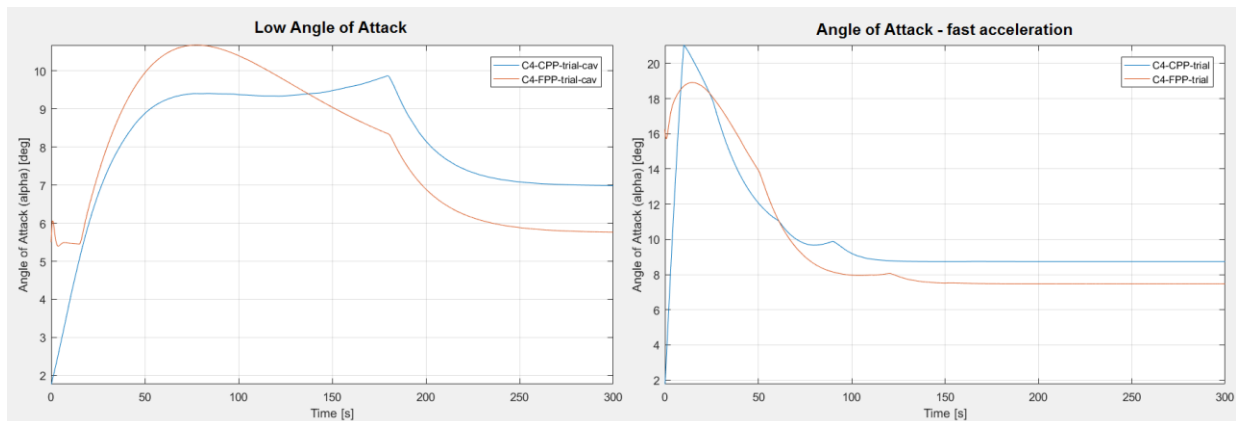


Figure 6.69: Angle of attack for concept 4, FPP vs CPP

Figure 6.70 shows the resulting ship speed and acceleration values for both propellers. While the acceleration maneuver takes roughly the same time for both propellers, the higher initial velocity of the FPP results in a slower acceleration. While maintaining a lower angle of attack, the maximum acceleration of the CPP is increased by 63% (0.062 m/s² vs 0.038 m/s²) and the average acceleration is increased by 86% (0.039 m/s² vs 0.021 m/s²).

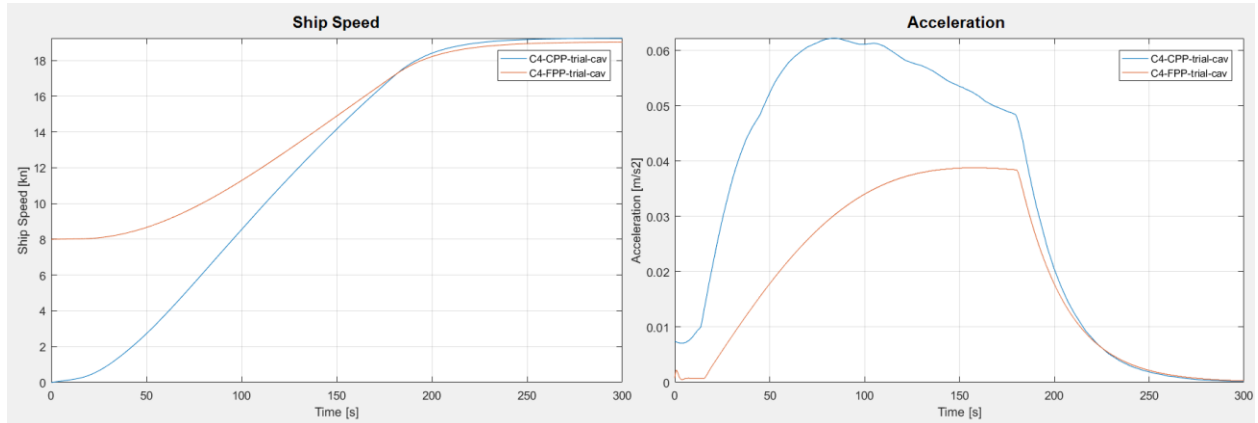


Figure 6.70: Ship speed and acceleration for low angle of attack concept 4, FPP vs CPP

7. Conclusions & Recommendations

Conclusions

The aim of this thesis is to answer the research questions that were posed in Chapter 1. To succeed in this endeavor, dynamic simulation models were developed based on the requirements of the future frigate. These simulation models represent different combinations of a hybrid propulsion system and were used to simulate constant speed and acceleration of the vessel in different sea states and with different operating conditions. Due to problems with overloading on the current M-frigate, special attention was given to prevent this issue.

To prevent overloading, the thermal loading of the engine was evaluated in case the load is increased as fast as the limiting load increase rates stipulated by the engine manufacturers. The thermal engine data obtained ($\Lambda_{\min} = 1.7$, $T_{\max} = 2070^{\circ}\text{C}$, $(dT/dt)_{\max} = 102^{\circ}\text{C/s}$) serves to evaluate whether the diesel engine is thermally overloaded. These values were obtained with the specific diesel engine model used, and are only valid for this model. However, this data proved useful for estimating the thermal load with very limited information on the engines.

For the acceleration simulations, different time-dependent setpoints were tested, resulting in ramp-up rates. Setpoints were developed for the diesel engines, electric drives and pitch, in the case of CPP, and their influence on acceleration performance and thermal loading was gauged. The ramp-up rates developed can serve as a guideline for the development of an adaptive controller.

If a hybrid drive system is considered, a CODLAD (also includes CODLADAD) system should be preferred. With this configuration, the diesel engine can be assisted until the maximum engine speed is reached, and the load limit margin can be increased. While maintaining the engine load constant, the average acceleration with assistance of electric drives can be improved by 19% compared to acceleration maneuver only on diesel engines (CODAD or CODLOD). Therefore, the electric drives have to be able to operate in field weakening range until reaching the maximum speed of the propeller shaft. Further, this system also offers assistance in off-design condition. In combination with electric energy storage, peak shaving of the load can be performed. With the electric drives providing power for the oscillating load caused by the waves, the thermal load on the engines can be reduced even more.

The results for the different concepts were compared with the performance of the current LCF (Luchtverdedigings – en Commando Fregat) in the Royal Netherlands Navy and are presented in the table below. Red values represent unfulfilled requirements; orange values meet the requirements by a small margin; and green values meet the requirements or, in case of the acceleration values, fulfill the desired standards.

| Concept | Ship speed SS3 | Average Acceleration | Thermal Limits | | Angle of Attack |
|-----------|----------------|------------------------|----------------|------------------|-----------------|
| | | | T_{\max} | $(dT/dt)_{\max}$ | α_{\max} |
| LCF - GT | 29 kn | 0.097 m/s ² | | | |
| LCF - DE | 19.4 kn | 0.057 m/s ² | | | |
| C1 – FPP | 27.3 kn | 0.08 m/s ² | 2086 °C | 156 °C/s | 17.5 ° |
| C1 – CPP | 27.5 kn | 0.1 m/s ² | 1963 °C | 100 °C/s | 20.9 ° |
| C2 – FPP | 28.4 kn | 0.084 m/s ² | 2070 °C | 102 °C/s | 18 ° |
| C2 – CPP | 28.6 kn | 0.109 m/s ² | 1895 °C | 90 °C/s | 20.8 ° |
| C3 – FPP | 28.0 kn | 0.075 m/s ² | 2065 °C | 92 °C/s | 18.1 ° |
| C3 – CPP | 28.2 kn | 0.114 m/s ² | 1911 °C | 102 °C/s | 21 ° |
| C4 – FPP | 28.5 kn | 0.087 m/s ² | 2040 °C | 58 °C/s | 18.9 ° |
| C4 – CPP | 28.6 kn | 0.128 m/s ² | 1850 °C | 69 °C/s | 21 ° |
| C4 – CPP* | 28.6 kn | 0.108 m/s ² | 1853 °C | 74 °C/s | 21 ° |

Table 7.1: Summarized results of acceleration maneuvers for all concepts in design conditions (EOL displacement, 6 months out of dock, with towed sonar array, sea state 3) * without electric drives (CODLOD/CODAD)

These results show that propulsion plants with a combination of diesel engines and electric drives can achieve high acceleration values while simultaneously limiting the thermal loading of the diesel engines. If the NATO standards for required and desired acceleration are taken into account, only propulsion plant concepts contemplating the use of CPP can fulfill the requirements. Concepts including CPP can perform better than the LCF on gas turbines, which also fails to meet the standards. Key to achieving high acceleration while reducing thermal load is the fast ramp up of the diesel engine with the increase in pitch lagging behind. Results from the Iver Huitfeldt-class frigates show that this has already been successfully implemented, with a maximum speed of 29.3 knots being reached in 120 seconds, resulting in an average acceleration of 0.126 m/s².

Both CPP and FPP propulsion plants benefit from the assistance of electric drives. FPP perform fairly well with electric drives, although without the assistance of electric drives, the vessel will display poor performance and the diesel engines are prone to overloading. Compared to CPP with the possibility of pitch reduction, larger engine margins are needed due to the dynamic effects of the waves that influence the requested power from the engine and the engine limits. As a result, the performance and engine loading of FPP propulsion plants will always be inferior to that of CPP propulsion plants.

The difference in service margin between FPP and CPP is also demanded by diesel engine manufacturers. By relying on larger electric drives, the effect of dynamic wave loading on the diesel engines increases and larger service margins are required. Thus, the exact magnitude of the margin for hybrid propulsion can only be determined with dynamic simulations.

The actual sizing of the diesel engine and electric drives is of less importance to maneuverability, as long as enough power can be provided to propel the frigate to maximum speed. The control strategy during the acceleration maneuver is, however, of critical importance. In this research, the models were controlled by providing ramp-up rates which are easily implemented into a real controller but require a lot of fine tuning for optimal results. These ramp-up rates needed to be retuned according to the different operating conditions, including sea states, acceleration without e-drive, and one-shaft operation. Therefore, an adaptive controller is needed to ensure high maneuverability and low engine loading under all operational conditions. An adaptive controller increases the complexity and the costs of the controller, but without adaptive control, large margins are needed to prevent overloading of the diesel engines in all operational conditions. In the absence of an adaptive controller, the performance of the propulsion plant is significantly reduced.

The FPP might achieve better cavitation performance in static conditions due to its design, but once equipped to the vessel very low acceleration is the only option to prevent cavitation in dynamic conditions. With CPP, on the contrary, the cavitation inception can be influenced by propeller speed and pitch. This results in a lower angle of attack of the CPP and probably also less underwater noise.

| | Ship speed trial | Average Acceleration | Angle of Attack |
|-----------|------------------|------------------------|-----------------|
| Concept | | | α_{\max} |
| C4 – FPP* | 19 kn | 0.021 m/s ² | 10.7 ° |
| C4 – CPP* | 19 kn | 0.039 m/s ² | 9.8 ° |

Table 7.2: Results of acceleration maneuvers with low angle of attack.
*without electric drives.

Diesel hybrid propulsion is definitely worth considering for the future M-frigate. High acceleration and low thermal loading can be achieved with a CODLAD system in combination with CPP and an adaptive controller. This system can compete with the acceleration performance of propulsion plants relying on gas turbines while reducing the fuel consumption.

Recommendations

CODLAD and CODLOD are both possible for concept 4. Concept 2 & 3 can only reach maximum speed in a CODLAD configuration due to decreased size of the diesel engines. With concept 1, the maximum speed is narrowly missed with 1 diesel engine and 1 large electric drive per shaft. However, large electric drives significantly increase the weight of the propulsion plant and require more generator sets to provide sufficient electrical power. Further research on the weight of all necessary components is required to show if reducing the amount and/or size of propulsion diesel engines outweighs the increasing size and amount of generator sets and electric drives.

Although the propulsion model was partly verified and validated, in order to ensure its complete validation, engine and propulsion control system measurement data for the LCF is absolutely essential. Aside from this validation, this data can also reveal the current performance of the frigates and might in addition offer solutions for improving their acceleration performance.

Beyond the general readings for the vessel and the engine, the charge air pressure and exhaust gas temperature are particularly important. This data can provide insight into the behavior of the turbocharger in dynamic conditions and the impact of the charge air pressure on the engine's thermal load. With it, the turbocharger model can be improved and thermal load limit predictions made more accurately. For a one-stage turbocharged engine, implementing the Büchi equation for the turbocharger might be sufficient. However, for predicting the performance of sequentially turbocharged engines a more advanced turbocharger model is needed.

During acceleration maneuvers, performance can be boosted by delivering the electric drives' maximum amount of torque. However, this research has already confirmed that the oscillating load on diesel engines in increased sea states can be reduced with advanced control of the electric drives. To investigate the possibilities of improved load sharing between the diesel engine and the electric drive, the simple model of the electric drive is insufficient because a speed control strategy is not possible. A more suitable model of the electric drive should be based on the equivalent circuit.

For this research, the thrust produced by the propeller is estimated as quasi-static with the open water diagram and only dependent on ship speed (advance speed) and propeller speed. During a real acceleration maneuver, the advance velocity will lag in comparison to the quasi-static estimations. Due to the water's inertia, the effective inflow is not instantly restored if the propeller speed or pitch is changed, thus increasing the thrust coefficient of the propeller. The effect is considered negligible as the quasi-static approach is used in several important research publications for marine engineering [e.g. (Vrijdag, 2009); (Geerstma, Negenborn, Visser, & Hopman, 2016)]. However, including the effect for fast acceleration maneuvers might affect the performance.

This research shows the possibilities for high-performance propulsion and low loading on diesel engines. The combination of pitch and engine speed for the propulsion plants with CPP are loosely based on the settings of the Danish Iver Huitfeldt-class frigate. Data on the acceleration performance was provided by the Danish Navy, but their considerations and limits regarding the control strategy remain unknown. An exchange of more detailed information might result in a new and more accurate insight into high performance with diesel propulsion, in addition to unveiling the effect on the required maintenance.

Predicting the exact cavitation behavior of propellers is very difficult. The only option investigated in this research was reducing the angle of attack during the acceleration maneuver in trial condition (with calm sea). Further research on more aspects of cavitation is needed to examine whether a CPP might offer better cavitation performance in real dynamic conditions. Simulations with finite element methods or model tests can offer more insight in the cavitation behavior.

8. References

- ABB. (2011). *HV induction motors, technical catalog for IEC motors EN 06-2015*. Zurich: ABB Asea Brown Boveri Ltd.
- ABB. (2011). *Technical guide No. 7 - Dimensioning of a drive system*. Zurich: ABB Asea Brown Boveri Ltd.
- Alexander, D. (2015, December). Hybrid Electric Drive for Naval Combatants. *Proceedings of the IEEE*, 103(12).
- Amini, H., & Steen, S. (2012). Theoretical and experimental investigation of propeller shaft loads in transient conditions. *International Shipbuilding Progress*(59), pp. 55-82.
- Amrhein, M., Krein, P. T., Chapman, P. L., & Fierro, B. I. (2007, November/December). Speed it up – Applications of faster rerated motors. *IEEE Industry Applications Magazine*, pp. 28-37.
- Betz, A., & Woschni, G. (1986). Umsetzungsgrad und Brennverlauf aufgeladener Dieselmotoren im instationären Betrieb. *Motortechnische Zeitung*(47), pp. 263-267.
- Bille, T. (1970). Experiences With Controllable Pitch Propellers. (IMarEst, Ed.) *Transactions IMarEst*, 82, p. 8.
- Boetius, D., & Baan, P. (1998). *Modulair simulatiemodel van een dieselmotor*. Delft: Delft University of Technology.
- Bolwell, R. (2001). *Through Life Management of Naval Gas Turbines for Extended Service Lives and Reduced Lifetime Costs*. Bath: Warship Support Agency.
- Brady, R. F. (2005). Fouling-Release Coatings for Warships. *Defense Science Journal*, 55(1), 75-81.
- Buckley, J., & Crane, A. (2007). Electric Propulsion Architectures in (Non) Capital Warships. *All Electric Ship Conference "The Vision Redrawn"*. London: IMarEst.
- Burril, L. C. (1949). Latest Developments in Reversible Propellers. *Transactions IMarEst*(61).
- Butcher, M., Maltby, R., & Parvin, P. S. (2009). Compact DC power and propulsion systems – the definitive solution? *"The Engine as a Weapon III" symposium*. Portsmouth: IEEE.
- Chen, S., & Flynn, P. (1965). *Development of a Single Cylinder Compression Ignition Research Engine*. SAE.
- Dang, J., van den Boom, H. J., & Ligtelijn, J. T. (2013). The Wageningen C- and D-Series Propellers. *International Conference on Fast Sea Transportation (FAST)*. Amsterdam.
- de Boer, M. J., & Hardy, I. J. (2014). Dynamic simulation as a tool to integrate, verify and optimise hybrid propulsion control systems. *Conference Proceedings, INEC 12th international Naval Engineering Conference and Exhibition "Innovative solutions to global trends"*. Amsterdam.
- de Jong, R., Rollema, I., Volger, C., & Schillings, R. (2015). *Geardrive - Gearbox power loss models and validation in hybrid propulsion configurations*. Delft: Bachelor Research Project, Delft University of Technology.
- de Waard, D. S. (2013). *Parameterization of ship propulsion drives*. Delft: Master's Thesis, Delft University of Technology.
- Defensie. (2007). *Hoofddlijnen Defensie Materieel Proces en Defensie Materieelprojectenoverzicht*. Retrieved from www.rijksoverheid.nl: <https://www.rijksoverheid.nl/documenten/kamerstukken/2007/09/18/hoofddlijnen-defensie-materieel-proces-en-defensie-materieelprojectenoverzicht>

- Drijver, J. (2013). *Evaluation of Transmission Losses, Heat Flows and Temperatures of Propulsive Drive Lines*. Delft: Master's thesis, Delft University of Technology.
- Drijver, J., Godjevac, M., de Vries, M. L., & Stapersma, D. (2015). Evaluation of losses in maritime gearboxes. *Proceedings of the Institution of Mechanical Engineers, Part M: Journal of Engineering for the Maritime Environment*.
- European Commission. (2014). *A policy framework for climate and energy in the period from 2020 to 2030*. Retrieved from ec.europa.eu: <http://eur-lex.europa.eu/legal-content/EN/TXT/?uri=CELEX%3A52014DC0015>
- GE Aviation. (2016). *LM2500+ Marine Gas Turbine*. Retrieved from www.geaviation.com: <http://www.geaviation.com/marine/engines/military/lm2500plus/>
- Geerstma, R. D., Negenborn, R. R., Visser, K., & Hopman, J. J. (2016). Torque control for diesel mechanical and hybrid propulsion on naval vessels. *INEC 13th international Naval Engineering Conference and Exhibition "Engineering the Triple A Navy: Active, Adaptive, Affordable"*, IMarEST. Bristol: IMarEst.
- Grimmelius, H. T., & Stapersma, D. (2001). The impact of propulsion plant control on diesel engine thermal loading. *22nd CIMAC World Congress*. Hamburg.
- Grimmelius, H. T., Shi, W., & Stapersma, D. (2010). Analysis of ship propulsion system behaviour and the impact on fuel consumption. *International Shipbuilding Progress*, 57, pp. 35-64.
- Grimmelius, H., Boetius, D., & Baan, P. (1999). The influence of sequential turbocharging control on propulsion behavior. *12th Ship Control System Symposium*. The Hague.
- Guillemette, J., & Bussieres, P. (1997). Proposed optimal controller for the Canadian Patrol frigate. *11th Ship Control System Symposium*. Southampton.
- Heising, C., Staudt, V., & Steimel, A. (2011). Optimized Energy-Efficient Drive System for Ship Propulsion. *IEEE Electric Ship Technologies Symposium* (pp. 292 – 295). Alexandria: IEEE.
- Hendriks, B. R. (2010). Designing warships under peacetime policy. *INEC 10th international Naval Engineering Conference and Exhibition "The Affordable Future Fleet"*. Portsmouth: IMarEst.
- Holtrop, J., & Mennen, G. (1982). An approximate power prediction method. *International Shipbuilding Progress*, 29, pp. 166-170.
- Hoppe, F. (2012). Hybrid propulsion combining gears and systems for naval vessels. *INEC 11th international Naval Engineering Conference and Exhibition "Engineering Naval Capability"*. Edinburgh: IMarEst.
- Klein Woud, H., & Sapersma, D. (2002). *Design of Propulsion and Electric Power Generation Systems*. London: IMarEst.
- Klein Woud, H., & Sapersma, D. (2005). Matching Propulsion Engine With Propulsor. *Journal of Marine Engineering and Technology*(A7), pp. 25-38.
- Koumbarelis, I., & Kyrtatos, N. P. (1991). Performance prediction of next generation slow speed diesel engines during ship maneuvers. *Transactions of The Institute of Marine Engineers*, 106(1), pp. 1-26.
- Kuphaldt, T. R. (1999). *Lessons in Electric Circuits*. Retrieved from [allaboutcircuits.com](http://www.allaboutcircuits.com): <http://www.allaboutcircuits.com/textbook/>

- Lamerton, R. F., Moss, N., Maltby, R. E., & Uhbi, W. (2008). Propulsion options for future frigates - power dense solutions for medium sized warships. *INEC 9th International Naval Engineering Conference and Exhibition "Embracing The Future"*. Hamburg: IMarEST.
- Lewis, C. (2002). The Advanced Induction Motor. *Power Engineering Society Summer Meeting, 1*, pp. 250-253.
- Lewis, E. V. (1988). *Principles of Naval Architecture – Volume II Resistance, Propulsion and Vibration*. Jersey City: Society of Naval Architects & Marine Engineers (SNAME).
- Loonstijn, M. (2016). *Sequential turbocharging for marine 4-stroke diesel engines*. Delft: Master's Thesis - Literature Study, Delft University of Technology.
- MAN. (2012). *V28/33D STC Project Guide – Marine*. Augsburg: MAN Diesel & Turbo SE.
- MAN. (2015). *Four-Stroke Propulsion Engines*. Augsburg: MAN Diesel & Turbo SE.
- MET Office. (2010). *Fact sheet 6 — The Beaufort Scale*. Exeter: National Meteorological Library and Archive.
- Miedema, S. A., & Lu, Z. (2002). The dynamic behaviour of a diesel engine. *WEDA XXII Technical Conference and 34th Texas A and M Dredging Seminar*. Denver: Western Dredging Association.
- Moran, M., & Shapiro, H. (2006). *Fundamentals of Engineering Thermodynamics SI-Version* (5 ed.). New York: Wiley and Sons.
- MTU. (2016). *Diesel Engines 20V 1163*. Friedrichshafen: MTU Friedrichshafen GmbH.
- Nadkarni, N. (2015).uspicious seas: Navies in Australasia are looking at fleet renewal in light of growing territorial tensions brought on by an increasingly strident Chinese navy. *Naval Focus*.
- NEMA. (2009). *NEMA Standards Publication MG 1-2009*. Rosslyn: National Electrical Manufacturers Association (NEMA).
- OES. (2015). *Operationele Energie Strategie*. Retrieved from www.rijksoverheid.nl:
<https://www.rijksoverheid.nl/documenten/kamerstukken/2016/02/15/kamerbrief-over-operationele-energie-strategie>
- OMT. (2014). *Danish frigate program*. Retrieved from Odense Maritime Technology:
<http://www.aspistrategist.org.au/wp-content/uploads/2014/11/OMT-Dansh-Frigate-Programme-April-2014.pdf>
- Oosterveld, M., & van Oossanen, P. (1975). *Further Computer-Analyzed Data of the Wageningen B-Screw Series*. Rotterdam: MARIN, former Netherlands Ship Model Basin (NSMB).
- Partridge, R., & Thorp, B. (2014). Re-Writing the propulsion rule book for the 21st century. *INEC 12th International Naval Engineering Conference and Exhibition "Innovative solutions to global trends"*. Amsterdam: IMarEST.
- Rajkumar, S., & Sudarshan, G. (2015). Multi-zone phenomenological model of combustion and emission characteristics and parametric investigations for split injections and multiple injections in common-rail direct-injection diesel engines. *Proceedings of the Institution of Mechanical Engineers, Part D: Journal of Automobile Engineering*.
- Reitz, R. D. (1995). Development and testing of diesel engine CFD models. *Progress in Energy and Combustion Science, 21*(2).

-
- Ross, R., Stapersma, D., & Bosklopper, J. (2010). Fuel efficiency of diesel, electric and superconductive propulsion systems. *INEC 10th International Naval Engineering Conference and Exhibition "The Affordable Future Fleet"*. Portsmouth: IMarEST.
- Schulten, P. J. (1998). *Quasi stationair model voor het cilindermodel van een dieselmotor*. Delft: Master's Thesis, Delft University of Technology.
- Schulten, P. J. (2005). *The Interaction between Diesel Engines, Ship and Propellers during Manoeuvring*. Delft: PhD Thesis, Delft University of Technology.
- Schulten, P. J., & Stapersma, D. (2003). *Mean Value Modelling of the Gas Exchange of a 4-stroke Diesel Engine For Use in Powertrain Applications*. SAE.
- Seiliger, M. (1922). *Graphische Thermodynamik und Berechnen der Verbrennungsmaschinen und Turbinen*. Berlin: Springer Verlag.
- Shumei, C., Chen, L., & Liwei, S. (2008). Study on Efficiency Calculation Model of Induction Motors for Electric Vehicles. *IEEE Vehicle Power and Propulsion Conference (VPPC)*. Harbin: IEEE.
- Siemens. (2009). *Three-phase Induction Motors - Catalog D 84.1*. München: Siemens AG.
- Simmonds, O. J. (2016). DC: Is it the Alternative Choice for Naval Power Distribution? *INEC 13th International Naval Engineering Conference and Exhibition "Engineering the Triple A Navy: Active, Adaptive, Affordable"*. Bristol: IMarEST.
- Slade, S. L. (2015). *Competing Manufacturers of MARINE GAS TURBINES - A Special Descriptive Market Analysis*. Newton: Forecast International.
- Stapersma, D. (2001). *Prime movers in an AES powerplant; number of units, size and costs*. Den Helder: Royal Netherlands Navy College.
- Stapersma, D. (2010). *Diesel Engines - A Fundamental Approach to Performance Analysis, Turbocharging, Combustion, Emissions and Heat Transfer Vol. 1-6* (8 ed.). Utrecht: Netherlands Defense Academy.
- USDE. (2012). *Adjustable Speed Drive Part-Load Efficiency*. Retrieved from U.S. Department of Energy: https://www1.eere.energy.gov/manufacturing/tech_assistance/pdfs/motor_tip_sheet11.pdf
- van Es, F. (2011). *Designing and evaluating propulsion concepts of surface combatants*. Delft: Master's Thesis, Delft University of Technology.
- van Spronsen, P., & Tousain, R. (2001). An optimal control approach to preventing marine diesel engine overloading aboard Karel Doorman Class frigates. *Selected Topics in Signals, Systems and Control*, 12.
- van Straten, O., & de Boer, M. (2012). Optimum propulsion engine configuration from fuel economic point of view. *INEC 11th international Naval Engineering Conference and Exhibition "Engineering Naval Capability"* (pp. 543 – 554). Edinburgh: IMarEST.
- Vrijdag, A. (2009). *Control of Propeller Cavitation in Operational Conditions*. Delft: PhD Thesis, Delft University of Technology.
- Wärtsilä. (2003). *Marine Project Guide W26A*. Trieste: Wärtsilä Italia S.p.A.
- Wärtsilä. (2015). *Wärtsilä 26 Product Guide*. Vaasa: Wärtsilä Finland.
- Wiesmann, A. (2010). Slow steaming – a viable long term option? *Wärtsilä Technical Journal*, pp. 49 – 55.
-

- Witt, D. L., Motley, M. R., Helfers, D. P., & Young, Y. L. (2012). Analysis of Controllable Pitch Propellers for an All-Electric Naval Combatant. *Society of Naval Architects and Marine Engineers*.
- Yabuki, H., Yoshimura, Y., Ishiguro, T., & Ueno, M. (2006). Turning motion of a ship with single CPP and single rudder during stopping maneuver under windy condition. *International Conference on Marine Simulation and Ship Manoeuvrability, MARSIM*. Terschelling: International Marine Simulator Forum.

9. Appendix

Appendix A: Coefficients Wageningen B-series Oosterveld and Oossanen

| KT: | C _{s,t,u,v} | (J) ^s | (P/D) ^t | (AE/A0) ^u | (Z) ^v | KQ: | C _{s,t,u,v} | (J) ^s | (P/D) ^t | (AE/A0) ^u | (Z) ^v |
|-----|----------------------|------------------|--------------------|----------------------|------------------|-----|----------------------|------------------|--------------------|----------------------|------------------|
| | 8.80E-03 | 0 | 0 | 0 | 0 | | 3.79E-03 | 0 | 0 | 0 | 0 |
| | -2.05E-01 | 1 | 0 | 0 | 0 | | 8.87E-03 | 2 | 0 | 0 | 0 |
| | 1.66E-01 | 0 | 1 | 0 | 0 | | -3.22E-02 | 1 | 1 | 0 | 0 |
| | 1.58E-01 | 0 | 2 | 0 | 0 | | 3.45E-03 | 0 | 2 | 0 | 0 |
| | -1.48E-01 | 2 | 0 | 1 | 0 | | -4.09E-02 | 0 | 1 | 1 | 0 |
| | -4.81E-01 | 1 | 1 | 1 | 0 | | -1.08E-01 | 1 | 1 | 1 | 0 |
| | 4.15E-01 | 0 | 2 | 1 | 0 | | -8.85E-02 | 2 | 1 | 1 | 0 |
| | 1.44E-02 | 0 | 0 | 0 | 1 | | 1.89E-01 | 0 | 2 | 1 | 0 |
| | -5.30E-02 | 2 | 0 | 0 | 1 | | -3.71E-03 | 1 | 0 | 0 | 1 |
| | 1.43E-02 | 0 | 1 | 0 | 1 | | 5.14E-03 | 0 | 1 | 0 | 1 |
| | 6.07E-02 | 1 | 1 | 0 | 1 | | 2.09E-02 | 1 | 1 | 0 | 1 |
| | -1.26E-02 | 0 | 0 | 1 | 1 | | 4.74E-03 | 2 | 1 | 0 | 1 |
| | 1.10E-02 | 1 | 0 | 1 | 1 | | -7.23E-03 | 2 | 0 | 1 | 1 |
| | -1.34E-01 | 0 | 3 | 0 | 0 | | 4.38E-03 | 1 | 1 | 1 | 1 |
| | 6.38E-03 | 0 | 6 | 0 | 0 | | -2.69E-02 | 0 | 2 | 1 | 1 |
| | -1.33E-03 | 2 | 6 | 0 | 0 | | 5.58E-02 | 3 | 0 | 1 | 0 |
| | 1.68E-01 | 3 | 0 | 1 | 0 | | 1.62E-02 | 0 | 3 | 1 | 0 |
| | -5.07E-02 | 0 | 0 | 2 | 0 | | 3.18E-03 | 1 | 3 | 1 | 0 |
| | 8.55E-02 | 2 | 0 | 2 | 0 | | 1.59E-02 | 0 | 0 | 2 | 0 |
| | -5.04E-02 | 3 | 0 | 2 | 0 | | 4.72E-02 | 1 | 0 | 2 | 0 |
| | 1.05E-02 | 1 | 6 | 2 | 0 | | 1.96E-02 | 3 | 0 | 2 | 0 |
| | -6.48E-03 | 2 | 6 | 2 | 0 | | -5.03E-02 | 0 | 1 | 2 | 0 |
| | -8.42E-03 | 0 | 3 | 0 | 1 | | -3.01E-02 | 3 | 1 | 2 | 0 |
| | 1.68E-02 | 1 | 3 | 0 | 1 | | 4.17E-02 | 2 | 2 | 2 | 0 |
| | -1.02E-03 | 3 | 3 | 0 | 1 | | -3.98E-02 | 0 | 3 | 2 | 0 |
| | -3.18E-02 | 0 | 3 | 1 | 1 | | -3.50E-03 | 0 | 6 | 2 | 0 |
| | 1.86E-02 | 1 | 0 | 2 | 1 | | -1.07E-02 | 3 | 0 | 0 | 1 |
| | -4.11E-03 | 0 | 2 | 2 | 1 | | 1.11E-03 | 3 | 3 | 0 | 1 |
| | -6.07E-04 | 0 | 0 | 0 | 2 | | -3.14E-04 | 0 | 6 | 0 | 1 |
| | -4.98E-03 | 1 | 0 | 0 | 2 | | 3.59E-03 | 3 | 0 | 1 | 1 |
| | 2.60E-03 | 2 | 0 | 0 | 2 | | -1.42E-03 | 0 | 6 | 1 | 1 |
| | -5.61E-04 | 3 | 0 | 0 | 2 | | -3.84E-03 | 1 | 0 | 2 | 1 |
| | -1.64E-03 | 1 | 2 | 0 | 2 | | 1.27E-02 | 0 | 2 | 2 | 1 |
| | -3.29E-04 | 1 | 6 | 0 | 2 | | -3.18E-03 | 2 | 3 | 2 | 1 |
| | 1.17E-04 | 2 | 6 | 0 | 2 | | 3.34E-03 | 0 | 6 | 2 | 1 |
| | 6.91E-04 | 0 | 0 | 1 | 2 | | -1.83E-03 | 1 | 1 | 0 | 2 |
| | 4.22E-03 | 0 | 3 | 1 | 2 | | 1.12E-04 | 3 | 2 | 0 | 2 |
| | 5.65E-05 | 3 | 6 | 1 | 2 | | -2.97E-05 | 3 | 6 | 0 | 2 |
| | -1.47E-03 | 0 | 3 | 2 | 2 | | 2.70E-04 | 1 | 0 | 1 | 2 |
| | | | | | | | 8.33E-04 | 2 | 0 | 1 | 2 |
| | | | | | | | 1.55E-03 | 0 | 2 | 1 | 2 |
| | | | | | | | 3.03E-04 | 0 | 6 | 1 | 2 |
| | | | | | | | -1.84E-04 | 0 | 0 | 2 | 2 |
| | | | | | | | -4.25E-04 | 0 | 3 | 2 | 2 |
| | | | | | | | 8.69E-05 | 3 | 3 | 2 | 2 |
| | | | | | | | -4.66E-04 | 0 | 6 | 2 | 2 |
| | | | | | | | 5.54E-05 | 1 | 6 | 2 | 2 |

Table 9.1: Coefficients Wageningen B-Series

Appendix B: Estimated Resistance vVMF

Resistance curve $\Delta = 5200$ ton

| V | R(t) DESP |
|------|--------------|------|--------------|------|--------------|------|--------------|------|--------------|------|--------------|
| 7 | 41.75898 | 12.1 | 130.1197 | 17.2 | 280.4574 | 22.3 | 539.756 | 27.4 | 1004.517 | 32.5 | 1805.459 |
| 7.1 | 42.97768 | 12.2 | 132.4251 | 17.3 | 284.7495 | 22.4 | 545.5715 | 27.5 | 1018.987 | 32.6 | 1823.561 |
| 7.2 | 44.21555 | 12.3 | 134.7541 | 17.4 | 289.0853 | 22.5 | 551.4269 | 27.6 | 1033.588 | 32.7 | 1841.784 |
| 7.3 | 45.47268 | 12.4 | 137.1068 | 17.5 | 293.4649 | 22.6 | 557.3222 | 27.7 | 1048.321 | 32.8 | 1860.128 |
| 7.4 | 46.74915 | 12.5 | 139.4832 | 17.6 | 297.8885 | 22.7 | 563.2577 | 27.8 | 1063.187 | 32.9 | 1878.594 |
| 7.5 | 48.04504 | 12.6 | 141.8836 | 17.7 | 302.3564 | 22.8 | 569.2335 | 27.9 | 1078.186 | 33 | 1897.181 |
| 7.6 | 49.36043 | 12.7 | 144.3079 | 17.8 | 306.8688 | 22.9 | 575.2496 | 28 | 1093.318 | 33.1 | 1915.891 |
| 7.7 | 50.69541 | 12.8 | 146.7562 | 17.9 | 311.426 | 23 | 581.3063 | 28.1 | 1108.585 | 33.2 | 1934.724 |
| 7.8 | 52.05006 | 12.9 | 149.2287 | 18 | 316.0281 | 23.1 | 587.4036 | 28.2 | 1123.987 | 33.3 | 1953.68 |
| 7.9 | 53.42446 | 13 | 151.7254 | 18.1 | 320.6754 | 23.2 | 593.5417 | 28.3 | 1139.524 | 33.4 | 1972.759 |
| 8 | 54.81869 | 13.1 | 154.2465 | 18.2 | 325.3681 | 23.3 | 599.7207 | 28.4 | 1155.197 | 33.5 | 1991.962 |
| 8.1 | 56.23285 | 13.2 | 156.792 | 18.3 | 330.1064 | 23.4 | 605.9407 | 28.5 | 1171.007 | 33.6 | 2011.29 |
| 8.2 | 57.667 | 13.3 | 159.362 | 18.4 | 334.8906 | 23.5 | 612.2019 | 28.6 | 1186.954 | 33.7 | 2030.743 |
| 8.3 | 59.12125 | 13.4 | 161.9566 | 18.5 | 339.7209 | 23.6 | 618.5044 | 28.7 | 1203.039 | 33.8 | 2050.32 |
| 8.4 | 60.59566 | 13.5 | 164.5759 | 18.6 | 344.5975 | 23.7 | 624.8483 | 28.8 | 1216.867 | 33.9 | 2070.024 |
| 8.5 | 62.09034 | 13.6 | 167.22 | 18.7 | 349.5207 | 23.8 | 631.2338 | 28.9 | 1230.785 | 34 | 2089.853 |
| 8.6 | 63.60535 | 13.7 | 169.8889 | 18.8 | 354.4906 | 23.9 | 637.661 | 29 | 1244.81 | 34.1 | 2109.809 |
| 8.7 | 65.14079 | 13.8 | 172.5828 | 18.9 | 359.5075 | 24 | 645.7902 | 29.1 | 1258.94 | | |
| 8.8 | 66.69675 | 13.9 | 175.3018 | 19 | 364.5716 | 24.1 | 654.3778 | 29.2 | 1273.178 | | |
| 8.9 | 68.2733 | 14 | 178.0459 | 19.1 | 369.6831 | 24.2 | 663.0419 | 29.3 | 1287.522 | | |
| 9 | 69.87053 | 14.1 | 180.8153 | 19.2 | 374.8424 | 24.3 | 671.7827 | 29.4 | 1301.974 | | |
| 9.1 | 71.48854 | 14.2 | 183.61 | 19.3 | 380.0495 | 24.4 | 680.6007 | 29.5 | 1316.533 | | |
| 9.2 | 73.1274 | 14.3 | 186.4302 | 19.4 | 385.3047 | 24.5 | 689.4962 | 29.6 | 1331.201 | | |
| 9.3 | 74.7872 | 14.4 | 189.2759 | 19.5 | 390.6083 | 24.6 | 698.4695 | 29.7 | 1345.977 | | |
| 9.4 | 76.46803 | 14.5 | 192.1471 | 19.6 | 395.9605 | 24.7 | 707.5209 | 29.8 | 1360.863 | | |
| 9.5 | 78.16997 | 14.6 | 195.0441 | 19.7 | 401.3615 | 24.8 | 716.6509 | 29.9 | 1375.857 | | |
| 9.6 | 79.89312 | 14.7 | 197.9669 | 19.8 | 406.8115 | 24.9 | 725.8598 | 30 | 1390.962 | | |
| 9.7 | 81.63756 | 14.8 | 200.9156 | 19.9 | 411.8032 | 25 | 735.1478 | 30.1 | 1406.177 | | |
| 9.8 | 83.40337 | 14.9 | 203.8902 | 20 | 416.7012 | 25.1 | 744.5154 | 30.2 | 1421.503 | | |
| 9.9 | 85.19065 | 15 | 206.891 | 20.1 | 421.6358 | 25.2 | 753.9629 | 30.3 | 1436.939 | | |
| 10 | 86.99947 | 15.1 | 209.9178 | 20.2 | 426.6073 | 25.3 | 763.4906 | 30.4 | 1452.487 | | |
| 10.1 | 88.82994 | 15.2 | 212.971 | 20.3 | 431.6158 | 25.4 | 773.0989 | 30.5 | 1468.147 | | |
| 10.2 | 90.68213 | 15.3 | 216.0505 | 20.4 | 436.6615 | 25.5 | 782.7881 | 30.6 | 1483.92 | | |
| 10.3 | 92.55614 | 15.4 | 219.1565 | 20.5 | 441.7444 | 25.6 | 792.5586 | 30.7 | 1499.804 | | |
| 10.4 | 94.45205 | 15.5 | 222.289 | 20.6 | 446.8647 | 25.7 | 802.4108 | 30.8 | 1515.802 | | |
| 10.5 | 96.36995 | 15.6 | 225.4481 | 20.7 | 452.0225 | 25.8 | 812.3448 | 30.9 | 1531.914 | | |
| 10.6 | 98.30993 | 15.7 | 228.6339 | 20.8 | 457.2179 | 25.9 | 822.3612 | 31 | 1548.139 | | |
| 10.7 | 100.2721 | 15.8 | 231.8466 | 20.9 | 462.4512 | 26 | 832.4603 | 31.1 | 1564.479 | | |
| 10.8 | 102.2565 | 15.9 | 235.0862 | 21 | 467.7223 | 26.1 | 842.6423 | 31.2 | 1580.933 | | |
| 10.9 | 104.2632 | 16 | 238.3528 | 21.1 | 473.0315 | 26.2 | 852.9076 | 31.3 | 1597.502 | | |
| 11 | 106.2924 | 16.1 | 241.6465 | 21.2 | 478.3788 | 26.3 | 863.2567 | 31.4 | 1614.187 | | |
| 11.1 | 108.3441 | 16.2 | 244.9673 | 21.3 | 483.7645 | 26.4 | 873.6897 | 31.5 | 1630.988 | | |
| 11.2 | 110.4185 | 16.3 | 248.3155 | 21.4 | 489.1886 | 26.5 | 884.2072 | 31.6 | 1647.905 | | |
| 11.3 | 112.5155 | 16.4 | 251.691 | 21.5 | 494.6512 | 26.6 | 894.8093 | 31.7 | 1664.939 | | |
| 11.4 | 114.6353 | 16.5 | 255.094 | 21.6 | 500.1525 | 26.7 | 906.8622 | 31.8 | 1682.09 | | |
| 11.5 | 116.778 | 16.6 | 258.5246 | 21.7 | 505.6926 | 26.8 | 920.4279 | 31.9 | 1699.358 | | |
| 11.6 | 118.9437 | 16.7 | 261.9828 | 21.8 | 511.2717 | 26.9 | 934.121 | 32 | 1716.744 | | |
| 11.7 | 121.1324 | 16.8 | 265.4688 | 21.9 | 516.8899 | 27 | 947.942 | 32.1 | 1734.249 | | |
| 11.8 | 123.3443 | 16.9 | 268.9827 | 22 | 522.5473 | 27.1 | 961.8916 | 32.2 | 1751.872 | | |
| 11.9 | 125.5794 | 17 | 272.5244 | 22.1 | 528.244 | 27.2 | 975.9703 | 32.3 | 1769.615 | | |
| 12 | 127.8379 | 17.1 | 276.2086 | 22.2 | 533.9802 | 27.3 | 990.1788 | 32.4 | 1787.477 | | |

Table 9.2: Resistance Curve future M-frigate, $\Delta = 5200$ ton

9. Appendix

Resistance curve $\Delta = 5970$ ton

| V | R(t) DESP |
|------|--------------|------|--------------|------|--------------|------|--------------|------|--------------|------|--------------|
| 7 | 47.12905 | 12.1 | 146.5163 | 17.2 | 314.3084 | 22.3 | 604.2529 | 27.4 | 1091.98 | 32.5 | 1986.574 |
| 7.1 | 48.50218 | 12.2 | 149.1059 | 17.3 | 318.3718 | 22.4 | 610.7424 | 27.5 | 1107.816 | 32.6 | 2006.503 |
| 7.2 | 49.89681 | 12.3 | 151.7218 | 17.4 | 322.4668 | 22.5 | 617.2762 | 27.6 | 1123.796 | 32.7 | 2026.564 |
| 7.3 | 51.31305 | 12.4 | 154.3643 | 17.5 | 327.3281 | 22.6 | 623.8544 | 27.7 | 1139.921 | 32.8 | 2046.76 |
| 7.4 | 52.75098 | 12.5 | 157.0333 | 17.6 | 332.2449 | 22.7 | 630.4772 | 27.8 | 1156.192 | 32.9 | 2067.089 |
| 7.5 | 54.21069 | 12.6 | 159.729 | 17.7 | 337.2107 | 22.8 | 637.1447 | 27.9 | 1172.609 | 33 | 2087.552 |
| 7.6 | 55.69227 | 12.7 | 162.4515 | 17.8 | 342.2258 | 22.9 | 643.8569 | 28 | 1189.174 | 33.1 | 2108.15 |
| 7.7 | 57.19582 | 12.8 | 165.2008 | 17.9 | 347.2903 | 23 | 650.6142 | 28.1 | 1205.885 | 33.2 | 2128.884 |
| 7.8 | 58.72142 | 12.9 | 167.9772 | 18 | 352.4046 | 23.1 | 657.4166 | 28.2 | 1222.746 | 33.3 | 2149.753 |
| 7.9 | 60.26916 | 13 | 170.7806 | 18.1 | 357.569 | 23.2 | 664.2643 | 28.3 | 1239.755 | 33.4 | 2170.758 |
| 8 | 61.83914 | 13.1 | 173.6111 | 18.2 | 362.7835 | 23.3 | 671.1573 | 28.4 | 1256.913 | 33.5 | 2191.9 |
| 8.1 | 63.43144 | 13.2 | 176.469 | 18.3 | 368.0486 | 23.4 | 678.096 | 28.5 | 1274.222 | 33.6 | 2213.178 |
| 8.2 | 65.04617 | 13.3 | 179.3542 | 18.4 | 373.3645 | 23.5 | 685.0803 | 28.6 | 1291.682 | 33.7 | 2234.594 |
| 8.3 | 66.68341 | 13.4 | 182.2668 | 18.5 | 378.7313 | 23.6 | 692.1105 | 28.7 | 1309.293 | 33.8 | 2256.149 |
| 8.4 | 68.34325 | 13.5 | 185.2071 | 18.6 | 384.1494 | 23.7 | 699.1866 | 28.8 | 1327.057 | 33.9 | 2277.841 |
| 8.5 | 70.0258 | 13.6 | 188.175 | 18.7 | 389.619 | 23.8 | 706.3089 | 28.9 | 1344.973 | 34 | 2299.672 |
| 8.6 | 71.73113 | 13.7 | 191.1707 | 18.8 | 395.1403 | 23.9 | 713.4775 | 29 | 1363.042 | 34.1 | 2321.643 |
| 8.7 | 73.45935 | 13.8 | 194.1943 | 18.9 | 400.7136 | 24 | 720.6925 | 29.1 | 1381.265 | 34.2 | 2343.753 |
| 8.8 | 75.21055 | 13.9 | 197.2459 | 19 | 406.3392 | 24.1 | 727.9541 | 29.2 | 1399.643 | 34.3 | 2366.003 |
| 8.9 | 76.98482 | 14 | 200.3255 | 19.1 | 412.0173 | 24.2 | 735.2624 | 29.3 | 1416.419 | 34.4 | 2388.394 |
| 9 | 78.78225 | 14.1 | 203.4333 | 19.2 | 417.7481 | 24.3 | 742.6175 | 29.4 | 1432.327 | 34.5 | 2410.926 |
| 9.1 | 80.60295 | 14.2 | 206.5694 | 19.3 | 423.5319 | 24.4 | 750.8326 | 29.5 | 1448.353 | 34.6 | 2433.599 |
| 9.2 | 82.44701 | 14.3 | 209.7339 | 19.4 | 429.3689 | 24.5 | 760.6394 | 29.6 | 1464.498 | 34.7 | 2456.414 |
| 9.3 | 84.31451 | 14.4 | 212.9269 | 19.5 | 435.2595 | 24.6 | 770.532 | 29.7 | 1480.764 | 34.8 | 2479.372 |
| 9.4 | 86.20556 | 14.5 | 216.1484 | 19.6 | 441.2038 | 24.7 | 780.5108 | 29.8 | 1497.149 | | |
| 9.5 | 88.12025 | 14.6 | 219.3987 | 19.7 | 447.2021 | 24.8 | 790.5761 | 29.9 | 1513.655 | | |
| 9.6 | 90.05868 | 14.7 | 222.6777 | 19.8 | 453.2546 | 24.9 | 800.7283 | 30 | 1530.281 | | |
| 9.7 | 92.02094 | 14.8 | 225.9856 | 19.9 | 459.3616 | 25 | 810.9678 | 30.1 | 1547.029 | | |
| 9.8 | 94.00712 | 14.9 | 229.3225 | 20 | 465.5234 | 25.1 | 821.295 | 30.2 | 1563.9 | | |
| 9.9 | 96.01733 | 15 | 232.6885 | 20.1 | 471.7402 | 25.2 | 831.7102 | 30.3 | 1580.892 | | |
| 10 | 98.05166 | 15.1 | 236.0837 | 20.2 | 477.9427 | 25.3 | 842.2139 | 30.4 | 1598.007 | | |
| 10.1 | 100.1102 | 15.2 | 239.5082 | 20.3 | 483.5359 | 25.4 | 852.8064 | 30.5 | 1615.246 | | |
| 10.2 | 102.1931 | 15.3 | 242.9621 | 20.4 | 489.1704 | 25.5 | 863.4881 | 30.6 | 1632.608 | | |
| 10.3 | 104.3003 | 15.4 | 246.4455 | 20.5 | 494.8462 | 25.6 | 874.2593 | 30.7 | 1650.094 | | |
| 10.4 | 106.4321 | 15.5 | 249.9585 | 20.6 | 500.5636 | 25.7 | 885.1205 | 30.8 | 1667.704 | | |
| 10.5 | 108.5885 | 15.6 | 253.5012 | 20.7 | 506.3227 | 25.8 | 896.072 | 30.9 | 1685.44 | | |
| 10.6 | 110.7696 | 15.7 | 257.0738 | 20.8 | 512.1235 | 25.9 | 907.1142 | 31 | 1703.301 | | |
| 10.7 | 112.9754 | 15.8 | 260.6762 | 20.9 | 517.9664 | 26 | 918.2476 | 31.1 | 1721.288 | | |
| 10.8 | 115.2062 | 15.9 | 264.3086 | 21 | 523.8514 | 26.1 | 929.4724 | 31.2 | 1739.402 | | |
| 10.9 | 117.462 | 16 | 267.9712 | 21.1 | 529.7786 | 26.2 | 940.789 | 31.3 | 1757.642 | | |
| 11 | 119.7428 | 16.1 | 271.664 | 21.2 | 535.7482 | 26.3 | 952.1979 | 31.4 | 1776.009 | | |
| 11.1 | 122.0489 | 16.2 | 275.3871 | 21.3 | 541.7603 | 26.4 | 963.6993 | 31.5 | 1794.504 | | |
| 11.2 | 124.3802 | 16.3 | 279.1406 | 21.4 | 547.8151 | 26.5 | 975.2938 | 31.6 | 1813.127 | | |
| 11.3 | 126.7369 | 16.4 | 282.9246 | 21.5 | 553.9128 | 26.6 | 986.9816 | 31.7 | 1831.879 | | |
| 11.4 | 129.1191 | 16.5 | 286.7393 | 21.6 | 560.0534 | 26.7 | 998.7632 | 31.8 | 1850.76 | | |
| 11.5 | 131.5269 | 16.6 | 290.5847 | 21.7 | 566.2371 | 26.8 | 1010.639 | 31.9 | 1869.77 | | |
| 11.6 | 133.9603 | 16.7 | 294.461 | 21.8 | 572.4641 | 26.9 | 1022.609 | 32 | 1888.91 | | |
| 11.7 | 136.4196 | 16.8 | 298.3682 | 21.9 | 578.7345 | 27 | 1034.674 | 32.1 | 1908.18 | | |
| 11.8 | 138.9047 | 16.9 | 302.3064 | 22 | 585.0484 | 27.1 | 1046.835 | 32.2 | 1927.581 | | |
| 11.9 | 141.4158 | 17 | 306.2758 | 22.1 | 591.406 | 27.2 | 1060.74 | 32.3 | 1947.114 | | |
| 12 | 143.9529 | 17.1 | 310.2764 | 22.2 | 597.8075 | 27.3 | 1076.289 | 32.4 | 1966.778 | | |

Table 9.3: Resistance Curve future M-frigate, $\Delta = 6000$ ton

Appendix C: Estimated Resistance LFAS

| v | R(t) LFAS |
|----|--------------|
| 5 | 4.297371 |
| 6 | 5.478393 |
| 7 | 6.750562 |
| 8 | 8.129728 |
| 9 | 9.631473 |
| 10 | 11.27107 |
| 11 | 13.06346 |
| 12 | 15.02312 |
| 13 | 17.16409 |
| 14 | 19.49983 |
| 15 | 22.0432 |
| 16 | 24.80637 |
| 17 | 27.80079 |
| 18 | 31.03708 |
| 19 | 34.52501 |
| 20 | 38.27342 |
| 21 | 42.2902 |
| 22 | 46.5822 |
| 23 | 51.15519 |
| 24 | 56.01384 |
| 25 | 61.16166 |
| 26 | 66.60097 |
| 27 | 72.33286 |
| 28 | 78.35716 |
| 29 | 84.67241 |
| 30 | 91.27587 |
| 31 | 98.16346 |
| 32 | 105.3298 |

Table 9.4: Added resistance towed sonar array

Appendix D: Open Water Results

Propeller model: 7496L
Propeller test: 2475701030
P/0.7D: 1.705
AE/A0: 0.922

Table data contains restricted information and is not included in the public version

Appendix E: Rolls Royce Spey SM1C – non dimensional performance data points

| n/n_{nom} | $m_f/m_{f,nom}$ | P/P_{nom} |
|-------------|-----------------|-------------|
| 1.000 | 1.000 | 1.000 |
| 0.818 | 0.346 | 0.239 |
| 0.364 | 0.346 | 0.200 |
| 0.182 | 1.000 | 0.444 |
| 0.182 | 0.866 | 0.383 |
| 0.727 | 0.779 | 0.733 |
| 0.909 | 0.693 | 0.656 |
| 1.000 | 0.606 | 0.539 |
| 0.545 | 0.606 | 0.494 |
| 0.909 | 0.519 | 0.433 |
| 0.182 | 0.519 | 0.239 |
| 0.364 | 0.433 | 0.278 |
| 0.909 | 0.346 | 0.228 |
| 0.182 | 0.346 | 0.144 |
| 1.000 | 0.173 | 0.050 |
| 0.909 | 0.173 | 0.050 |
| 0.364 | 0.173 | 0.067 |
| 0.182 | 0.173 | 0.044 |
| 0.909 | 0.260 | 0.133 |
| 0.727 | 0.260 | 0.144 |
| 0.455 | 0.260 | 0.144 |
| 0.273 | 0.260 | 0.117 |

Table 9.6: non-dimensional performance data RR Spey SM1C

Appendix F: Model Parameters

Reference - LCF

| Ship | | | Diesel Engine | | 2 per shaft |
|------------------------------|--------------------|------------------------|--------------------------------|------------------|------------------------|
| ship mass | m | 6050e ³ kg | nominal power | P _{nom} | 5440 kW |
| number of propellers | k _p | 2 | nominal speed | n _{nom} | 1000 rpm |
| thrust deduction factor | t | 0.06 | number of cylinders | i _{eng} | 16 |
| design resistance | R _D | 1658 kN | fuel pump time delay | τ _X | 0.01 s |
| design speed | v _D | 28.45 kn | heat release efficiency | η _q | 0.774 |
| Propeller | | | effective compression ratio | r _c | 15 |
| wake fraction | w | 0.09 | nominal charge air pressure | p ₁ | 3.8e ⁵ Pa |
| diameter | D | 5.0 m | nominal charge air temperature | T ₁ | 328 K |
| pitch | P _d | 1.47 | nominal mechanical efficiency | η _m | 0.9 |
| total propeller inertia | I _{prop} | 39915 kgm ² | turbocharger time delay | τ _{TC} | 1 s |
| relative rotative efficiency | η _r | 1 | inertia | I _{eng} | 279 kgm ² |
| Gearbox | | | Gas Turbine | | 2 per shaft |
| reduction ratio DE | i _{GB,DE} | 9.7087 | nominal power | P _{nom} | 18000 kW |
| reduction ratio GT | i _{GB,GT} | 34.516 | nominal speed | n _{syn} | 5350 rpm |
| gearbox loss coefficient a | a _{GB} | 0.6725 | inertia power turbine | I _{GT} | 49.45 kgm ² |
| gearbox loss coefficient b | b _{GB} | 0.1613 | gas turbine coefficient a | a _{GT} | -0.0470 |
| gearbox loss coefficient c | c _{GB} | 0.1609 | gas turbine coefficient b | b _{GT} | -0.8884 |
| gearbox inertia | I _{GB} | 10150 kgm ² | gas turbine coefficient c | c _{GT} | 1.1724 |
| | | | gas turbine coefficient d | d _{GT} | -0.1904 |
| | | | gas turbine coefficient e | e _{GT} | 0.4540 |

Table 9.7: Model parameters reference - LCF

Concept 1 - FPP

| Ship | | | Diesel Engine | | 1 per shaft |
|------------------------------|-------------------|------------------------|--------------------------------|------------------|-----------------------|
| ship mass | m | 5200e ³ kg | nominal power | P _{nom} | 10000 kW |
| number of propellers | k _p | 2 | nominal speed | n _{nom} | 1035 rpm |
| thrust deduction factor | t | 0.068 | number of cylinders | i _{eng} | 20 |
| design resistance | R _D | 1093 kN | fuel pump time delay | τ _X | 0.01 s |
| design speed | v _D | 28 kn | heat release efficiency | η _q | 0.8 |
| Propeller | | | effective compression ratio | r _c | 14.2 |
| wake fraction | w | 0.05 | nominal charge air pressure | p ₁ | 4.52e ⁵ Pa |
| diameter | D | 4.8 m | nominal charge air temperature | T ₁ | 322 K |
| pitch | P _d | 1.705 | nominal mechanical efficiency | η _m | 0.9 |
| total propeller inertia | I _{prop} | 37000 kgm ² | turbocharger time delay | τ _{TC} | 1 s |
| relative rotative efficiency | η _r | 1 | inertia | I _{eng} | 1070 kgm ² |
| Gearbox | | | Electric Drive | | 1 per shaft |
| reduction ratio | i _{GB} | 7.4981 | nominal power | P _{nom} | 4900 kW |
| gearbox loss coefficient a | a _{GB} | 0.6725 | synchronous speed | n _{syn} | 900 rpm |
| gearbox loss coefficient b | b _{GB} | 0.1613 | inertia | I _{ED} | 300 kgm ² |
| gearbox loss coefficient c | c _{GB} | 0.1609 | gearbox ratio Edrive | I _{ED} | 9.47 |
| gearbox inertia | I _{GB} | 10150 kgm ² | total shaft inertia | I _{sh} | 800 kgm ² |

Table 9.8: Model parameters Concept 1 - FPP

Concept 1 – CPP

| Ship | | | Diesel Engine | | 1 per shaft |
|------------------------------|-------------------|------------------------|--------------------------------|------------------|-----------------------|
| ship mass | m | 5200e ³ kg | nominal power | P _{nom} | 10000 kW |
| number of propellers | k _p | 2 | nominal speed | n _{nom} | 1035 rpm |
| thrust deduction factor | t | 0.068 | number of cylinders | i _{eng} | 20 |
| design resistance | R _D | 1093 kN | fuel pump time delay | τ _X | 0.01 s |
| design speed | v _D | 28 kn | heat release efficiency | η _q | 0.8 |
| Propeller | | | effective compression ratio | r _c | 14.2 |
| wake fraction | w | 0.05 | nominal charge air pressure | p ₁ | 4.52e ⁵ Pa |
| diameter | D | 4.8 m | nominal charge air temperature | T ₁ | 322 K |
| pitch | P _d | 1.8 | nominal mechanical efficiency | η _m | 0.9 |
| total propeller inertia | I _{prop} | 39915 kgm ² | turbocharger time delay | τ _{TC} | 1 s |
| relative rotative efficiency | η _r | 1 | inertia | I _{eng} | 1070 kgm ² |
| Gearbox | | | Electric Drive | | 1 per shaft |
| reduction ratio | i _{GB} | 7.4378 | nominal power | P _{nom} | 4900 kW |
| gearbox loss coefficient a | a _{GB} | 0.6725 | synchronous speed | n _{syn} | 900 rpm |
| gearbox loss coefficient b | b _{GB} | 0.1613 | inertia | I _{ED} | 300 kgm ² |
| gearbox loss coefficient c | c _{GB} | 0.1609 | gearbox ratio Edrive | I _{ED} | 9.47 |
| gearbox inertia | I _{GB} | 10150 kgm ² | total shaft inertia | I _{sh} | 800 kgm ² |

Table 9.9: Model parameters Concept 1 - CPP

Concept 2 – FPP

| Ship | | | Diesel Engine | | 2 per shaft |
|------------------------------|-------------------|------------------------|--------------------------------|------------------|------------------------|
| ship mass | m | 5200e ³ kg | nominal power | P _{nom} | 7280 kW |
| number of propellers | k _p | 2 | nominal speed | n _{nom} | 1000 rpm |
| thrust deduction factor | t | 0.068 | number of cylinders | i _{eng} | 16 |
| design resistance | R _D | 1231 kN | fuel pump time delay | τ _X | 0.01 s |
| design speed | v _D | 28.9 kn | heat release efficiency | η _q | 0.795 |
| Propeller | | | effective compression ratio | r _c | 14.2 |
| wake fraction | w | 0.05 | nominal charge air pressure | p ₁ | 4.31e ⁵ Pa |
| diameter | D | 4.8 m | nominal charge air temperature | T ₁ | 322 K |
| pitch | P _d | 1.705 | nominal mechanical efficiency | η _m | 0.9 |
| total propeller inertia | I _{prop} | 37000 kgm ² | turbocharger time delay | τ _{TC} | 1 s |
| relative rotative efficiency | η _r | 1 | inertia | I _{eng} | 830 kgm ² |
| Gearbox | | | Electric Drive | | 1 per shaft |
| reduction ratio | i _{GB} | 7.1677 | nominal power | P _{nom} | 2600 kW |
| gearbox loss coefficient a | a _{GB} | 0.6725 | synchronous speed | n _{syn} | 900 rpm |
| gearbox loss coefficient b | b _{GB} | 0.1613 | inertia | I _{ED} | 120.7 kgm ² |
| gearbox loss coefficient c | c _{GB} | 0.1609 | gearbox ratio Edrive | I _{ED} | 12 |
| gearbox inertia | I _{GB} | 10150 kgm ² | total shaft inertia | I _{sh} | 800 kgm ² |

Table 9.10: Model parameters Concept 2 - FPP

Concept 2 – CPP

| Ship | | | Diesel Engine | | 2 per shaft |
|------------------------------|-------------------|------------------------|--------------------------------|------------------|------------------------|
| ship mass | m | 5200e ³ kg | nominal power | P _{nom} | 7280 kW |
| number of propellers | k _p | 2 | nominal speed | n _{nom} | 1000 rpm |
| thrust deduction factor | t | 0.068 | number of cylinders | i _{eng} | 16 |
| design resistance | R _D | 1231 kN | fuel pump time delay | τ _X | 0.01 s |
| design speed | v _D | 28.9 kn | heat release efficiency | η _q | 0.795 |
| Propeller | | | effective compression ratio | r _c | 14.2 |
| wake fraction | w | 0.05 | nominal charge air pressure | p ₁ | 4.31e ⁵ Pa |
| diameter | D | 4.8 m | nominal charge air temperature | T ₁ | 322 K |
| pitch | P _d | 1.8 | nominal mechanical efficiency | η _m | 0.9 |
| total propeller inertia | I _{prop} | 39915 kgm ² | turbocharger time delay | τ _{TC} | 1 s |
| relative rotative efficiency | η _r | 1 | inertia | I _{eng} | 830 kgm ² |
| Gearbox | | | Electric Drive | | 1 per shaft |
| reduction ratio | i _{GB} | 7.1101 | nominal power | P _{nom} | 2600 kW |
| gearbox loss coefficient a | a _{GB} | 0.6725 | synchronous speed | n _{syn} | 900 rpm |
| gearbox loss coefficient b | b _{GB} | 0.1613 | inertia | I _{ED} | 120.7 kgm ² |
| gearbox loss coefficient c | c _{GB} | 0.1609 | gearbox ratio Edrive | I _{ED} | 12 |
| gearbox inertia | I _{GB} | 10150 kgm ² | total shaft inertia | I _{sh} | 800 kgm ² |

Table 9.11: Model parameters Concept 2 - CPP

Concept 3 – FPP

| Ship | | | Diesel Engine | | 2 per shaft |
|------------------------------|-------------------|------------------------|--------------------------------|------------------|------------------------|
| ship mass | m | 6000e ³ kg | nominal power | P _{nom} | 7280 kW |
| number of propellers | k _p | 2 | nominal speed | n _{nom} | 1000 rpm |
| thrust deduction factor | t | 0.068 | number of cylinders | i _{eng} | 16 |
| design resistance | R _D | 1257 kN | fuel pump time delay | τ _X | 0.01 s |
| design speed | v _D | 28.4 kn | heat release efficiency | η _q | 0.795 |
| Propeller | | | effective compression ratio | r _c | 14.2 |
| wake fraction | w | 0.05 | nominal charge air pressure | p ₁ | 4.31e ⁵ Pa |
| diameter | D | 4.8 m | nominal charge air temperature | T ₁ | 322 K |
| pitch | P _d | 1.705 | nominal mechanical efficiency | η _m | 0.9 |
| total propeller inertia | I _{prop} | 37000 kgm ² | turbocharger time delay | τ _{TC} | 1 s |
| relative rotative efficiency | η _r | 1 | inertia | I _{eng} | 830 kgm ² |
| Gearbox | | | Electric Drive | | 1 per shaft |
| reduction ratio | i _{GB} | 7.1815 | nominal power | P _{nom} | 2600 kW |
| gearbox loss coefficient a | a _{GB} | 0.6725 | synchronous speed | n _{syn} | 900 rpm |
| gearbox loss coefficient b | b _{GB} | 0.1613 | inertia | I _{ED} | 120.7 kgm ² |
| gearbox loss coefficient c | c _{GB} | 0.1609 | gearbox ratio Edrive | I _{ED} | 12 |
| gearbox inertia | I _{GB} | 10150 kgm ² | total shaft inertia | I _{sh} | 800 kgm ² |

Table 9.12: Model parameters Concept 3 - FPP

Concept 3 – CPP

| Ship | | | Diesel Engine | | 2 per shaft |
|------------------------------|-------------------|------------------------|--------------------------------|------------------|------------------------|
| ship mass | m | 6000e ³ kg | nominal power | P _{nom} | 7280 kW |
| number of propellers | k _p | 2 | nominal speed | n _{nom} | 1000 rpm |
| thrust deduction factor | t | 0.068 | number of cylinders | i _{eng} | 16 |
| design resistance | R _D | 1257 kN | fuel pump time delay | τ _X | 0.01 s |
| design speed | v _D | 28.4 kn | heat release efficiency | η _q | 0.795 |
| Propeller | | | effective compression ratio | r _c | 14.2 |
| wake fraction | w | 0.05 | nominal charge air pressure | p ₁ | 4.31e ⁵ Pa |
| diameter | D | 4.8 m | nominal charge air temperature | T ₁ | 322 K |
| pitch | P _d | 1.8 | nominal mechanical efficiency | η _m | 0.9 |
| total propeller inertia | I _{prop} | 39915 kgm ² | turbocharger time delay | τ _{TC} | 1 s |
| relative rotative efficiency | η _r | 1 | inertia | I _{eng} | 830 kgm ² |
| Gearbox | | | Electric Drive | | 1 per shaft |
| reduction ratio | i _{GB} | 7.1237 | nominal power | P _{nom} | 2600 kW |
| gearbox loss coefficient a | a _{GB} | 0.6725 | synchronous speed | n _{syn} | 900 rpm |
| gearbox loss coefficient b | b _{GB} | 0.1613 | inertia | I _{ED} | 120.7 kgm ² |
| gearbox loss coefficient c | c _{GB} | 0.1609 | gearbox ratio Edrive | I _{ED} | 12 |
| gearbox inertia | I _{GB} | 10150 kgm ² | total shaft inertia | I _{sh} | 800 kgm ² |

Table 9.13: Model parameters Concept 3 - CPP

Concept 4 – FPP

| Ship | | | Diesel Engine | | 2 per shaft |
|------------------------------|-------------------|------------------------|--------------------------------|------------------|------------------------|
| ship mass | m | 6000e ³ kg | nominal power | P _{nom} | 9100 kW |
| number of propellers | k _p | 2 | nominal speed | n _{nom} | 1000 rpm |
| thrust deduction factor | t | 0.068 | number of cylinders | i _{eng} | 20 |
| design resistance | R _D | 1309 kN | fuel pump time delay | τ _X | 0.01 s |
| design speed | v _D | 28.7 kn | heat release efficiency | η _q | 0.795 |
| Propeller | | | effective compression ratio | r _c | 14.2 |
| wake fraction | w | 0.05 | nominal charge air pressure | p ₁ | 4.31e ⁵ Pa |
| diameter | D | 4.8 m | nominal charge air temperature | T ₁ | 322 K |
| pitch | P _d | 1.705 | nominal mechanical efficiency | η _m | 0.9 |
| total propeller inertia | I _{prop} | 37000 kgm ² | turbocharger time delay | τ _{TC} | 1 s |
| relative rotative efficiency | η _r | 1 | inertia | I _{eng} | 1037 kgm ² |
| Gearbox | | | Electric Drive | | 1 per shaft |
| reduction ratio | i _{GB} | 7.0732 | nominal power | P _{nom} | 2600 kW |
| gearbox loss coefficient a | a _{GB} | 0.6725 | synchronous speed | n _{syn} | 900 rpm |
| gearbox loss coefficient b | b _{GB} | 0.1613 | inertia | I _{ED} | 120.7 kgm ² |
| gearbox loss coefficient c | c _{GB} | 0.1609 | gearbox ratio Edrive | I _{ED} | 12 |
| gearbox inertia | I _{GB} | 10150 kgm ² | total shaft inertia | I _{sh} | 800 kgm ² |

Table 9.14: Model parameters Concept 4 - FPP

Concept 4 – CPP

| Ship | | | Diesel Engine | | |
|------------------------------|-------------------|------------------------|--------------------------------|------------------|------------------------|
| ship mass | m | 6000e ³ kg | nominal power | P _{nom} | 9100 kW |
| number of propellers | k _p | 2 | nominal speed | n _{nom} | 1000 rpm |
| thrust deduction factor | t | 0.068 | number of cylinders | i _{eng} | 20 |
| design resistance | R _D | 1309 kN | fuel pump time delay | τ _X | 0.01 s |
| design speed | v _D | 28.7 kn | heat release efficiency | η _q | 0.795 |
| Propeller | | | effective compression ratio | r _c | 14.2 |
| wake fraction | w | 0.05 | nominal charge air pressure | p ₁ | 4.31e ⁵ Pa |
| diameter | D | 4.8 m | nominal charge air temperature | T ₁ | 322 K |
| pitch | P _d | 1.8 | nominal mechanical efficiency | η _m | 0.9 |
| total propeller inertia | I _{prop} | 39915 kgm ² | turbocharger time delay | τ _{TC} | 1 s |
| relative rotative efficiency | η _r | 1 | inertia | I _{eng} | 1037 kgm ² |
| Gearbox | | | Electric Drive | | |
| reduction ratio | i _{GB} | 7.0163 | nominal power | P _{nom} | 2600 kW |
| gearbox loss coefficient a | a _{GB} | 0.6725 | synchronous speed | n _{syn} | 900 rpm |
| gearbox loss coefficient b | b _{GB} | 0.1613 | inertia | I _{ED} | 120.7 kgm ² |
| gearbox loss coefficient c | c _{GB} | 0.1609 | gearbox ratio Edrive | I _{ED} | 12 |
| gearbox inertia | I _{GB} | 10150 kgm ² | total shaft inertia | I _{sh} | 800 kgm ² |

Table 9.15: Model parameters Concept 4 - CPP

Operational conditions

For the sake of completeness the parameters defining the operational conditions are given in the following table.

| | Trial | Design | Off-Design |
|--------------------------|-----------|---------|------------|
| Service Margin | 1.0 | 1.203 | 1.6 |
| Resistance of LFAS | Not added | Added | Not added |
| Sea state | 0 | 3 | 6 |
| Wave frequency | 0 Hz | 0.14 Hz | 0.1 Hz |
| Wave amplitude | 0 m | 0.625 m | 3 m |
| Wave number | 0 | 0.08 | 0.04 |
| Water depth HL propeller | 4.5 m | 4.5 m | 4.5 m |

Table 9.16: Operational conditions

Appendix G: Results simulation model Imtech

Figures contain restricted information and are not included in the public version